Expression of α3 and FXYD subunits comprising dynamic sodium pumps in young *Xenopus* frog tadpoles

Dorothy MacFarlane

A thesis submitted for the degree of PhD
at the
University of St Andrews

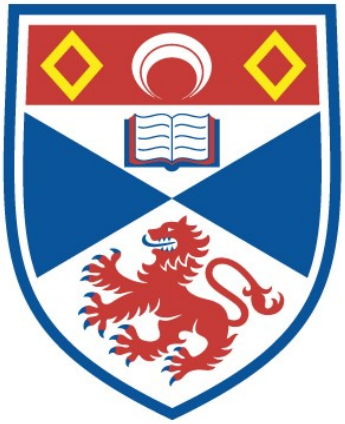

2024

DECLARATION

Candidate's declaration

I, Dorothy MacFarlane, do hereby certify that this thesis, submitted for the degree of PhD, which is approximately 50,000 words in length, has been written by me, and that it is the record of work carried out by me, or principally by myself in collaboration with others as acknowledged, and that it has not been submitted in any previous application for any degree. I confirm that any appendices included in my thesis contain only material permitted by the 'Assessment of Postgraduate Research Students' policy.

I was admitted as a research student at the University of St Andrews in September 2019.

I received funding from an organisation or institution and have acknowledged the funder(s) in the full text of my thesis.

Date 18th March, 2024 Signature of candidate

Supervisor's declaration

We hereby certify that the candidate has fulfilled the conditions of the Resolution and Regulations appropriate for the degree of PhD in the University of St Andrews and that the candidate is qualified to submit this thesis in application for that degree. We confirm that any appendices included in the thesis contain only material permitted by the 'Assessment of Postgraduate Research Students' policy.

Date 11th March, 2024 Signature of supervisor

Date 11th March, 2024 Signature of supervisor

Permission for publication

In submitting this thesis to the University of St Andrews we understand that we are giving permission for it to be made available for use in accordance with the regulations of the University Library for the time being in force, subject to any copyright vested in the work not being affected thereby. We also understand, unless exempt by an award of an embargo as requested below, that the title and the abstract will be published, and that a copy of the work may be made and supplied to any bona fide library or research worker, that this thesis will be electronically accessible for personal or research use and that the library has the right to migrate this thesis into new electronic forms as required to ensure continued access to the thesis.

I, Dorothy MacFarlane, confirm that my thesis does not contain any third-party material that requires copyright clearance.

The following is an agreed request by candidate and supervisor regarding the publication of this thesis:

Printed copy

No embargo on print copy.

Electronic copy

No embargo on electronic copy.

Date 18th March, 2024 Signature of candidate

Date 11th March, 2024 Signature of supervisor

Date 11th March, 2024 Signature of supervisor

Underpinning Research Data or Digital Outputs

Candidate's declaration

I, Dorothy MacFarlane, understand that by declaring that I have original research data or digital outputs, I should make every effort in meeting the University's and research funders' requirements on the deposit and sharing of research data or research digital outputs.

Date 18th March, 2024 Signature of candidate

Permission for publication of underpinning research data or digital outputs

We understand that for any original research data or digital outputs which are deposited, we are giving permission for them to be made available for use in accordance with the requirements of the University and research funders, for the time being in force.

We also understand that the title and the description will be published, and that the underpinning research data or digital outputs will be electronically accessible for use in accordance with the license specified at the point of deposit, unless exempt by award of an embargo as requested below.

The following is an agreed request by candidate and supervisor regarding the publication of underpinning research data or digital outputs:

No embargo on underpinning research data or digital outputs.

Date 18th March, 2024 Signature of candidate

Date 11th March, 2024 Signature of supervisor

Date 11th March, 2024 Signature of supervisor

CONTRIBUTIONS

Tadpole Provision and Rearing

Tadpoles were provided by the breeding of paired adult *Xenopus* frogs from an in-house frog colony managed by the home office (HO). Preparation and injection of the breeding pairs with human chorionic gonadotropin (hCG) was conducted by the Sillar and Li lab primary investigators, Keith T Sillar and Wenchang Li respectively. Collection of fertilized eggs and tadpole rearing was handled by Lamia Hachoumi, Jessica Barclay, Rebecca Rensner, Valentina Saccomanno and Hong Yan Zhang.

Immunocytochemistry

Completion of the western blot protocol was accomplished with help from fellow Neuroscience PhD candidates James Grey and Chloe O' Rourke.

Microscopy Training

A variety of microscopes within the School of Psychology and Neuroscience and the School of Biology were accessed over the course of my degree. Training for these microscopes was provided by the following colleagues: Postdoctoral students Mizuki Morisaki, Pierce Mullen and Lamia Hachoumi. Maarten Zwart also kindly lent his time to me to explain the mechanical function of confocal microscopes which enabled me to ensure I produced high-quality images.

Research Data/Digital Outputs access statement Research data underpinning this thesis are available at:

https://doi.org/10.17630/6704b4d4-512d-4816-86d2-438fd4d0de89

FUNDING

This work was supported in part by a Biotechnology and Biology Sciences Research Council grant to Prof Keith T. Sillar (Award ref BB/T015705/1).

“This I’ll Defend”
---MacFarlane Clan Motto

ACKNOWLEDGMENTS

I cannot, in good faith, submit this thesis without acknowledging and thanking the people who have helped me to complete my graduate programme these past few years, keeping me sane and sensible in equal measure all the while.

First and foremost, I want to express my sincere gratitude for the unwavering support and kindness provided by my supervisors Keith Thomas Sillar and Gayle Helane Doherty. Their considerable guidance, accumulated experience and shared wisdom have made a profound impact on my graduate studies and I will carry the lessons they have taught me for the rest of my days. Keith took a chance on me at a time when I was at my lowest and offered me a position in his lab first as an MSc candidate and then by granting me an extension to instead pursue my PhD. This has proven to be a generosity that I cannot ever repay but for which I am forever grateful. His candour and wit were instrumental in raising my confidence and shaping me into the scientist that I am today. Even prior to my graduate studies, Gayle has been an unshakeable supporter of my studies. She has proven herself to be an unerring force of nature and her keen intellect and sardonic humour have provided me with immeasurable joy through my near decade of acquaintance with her. Together, Gayle and Keith have been my rock, my safe harbour, my mentors. From the bottom of my heart, thank you both.

I would be greatly remiss if I did not mention my marvellous lab mates in the Sillar Lab who have kept me sane both inside and outside our workplace. Their presence in my life has brought joy, laughter, and countless cherished memories. Whether we were battling dragons during DnD or spontaneously swimming tadpoles, these ladies always found a way to make me laugh until my sides ached. They also were a much-needed shoulder to cry over the woes of a thousandth failed experiment. Their good-humour, world-weary wisdom and unceasing generosity were truly unparalleled and I am so grateful to have had you guys as my friends these past few years. And so for all of this, I wanted to take this little bit of space in my thesis to give an extra special thanks to Lamia Hachoumi, Rebecca Rensner and Jessica Barclay. Never change.

I cannot ignore my fellow PhD candidates who have been my rock through this experience. James Grey and Chloe O’Rourke wholeheartedly breath truth into the phrase truth misery loves company. From sharing work benches to sharing bar space, your friendship has made me incredibly happy and I hate the thought of never getting to trudge the ghost and dead-bee ridden hallways of Bute’s eery top floor with you guys again - a sentiment I never thought I could have before my ill-spent time with you both. From the drudge-filled abyss of my traumatized graduate school heart: thank you.

Of course, I could not have done any of this without the help of my wonderful parents and my older brother. Your unwavering support during this busy time helped me to become the woman that I am today. Thank you for all the sacrifices you've made, the lessons you've taught, and the memories we've shared. It is with a glad heart and a bettered mind that I dedicate this thesis to you.

I would also like to express my appreciation to all the amazing staff and colleagues employed in St Mary’s quad. Never have I worked in a more kind or welcoming environment before this. I can’t imagine any place else ever measuring up to the quality of people I have gotten to know in my time as a PhD candidate.

CONTENTS

FIGURE LIST

ABBREVIATIONS

A	**Actuator Domain**
ACh	**Acetylcholine**
ADP + P	**Adenosine Diphosphate + Phosphate**
AHC	**Alternating Hemiplegia of Childhood**
aIN	**Ascending Interneuron**
AP	**Action Potential**
ATP	**Adenosine Triphosphate**
CC	**Central Canal**
CE	**Ciliated Ependymal Cells**
CG	**Cement Gland**
cIN	**Commissural Interneuron**
CMZ	**Central Marginal Zone**
CNS	**Central Nervous System**
CPG	**Central Pattern Generator**
CSF	**Cerebrospinal Fluid**
CTCF	**Combined Total Cellular Fluorescence**
CTF	**Combined Total Fluorescence**
dla	**Dorsolateral Ascending Interneuron**
dlc	**Dorsolateral Commissural Interneuron**
dIN	**Descending Interneuron**
ELISA	**Enzyme-Linked Immunosorbent Assay**
FB	**Forebrain**
GABA	**γ-aminobutyric acid**
GCL	**Ganglion Cell Layer**
GIRK	**G Protein-Coupled Inward-Rectifying Potassium Channels**
Glu	**Glutamate**
Gly	**Glycine**
H&E	**Haematoxylin and Eosin**
HB	**Hindbrain**
HCG	**Human Chorionic Gonadotropin**
HCN	**Hyperpolarization-Activated Cyclic Nucleotide–Gated Channels**

HO	**Home Office**
IHC	**Immunohistochemistry**
IKr	**delayed-rectifying K+ current**
INL	**Inner Nuclear Layer**
IPL	**Inner Plexiform Layer**
ISI	**Inter-Swim Interval**
KA	**Kolmer–Agduhr cells**
KOH	**Potassium hydroxide**
LA	**Low Activity**
LT	**Lateral Tract**
LV	**Lateral Ventricle**
MB	**Midbrain**
mhr	**Midhindbrain reticulospinal neurons**
MN	**Motoneuron**
MS-222	**Tricaine methanesulfonate**
N	**Nucleotide Binding Domain**
NF	**Nieuwkoop and Faber, 1965**
NKA	**Na,K-ATPase**
NMDA	**N-methyl-D-aspartate**
ON	**Optic Nerve**
ONL	**Outer Nuclear Layer**
OPL	**Outer Plexiform Layer**
P	**Phosphorylation Domain**
PE	**Protein Extract**
PKA	**Protein Kinase A**
PKC	**Protein Kinase C**
PTH	**Post-tetanic Hyperpolarization**
RDP	**Rapid-Onset Dystonia Parkinsonism**
RMP	**Resting Membrane Potential**
SC	**Spinal Cord**
SEM	**Standard Error of the Mean**
SD	**Standard Deviation**

STMM	**Short-Term Motor Memory**
S1K	**Schedule 1 Kill**
TBS	**Tris-buffered saline**
TBS-T	**TBS with 0.1% tween20**
TM	**Transmembrane Domain**
TRPV1	**transient receptor potential channel V1**
usAHP	**Ultra-Slow Afterhyperpolarization**
Vmax	**Maximal Pump Rate**
VR	**Ventral Root**
WT	**Wild Type**

ABSTRACT

Animal behaviour relies on output from neuronal networks in the central nervous system (CNS). Evidence has demonstrated that a sub-population of sodium pumps play a dynamic role in modifying network output. Following a period of intense neuronal firing, some sodium pumps are recruited and mediate a minute-long hyperpolarization of the cell membrane known as the ultraslow afterhyperpolarization (usAHP). Previous research has proposed that the usAHP, which is found in only a subset of spinal neurons, is mediated by sodium pumps expressing a subtype of their catalytic α subunit found exclusively in neurons, termed α3. Though α3 is postulated to be heterogeneously expressed in the CNS, until now, there has been no research on the localisation of α3 to neurons in that region. Similarly, no previous research has investigated the distribution of FXYD1, a regulatory subunit in the sodium pump, which is broadly expressed in brain and muscle tissue.

Here, I present the first evidence for α3, FXYD1 and FXYD6 expression within neurons that comprise the rostrocaudal CNS of stage 42 *Xenopus* laevis larvae, as well as in other tissues, using immunohistochemical labelling techniques I have developed for this project. Furthermore, I outline the potential specific roles for these subunits both throughout locomotor development and their contribution to swimming function by the tadpole larval stage. This was done by developing movement deprivation experiments from embryonic to larval stages in *Xenopus* using tricaine methanesulfonate (MS-222) and then subsequent fluorescent co-labelling of α3 and FXYD1 with cross-comparison to previous immunolabelling results.

1. CHAPTER 1: GENERAL INTRODUCTION

Project Outline and Summary

Distinct motor behaviours in animals depend upon output from specific neural networks comprised of central pattern generator (CPG) neurons located in the brainstem and spinal cord (SC). It has long been considered necessary to develop optimal methods for identifying these neuronal subtypes to better bridge this gap between neuron output and behaviour (Roberts and Clarke, 1982; Roberts *et al.*, 1987; Picton, Sillar and Zhang, 2018). The intrinsic electrical properties of the spinal neuron types is dependent upon the different ion channels expressed in their cell membrane (Harris-Warrick and Marder, 1991). An accumulation of recent evidence has highlighted certain ion pumps, the Na+ /K+ -ATPase, or sodium pump, as influential regulators of neuronal activity and, consequently, network output (Zhang and Sillar, 2012; Picton et al., 2017; Hachoumi et al., 2022). Sodium pump function can vary depending upon the type of subunit expressed in their heterotrimeric structure, which is typically comprised of α, β, and FXYD proteins (Clausen, Hilbers and Poulsen, 2017). One sodium pump subtype has been implicated in halting network output by hyperpolarising the membrane potential of neurons for a prolonged time period lasting up to one minute (Zhang and Sillar, 2012). It is theorised that these pump types, termed “dynamic sodium pumps,” express a specific catalytic α subunit: α3. My project aims to identify where the α3 subunit is expressed in the central nervous system (CNS) and surrounding tissue of developing *Xenopus* frog tadpoles. Furthermore, since the auxiliary sodium pump subunits, FXYD1 and FXYD6 (Meyer et al., 2020), have been implicated in modulating the function of sodium pumps, my project also focused on identifying the distribution of these two proteins within the CNS in relation to each other and to α3.

In this thesis I present novel data on the tissue and cell-specific distribution of three sodium pump subunit isoforms: α3, FXYD1 and FXYD6. My first results chapter presents the expression patterns of α3 within *Xenopus* tissue while also investigating its comparative expression level over the course of development, as established by Nieuwkoop & Faber (Nieuwkoop and Faber, 1956). I also compare α3 expression levels between two genetic

mutations: wild-type (WT) and albinos to deduce whether the contributive function of α3 is potentially different between the two phenotypes. My second results chapter labels the expression of FXYD1 and FXYD6 subunits, mainly focusing on cells within the CNS and other tissue types such as skin and myotome of NF stage 42 *Xenopus* laevis larvae (Crambert and Geering, 2003; Zhang and Sillar, 2012). In my third results chapter, I present findings from a set of movement deprivation experiments I conducted where tadpoles were reared from embryonic to larval stages in the anaesthetic tricaine methanesulfonate (MS-222). I then compared the differences in swimming behaviour, tadpole anatomy and expression of α3 and FXYD1 in the CNS of tadpoles reared in MS-222 to control tadpoles. The lattermost research aim was to evaluate how these α3 and FXYD1 subunits, identified via immunolabelling, change when swimming function is pharmacologically blocked over the course of development. Finally, I will outline how my project findings contribute to current research into dynamic sodium pumps and offer avenues for further advancement on pump function research based upon the expression patterns of its constituent subunits (Zhang and Sillar, 2012; Picton et al., 2017; Hachoumi et al., 2022).

1.1 The Sodium Potassium Pump

The sodium pump is a ubiquitously expressed enzyme complex that is highly conserved across vertebrate and invertebrate animal species localized to the plasma membrane of all cell types (Kaplan, 2002; Blanco, 2005a; Clausen, Hilbers and Poulsen, 2017). This omnipresence demonstrates its essential role in establishing and maintaining Na+ and K+ gradients across the intracellular and extracellular domains, which is essential for the survival of eukaryotic cells. Different sodium pump types contribute to the specific function of cell types in essential organs (Suhail, 2010; Clausen, Hilbers and Poulsen, 2017).

In the CNS, there is a constant ionic imbalance in neurons where the K+ concentration is high intracellularly but low extracellularly, whilst Na+ concentration is high extracellularly but low intracellularly (Baccaglini and Spitzer, 1977). While the neuronal membrane is more permeable to K+ than Na+ at rest, which results in the passive influx and efflux of K+ ions, there is also efflux of K+ occurring via AMPARs and other leak channels (Wasser and Kavalali, 2009). Sodium pumps counter this passive loss of in K+, and maintain intracellular ion gradient, by using ATP to actively transport Na+ and K+ against their concentration gradients. Per exchange, 3 Na+ are exported and 2 K+ ions are imported (Post, Hegyvahy and Kume, 1972) (Figure 1.1A). In neurons, this continuous unequal exchange of positive ions enables sodium pumps to maintain a steady resting membrane potential (RMP) (Kaplan, 2002).

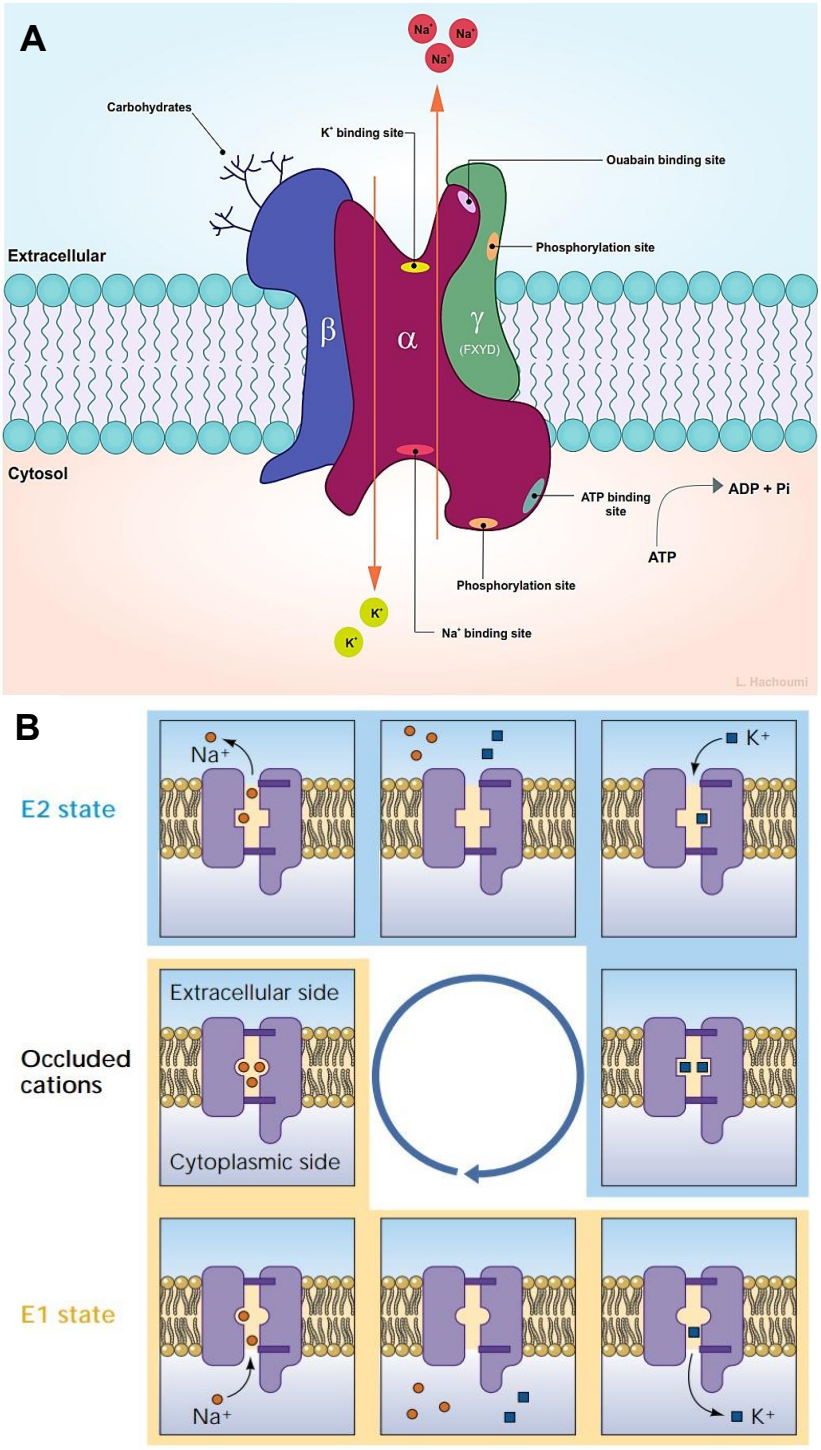

Figure 1.1: Sodium Pump Structure and Conformational States. A. Diagram of Na+/K+ pump detailing its heterotrimeric structure (comprised of α, β and FXYD subunits) and binding sites B. Simplified illustration demonstrating where the K+ (blue box) and Na+ (red circle) ion-binding sights are located within the transmembrane portion of the sodium pump. Access to each binding sight is available via the pump alternating between two states, E1 (bottom panels, illustrated in yellow) and E2 (top panels, illustrated in blue). Affinity for each cation is demonstrated by the round and square shapes of the binding sites (Panel A illustration courtesy of L. Hachoumi; Panel B adapted from review by (Horisberger, 2004).

However, different sodium pump isoforms display varying affinity to Na+ and K+ depending upon the subunits expressed within their structure. This means that kinetic activity within a cell varies depending upon the population of sodium pump isoforms expressed in different cell types. Different sodium pump subunit isoforms, which comprise each sodium pump complex, can therefore affect the firing properties of electrogenic cells due to this variation in the sodium pump architecture (Blanco and Mercer, 1998; Crambert et al., 2000; Suhail, 2010; Clausen, Hilbers and Poulsen, 2017; Murata et al., 2020).

1.2 Sodium Pump Isoforms

The sodium pump structure is heterotrimeric and comprised of two main subunits, a catalytic α subunit and a structural β subunit, plus an auxiliary tertiary FXYD subunit (Figure 1.1A). The broad expression and functional contribution of sodium pumps across various cell types is attributed to each sodium pump structure being comprised of different α, β and FXYD isoforms. The catalytic α subunit is a transmembrane (TM) domain comprised of 10 helices embedded in the cell membrane (M1–M10) with three cytosolic domains: the actuator (A) domain, the nucleotide-binding (N) domain, and the phosphorylation (P) domain (Cornelius and Mahmmoud, 2003; Morth et al., 2007). The A, N, and P domains power active cationic exchange through ATP phosphorylation which enables the unequal exchange of 2 K+ ions in for 3 Na+, all of which are transported against their concentration gradients.

This active exchange of K+ and Na+ involves alternating access to the cation binding sites, located in the TM domain within the catalytic α subunit. This requires shifting between two conformation states known as E1 and E2 (Albers, 1967; Post, Hegyvahy and Kume, 1972; Robinson and Pratap, 1993) (Figure 1.1 B). However, it should be noted that these two states are not the full range of conformational changes through which the sodium pump can shift but have proven to be a reliable outline for the physical ionic exchange that this pump mediates (Guo et al., 2022). When in the E1 state, the cation binding sites are open intracellularly allowing Na+ to bind to the α subunit and be briefly taken up into the pump. Following a shift into the E2 state, the Na+ is released into the extracellular space and the cation binding site changes affinity to accept K+ (Jorgensen, Håkansson and Karlish, 2003) (Figure 1.1 B). The kinetic dynamics of this change in conformational states is modulated significantly by the FXYD isoforms (Meyer et al., 2020) whereas ion affinity and ouabain sensitivity of the pump is believed to be conferred by each α isoform as that this subunit hosts their respective binding sites (Zahler et al., 1997) (Figure 1.1A).

Currently four α (α1-α4) (Kaplan, 2002), three β (β1-β3) (Antonicek, Persohn and Schachner, 1987), and seven FXYD (FXYD1-FXYD7) (Meyer et al., 2020) isoforms have

been identified, each of which contributes differentially to the sodium pump complex structure and functional properties (Forbush, Kaplan and Hoffman, 1978; Blanco and Mercer, 1998). Expression of most subtype isoforms has been found to be conserved across different species in a tissue-specific manner indicating that their function is also conserved by organ and cell type (Blanco and Mercer, 1998; Blanco, 2005b).

1.2.1 The Catalytic Subunit: α

Of the four α subunits α1 is the only isoform that is expressed ubiquitously across all cell types, including neurons (McGrail, Phillips and Sweadner, 1991; Sweadner et al., 1994; De Carvalho Aguiar et al., 2004). This broad expression is conserved in *Xenopus* with mRNA transcripts of ATP1A1, the gene that codes for α1, being found to be present in all tissue types (Session et al., 2016a). In the CNS, mRNA transcripts of the ATP1A2 and ATP1A3 genes, which code for α2 and α3 respectively, are present in the brain however they are differentially expressed across cell types with α2 being found in glial cells while α3 is restricted to neurons (Bøttger et al., 2011a; Session et al., 2016a; Sweadner et al., 2019). The final subunit, α4, is found in the testes and has been implicated in male fertility (Shamraj and Lingrel, 1994). Each of these catalytic subunit subtypes can work conjunctively to endow unique electrochemical properties onto the cell types in which they are expressed (Shamraj and Lingrel, 1994; Therien and Blostein, 2000; Bøttger *et al.*, 2011a).

The α1 subunit has a high Na+ affinity and so is tonically active at comparatively low intracellular Na+ concentrations present at the RMP (~10 mM) (Zahler *et al.*, 1997; Azarias *et al.*, 2013; Shrivastava, Triller and Melki, 2020). As such, α1 is primarily responsible for the constant ionic exchange that maintains the RMP. Contrastingly the other α subtypes, such as α3 are only active when there is a high concentration of intracellular Na+ due to possessing a comparatively lower intracellular Na+ affinity (Zahler et al., 1997; Zhang and Sillar, 2012; Zhang et al., 2015). The neurons believed to express α3-expressing, “dynamic sodium pumps” exhibit a unique phenomenon whereby intense neuronal firing leads to a hyperpolarized membrane potential that can last for a period of 1 minute, termed the an

ultra-slow afterhyperpolarisation (usAHP) (Zhang and Sillar, 2012). Expression of this function is conserved across vertebrate and invertebrate species such as *Xenopus* tadpoles (Zhang and Sillar, 2012), mice (Picton et al., 2017) and Drosophila (Pulver and Griffith, 2009). It has been reported that during the usAHP, the neuronal membrane potential is hyperpolarised by up to 10 mV (Zhang and Sillar, 2012). Therefore, the usAHP weakens neuronal excitability in the spinal networks of tadpoles (Zhang and Sillar, 2012) and mice (Picton *et al.*, 2017). This has been shown to consequently lead to a decrease in locomotor output in subsequent motor episodes (Zhang and Sillar, 2012; Hachoumi *et al.*, 2022).

Notably, the usAHP was not found to be present within all spinal cell populations (measured in ~42% of neurons) indicating that this function is not mediated by pumps expressing the α1 subunit isoform (Zhang and Sillar, 2012; Picton *et al.*, 2017). This has raised strong, albeit circumstantial, evidence that only one specific isoform, α3, underlies the usAHP. Therefore, α3 has been expected to also only be expressed by a subset of spinal neurons which became an investigative aim for my graduate studies (See Chapter 2.3.1). All four α catalytic subunit types are capable of being blocked via binding of various cardiac glycoside inhibitors to their extracellular ouabain binding site (Figure 1.1A). These glycoside inhibitors include digoxin, digitoxin and ouabain with the latter being a potent inhibitor for all four α isoforms (Laursen *et al.*, 2013, 2015). Notably, the α subunits are variably sensitive to ouabain with α3 possessing the highest affinity for ouabain due to its functional abolishment when incubated with sub-micromolar concentrations of ouabain (≤0.5 μM) (Dobretsov and Stimers, 2005). The usAHP is also abolished following exposure to these same low ouabain concentrations (Zhang and Sillar, 2012; Hachoumi *et al.*, 2022). It should be noted that these concentrations are too low for inhibiting tonic sodium pumps the α1 affinity for ouabain is much lower (3 μM) therefore the RMP can be conserved (Dobretsov and Stimers, 2005; Hachoumi *et al.*, 2022). This similarity in high ouabain affinity therefore implicates α3-expressing pump complexes as being the dynamic sodium pumps that underly the usAHP (Dobretsov and Stimers, 2005; Picton *et al.*, 2017; Picton, Sillar and Zhang, 2018).

1.2.2 The Structural Subunit: β

The β subunit is considered the “anchor” of the pump complex (Antonicek, Persohn and Schachner, 1987). Like the α subunit the β structure is transmembrane, spanning from the intracellular to the extracellular space. It is comprised of a small N domain, which is intracellular, a TM domain, and a large extracellular C domain (Antonicek, Persohn and Schachner, 1987; Noguchi, Mutoh and Kawamura, 1994; Clausen, Hilbers and Poulsen, 2017). The formation of a pump complex relies upon glycosylation of the extracellular domain resulting in carbohydrates being attached to the glycoside binding sites (Noguchi, Mutoh and Kawamura, 1994) (Figure 1.1 A). The number of glycoside binding sites differ between β1 (3 sites), β2 (8 sites) and β3 (2 sites) isoforms indicating that the stability of the pump also varies across sodium complexes and likely allowing for a higher assembly of complexes formed with β1 and β3 (Tokhtaeva *et al.*, 2010, 2012).

Each of the 3 β isoforms are expressed differentially across tissue types: β1 is found primarily in epithelial cells and is more broadly expressed within the body making it the preferred binding partner for α1 (Tokhtaeva *et al.*, 2012; Murata *et al.*, 2020). The latter two β isoforms are more tissue specific with β2 being expressed, to varying degrees, in neurons and glia within the brain (Antonicek, Persohn and Schachner, 1987; Murata *et al.*, 2020) and in smooth muscle (Floyd *et al.*, 2010). β3 is mainly expressed in the lung, testis, skeletal muscle, and liver of humans and mice (Clausen, Hilbers and Poulsen, 2017). In *Xenopus*, the mRNA transcripts (Zhao *et al.*, 2021) of the ATP1B1, ATP1B2, and ATP1B3 genes that code for the 3 β isoforms have been variably detected in the brain, eye and skin of tadpoles indicating that pump complexes subtypes are likely very diverse within these tissue types which could affect ion affinity (Session et al., 2016a). Though the role of β in pump function is considered primarily structural there have been findings that hint at the 3 β isoforms contributing to regulating enzymatic activity (Tokhtaeva *et al.*, 2012) mainly by impacting ion binding. For example β2 has been implicated in the occlusion of the K+ binding site and in modulating α affinity to K+ and Na+ (Larsen *et al.*, 2014). Furthermore, changes to β1

expression have been reported to differentially influence contractibility in heart muscle of rats (Barwe *et al.*, 2009) however there remains some debate as to whether this effect isn't mainly due to the α1 or α2 isoforms it is bound to in the pump complex (James *et al.*, 1999). Therefore, the direct contributions of the β isoforms to sodium pump kinetics are still largely unconfirmed.

1.2.3 The Auxiliary Subunit: FXYD

When compared to the structural support provided by the β subunit and the active changes conferred by the catalytic α subunit on the sodium pump, the auxiliary FXYD subunit has often been overlooked. Only recently has this subunit received more critical evaluation in how it, and its many isoforms, potentially directly modulate sodium pump activity (Meyer *et al.*, 2020). Previously, FXYDs were perceived as contributing very little to sodium pump function due to their comparatively smaller size and that they frequently assemble to the heterotrimeric complex post membrane insertion of the α/β complex (Zouzoulas *et al.*, 2003). Structurally, FXYDs are composed of cytoplasmic, TM and extracellular domains with their structure and conformation varying by subtype (Crambert *et al.*, 2000) (See Chapter 1.2.3 and Chapter 3.1.1 for further detail).

FXYD isoforms are also expressed in a tissue-specific manner with FXYD1 (initially termed phospholemman) (Feschenko *et al.*, 2003; Banine *et al.*, 2011), FXYD6 (initially termed phosphohippolin) (Saito *et al.*, 2001) and FXYD7 (Béguin *et al.*, 2002) being the only FXYD subtypes found in the CNS, an expression pattern that is conserved in humans (Floyd *et al.*, 2010; Mishra *et al.*, 2011), rats (Reis *et al.*, 2005) and in *Xenopus* (Béguin et al., 1997; Crambert et al., 2004; Session et al., 2016a; Meyer et al., 2020). The heterogeneous distribution of these FXYD isoforms indicates that they may make more specialized contributions to sodium pump activity than their initially perceived role as an auxiliary subunit might suggest (Schneider and Kraig, 1990; Mercer *et al.*, 1993; Blanco, 2005b; Meyer *et al.*, 2020).

Out of all the FXYD isoforms, FXYD1 and FXYD6 are the most structurally similar sharing ~48.1% homology in rats (Kadowaki *et al.*, 2004). FXYD6 was initially termed "phospholemman-like protein" prior to being officially classified due to this high homology (Yamaguchi *et al.*, 2001). This strongly indicates that these two isoforms likely share a functional overlap as well, based off previous comparisons between other FXYD isoforms (Geering, 2006a). Functional overlap has already been detected in recent work which demonstrated that FXYD1 and FXYD6 induce small but notable changes to established α1β1 pump function in *Xenopus* oocytes by reducing the ion exchange rate of the sodium pump, subsequently reducing the total charge carried by the pump (Meyer *et al.*, 2020). The α1-expressing tonic sodium pumps are ubiquitously expressed, and constitutively active, across a broad range of cell and tissue types. Each FXYD isomer is thought to confer unique kinetic properties upon the sodium pump complex to which they are bound. This functional diversity likely enables each pump to contribute to the distinct kinetic properties required for the broad range of cell and tissue types in which the NKA pump is expressed (Cornelius and Mahmmoud, 2003; Chang, Lowery and Sive, 2012; Meyer *et al.*, 2020). Investigations have shown that FXYDs can alter tonic sodium pump transport efficacy and rate of function by actively manipulating the Na+ ion de-occlusion rate in the E2 conformation, likely by actively affecting pump transition between phosphorylated and dephosphorylated states via the phosphorylation site located on the subunit (Meyer *et al.*, 2020) (Figure 1.1A). FXYD1 in particular has been noted to decrease pump affinity for intracellular Na+ in the α1/β complex (Crambert and Geering, 2003; Meyer *et al.*, 2020). FXYD1 has also been shown to be involved in the trafficking sodium pumps to and from the intracellular space to the cellular membrane and thus determining the overall transmembrane sodium pump concentration, particularly in response to changes in locomotor output brought about by exercise (Rasmussen, Kristensen and Juel, 2008; Christiansen *et al.*, 2017; Meyer *et al.*, 2020). In conjunction with this, aging has been noted to impact pump function through altering FXYD1 availability in the intracellular matrix (Reis *et al.*, 2005). All these findings indicate that FXYD1 and FXYD6 could conceivably overlap in how they both influence locomotor output

due to the conserved structure of these two isomers (Kadowaki *et al.*, 2004; Meyer *et al.*, 2020). It is therefore worthwhile to compare whether FXYD1 and FXYD6 overlap in where they are both expressed within the tadpole CNS.

α3 has also been implicated with affecting motor development as mutations to the ATP1A3 gene that codes for the catalytic subtype often result in disorders characterized by motor dysfunction (Heinzen *et al.*, 2014). This featured pathology is highly conserved across species including in humans (Oblak *et al.*, 2014) zebrafish (Doğanli *et al.*, 2013) and mice (Allocco *et al.*, 2019) as well as potentially in *Xenopus*. It is important to mention that until this project, this latter model organism had yet to be investigated for any potential differences in motor output in response to a change in α3 expression. This functional overlap between these subunits further supports investigation into expression patterns, and potential environmental changes to expression, of these isoforms in a well-established vertebrate CNS, such as *Xenopus*.

1.3 The *Xenopus* laevis Model Organism

Xenopus laevis, also known as the African clawed frog, has been extensively utilised as a model organism in several scientific fields, including developmental biology and neuroscience, due to its well-established anatomy (Nieuwkoop and Faber, 1956; Bernhardt *et al.*, 1990) and relatively simple CNS (van Mier, Armstrong and Roberts, 1989a). This project relies upon investigating both the tissue-specific expression of α3, FXYD1 and FXYD6 within the tadpole CNS and surrounding tissue. Furthermore, this project will also limit motor function during early development in order to establish whether there are any subsequent changes to isoform expression. Though experiments in this field have mainly utilized tissue derived from *Xenopus* oocytes to investigate sodium subunit expression and formation of its pump complex (Béguin *et al.*, 1997; Crambert *et al.*, 2000, 2004; Larsen *et al.*, 2014; Meyer *et al.*, 2020), the high conservation of sodium pump function combined with the extensive background research on its CNS make *Xenopus* an ideal model organism for this project (Combes, Sillar and Simmers, 2020a).

1.3.1 Tadpole Development: Relevant Anatomy and Swimming Behaviour

During *Xenopus* mating, a female frog releases hundreds of eggs that are then fertilised externally by sperm released from a male frog. During the first 7 hours post-fertilisation (pf), eggs undergo rapid cleavage divisions that leads to the generation of thousands of cells and thus forming the blastula by NF stage 9. Gastrulation commences about NF stage 10 (~10 hrs pf) and this is followed by neurulation which characterises the embryogenesis between NF stages 13-21 (15-22 hrs pf) (Figure 1.2Ai). The embryo then undergoes organogenesis, which leads to the formation and differentiation of tissues and organs. Later *Xenopus* developmental stages are not only characterised by anatomical changes but also by changes in behavioural repertoire (Nieuwkoop & Faber, 1956).

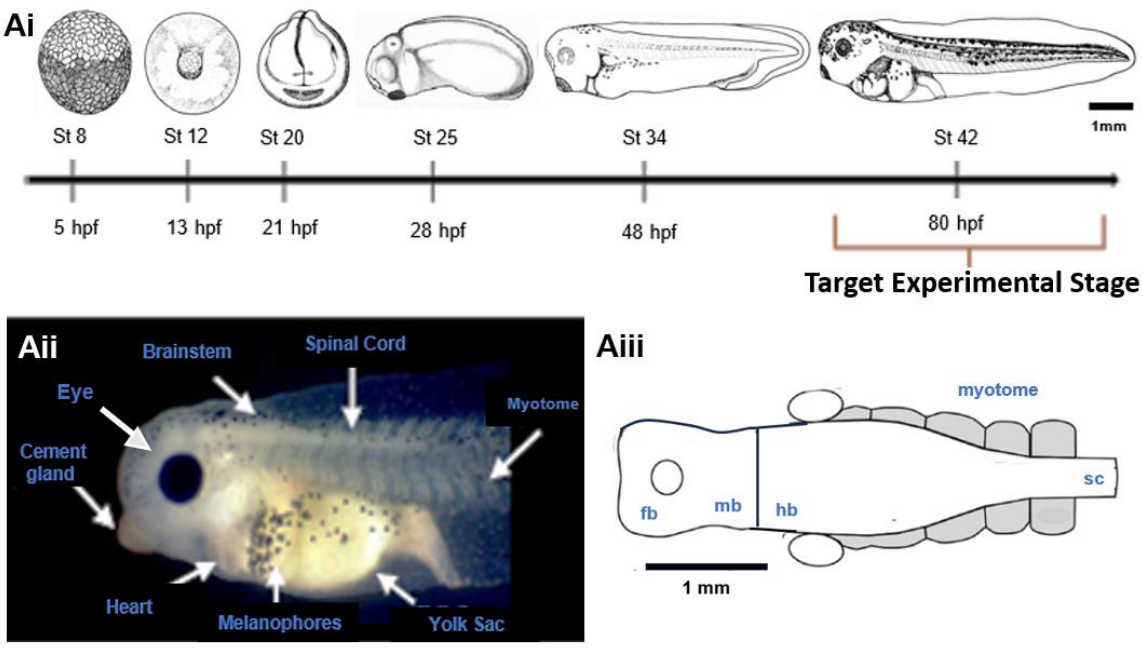

Figure 1.2: *Xenopus* laevis NF Developmental Stages and Relevant Tadpole Anatomy. A. Schematic illustrating WT *Xenopus* tadpole development from fertilized stage 8 blastocyte to target larval stage 42 as described by Nieuwkoop and Faber (1965) from rearing experiments conducted at 23°C (Ai). Photograph of a stage 42 tadpole highlighting key anatomical features (Aii). Rostrocaudal distribution of relevant CNS regions (labelled in blue): forebrain (fb), midbrain (mb), hindbrain (hb) and spinal cord (sc) as well as the myotomes including the clefts which are the boundary between each myotomal segment (grey) (Aiii).

At NF stage 20 (~21 hrs pf, reared at 23°C), *Xenopus* have reached the embryonic stage and neurolation is nearly complete, as testament to the nearly closed neural suture which will begin to develop the anatomical structures which comprise the rostral CNS (Figure 1.2Ai). By NF stage 32-35/36 (~30 hrs to 50 hrs pf, reared at 23°C) the rostral CNS has formed the forebrain, midbrain and hindbrain structures (Figure 1.2Aiii). The SC has also begun forming with rostral SC developing in advance of caudal locations in conjunction with a consistently lengthening tail (Roberts et al., 1987; van Mier, Armstrong and Roberts, 1989a). At this stage animals are largely sessile and do not demonstrate complex swimming behaviour beyond tail-twitching (van Mier, Armstrong and Roberts, 1989a). When induced, swim episodes are comparatively short and mainly serve as a reaction to changes in light or a mechanosensory stimulus applied to the tadpole skin (Figure 1.2Aii) (Nieuwkoop and Faber, 1956; Clarke et al., 1984; van Mier, Armstrong and Roberts, 1989a). This is because

early swimming in tadpoles is largely reactive as this behaviour functionally evolves as a method for evading predation (Roberts, Li and Soffe, 2010). An important reason why tadpoles can remain sessile at earlier developmental stages is because they are pre-feeding and syphon energy from their yolk sac prior to developing a mouth (Figure 1.2Aii) (Nieuwkoop and Faber, 1956).

Towards NF stage 37/38 (~53 hrs pf, reared at 23ºC), the tadpole tail has lengthened further (tadpole length is ~5mm) with the CPG extending along the caudal SC (Figure 1.2Aiii) and the rostrocaudally distributed myotomes (Figure 1.2Aii) become larger and are innervated by spinal motor neurons (Sillar, Wedderburn and Simmers, 1991). Swim behaviour begins to occur more frequently with movement ranging from simple flexion behaviour to more sophisticated manoeuvres such as turning (Boothby and Roberts, 1992). While earlier stage tadpoles remain sessile as a way of avoiding predation, tadpoles at this stage are faster and even demonstrate escape behaviours such as struggling when clasped by forceps (Kahn and Roberts, 1982; Boothby and Roberts, 1995).

The range of stimuli capable of inducing swimming in tadpoles can be quite broad and dependent upon the anatomical or sensory region where the stimulus is applied. Mechanical touch (Li, Wagner and Porter, 2014), light (Li, Wagner and Porter, 2014; Bertolesi *et al.*, 2021), water current (Roberts *et al.*, 2009a) and temperature changes are all capable of initiating various sensory pathways that activate the CNS-located neuronal networks underlying locomotor output (Clarke *et al.*, 1984; Roberts, Li and Soffe, 2010). These stimuli are registered by different sensory organs with the pineal gland inducing movement in tadpoles in response to light. Skin cells in particular impose different specific sensory pathways which are activated depending upon where the mechanical stimuli are registered. In this organ there are specific receptors located in the electrically excitable cell types comprising the skin (Figure 1.2Aii) such as mechanoreceptors which respond to touch, nociceptors which activate in response to pain and lateral line neuromasts which detect

water current direction and influence swim direction (Clarke *et al.*, 1984; Roberts *et al.*, 2009a).

By NF developmental stage 42 (~80 hrs pf, reared at 23^{o}C) (Figure 1.2Ai-Aii), the main stage used this project, tadpoles have lengthened further (~7mm) and have developed their swimming behaviour has become more flexible. Tadpoles at this stage are capable of varying their velocity and initiating more complex manoeuvres such as changing directions mid-swim episode (Sillar, Wedderburn and Simmers, 1991). This ensures that tadpole can manoeuvre away from predators or environmental barrier which will increase the possibility of survival. Tadpoles are also more predisposed to initiating spontaneous swimming or escape behaviour in response to sensory stimulus (van Mier, Armstrong and Roberts, 1989a; Zhang, Issberner and Sillar, 2011). However, this behavioural response can be limiting as constant and frequent movement in water can also serve to attract predators (Li, Wagner and Porter, 2014). The complexity of the swim network at this stage combined with the well-established research describing their anatomy, swim behaviour and spinal neuron output therefore facilitate constructive research into sodium pump subunit expression featured in this project.

1.3.2 Behavioural and Developmental Conservations Across *Xenopus* Phenotypes

The same developmental rate, and behavioural milestones, described in the above section remain conserved in the *Xenopus* albino phenotype. Albino tadpoles are characterised by expressing periodic albinism through a recessive mutation on their hps4 gene and have been widely utilised in *Xenopus* research over the past half century (Hoperskaya, 1975). They have long been viewed as an effective stand-in for WT tadpoles in various fields of research (Hewapathirane and Haas, 2009). This is because unlike WT tadpoles, albinos lack pigmented skin cells. This trait can enable unrestricted visualisation of their anatomy and previous studies have used them to visualise skeletal structure development and cerebrospinal fluid flow through their ventricles (Hewapathirane and Haas, 2009; Mogi *et al.*, 2012; Shan *et al.*, 2023). However there has remained some debate as to whether they

reflect WT tadpole physiology accurately, beyond sharing similarities in their anatomical structure (Hewapathirane and Haas, 2009; Fukuzawa, 2021; Shan *et al.*, 2023).

In terms of development, albino tadpoles age at the same temperature-dependent rate as their WT counterparts including through metamorphosis and evolvultion into adult frogs (Shan *et al.*, 2023). Their albinism does raise the possibility that their sensory pathways likely respond differently to light-based stimulus (Hoperskaya, 1975; Adebogun *et al.*, 2023). Both WT and albino tadpoles primarily register changes in light-based stimuli via their pineal eye (Roberts and Clarke, 1982) however they also register light through other means such as through melanophores, which are light sensitive and will alter their shape from punctate (aggregated) to stellate (dispersed) in response to light (Figure 1.2Aii) (Binkley *et al.*, 1988). The primary inference is that melanophores are meant to provide camouflage (Bertolesi *et al.*, 2021; Liedtke *et al.*, 2023) though previous research has also implicated these sensory cells in impacting tadpole phototaxis by affecting skin sensitivity to certain light wavelengths by occluding activation of the pineal gland and deep brain photoreceptors as well (Becker and Cone, 1966).

Like their WT counterparts, albino tadpoles express pigmented melanophore cells though they tend to produce a smaller population, and the colour of these cells tends to lighten later in development as the tadpole approaches metamorphosis (Hoperskaya, 1975; Shan *et al.*, 2023). The only direct behavioural difference between the two phenotypes appears to be a measured preference for darker environments in albinos compared to WT tadpoles post stage 42 (Adebogun *et al.*, 2023). However, this preference for darker environments could be due to an increased reliance on eye-based vision in pre-metamorphic stages resulting in albino tadpoles shunning light while WT adapt their swimming behaviour around this stimulus (Butler *et al.*, 2022). Outside of this observation, there are minimal noted differences in swimming behaviour output in response to sensory stimuli, including light, between the two phenotypes (Fukuzawa, 2021). It would be worthwhile to investigate whether this behavioural similarity extends to sodium pump expression by tracking and

comparing α3 within their respective SC to assess whether patterning differs between WT and albino tadpoles.

1.4 The Xenopus Swimming CPG: Bridging the Gap Between Cellular Function and Behaviour

While it is now understandable that swimming can be initiated in tadpoles via various external stimuli acting upon sensory receptors (Figure 1.3A), the mechanism by which this signalling translates into movement remains to be addressed. Movement in tadpoles is initiated via signalling within the caudal hindbrain and rostral SC where the central pattern generator (CPG) resides (Kahn and Roberts, 1982; Clarke *et al.*, 1984; Sillar, Wedderburn and Simmers, 1991). The CPG refers to the spinal cord network that produces locomotor output from rhythmic firing of various neuronal subtypes. When embryos, tadpoles are considered to have ten spinal neuron subtypes (Sautois *et al.*, 2007), only four of which are sufficient to produce swimming (Roberts, Li and Soffe, 2010). These four are known as descending interneurons (dINs), motoneurons (MNs), commissural interneurons (cINs) and ascending interneurons (aINs) (Figure 1.3B) (Roberts, Li and Soffe, 2012). The swim circuits that are comprised of these neuronal subtypes can induce a flexible array of movement through signalling that is sustained and propagated both within the network and to adjacent caudal networks along the tadpole CNS (Li and Moult, 2012). The output from the half-centre circuits on the left and right sides that comprise the CPG translates directly into swimming behaviour in larval *Xenopus* and therefore is carefully organized within the tadpole SC: both in regard to which spinal neuron types are present within each circuit as well as the spatial and anatomical alignment of these neuron populations within the tadpole CNS. This circuit output can be modulated both by membrane bound dynamic sodium pumps measured within spinal neuron subtypes (expanded in Chapter 1: Heterogeneity of the usAHP Across Spinal Neurons) and by extracellular neurotransmitters that act upon them (expanded in Chapter 1: Neuromodulators That Influence the usAHP) which in turn influences the duration and intensity of swim episodes (Zhang and Sillar, 2012; Hachoumi *et al.*, 2022).

1.4.1 The Mechanics of Tadpole Swimming

Swimming behaviour in NF stage 42 tadpoles is characterised by repeated lateral undulations of the tail (typically at 10-30 Hz frequency at RT or ~18^{o}C) which induces forward propulsion of the tadpole body. This undulation is the result of a left-right alternation in flexion, in combination with a rostrocaudal-propagated temporal delay in myotomal muscle contractions along the length of the tadpole body (Stehouwer and Farel, 1985; van Mier, Armstrong and Roberts, 1989b). Rhythmic tail movement forces water backwards, in turn providing the forward thrust that enables tadpoles to manoeuvre within their aquatic environment (Stehouwer and Farel, 1985; Li, Roberts and Soffe, 2010; Roberts, Li and Soffe, 2010) (Figure 1.3A).

Myotome segments are innervated by MNs which are driven to fire by dINs. Rostral dINs are responsible for initiating the firing of ipsilaterally organized motor circuits which are distributed throughout the caudal CNS: mainly in the caudal hindbrain and SC regions (Roberts and Clarke, 1982; Roberts, Li and Soffe, 2010). Swimming episodes rely on the repeated, sensory-induced firing of excitatory postsynaptic potentials (EPSPs) fired from rostral dINs which co-release glutamate and acetylcholine to excite CPG neurons on the same side (Wilson and Wyman, 1965; Roberts and Clarke, 1982; W. C. Li, Soffe and Roberts, 2004; Li, Roberts and Soffe, 2010) (Figure 1.3B, Red-Green). Importantly, dINs are electrically coupled to other dINs, localized up to 100μm away, and dIN firing leads to an initial EPSP that can recruit caudal ipsilateral CPG neurons (Zhang et al., 2009). These dINs fire an initial long duration (~2 ms) action potential (AP) and, via ascending axons, provide glutamatergic excitatory feedback onto themselves with the signal being received by N-methyl-D-aspartate (NMDA) receptors located on neighbouring dINs (W.-C. Li, Soffe and Roberts, 2004; Roberts, Li and Soffe, 2010).

Following the first AP fired by the initiating dIN, there is subsequently activation of ipsilateral cINs (Figure 1.3B). Furthermore, contralateral dINs, opposite to the initially excited dIN (Figure 1.3B, Left versus Right), are inhibited by these cINs via glycinergic signalling (Dale,

1985) (Figure 1.3B, Blue). The networks on opposite sides of the tadpole will then remain inhibited while the cIN is active (see Figure 1.3B).

Once this inhibition ceases, the contralateral circuit will be recruited and, following initial firing of the contralateral dIN and recruitment of the ipsilateral cIN, this starting side will be inhibited in turn. Therefore, cINs relay signals between the two sides through reciprocal inhibition (Sillar and Li, 2020). Compared to cINs, the role of aINs is to inhibit CPG neurons through glycinergic signalling of their ascending and descending axons (Moult, Cottrell and Li, 2013). While aINs are also glycinergic (Figure 1.3B) they restrict their inhibition to their own ipsilateral circuit and sensory interneurons (Clarke and Roberts, 1984; Li, Soffe and Roberts, 2002; Sillar and Li, 2020). This inhibition accomplishes two main functions. First, it prevents multiple firing by ipsilateral CPG neurons to ensure that each swim cycle is kept suitably brief. This function is similar to Renshaw Cells in mammals which inhibit MNs and maintain flexor-extensor alternation behind pedal movement (Li *et al.*, 2004). Secondly, inhibition of sensory interneurons prevents most other sensory input from interrupting or dysregulating swimming following the initiation of a swim episode (Sillar and Roberts, 1988).

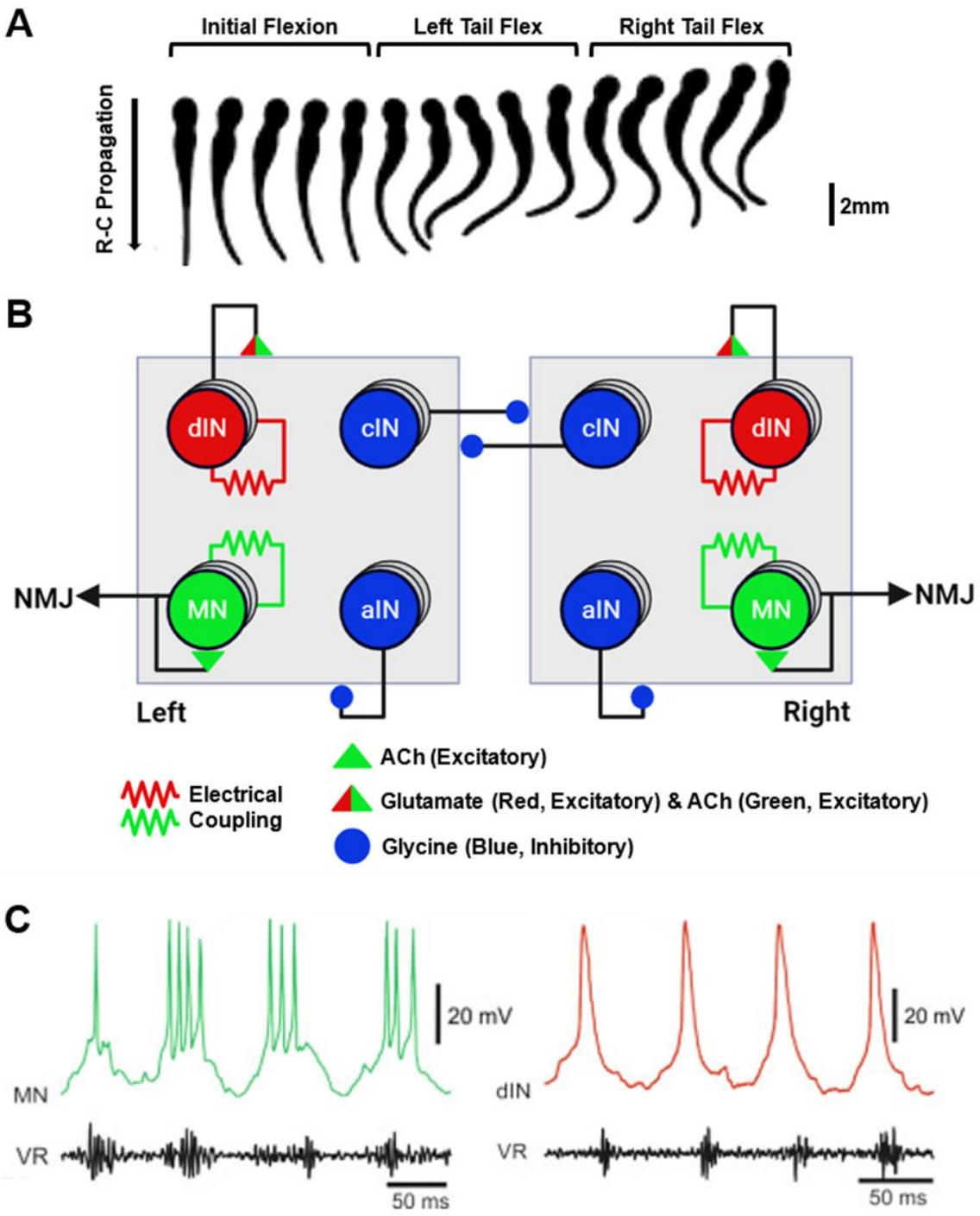

Figure 1.3: Tadpole Swimming Characterised by Left-Right Alteration of CPG Activity. A. Outline illustration of initial tadpole swim cycle (viewed from above and taken at 200 frames per second) (fps). Swimming begins with an initial flexion before transitioning into first swim cycle and follows the rostrocaudal propagation of this flexion (R-C, black arrow) along the tadpole tail. B. Diagram of spinal neurons within the tadpole CPG, organized into the half-centre model. Circuits repeat rostrocaudally along the tadpole SC and swimming rhythmicity is mediated through electrically coupled dINs (red) and MNs (green). C. Recordings of MN (green) and dIN (red) AP firing in NF stage 42 tadpoles during fictive swimming. Ventral root (VR) output was also recorded. (Zhang and Sillar, unpublished data, presented in Sillar and Li, 2020).(Panel A adapted from figure presented in Roberts, Li and Soffe, 2010; Panels B and C based on, and adapted from, figures presented in Sillar and Li, 2020).

MNs within the SC stimulate contraction of myotomal muscle segments by excitatory cholinergic transmission at neuromuscular junctions (NMJs) located along the intermyotomal clefts (Figure 1.3C). This induces muscle contraction ipsilaterally, which in turn lengthens the opposite side of the tadpole (Li and Moult, 2012; Moult, Cottrell and Li, 2013). Like dINs, stage 37/38 MNs are initially electrically coupled in order to synchronise their firing activity (Li, Roberts and Soffe, 2009; Zhang *et al.*, 2009b). Unlike dINs, which fire once per swim cycle, MNs demonstrate a reduction in electrical coupling at stage 42 leading to development of a burst firing pattern where during a swim cycle will fire multiple APs over a slightly longer time period (~50ms) (Zhang et al., 2009a) (Figure 1.3C). MN recruitment also becomes variable as within the same motor pool MNs will possess a range of different firing thresholds, with MNs that have higher firing thresholds requiring greater stimulation over a longer period of time in order to be recruited for swimming (Zhang, Issberner and Sillar, 2011).

1.4.2 The Spatial Orientation of the Tadpole CNS

The tadpole CNS is comprised of the forebrain, the rostral brainstem that contains the midbrain and hindbrain as well as a more caudal SC that extends along the tadpole trunk and tail (Figure 1.2Aiii). The CNS develops rapidly, forming within the 24 hours after the closure of the neural tube during embryogenesis (Nieuwkoop and Faber, 1956). In the hindbrain (Figure 1.4Ai) the axons extending from somata bordering the ventral hindbrain, a spatial region comprised of varying interneuron subtypes, form a “lateral tract” (LT) through which neuronal projections expand to receive “en-passant” synapses (Roberts and Clarke, 1982; Roberts, Li and Soffe, 2012). This tract allows for “top-down” signalling to pass from sensory organs in more rostral anatomical regions such as the light-sensitive pineal eye, cement gland and neuromasts that comprise the lateral line (Roberts *et al.*, 1987, 2009b; Li, Wagner and Porter, 2014). Within the SC (Figure 1.4 Aii-Aiv), the CPG neuron subtypes and supporting glial cells are organized along a dorsoventral spatial midline with most MNs located ventrally within the SC while interneurons are located more dorsally (Figure 1.4B).

Directly along the dorsal midline, and forming a rostrocaudal column of cell bodies, are the Rohon-Beard (RB) sensory neurons, named for the two researchers who identified them in the late 19th century (Rohon, 1885; Beard, 1890). RB neurons can be anatomically identified by their relatively large soma (~20μm diameter) and dorsal orientation within the tadpole SC (Figure 1.4B).

There is a population of midline neurons which border the central canal (CC) through which cerebrospinal fluid (CSF) flows caudally in tadpoles (Date *et al.*, 2019). Initially these neurons were simply termed ciliated ependymal (CE) cells (Roberts and Clarke, 1982) however are now more commonly termed Kolmer–Agduhr (KA) cells (Dale *et al.*, 1987) (Figure 1.4B, CE and KA). As the name suggests, these cells maintain contact with the CSF through their projecting cilia. While their primary function is debatable, KA are thought to provide mechanosensory input to neighbouring neurons and sensory cells by detecting both the flow of CSF and perhaps contribute to maintaining the ionic gradient as this pathway can be used to transport Na+ to caudal SC regions (Dale *et al.*, 1987; Speake *et al.*, 2001; Yang, Wang and Strähle, 2020).

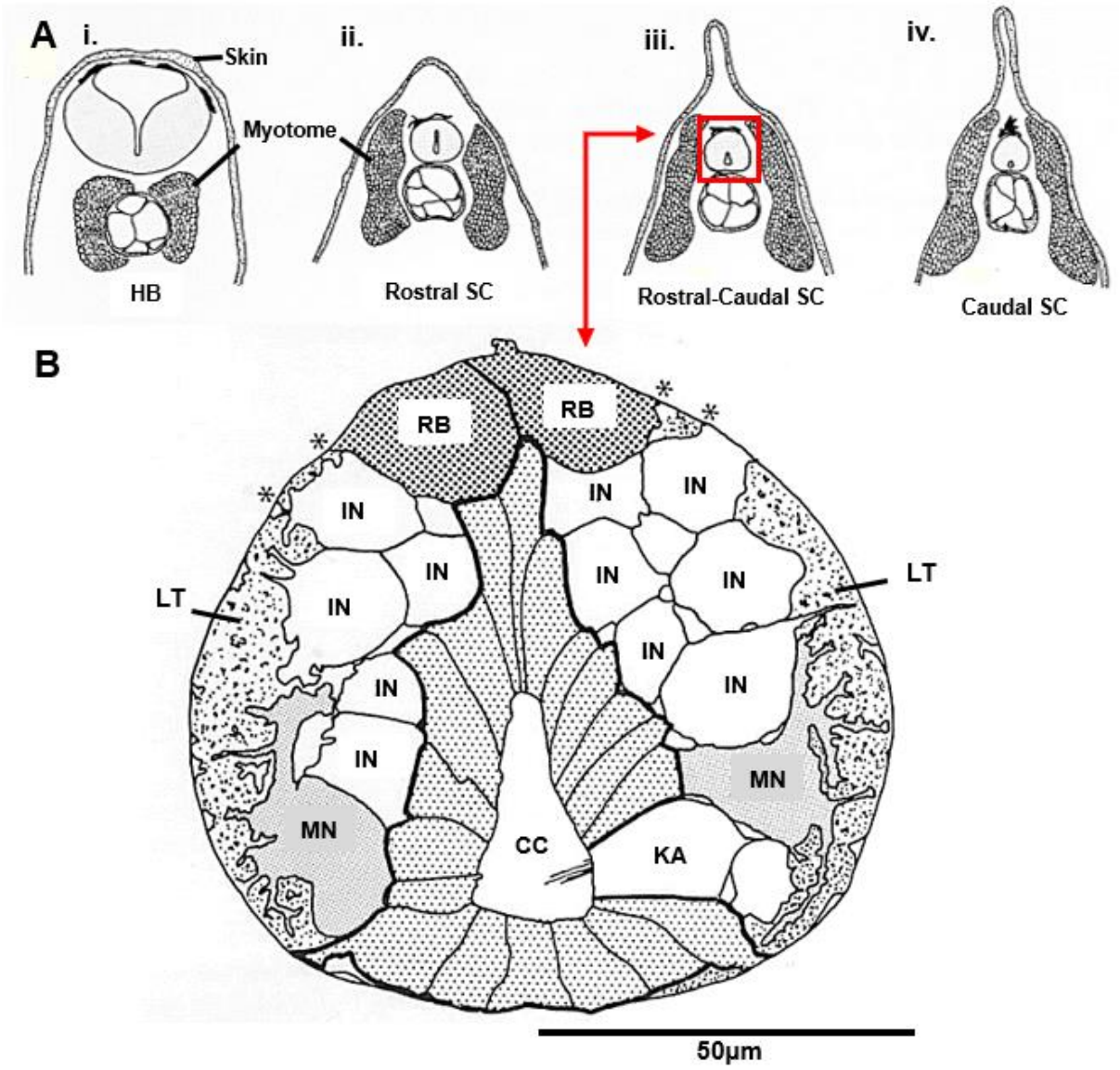

Figure 1.4: Anatomical and Spatial Locality of Specific Neuronal Subtypes Within *Xenopus* SC. A. Labelled anatomical drawing illustrating tadpole, oriented dorsal side, CNS cross-sections taken at the level of the myotome with structures ranging from the hindbrain (Ai) and the rostral to caudal spinal cord (Aii-Aiv). Each section is spaced approximately 1mm caudal from the preceding transverse section. B. Anatomical drawing of a rostral spinal cord structure (as drawn at lower magnification in panel Aiii; Red Box and Arrow) illustrated above as a cross-section taken from rostrocaudal section. The cell types and structures comprising the spinal cord are labelled and/or outlined with enclosed linings of varying thickness. Patterning was also utilized to differentiate cell types including unspecified interneurons (IN), Rohon-Beard sensory neurons (RB), motoneurons (MNs) including outlined projections from soma into the lateral tract (LT; Dorsal tract indicated by asterisks '*'). The central canal (CC) is bordered by ciliated ependymal cells (CE) termed Kolmer–Agduhr (KA) cells. Other ependymal cells were not all labelled but instead enclosed by a heavy black outline and filled with stippled patterning and cilia were represented by black lines directed into CC (Figure adapted from Roberts & Clarke, 1982).

The SC anatomy, neuron populations and CPG output in *Xenopus* vary rostrocaudally along the tadpole SC (Roberts and Clarke, 1982; Clarke and Roberts, 1984; Bernhardt et al., 1990; Zhang et al., 2009a). This is in part due to the caudal tadpole regions being comparatively younger compared to rostral CNS sections. Between NF stage 37/38 and 42, there are physical changes in MN structure (Zhang et al., 2009a; Zhang, Issberner and Sillar, 2011) characterized by the extension and retraction of their peripheral projections in order to restrict myotome innervation by motor pools to predominantly dorsal, medial or ventral regions (Zhang, Issberner and Sillar, 2011). During this developmental period, there is also a maturation of MN firing properties from firing a single AP per swim cycle to AP bursts. Given the developmental difference between rostral versus caudal SC regions, MN bursts first occur in rostral SC regions (Figure 1.4 Aii-iii) at stage 40 before progressing to caudal segments by stage 42 (van Mier, Armstrong and Roberts, 1989a; Sillar, Wedderburn and Simmers, 1991; Zhang, Issberner and Sillar, 2011). This delay is in conjunction with anatomical development as over this period the tadpole tail is continuing to lengthen and form new CPG circuits within that emerging caudal SC region (van Mier, Armstrong and Roberts, 1989a; Combes et al., 2004; Combes, Sillar and Simmers, 2020a) (Figure 1.4 Aiv). Therefore, the MNs in caudal SC regions will be the final region to switch from firing a single AP per swim cycle to bursts (van Mier, Armstrong and Roberts, 1989a; Zhang et al., 2009).

1.4.3 Heterogeneous Expression of the usAHP in Spinal Neurons

In the tadpole locomotor system, the appearance of the usAHP is not ubiquitously present in all CPG neurons, instead having been identified in only 40% of rhythmically active spinal neurons (Picton *et al.*, 2017) (Figure 1.5A). The presence of the usAHP also varies across interneuron populations and is theorized to only be present in 28.6% of all interneurons. It was therefore assumed that α3, which has been proposed to underlie the usAHP, will also be heterogeneously expressed (Picton *et al.*, 2017; Picton, Sillar and Zhang, 2018).

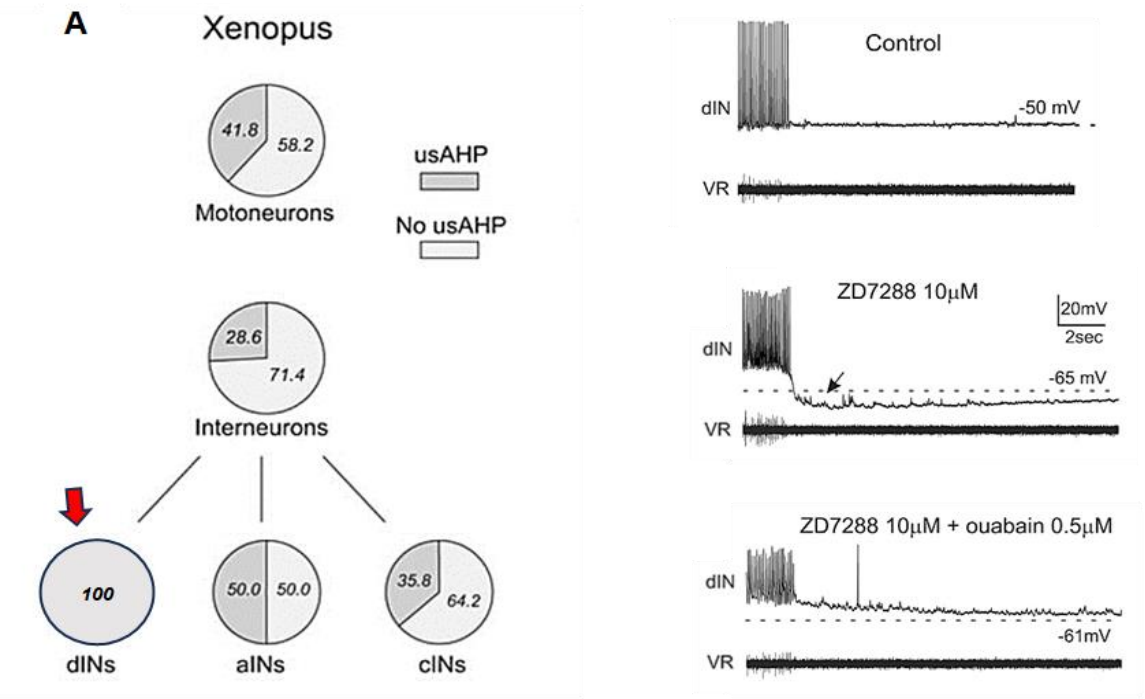

Figure 1.5: Expression of usAHP Is Masked by Ih in dINs. A. The usAHP has been recorded only in a subset (~40%) of spinal neurons with average usAHP occurrence also varying per cell type (expressed as %). The usAHP has been found to be expressed in all dINs (red arrow). B. Recording of dINs under control conditions demonstrate absence of a usAHP (Bi). The usAHP (black arrow) is revealed once the Ih was blocked by ZD7288 (Bii). The usAHP was no longer expressed once dynamic sodium pumps were blocked with a sub-micromolar concentration of ouabain (0.5 μm) (Biii). (Panel A adapted from Picton, Zhang & Sillar, 2017) (Panels B and C adapted from (Picton, Sillar and Zhang, 2018).

Initially, dINs were not thought to express a usAHP and while firing duration would shorten in subsequent episodes (Figure 1.5Bi) no break in firing would occur. However, this was found to be due to a specific modulatory current, hyperpolarization activated cation current (Ih; Biel et al., 2009;) that pacemaker neurons such as dINs possess in order to maintain the rhythmicity of their firing (Biel *et al.*, 2009; Zhang *et al.*, 2015; Picton, Sillar and Zhang, 2018). In dINs this stabilized membrane potential is maintained by an inward Ih current which counterbalance an efflux of positive Na^+ ions engaged by the recruitment of dynamic pumps. After bath application of ZD7288 (10 μM) to block cyclic nucleotide-gated (HCN) channels that underlie Ih, the usAHP was unmasked in all measured (8/8) dINs (Figure 1.5Bii). Furthermore, once ZD7288 was washed out, the usAHP was once more masked in a majority of these dINs (6/8) (Picton, Sillar and Zhang, 2018) (Figure 1.5Biii).

The differential expression of the usAHP in CPG neuron populations could be linked to the broader impact the usAHP has on motor circuit output. During tadpole swimming, the duration of subsequent episodes has been shown to be directly affected by the interval between swimming when the tadpole can recover known as the inter-swim interval (ISI) (Zhang and Sillar, 2012). When this interval period is reduced, the swimming duration also decreases accordingly (Figure 1.6 Ai).

The usAHP has been implicated in this process due to its ability to decrease network excitability by hyperpolarizing (up to 10 mV) the membrane potential of usAHP-expressing neurons within motor circuits (Zhang and Sillar, 2012; Zhang *et al.*, 2015). Through this function, the usAHP confers a short-term motor memory (STMM) mechanism on motor circuits by targeting low-threshold neurons known to fire reliably during swimming (Zhang and Sillar, 2012), which is why it is present in a sub-population of MNs. Furthermore, the usAHP has been shown to be directly involved in affecting ISI-dependent swim durations. When ouabain is applied to the tadpole CNS at a sub-micromolar concentration (0.5 μm which is proven to inhibit dynamic sodium pumps) (Zahler *et al.*, 1997; Hachoumi *et al.*, 2022), this results in subsequent swim episodes that are comparatively prolonged even after ISI durations of less than 5 seconds, demonstrating that the STMM is impaired by inhibition of the usAHP (Figure 1.6 Aii).

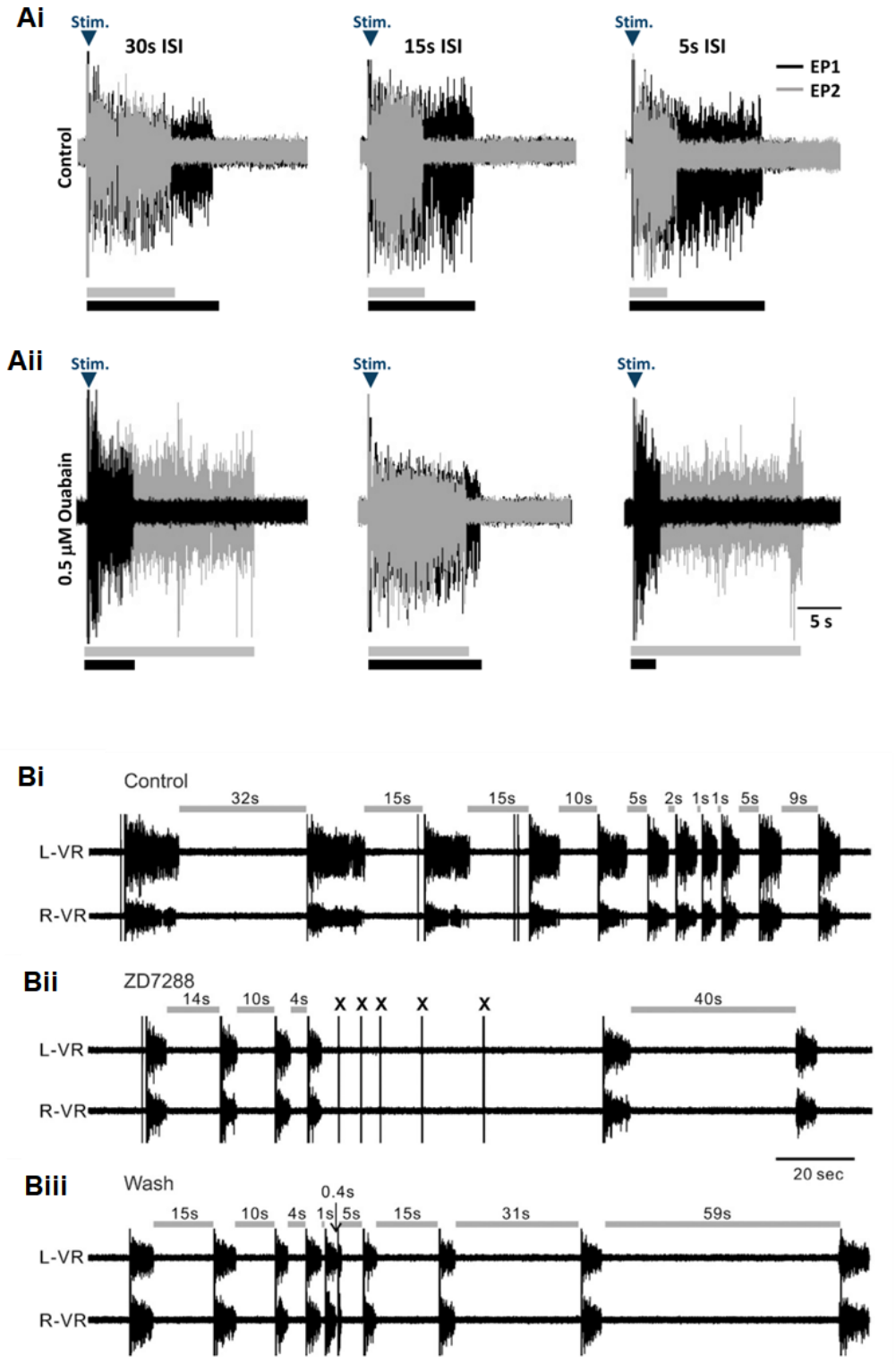

Figure 1.6: The usAHP Confers a STMM On Motor Circuits. A. VR traces of paired swim episodes with the second episode (grey trace, EP2) overlaid on the first (black trace, EP1) following ISI of 30s, 15s and 5s (Ai). Application of ouabain (0.5 µM) resulted in longer second episodes (Aii). B. VR traces showing episode duration decreasing but not ceasing after very short ISIs (2s) (Bi). Application of ZD7288 unmasked the usAHP in dINs which abolished swimming after a slightly longer ISI (4s) (Bii). Washing out ZD7288 reversed this effect. (Panel A adapted from Zhang et al., 2011; Panel B adapted from Picton et al., 2018).

The usAHP is thought to be masked in rhythm-generating neurons, dINs, to preserve their capability to induce swimming. When swimming episodes are continuously evoked across shorter and shorter ISIs there is a clear reduction in episode length, but subsequent episodes can still be reliably produced even after a very short ISI (2 s) (Figure 1.6 Bi). This is because dINs are still able to recruit high-threshold neurons uninhibited by the usAHP and activate motor circuits to initiate swimming (Zhang and Sillar, 2012; Picton, Sillar and Zhang, 2018). However, when the Ih current is blocked by ZD7288, and the usAHP is no longer counterbalanced by its positive ionic intake, these episodes are abolished after an ISI of less than 5 seconds (Figure 1.6 Bii). Unmasking the usAHP in dINs halts activation of the motor circuit by inhibiting dIN from firing their single prolonged AP which means it cannot excite itself or nearby cINs and electrically coupled dINs.

While the Ih current is not present in any other CPG neuron- other than dINs -at stage 42, other mechanisms could affect the expression of the usAHP and therefore could mask its presence in these other neuronal types (such as MNs). This is through neuromodulators such as NO or 5-HT or more specifically, in the case of 5-HT, through their varied receptor subtypes (Halberstadt, Powell and Geyer, 2013; Hachoumi et al., 2022). It is therefore possible that α3 could be more broadly expressed across neurons within the SC than previously documented (Figure 1.5A).

1.4.4 Neuromodulators Affect the Duration and Magnitude of the usAHP

During tadpole swimming, neuromodulators can modify swimming behaviour by affecting the firing behaviour of MNs, CPG neurons acting on MNs, or both CPG neurons and MNs (Sillar, Wedderburn and Simmers, 1991; Currie and Sillar, 2018). Motor output can therefore be influenced in a variety of ways, including by influencing the VR burst amplitude, the frequency of AP spikes, or both (Harris-Warrick and Marder, 1991; Sillar, Wedderburn and Simmers, 1991; Currie and Sillar, 2018; Hachoumi et al., 2022).

Neuromodulators themselves comprise a fairly broad, heterogenous class of signalling molecules which include classic neurotransmitters, biogenic amines, gaseous molecules and peptides (reviewed in (Combes, Sillar and Simmers, 2020b). Many neuromodulators influence sodium pump activity through targeting specific receptor subtypes expressed in the same cell as the sodium pump. This binding can initiate intracellular signalling pathways which influence pump function, such as PKA and PKC, pathways that are similarly targeted by FXYDs (Barbas et al., 2003; Meyer et al., 2020). Two main neuromodulators have been investigated as specifically targeting dynamic sodium pumps through their net inhibitory effect on the usAHP: 5-HT and NO (Miles and Sillar, 2011; Hachoumi et al., 2022).

Initially, bath application of 5-HT alone did not appear to affect the usAHP or STMM (Hachoumi et al., 2022). However, 5-HT is known to modulate neurons by acting on a range of receptor subtypes which can differentially impact neuronal firing, which often resulting in contradictory motor output. This was found to be the case when investigating the opposing impact that the receptors 5-HT2a (5-HT2aR) and 5-HT7 (5HT7R) has on the usAHP. In mice (Halberstadt, Powell and Geyer, 2013), rats (Liu and Jordan, 2005) and most recently tadpoles (Hachoumi et al., 2022), the 5-HT2aR has been shown to increase network excitability particularly by acting on cells at the locomotor output stage such as MNs and premotor interneurons. When a 5-HT2aR agonist, NBOH (30 μM) was applied to stage 42 tadpoles, the usAHP was attenuated, demonstrating a less negative peak amplitude compared to control conditions (Figure 1.7Ai). It also weakened the STMM as swim episode duration was not influenced by the either ISI or the duration of the preceding episode (Hachoumi et al., 2022). The opposite effect occurred when the 5-HT2aR antagonist, MDL 11939 (>15 μM) was applied leading to an enhanced negative peak and reduced network excitability. (Figure 1.7Aii). Meanwhile the 5-HTY7R is shown to enhance the usAHP, and subsequently strengthened the STMM, as its inhibition by 5-HTY7R antagonist SB-269970 (20 μM) results in a notable attenuation in the usAHP amplitude (Figure 1.7Bii).

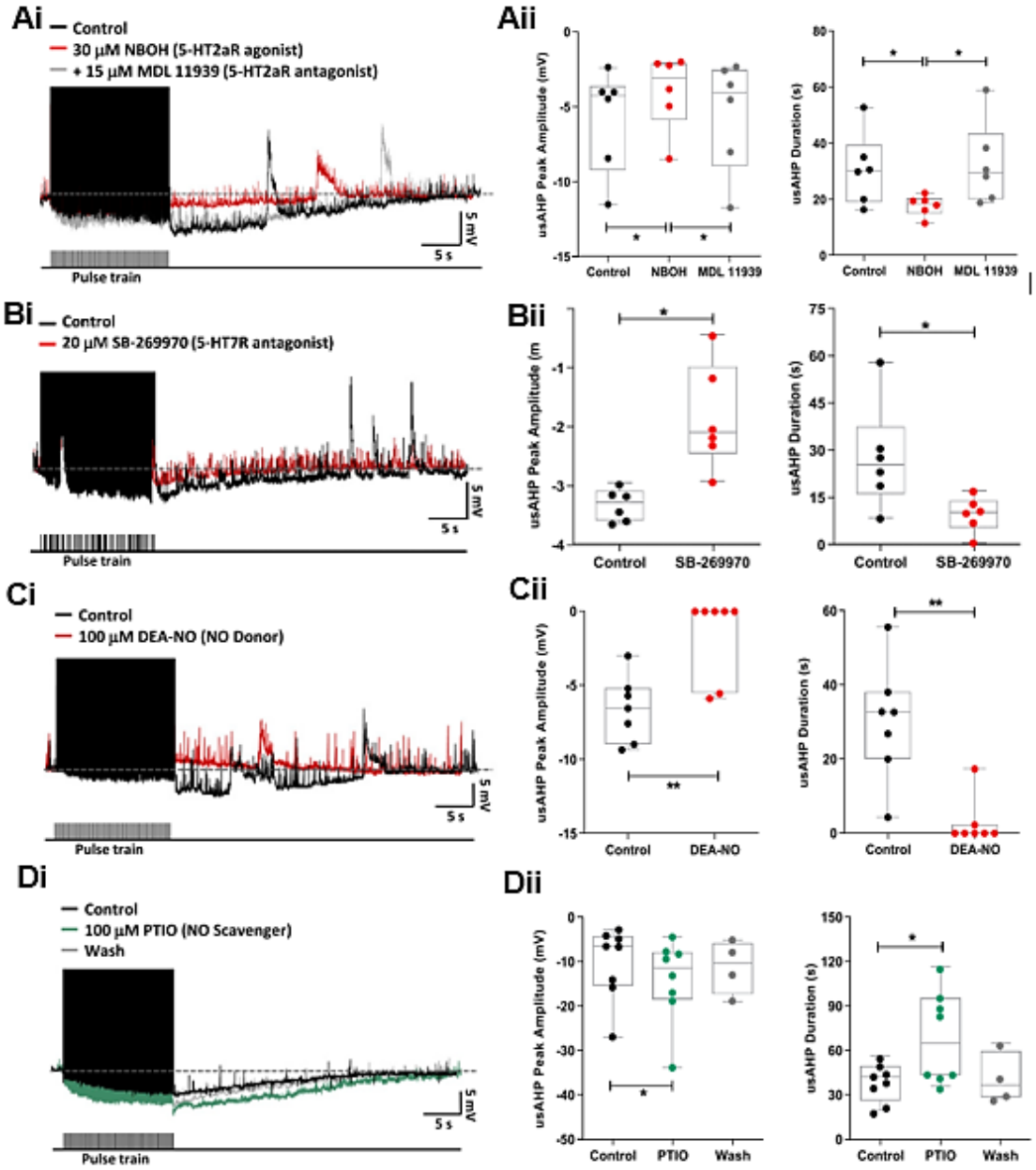

Figure 1.7: 5-HT and NO Differentially Modulate the usAHP Amplitude and Duration. A. The usAHP (black) is attenuated following application of 5-HT2a receptor agonist NBH (30 µM, red) (Ai). This is demonstrated by a decrease in the usAHP peak amplitude (mV) and decrease in duration (s) following application of NBOH, the latter effect of which is reversed following application of 5-HT2aR antagonist MDL 11939 (>15 µM) (grey) (Aii). B. Contrastingly, 5-HT7 does not inhibit the usAHP (usAHP) except in the presence of its antagonist, SB-269970 (20 µM) (red) (Bi) wherein it attenuates the usAHP by increasing peak amplitude (mV) and decreasing duration (s) (Bii). C. The NO donor, DEA-NO (100 µM), (red) also attenuates the usAHP (black) (Ci) by inducing a similar decrease in peak amplitude (mV) and decrease in duration (s) (Cii). D. When the NO scavenger, PTIO (100 µM) (green), was applied the usAHP increased (Di) in peak amplitude (mV) and duration (s) compared to the control (black). These effects were partially reversed once PTIO was washed out (grey) (Dii).

These findings indicate that 5-HT7R functions in direct contrast to 5-HT2aR which demonstrates the clear bimodal effects of 5-HT on the usAHP (Hachoumi et al., 2022). Furthermore, these differential effect by the antagonists when applied alone also provides direct evidence that these receptors are endogenously activated. For 5-HT2aR, this highlights its potential to successfully mask the presence of the usAHP in cell types where it is expressed. Given this finding, it is worthwhile to investigate whether α3 is more widely expressed than previously estimated given the strong potential for its activation to be masked or attenuated following upregulation of 5-HT2aR or downregulation of 5-HT7R.

NO is a diffusible signalling molecule that, like 5-HT, can induce widespread effects on neurons and networks (McLean and Sillar, 2004; Currie and Sillar, 2018). Furthermore, the effects of NO modulation can vary within the same CPG network as *Xenopus* larvae reach different stages of development (McLean and Sillar, 2000; Currie and Sillar, 2018). Prior to the advent of free-swimming at stages 37/38-42, NO has a primarily inhibitory effect on swimming by shortening episode duration and reducing the spike frequency within these episodes by facilitating presynaptic inhibitory GABA-ergic and glycinergic signalling (Nieuwkoop and Faber, 1956; McLean and Sillar, 2000, 2002, 2004).

In contrast to this net inhibitory effect, direct application of NO has been shown to excite spinal neurons, much like noradrenaline (NA) on which pathway NO acts as a 'meta-modulator' on in order to potentiate inhibitory glycinergic signalling (McLean and Sillar, 2004). However, once the tadpole reaches NF stage 42 and beyond, NO modulation appears to switch to having a net positive effect on swimming in part by acting on the usAHP and STMM (Currie et al., 2016; Currie and Sillar, 2018; Hachoumi et al., 2022). When the NO donor, diethylamine (DEA-NO, 100 μm), was applied to the CNS of stage 42 tadpoles, there was a profound attenuation of the usAHP, an effect that indicated that NO receptors, like 5-HTa2R, also inhibit the usAHP in the tadpole CNS (Hachoumi et al., 2022). There was a stronger inhibition of the usAHP by DEA-NO as in many neurons (~60%), the usAHP was abolished entirely (Figure 1.5Cii). To ascertain whether NO was directly affecting the usAHP,

and by extension modulating dynamic sodium pumps, the NO scavenger 2-Phenyl-4,4,5,5-tetramethylimidazoline-1-oxyl 3-oxide (PTIO, 100 μm) was applied to downregulate the effects of endogenous NO (Figure 1.5Di-Dii). The usAHP was enhanced with application of PTIO, demonstrating a more negative peak amplitude and lasting for a longer duration compared to the measured properties of the usAHP under control conditions (Figure 1.6Dii).

1.5 Sensory Pathways: Skin and Cement Gland

As referenced previously, there are many sensory pathways that impact spinal neuron function (Roberts, 1971; Roberts and Clarke, 1982; Roberts et al., 1998; Li, Wagner and Porter, 2014). RB neurons possess two primary central axons and a peripheral one that projects into the skin. The two primary axons project bidirectionally along a dorsal tract within the SC with one extending towards the rostral hindbrain regions and another extending into caudal SC regions. The peripheral axon runs through the myotomal muscle layer and between the two cell layers comprising the skin where peripheral neurites ramify forming a network underneath the skin (Roberts and Hayes, 1977; Clarke et al., 1984). In response to direct mechanical pressure, APs are propagated along these axons into the SC and to the RB soma which in turn produces an EPSP onto sensory interneurons: dorsolateral commissural (dlc) and dorsolateral ascending (dla) interneurons (Sautois et al., 2007). These interneurons then excite CPG neurons on the opposite (dlc) side and on the same side (dla) therefore activating these motor circuits to initiate swimming (Figure 1.8A).

Skin cell excitability, like dynamic sodium pumps, is modulated by NO. Application of an NO scavenger, SNAP, was found to increase the duration of the excitatory skin impulse (Roberts, 1971; Alpert et al., 2007). Furthermore, NO also slowed the rate at which this excitability could be propagated to neighbouring skin cells and lead to increased excitability by depolarizing the membrane potential (Alpert et al., 2007). Given the increase in excitability following NO application, combined with NO's known history as a sodium pump inhibitor, it is highly likely that α3 will be found in the skin cells of tadpoles.

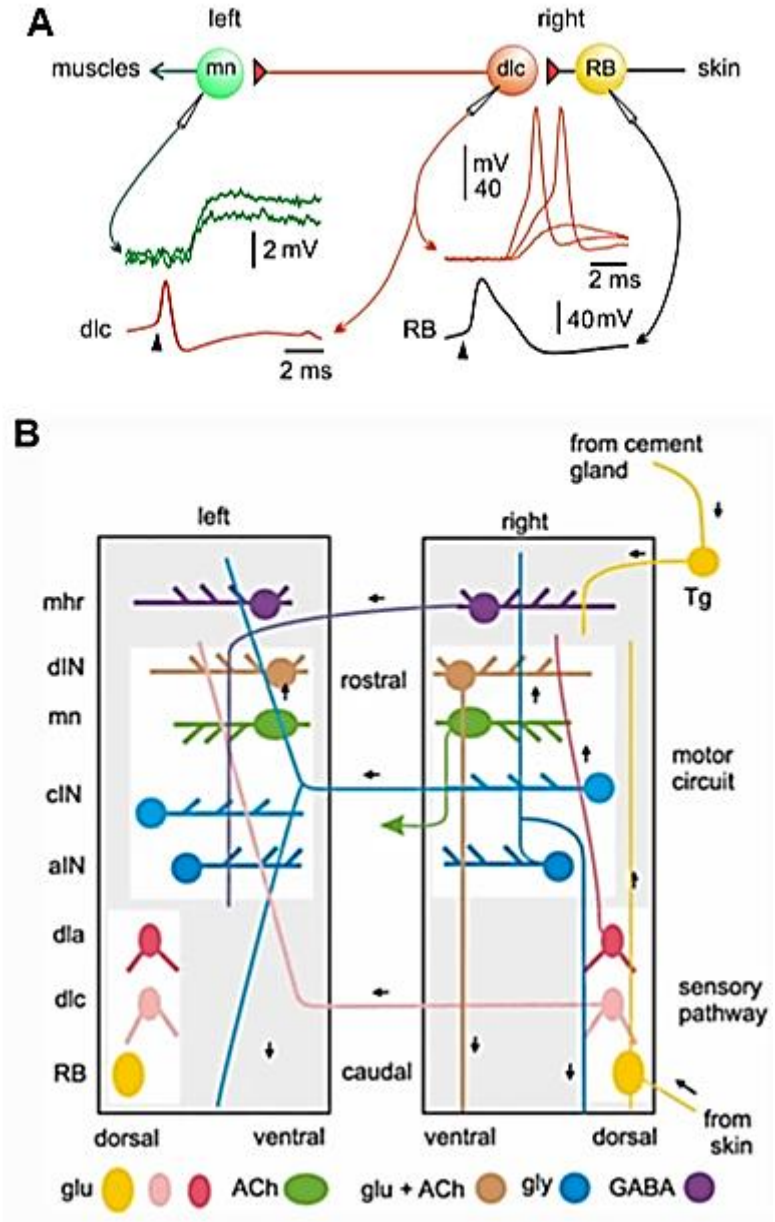

Figure 1.8: Interneuron-Mediated Swimming via Mechanosensory Excitation of RB Neurons and Subsequent Halting via Trigeminal Pathway. A. Diagram demonstrating post-mechanical stimulation to RB sensory peripheral neurites situated beneath the tadpole skin. The signal is propagated along the neurites extending from the RB soma (RB in yellow; AP recording in black) which in turn excites dlc interneurons (cell body and intracellular recording illustrated in red). These interneurons then excite MNs (cell body and intracellular recording illustrated in green) which stimulates muscle contraction through cholinergic signalling. B. Illustration (via yellow diagram) of initiation and halting of swimming via respective sensory pathway and trigeminal pathway (Tg). Both signalling pathways are initiated by stimulating sensory organs (skin, cement gland) which reside outside of the CNS. Swim function in response to either pathway is regulated by the spinal neurons which comprise the motor circuit (white box). (Note: Panel is set along tadpole HB/SC with view split evenly down tadpole dorsal midline, providing lateral view of both the left and right tadpole sides, axons are only shown for neurons on the right side) (Panel A adapted from Li et al., 2003; Panel B adapted from Roberts et al., 2008).

To terminate swim behaviour initiated by skin stimuli there is another signalling pathway that also originates from a sensory organ extrinsic to the tadpole CPG, the cement gland (CG), a mucous-producing organ located at the tadpole's most rostral point on the head (Figure 1.8 Aii) (Boothby and Roberts, 1995; Li, Wagner and Porter, 2014). Tactile pressure to the cement gland excites trigeminal sensory neurons that project into the hindbrain to excite inhibitory midhindbrain reticulospinal neurons (mhr) which, in turn, inhibit CPG neurons via GABA-ergic signalling. This inhibition results in a barrage of inhibitory post-synaptic potentials (IPSPs) that ensure swimming is halted abruptly, with little chance of the self-activating CPG circuit reinitiating it (Figure 1.8 B) (Li et al., 2003). This pathway is tonically active earlier in development when tadpoles suspend themselves from the water meniscus by the mucosal secretion produced by their CG, therefore inducing pressure on this gland through their own body weight. When tadpoles become free-feeding and begin to swim more frequently, the CG pathway begins to degenerate, as do RB neurons which decline from NF stage 42 onwards (Baccaglini and Spitzer, 1977; Roberts and Hayes, 1977; Roberts and Clarke, 1982). The mhr input does remain though and can become a target for neuromodulation later in development, notably also by NO which increases network excitability by raising the membrane potential of target neurons (Therien and Blostein, 2000; Alpert et al., 2007; Hachoumi and Sillar, 2019; Hachoumi et al., 2022).

1.5.1 Myotome Function Relies Upon Sodium Pump Kinetics

Myotomes are the essential components and drivers of tadpole swimming, mainly through mechanically facilitating tail movement in response to CPG output. There is compelling evidence that indicates myotomes mature alongside motor circuit complexity during larval tail growth in early development (Boudjelida and Muntz, 1987; P, J and A, 1989; Zhang, Issberner and Sillar, 2011). There is even the potential that mechanical feedback directly influences neuronal circuit function and that limited interactions between the myotomes and neurons could drastically affect future network connectivity and neuronal fate within the CNS (Gangatharan, Schneider-Maunoury and Breau, 2018).

In previous research, α3 expression has been documented as present in the brain tissue of rats (Orlowski and Lingrel, 1988) and humans (Hundal et al., 1994; Murphy et al., 2004). Tracking of ATP1A3 mRNA transcripts did also reveal the quantifiable presence of α3 (0.69 TPM) in the myotome of adult *Xenopus* (Session et al., 2016a) indicating a strong probability of positive immunolabelling in the tadpoles from my project. Though little research has been conducted into the exact role of α3 in skeletal muscle there is potential functional overlap with its role in smooth muscle where α3 has also been shown to be highly expressed in the cardiomyocytes of mice (Zheng et al., 2022), humans (Jaffer et al., 2015; Balestrini et al., 2020; Zheng et al., 2022), and *Xenopus* (Rahman et al., 2015; Liao et al., 2022a) where it has been identified as contributing to rhythmic contractibility. This is demonstrated through identifying the effects from the pathologies of ATP1A3-related disorders such as Alternating Hemiplegia of Childhood (AHC) where patients have been shown to present with arrhythmia attributed to a p.D801N loss of function mutation in the ATP1A3 gene (Jaffer et al., 2015). Inhibited function has been shown to cause this arrhythmia by shortening cardiomyocyte AP duration leading to a dysregulated Na+ and intracellular Ca2+ influx which depolarizes cardiomyocyte membrane potential and inhibits repolarization (Jaffer et al., 2015; Zheng et al., 2022). These findings highlight how α3-expressing pump mediated extrusion of Na+ helps to regulate smooth muscle contraction, often by operating with the Na+/Ca2+ exchanger pump to regulate intracellular Ca2+(Zheng et al., 2022).

I would hypothesize a functional overlap with its familial α2 isoform which is documented to be highly expressed in *Xenopus* skeletal and cardiac muscle tissue (Session et al., 2016a; Liao et al., 2022a). α2 activates in response to increased intracellular Na+ which occurs when the cell membrane potential is depolarized (Stanley et al., 2015). It then functions to directly reduce intracellular Na+ (Blanco and Mercer, 1998; Stanley et al., 2015). It has been shown that α2 also counterbalances the Na+/Ca2+ exchanger pump which transports Ca2+ into the myocyte in exchange for extruding Na+ ions at a 1:3 ratio (Stanley et al., 2015). The extent to which α3 is expressed within the tadpole myotome is certainly worth further

scrutiny particularly in regards to the potential that its cationic regulatory function in cardiomyocytes is likely conserved in skeletal myocytes.

FXYD1, and to a lesser quantity FXYD6, are expected to be present in the myotomes of *Xenopus* tadpoles given their previously detected presence in the skeletal muscle of *Xenopus* (Stanley et al., 2015; Session et al., 2016a; Liao et al., 2022a). Its high prevalence in skeletal muscle ranges across many different species (Crambert and Geering, 2003; Lifshitz et al., 2006; Christiansen et al., 2017) indicating a conserved expression and potentially conserved function for this protein. Functionally, FXYD1 and FXYD6 are reported to significantly reduce pump affinity for Na^+, and to a lesser extent K^+ in *Xenopus* while not affecting the transport rate of these ions (Feschenko et al., 2003; Bibert et al., 2008; Meyer et al., 2020). They are also implicated in reducing the population of sodium pumps within the cell membrane which induces activation of PKA intracellular pathways (Meyer et al., 2020). In the heart, concomitant activation of PKA (and PKC) pathways promotes the extrusion of Na+ which results in a low intracellular Na+ concentration. In response the Na+/Ca2+ exchanger pump is activated and shuttles Ca+ out of the cell to replenish intracellular Na+. Therefore, FXYD1 expressing pumps likely help to indirectly regulate the intracellular Ca2+ concentration in myocytes, which is likely to be high following periods of high locomotor activity during which muscle contractility increases acutely (Bibert et al., 2008). Similarly, when paired with a α2/β sodium pump complex following membrane depolarization, FXYD1 increases the pump affinity for K+ significantly and enables increased clearing of K+ (Stanley et al., 2015). It is therefore highly likely that the shuttling of FXYD1 pumps into and out of the cell membrane functionally induces downstream effects which help to regulate the intracellular concentration of positively charged ions.

Another downstream effect of PKA activation is that it promotes the rescue of FXYD1-expressing sodium pumps back into the cell membrane (Meyer et al., 2020). This likely underlies the functional upregulation of FXYD1 that has been identified following intense muscle training (Clausen, 2003; Rasmussen, Kristensen and Juel, 2008; Thomassen et al.,

2016; Wyckelsma et al., 2019). This increase in FXYD1 specifically is theorized to also increase the shuttling of more sodium pumps to the cell membrane and increase overall sodium pump activity in human and rat locomotor systems (Rasmussen, Kristensen and Juel, 2008; Meyer et al., 2020) all of which provides rationale for investigating FXYD subunit expression in tadpole myotomes. Given its seemingly transient role in intracellular regulation of positive ions, like K+ and Ca2+ it is worthwhile to investigate how restricting movement during early tadpole development impacts FXYD1 expression within muscle tissue.

1.5.2 Sodium Pump Function Within the Photosensitive Retinal Layers of the Eye

The eyes of tadpoles during early embryogenesis are not yet functionally connected to the brain, with the developing tadpole instead relying upon its light sensitive pineal eye which can induce vertical swimming when the light is dimmed (Roberts, Li and Soffe, 2010; Li, Wagner and Porter, 2014). However, while there is very little behavioural evidence indicating that the eye is functional in these early stages, this complex biological structure is undergoing prominent embryonic morphogenesis during this period. While transcription factors are important to this development, recent findings have shown that bioelectric signalling can provide an upstream determinant for cellular differentiation within the various retinal layers (Figure 1.9 A). This is induced by carefully patterned endogenous plasma membrane voltage gradients, namely bilateral hyperpolarized cell populations located in the anterior neural field (Pai et al., 2012). Furthermore, any perturbation in the hyperpolarized membrane potential by, enabling an efflux of chloride, lead to eye defects including incomplete eye formation and direct fusion to the brainstem.

These changes can be ameliorated by simply reintroducing a negative intracellular charge in neighbouring cell populations surrounding the undifferentiated cells, most directly by hyperpolarizing the membrane potential of these cells. This further emphasizes that bioelectric signalling plays a significant role in retinal layer patterning within the tadpole eye. Furthermore, cellular differentiation can be impacted by bioelectric signalling as hyperpolarizing the membrane potential of non-eye cells induces de novo expression of Rx1

and Pax6 transcription factors. This in turn influences the expression of an ectopic eye complete with differentiated Muller glia, amacrine cells, and photoreceptors such as rods and cones within the expected retinal layers (see Figure 1.9 B for reference) (Pai et al., 2012).

A previous study on the developmental expression of ATP1A3 in *Xenopus* found positive α3 expression in the inner nuclear layer (INL), outer nuclear layer (ONL), ganglion cell layer (GCL) and ciliary marginal zone (CMZ) retinal layers by larval NF stage 35/36 (Figure 1.5A) (Rahman et al., 2015). While the inner and outer plexiform layers (ONL and OPL, respectively) were not explicitly included it is likely that α3 is present within these regions given its prominent expression in the axons of neurons (Brines and Robbins, 1992). Furthermore, quantification and tracking of mRNA ATP1A3 transcripts in *Xenopus* tissue have revealed that it is quite highly (121.3 TPM) present in the eye (Session et al., 2016a).

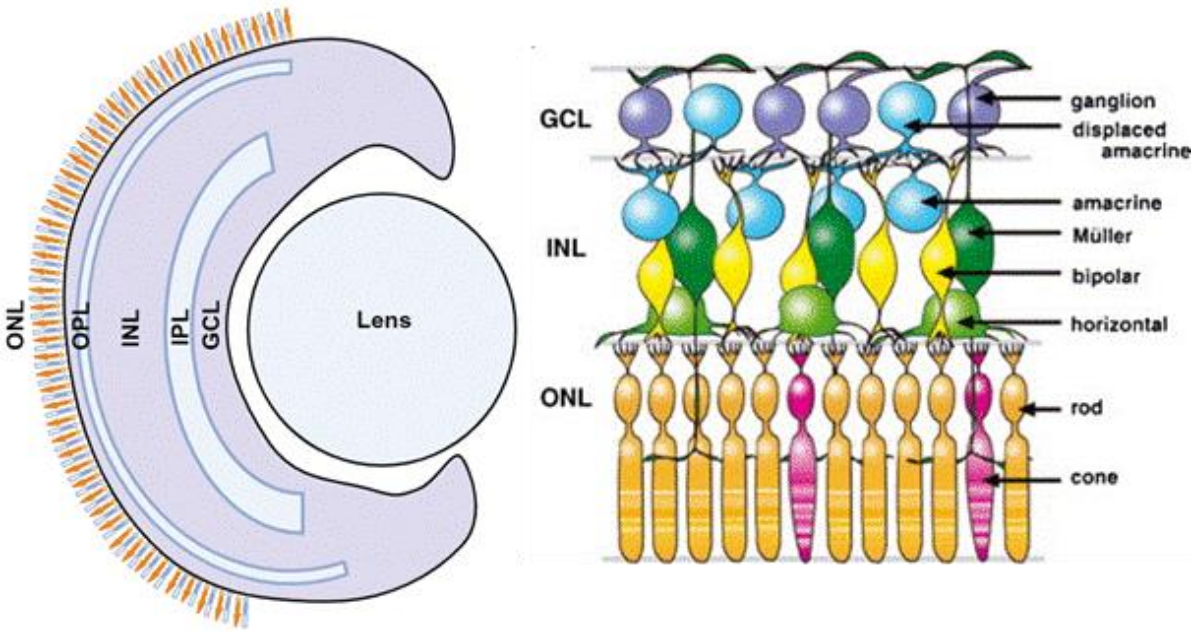

Figure 1.9: Retinal Layers Within *Xenopus* Eye. A. Outline retinal layers comprising the transverse cross-section of the stage 42 tadpole eye, taken at the midbrain level of the CNS. The retinal layers are comprised of the outer nuclear layer (ONL) outer plexiform layer (OPL) inner nuclear layer (INL), inner plexiform layer (IPL), the ganglion cell layer (GCL), and the lens (Lens). B. These retinal layers are made up of different cell types with axons ascending into the plexiform layers between the INL and ONL (Panel A is an outline retinal taken from a cross-section of a tadpole eye which was fixed and imaged by me; Panel B adapted from (Hatakeyama and Kageyama, 2004).

Another study which tracked gene expression across specific cell types also noted high mRNA transcripts within the eye with α3 expected in the photoreceptor cells, rods and cones, as well as microglia with minimal expression also quantified in the lens (Liao et al., 2022a). These findings could indicate that α3 provides an important function within the eye, perhaps even being involved moderating the bioelectric signalling that underlies cellular differentiation in the tadpole retinal layers during early tadpole development. As such, by NF stage 42 it is likely that α3 will be present in the aforementioned retinal layers given the temporal proximity to metamorphosis when eye development is expected to be far more complex than in embryonic stages.

1.6 Research Aims

My project was organized around two main aims to better elucidate the processes underlying tadpole motor behaviour. First, by investigating specific subunits that comprise the sodium pump complex as well as their potential contribution to kinetic function via their expression along different tissue types and within the tadpole CNS.

The first portion of this aim focussed on α3, a sodium pump subunit thought to be predominantly expressed in neurons however previous research has neglected to immunolabel this enzyme within the tadpole CNS and so this project sought to fill in this gap. Given previous research findings it is expected that α3 will be present in approximately ≤60% of all spinal neurons, regardless of subtype. This is examined by labelling the entire SC and quantifying total expression within a cross-section as well as quantifying and comparing whether expression varies dorsoventrally. MNs will be identified by backfilling and co-labelling with α3 to assess whether it is indeed only present in approximately 42% of MNs (Picton, Sillar and Zhang, 2018). This experiment will further elucidate the degree to which functional expression of the usAHP is affected by neuromodulator-driven inhibition rather than a lack of dynamic sodium pumps being expressed in this spinal neuron subtype as proposed by Hachoumi et al., (2022). Regarding non-CNS tissue, α3 is expected to be present in skin cells and in the retinal layers that comprise the eye as well as the lens

(Rahman et al., 2015). Due to previous research identifying that ATP1A3 mRNA transcripts are present in *Xenopus* muscle (Session et al., 2016a), α3 is anticipated to be expressed in the myotome tissue but, as referenced previously, likely is highly concentrated within the presynaptic NMJ.

For the latter portion of my immunolabelling project I present data on the expression patterning of FXYD1 and FXYD6 subunits within the tadpole CNS and related tissue. Both FXYD1 and FXYD6 are expected to be present in spinal neurons though it is uncertain whether expression within neuronal populations will vary or not between these two structurally similar FXYD isoforms. FXYD1 is expected to be more prominently expressed within the myotomes given that it is present in the skeletal muscle of a variety of species including humans (Crambert and Geering, 2003; Rasmussen, Kristensen and Juel, 2008).

For my second aim, I examined how expression of target pump subunits was affected by altering tadpole mobility during formative developmental stages through halting tadpole movement during early development. This was accomplished by exposing embryos from NF stage 20 until stage 42 to low concentrations of fish anaesthetic MS-222 which is permeable to skin and binds reversibly to voltage-dependent Na+ channels on sensory and motor neurons (Ramlochansingh et al., 2014; Félix et al., 2018a).

By the end of this project my research aims to provide a better understanding of the expression pattern of α3, FXYD1 and FXYD6 within key anatomical regions of *Xenopus* tadpoles. Furthermore, limiting motor function over the course of early tadpole development will enhance our current understanding of how α3 and FXYD1/FXYD6 expression is influenced by mechanical and sensory feedback from non-neuronal tissue during spinal network formation.

2. CHAPTER 2: α3 IS BROADLY EXPRESSED IN THE TADPOLE TISSUE TYPES

2.1 Introduction

The sodium pump is ubiquitously expressed within the CNS where it confers an electrochemical gradient through the unequal exchange of positive K+ and Na+ ions. The exchange rate of these ions can differ based upon which subunit isoform is present within the sodium pump's heterotrimeric structure with the variation in their catalytic properties being conferred by their α subunits, of which there are four (labelled numerically as α1- α4) (Blanco et al., 1994). The expression of each subunit subtype varies across tissue types with α1 and α3 being prominently ~~e~~xpressed in neurons within the vertebrate CNS (Shull, Greeb and Lingrel, 1986; Lingrel et al., 2007; Tokhtaeva et al., 2012). The functional properties of the α3 subunit within the heterotrimeric sodium pump complex has been broadly studied and arguably its best understood property is shown in how pumps expressing α3 are thought to underlie the usAHP in neurons and other electrogenic cells (Zhang and Sillar, 2012). As mentioned in the General Introduction, the usAHP is characterized by a prolonged period, lasting up to one minute, during which the cell membrane is hyperpolarized following an intense period of neuronal firing (Figure 2.1). During this period the cell is less likely to reach spike threshold therefore making firing more difficult to stimulate. This usAHP has been described in several locomotor systems including Drosophila larvae (Pulver and Griffith, 2009), *Xenopus* tadpoles (Zhang and Sillar, 2012; Picton, Sillar and Zhang, 2018; Hachoumi et al., 2022) and neonatal mice (Picton et al., 2017).

The following introductory sections will review the function and kinetic properties that have been found in relation to the catalytic α3 subunit and explore the ensuing relationship between α3 expression and cellular function. The ensuing results chapter will detail the protocols and statistical analyses developed for labelling α3 and documenting its expression pattern within the tadpole CNS and other tissue types.

2.1.1 Tonic Versus Dynamic Sodium Pumps

Prior to tracking the expression of dynamic sodium pumps it is essential to outline the unique kinetic properties that α3-expressing sodium pumps confer onto cells where this pump type is expressed. Dynamic sodium pumps are mainly inactive at RMP (~-65 to -80 mV) but when activated contribute to an important neuronal function, known as the usAHP. α3 is believed to be the main catalytic drive behind this dynamic sodium pump function and a wide range of experiments have presented evidence supporting this finding.

First, there is strong overlap in usAHP and α3 expression within neurons, as well as in other electrogenic cell types. However, other α isoforms, α1 and α2, are also expressed in neurons though α2 expression is mainly confined to glial cells making it less likely to be the contributing catalytic subunit within dynamic sodium pumps. Since α1 is far more widely expressed across neurons it was briefly considered a likely candidate for residing within the dynamic sodium pump complex (Picton et al., 2017; Picton, Sillar and Zhang, 2018; Murata et al., 2020). While the basic structure and catalytic function of α subunits does not vary significantly between pump subtypes, α isoforms do differ in their kinetic properties and ion affinities which can affect Na+ and K+ transport under certain conditions (Blanco and Mercer, 1998; Therien and Blostein, 2000).

For example, compared to α1, α2 and α3 containing pumps have a high affinity for the cardiac glycoside ouabain, a drug that inhibits sodium pump function by blocking ion transport at the α binding sites (Brines and Robbins, 1992). The activity of sodium pumps expressing α2 and α3 isoforms can be abolished at low concentrations (≤1μM). In contrast, the activity of α1 expressing pumps remains largely unaffected at these same concentrations due to α1 being relatively insensitive to ouabain (≥3μM, up to 100μM) (Blanco et al., 1994; Zahler et al., 1997; Hachoumi et al., 2022).Among the α subunits, α1 has the highest affinity for intracellular Na+ followed next by α2. In contrast, α3 pumps have a much lower Na+ affinity and pumps expressing α3 are likely to be inactive at low resting intracellular Na+ concentrations, such as those present at the RMP (Zahler et al., 1997; Blanco, 2005a)

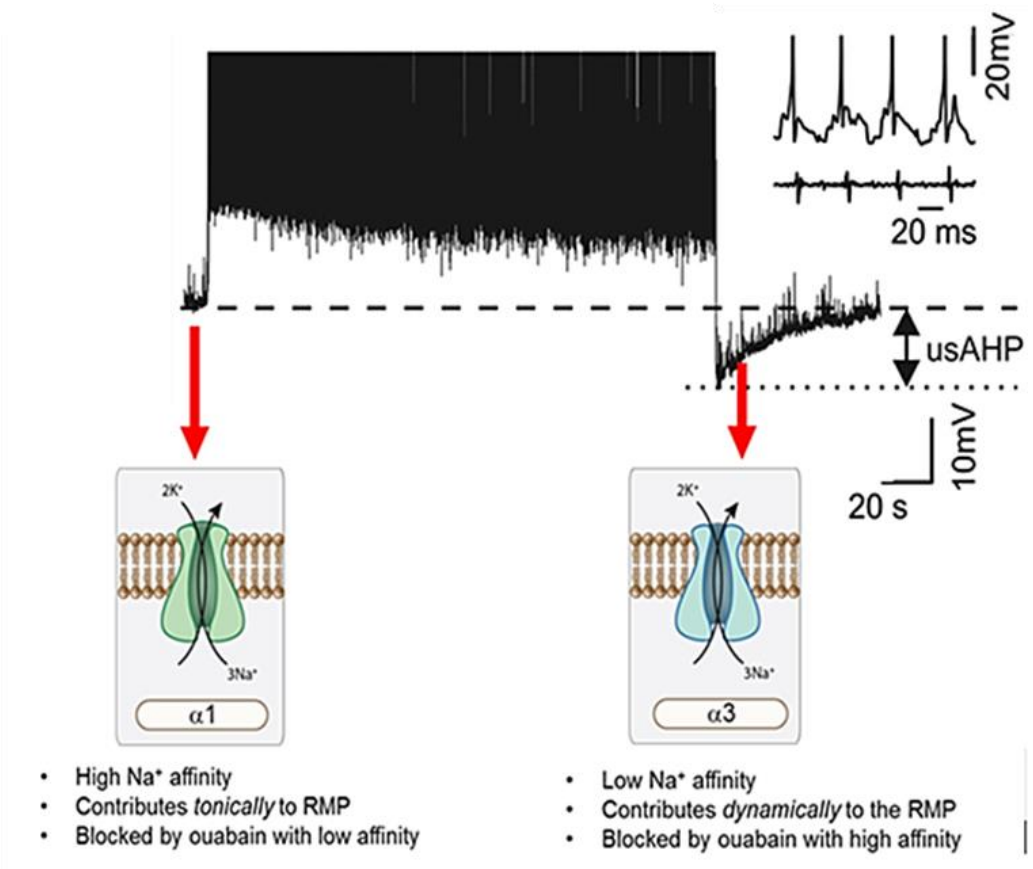

Figure 2.1: Tonic versus Dynamic Sodium Pump Function. Current clamp recording of rhythmically active spinal neurons during *Xenopus* tadpole swimming episode and the hypothesized functional contribution of α subunits, α1 and α3, to resting membrane potential (RMP) and the usAHP (Figure adapted from recordings by Zhang & Sillar, 2012 and cartoons courtesy of Professor L. Picton 2017).

In the nervous system, the different kinetic properties of α1 and α3 may allow sodium pumps to contribute to the electrical properties of neurons in two important ways: either “tonically” by contributing to the maintenance of the RMP (α1) or “dynamically”, recruited by neuronal activity and mediating a post-activity hyperpolarization (α3) often referred to as a usAHP (Picton et al., 2017) (Figure 2.1). Tonic sodium pumps are thought to solely express the α1 subunit allowing them to be continuously active at the RMP due to their high Na+ sensitivity and to contribute to the setting and homeostatic maintenance of the RMP. In contrast, α3-expressing pumps are normally silent (due to low intracellular Na+ at the RMP) and only activate during periods of high frequency neuronal firing when Na+ levels are elevated sufficiently to recruit them; putatively they help to return the ionic gradients to resting levels

by exporting intracellular Na+ ions that have entered during trains of Na+ spikes. Therefore, the recruitment of α3 pumps and their extrusion of positive charge results in the membrane potential becoming hyperpolarized for up to approximately one minute (Figure 2.1) (Zhang and Sillar, 2012; Zhang et al., 2015; Picton et al., 2017).

During the usAHP period, subsequent attempts to evoke bouts of locomotor activity result in a network output that is shorter, slower and weaker, the extent of which is influenced directly by the ISI duration between each motor episode (Zhang and Sillar, 2012; Zhang et al., 2015). Previous studies have shown that the usAHP is selectively abolished by sub-micromolar concentrations of ouabain (~1-0.5 μM). Since α3 is highly sensitive to this cardiac glycoside inhibitor, the usAHP is more likely mediated by α3-expressing sodium pumps. By comparison, the RMP remains unaffected by these lower ouabain concentrations making the usAHP therefore unlikely to be mediated by α1-containing pumps (Zhang and Sillar, 2012; Picton et al., 2017; Hachoumi et al., 2022). Though not constitutively active like α1 pumps, α3 pumps play an essential, transient role in regulating for locomotor function. It does so by conferring an STMM on motor circuits where subsequent movement-based episodes, such as swimming episode duration, is impacted by preceding output (Zhang and Sillar, 2012). When the usAHP in *Xenopus* tadpoles is abolished by ouabain these animals become unable to properly regulate their swimming episodes and will swim almost continuously (Zhang and Sillar, 2012; Hachoumi et al., 2022).

2.1.2 Role of α3 in Neurological Diseases

As stated above, recruitment of α3 pumps effectively acts as a “break” on neuronal firing, which is important in tadpoles for preventing system fatigue (Zhang and Sillar, 2012). As a result, dysfunction or downregulation in α3 activity would allow intense activity to continue unabated and there are a growing number of neurological disorders resulting from α3 mutations, often linked to diseases affecting movement (Shrivastava, Triller and Melki, 2020). Mutations of the ATP1A3 gene, which encodes the α3 subunit, have been directly linked to a variety of neurological disorders characterized by motor dysfunction, including

muscle tremors and epilepsy (Arystarkhova et al., 2019; Zou et al., 2023). The most notable disorders are Rapid-onset Dystonia Parkinsonism (RDP) and AHC (Oblak et al., 2014; Capuano et al., 2020). The majority of these mutations are autosomal dominant with the onset of major symptoms often arising before upright walking in early childhood (Bøttger et al., 2011b; Clausen, Hilbers and Poulsen, 2017). Many of the neurological conditions caused by ATP1A3 mutations demonstrate similar clinical manifestations, including a rapid onset of acute symptoms, motor dysfunction and the appearance of impaired excitability in locomotor networks which have been directly linked to loss of function in α3 (Heinzen et al., 2014; Clausen, Hilbers and Poulsen, 2017). In RDP, these mutations can downregulate α3 expression and impair Na+/K+ transport in the remaining sodium pumps.

The decline of sodium pump activity is believed to result from a selective decrease in Na+ affinity mediated by RDP mutations while K+ affinity appears unaffected (Dobyns et al., 1993; De Carvalho Aguiar et al., 2004; Brashear et al., 2012). Behaviourally, RDP is characterized by involuntary, sustained muscle contractions, known as dystonic spasms, and slow movement (Dobyns et al., 1993). The onset of RDP tends to occur rapidly with symptoms developing over the course of hours or days and typically affects people between 10 and 30 years of age, although symptoms can begin from very early on in development. Some RDP diagnosed infants, typically 9 to 14 months exhibit delayed motor responses not long after birth (Dobyns et al., 1993; Brashear et al., 2012). Unlike in RDP, AHC-causing mutations do not affect Na+ affinity nor do they lead to a decrease in α3 expression. Symptomatically, AHC is characterized by transient but recurrent episodes of hemiplegia, the partial paralysis of one side of the body, along with other motor disturbances such as dystonia and even seizures (Rosewich et al., 2012).

In RDP and AHC, it has been noted that the severity of dystonia and parkinsonism symptoms appeared to follow a rostrocaudal gradient, characterized as “face>arm>leg”, along the human body. In this context, face symptoms, such as facial expressions, are more severe than arm symptoms and arm symptoms are more severe than leg symptoms

(Brashear et al., 2012; Heinzen et al., 2012). This evidence would indicate that tracking α3 expression in the spinal cord could shed light on the widely varied pathologies of motor disorders caused by ATP1A3 mutations (Bøttger et al., 2011a).

Beyond motor symptoms, ATP1A3 mutations have also been found to disrupt the normal flow of CSF through brain ventricles which can lead to hydrocephalus (Doğanli et al., 2013; Date et al., 2019; Dur et al., 2020). Previous research has noted that sodium pumps are expressed in the cells that line these ventricles and help to maintain CSF flow by contributing to an osmotic Na+ gradient, with α3 also being implicated specifically in this process (Speake et al., 2001). Knockdown of two different ATP1A3 orthologues, ATP1A3a and ATP1A3b, in zebrafish led to CSF accumulating in brain ventricles; this build-up is attributed to an imbalanced Na+ gradient disrupting the flow of CSF through the brain ventricles (Doğanli et al., 2013). This suggests that a loss in α3-expressing pumps, which maintain this gradient, could induce hydrocephalus. This link is supported by work from a separate study on congenital hydrocephalus in humans which identified two ATP1A3 germline mutations, p.Arg19Cys and p.Arg463Cys, with onset of hydrocephalus symptoms (Allocco et al., 2019).

Therefore, these studies investigating the expression of ATP1A3 have indicated that mutations in this gene lead to a wide variety of motor disorders, thus implicating α3 in contributing to the development of normal locomotor function. Despite the notable observations on usAHP and α3 kinetic function drawn from previous research, few studies have conducted an in-depth investigation into α3 expression within the vertebrate CNS nor cross compared how α3 expression could be linked to motor development and ultimately contribute to swimming function in tadpoles (Zhang and Sillar, 2012; Currie and Sillar, 2018; Hachoumi et al., 2022).

2.1.3 Project Aims

I had two main aims for the results presented in this chapter: The first aim was to establish an immunohistochemical protocol to accurately and selectively label α3 within the CNS and

related tissue such as the myotomes, skin and eyes. This step was crucial as to date there does not exist a primary antibody either reared or adapted for use in *Xenopus* tissue.

An important next step in this project was to develop analytical methods for investigating where α3 is expressed within tadpoles, mainly focussing on NF stage 42 although I do also compare α3 in protein extracted from tadpoles across different stages of development. I therefore begin my analysis by systematically describing the spatial regions where α3 is highly expressed within the rostrocaudal CNS by labelling transverse rostrocaudal anatomical sections taken from the tadpole head to at least mid-trunk level along the tadpole tail. I then highlight where α3 is distributed within each CNS region including an overview of the rostral forebrain and midbrain regions before focussing more closely on the caudal hindbrain and spinal cord.

Finally, I was able to use these quantitative techniques to differentiate positive α3 labelling versus autofluorescence (negative) labelling. this was done by comparing whether the fluorescence intensity taken from an auto fluorescing anatomical region was found to be higher in the α3 labelled section versus in the negative control. If so, these values indicate whether α3 is positively expressed in this anatomy. With these established measurable factors, I was able to develop analytical protocols for quantifying the positive labelling of α3 in the CNS and surrounding tissue, versus the appearance of labelling in tissue that is auto fluorescent. As I also wanted to compare whether α3 varied between wild-type (WT) tadpoles and albino tadpoles I also immunolabelled tadpoles from these phenotypes or if α3 expression is conserved. Notably, tadpole development does not differ between WT and albinos (Shan et al., 2023). Therefore, it is anticipated that there will be little to no difference between WT and albino tadpoles in terms of α3 expression in the CNS.

2.2 Materials & Methods

2.2.1 Experimental Animals

All experiments in this chapter were conducted on pre-feeding *Xenopus* laevis tadpoles at developmental stage 42, staged using the normal table of *Xenopus* development by Nieuwkoop and Faber (Nieuwkoop and Faber, 1956). WT tadpoles were reared at room temperature (~20^{o}C) from fertilized ova obtained from in-house adult *Xenopus* frog colony. Selected breeding pairs were given injections (by Home Office (HO) licenced personnel) of human chorionic gonadotropin (hCG, 1000U/ml, Sigma-Aldrich) into the dorsal lymph sac of the frogs to induce mating. Albino embryos were acquired from *Xenopus* Research Centre (EXRC, University of Portsmouth) and reared in-house under the same conditions as WT tadpoles. All experimental procedures were approved by the Animal Welfare Ethics Committee (AWEC) of the University of St Andrews and conformed to United Kingdom HO regulations.

2.2.2 Sequence homology of primary antibody

Before experiments could begin, the sequence homology was calculated by comparing the epitopes of the selected primary antibodies to the *Xenopus* protein sequence of α3. The α3 protein sequence for *Xenopus* was obtained from the Xenbase database and alignment was done using the NCBI BLASTP program (Altschul et al., 1990). The α3 antibody (Alomone Labs, ANP-003) shared 69% sequence homology with *Xenopus*. The immunogen sequence of the primary antibody was then compared to the *Xenopus* proteome and the positive identity outlined in red (Figure 2.2).

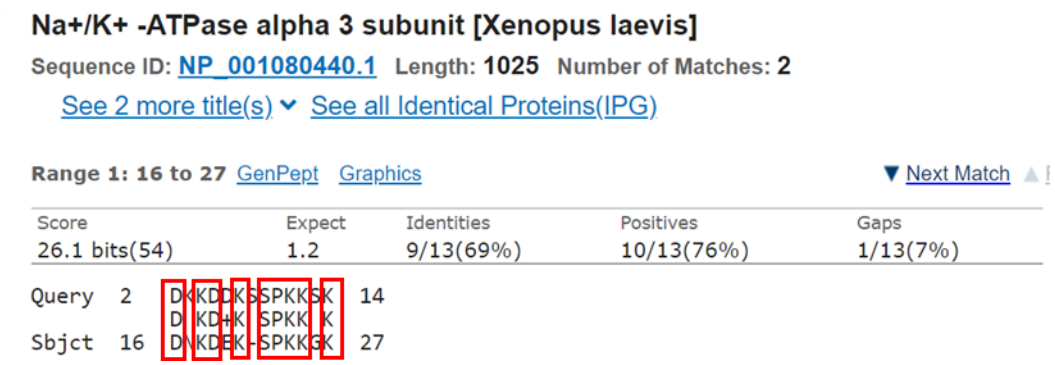

Figure 2.2: Alignment of chosen α3 primary antibody against X. laevis genome. Pairwise alignment of the immunogen sequence corresponding to amino acid residues 3-15 of rat ATP1A3 from which primary antibody was modelled to *Xenopus* laevis genome (gene id: 8355). (Positive identity between primary antibody and X. laevis genome outlined within red box).

2.2.3 Protein Extract Protocol

All *Xenopus* embryos and tadpoles between NF stage 20 and 45 were humanely euthanized, or Schedule 1 Killed (S1K), in 0.3% MS-222 (3-aminobenzoic acid ester; Sigma) and then washed twice in tris-buffered saline (TBS). The yolk sac was then excised from tadpoles and then tadpoles were suspended in an extraction solution comprised of 20% v/v 10mM Tris pH 8.0, 54% v/v methanol and 26% v/v chloroform. This solution was utilized as it allows for high protein yield with minimal contamination by extraneous lipids which can confer bind to other proteins and interfere with binding of the primary antibody. In conjunction with this step, the presence of the Tris detergent prevents protein aggregation (Ramola et al., 2019). Tissue was then homogenized in extraction solution until macerated. Eppendorf tube containing the sample was then spun at 13000rpm for 20 minutes at 4oC before being resuspended in fresh extraction solution before being spun again under the same conditions and then immersed in 100% ethanol before solution was removed and the tissue pellet was allowed to air dry for 1 hour to reduce moisture retained in pellet. The tissue was then resuspended in TBS with 0.1% tween20 (TBS-T), a gentle detergent that prevents protein aggregation, and again spun at 13000rpm for 10 minutes at room temperature. The final resultant supernatant (termed the protein extract or “PE”) does not contain the total protein

fraction but rather contains the soluble protein fraction, the concentration of which was measured using a Bradford Assay.

2.2.4 Dot Blots

Dot blot tests were conducted on the chosen α3 antibody (Alomone Labs, ANP-003) across a range of dilution concentrations (1:100, 1:250, 1:500, 1:1000; See Appendix Ai) to test specificity and approximate working concentration with the chosen antibody. Protein extract was denatured in boiling water for 10 minutes. Once cooled to room temperature, 2.5µl of protein extract was pipetted onto a nitrocellulose membrane and allowed to dry. Membranes were incubated in a blocking solution of 5% powdered milk mixed in TBS-T (termed milk block, 5% MB) for 30 minutes to block non-specific binding of the secondary antibody. Protein extract was then incubated with a range of primary antibody concentrations (1:100, 1:250, 1:500, 1:1000) made up in 5% MB overnight at room temperature. Protein was then washed 3 times in TBS-T before being incubated with goat anti-rabbit HRP-conjugated secondary antibody (1:10,000 dilution in TBS-T) for 1 hour. Protein was washed three more times in TBS-T and then stained with SigmaFast™ DAB (3,3'- Diaminobenzidine) (Sigma Aldrich, D0426) for approximately 3-5 minutes to visualise peroxidase activity. Once a colorimetric reaction was observed, membranes were washed three times with tap water to remove remaining DAB.

The darker coloration (at the 1:100 and 1:250 concentration) demonstrates that there was higher reactivity between protein, whereas the lighter shading indicates that reactivity was lower in the latter concentrations (1:500, 1:1000). As there was the potential that antibody specificity was lower in the higher antibody concentrations, it was determined that the 1:250 concentration was most optimal in terms of both reactivity and potential specificity in protein labelling. Regardless, as there was reactivity demonstrated in every concentration, the same concentration range was utilized for testing protein labelling in fluorescent IHC experiments.

2.2.5 Western Blot

A Western Blot was conducted to detect whether the target protein, α3, was present. This was done by labelling α3 with the chosen primary antibody. The specificity of the primary was also assessed using this method. Western immunoblotting was performed on protein extracted from NF stage 42 tadpoles. The protein weight for α3 (~112 kDa) and α-tubulin (~48.9 kDa) was estimated by entering the FASTA sequence into an online molecular weight calculator which takes into account the weight of each amino acid (Protein Molecular Weight Calculator (sciencegateway.org)). Tadpole protein was extracted via the methodology previously detailed in Protein Extract Protocol section above. The concentration of the soluble protein fraction was determined by running a Bradford Assay. Protein extract was denatured in boiling water for 10 minutes in 1X SDS sample buffer consisting of 1% SDS, 3% glycerol, 60 mM Tris, pH 8.8, and bromphenol blue. This denaturing in SDS buffer serves to unravel the protein and render them suitable for electrophoresis by granting the protein a uniform net negative charge. Denaturing in the SDS also helps to unravel and separate the subunits comprising the sodium pump by breaking apart the covalent bonds holding the structure together. The denatured proteins from the soluble fraction were then electrophoresed in NuPAGE 4-12% Bis-Tris Gel (Invitrogen, NP0323BOX) then transferred to nitrocellulose membrane. The membranes were blocked via incubation in 5% MB for two hours to prevent endogenous labelling. After washing twice in TBS-T, the blots were incubated with α3 primary antibody (Alomone Labs, ANP-003; 1:1000 concentration) and with α-tubulin (Santa Cruz Biotechnology, sc-32293; 1:1000 concentration), which acted as a positive control1 antibody, overnight at 4°C. Lower primary antibody concentrations were chosen in order to reduce any potential background labelling that could appear on the blot. Concentration was intended to be increased or decreased depending upon how strongly

[1] A positive control is a sample that has undergone the same procedure as the experimental group has but then is incubated with a separate reactive agent, in this case the α-tubulin primary antibody (Santa Cruz Biotechnology, sc-32293). A positive control is included in an experiment to evaluate the validity of an experiment my comparing labelling and reactivity of both reactive agents.

immunolabelled the protein was. Following incubation, Blots were washed and incubated with anti-rabbit or anti-mouse horseradish peroxidase-conjugated secondary antibody (1:10,000), respectively, and positive bands were detected using the Pierce CL Plus Western Blotting Substrate kit (Thermoscientific, 32134).

To ascertain the exact molecular weight of the protein being detected by the α3 primary antibody and deduce whether this protein was the target α3 protein, the weight of each protein band was calculated via comparison with an adjacent protein ladder (Thermoscientific, 26623) which was electrophoresed in the same gel as the protein extract. The protein band at approximately 100kDa was identified as the target α3 protein due to the band being positioned at around the estimated weight for this protein (~112 kDa) and that there was only one other positively labelled band on the membrane at the 50 kDa weight identified as positively labelled α-tubulin protein (estimated as ~48.9 kDa) which was included as a positive control (Appendix Bi).

2.2.6 Enzyme-Linked Immunosorbent Assay (ELISA)

Protein was extracted from *Xenopus* samples over a range of NF developmental stages and labelled using the chosen α3 primary antibody to measure and compare expression over the course of tadpole development. PE was pipetted into the wells, repeated in triplicate per condition, of a 96-well plate at a concentration of ~5 µg/ml, diluted with TBS. PE was left on a rocker for one hour to allow protein to coat the bottom of each well. Three sets of wells were set aside for controls. First control was a set of triplicate wells incubated solely with TBS rather than PE. The second control was incubated with PE but no primary antibody was added to this conditions. The third control was PE incubated with a separate primary antibody, α-tubulin (1:10000). As in the Western Blot, α-tubulin acted as the positive control. Endogenous binding of protein in wells was blocked by incubating with 5% MB (1 hr). PE was then incubated with primary antibody (1:10000; made up in 1% Milk Block) overnight at 4^{o}C. Primary solution was then discarded, and wells were washed three times in TBS, incubating for 5-10 min each time.

PE was then incubated overnight at 4°C with anti-rabbit or anti-mouse horseradish peroxidase-conjugated secondary antibody (1:10000) for α3 and α-tubulin incubated wells respectively. Secondary antibody solution was then removed and wells were washed three times with TBS, incubating for 5-10 min each time. PE was then incubated with TMB (abbreviation of 3,3',5,5' tetramethylbenzidine; Thermofisher, 34028), a chromagen that yields a blue colour when oxidized with hydrogen peroxide for approximately 10 min until reaction was observed to occur. Reaction was then halted with 1M HCl which resulted in a yellow colour.

Absorbance for each plate was read at 630nm. Values from each condition were averaged across triplicate wells and positively incubated PE values were compared to the controls incubated solely with TBS to determine if the latter values were higher. This would indicate if there was any degree of false labelling occurring. Averaged values of each independently conducted ELISA were normalized to the control lacking primary antibody by setting said control, in each developmental stage, to 100% and then comparing percentage absorbance in wells incubated with α3 primary antibody per developmental stage. This was to establish a quantifiable threshold where positive versus false positive labelling could be established. This was repeated for the α-tubulin incubated PE controls as well.

2.2.7 Tissue Preparation and Mounting

The following protocol was adapted for application in *Xenopus* from mammalian immunocytochemistry protocols provided on the manufacturers' websites of each primary antibodies. Stage 42 *Xenopus* tadpoles were used for all immunohistochemical labelling. Tadpoles were anaesthetized in 0.1% MS-222 before being fixed in formaldehyde, alcohol, acetic acid (FAA) overnight at 4oC. Fixed tadpoles were washed twice in TBS, for 5 minutes each time, and then taken through a series of dehydration and clearing steps consisting of 100% alcohol, 50% histoclear (HistoChoice® clearing agent (VWR, H103-4L)) and finally 100% histoclear. Tadpoles were embedded vertically (the head set vertical to bottom of mould) in paraffin wax and left to set overnight at room temperature. Serial transverse

sections were cut rostrocaudally at 9µm thickness using a rotary microtome (Microm, HM 310) and sections mounted onto polysine-coated microscope slides (VWR, 631-0107). After drying for 3 hours on a heat rack at 50°C, slides were stored for two days in an oven at 37°C to ensuring paraffin coated sections were sufficiently flattened. Slides were then stored at room temperature prior to labelling with primary antibody.

2.2.8 Primary Antibody Concentration Optimization

Slides were immersed twice in Histoclear to remove paraffin wax from sections. Sections were then taken through a series of rehydration steps in 100% alcohol, 96% alcohol and 70% alcohol before being washed once in TBS. Slides were then steamed in 0.1M citrate buffer for 25 minutes to retrieve cross-linked antigens, cooled to room temperature and washed twice in TBS. A blocking solution of 5% MB was added for 20 minutes to block non-specific binding by the secondary antibody, followed by incubation in primary antibody overnight at 4°C. In α3 optimisation experiments, goat anti-rabbit α3 antibody produced in rabbit (Alomone Labs, ANP-003) was tested at the following concentrations: 1:100, 1:250, 1:500, 1:1000. All images were compared to a negative control where the primary antibody was omitted, and sections were solely incubated with fluorescent secondary antibody.

Following incubation with the primary antibody, slides were washed twice in TBS, and incubated with goat anti-rabbit secondary antibody for 1 hour at room temperature in an IHC chamber to prevent mounted sections from drying. α3 labelled sections were incubated in fluorescein isothiocyanate (FITC) conjugated goat anti-rabbit secondary antibody (Vector Labs, FI-1000) at 1:1000 dilution in TBS. (Note: Following primary antibody optimisation, α3 labelled spinal cord sections were incubated solely in CY3 goat anti-rabbit secondary antibody (Vector Labs CY-1300) at 1:1000 dilution in TBS. The CY3 secondary antibody was initially purchased as an appropriate antibody for co-labelling with FITC (Vector Labs, FI-1000) due to their excitation ranges not overlapping (CY3 excitation at wavelength 550 nm, peak emission at 570 nm and FITC excitation at wavelength 495 nm, peak emission at 515 nm). Initial α3 experiments were labelled with FITC for a brief period while awaiting the CY3

order during the advent of the COVID-19 pandemic. Ultimately it was decided that CY3 would be used exclusively on α3 labelled sections and FITC with FXYD1 labelled sections going forward for the sake of consistency). After labelling with a secondary antibody, slides were then washed 5 times in TBS and mounted with a #1.5 thickness (0.17mm) coverslip.

2.2.9 Motoneuron Backfilling

A dextran-conjugated rhodamine dye (Invitrogen, D1824) was used to backfill, and therefore label, MNs in the tadpole CNS. The dye was mixed with a distilled water to make a paste and which was loaded onto a tungsten needle. Before dye-loading, the tungsten needle was sharpened by etching in a 10 M potassium hydroxide solution (KOH), which was is used as an electrolyte into which an applied potential could be generated from a generator. This potential was directed into the KOH solution via an anode/cathode set-up. The tungsten needle was then inserted into this solution leading to a controlled degradation of the metal until a sharpened point of tungsten remained at which point the newly formed needle was removed.

Once prepared, the sharp needle was inserted into the paste and left to crystallize on the needle. Selected stage 42 tadpoles were anaesthetised in 0.1% MS-222 as previously detailed earlier in this section (Chapter 2.2.6). Solution was drained until the alive tadpole was beached on a Sylgard (DOW, SYLGARD 184 Silicone Elastomer) platform in a dissection bath. The needle was then carefully inserted through the skin into the underlying myotome (Appendix B, panel Ai) while taking care not to damage the tissue nor penetrate beyond the segmented muscle. Tadpoles were then placed into saline to recover from anaesthetic until swimming behaviour returned. Tadpoles were allowed to swim, under reduced ambient light conditions, for around 2 hours to ensure dye uptake into VR.

Tadpole was then S1K-ed in 0.3% MS-222, as detailed previously (Chapter 2.2.3 Protein Extraction Protocol) and fixed overnight in FAA at 4^{o}C. Tadpoles were then washed twice in TBS and imaged briefly using Photometrics Moment fluorescent camera (Cairn Research) to ensure dye was still present in the tissue following fixation and washes (see Appendix C,

panel Aii). Backfilled tadpoles were then embedded in paraffin and sectioned following previously detailed protocol (See Chapter 2.2.7) before being co-labelled with α3 primary antibody incubated with FITC secondary antibody to prevent false positive labelling. Results were imaged using either Photometrics Moment Camera (Appendix B, panel Bi-iii) or Nikon AX/AX R Confocal Microscope System.

2.2.10 Fluorescent Microscopy and Image Processing

The majority of α3-labelled tadpole cross-sections were imaged using Zeiss Axio Imager M2 fluorescence microscope equipped with Apotome2. Follow-up or alternative imaging was done using either a Zeiss LSM800 confocal microscope or a Nikon AX/AX R Confocal Microscope System. Prior to mounting in paraffin, the uptake of MN-backfilled tadpoles were assessed using a Photometrics Moment Camera to visualize the fluorescent dye. All comparative analyses were restricted to images taken from the same camera. Positive antibody expression was identified from the presence of a positive signal and cross compared to a control tadpole labelled solely with secondary antibody. Cells were identified by their morphology: positively labelled cell bodies are outlined by a labelled membrane which exhibits as a fluorescent rings encompassing a rounded structure, as defined in Picton et al. (2017). As the initial images from antibody optimization experiments were acquired using the Leica confocal microscope and later images were acquired using the Zeiss microscope, any cross-comparisons of fluorescence intensity values were restricted to images taken from the same microscope.

2.2.11 Fluorescence Intensity and Data Analysis

Fluorescence intensity was measured using FIJI (ImageJ) software. Prior to image analysis, all files were duplicated and converted to 8-bit. All image analysis was also applied to negative control and compared to the experimental group by normalizing each fluorescent intensity value to said control. From there, cross comparisons could be made both between

tadpoles and within tadpole sections across independent repeats2. The following quantitative methods for measuring positive α3 expression were adapted from a previous study (Couto et al., 2020). To estimate total average fluorescence intensity, measurements for the Area, Integrated Density and Mean Gray values were taken from each imaged anatomical section. The background fluorescence was also measured and subtracted from the total fluorescent intensity in the same equation. Termed as combined total fluorescence (CTF), fluorescent intensity was calculated, per individual section, using the following equation: CTF = Integrated Density selected cell - (Area selected cell X Mean background fluorescence). To measure and compare average pixel intensity dorsoventrally or laterally across a section, the same previous measurements were selected. Using the line tool in FIJI, five independent lines were drawn across the cells within the CNS section and a plot profile was drawn. This method allows for quantitatively testing whether grey value intensity varied across the CNS sections within each tadpole. Each data set was then saved and averaged across the length of the chosen section and a graph was plotted to demonstrate variations in α3 expression within a target CNS section.

All statistical analysis was carried out using GraphPad Prism (v9.0, GraphPad Software). Data sets were tested for normality using the Kolmogorov-Smirnov (K-S) normality test. Testing the means between two independent experimental groups was used with either an unpaired t-test or a Mann-Whitney U test. Tests for significant average difference between positive versus negative labelling data sets were conducted using either a one sample t-test or a Wilcoxon ranked t-test nonparametric data sets. Testing statistical significance between multiple groups, eg testing α3 expression across different developmental stages, was conducted using either a one-way ANOVA with Bonferroni Corrections for normally distributed data sets and a Kruskal-Wallis test was conducted with Dunn's multiple

[2] An experimental repeat is defined as conducting the same experiment, across multiple independent sessions spaced out across different days but utilizing the same experimental protocol. This enables experimenter to test repeatability of a protocol and track whether the results are reproducible every time experiment is conducted. Every repeat in my project featured tadpoles spawned from different breeding pairs to allow for testing across a broader population genotype.

comparison test as a post-hoc test for non-parametric data sets. Box plots and bar graphs were represented as mean ± standard error of the data set (SEM). Significance was represented in the graphs as $p \leq 0.05$ (indicated by *) $p \leq 0.01$ (indicated by **), $p \leq 0.001$ (indicated by ***) or $p \leq 0.0001$ (indicated by ****). Total number of measured data points within a data set were detailed as “N= X”. If population featured measurements taken from a tadpole versus a cell population this is specified in-text. Measurement units were also specified in-text (e.g. mm).

2.3 Results

2.3.1 α3 Expression Is Widespread Across Cell-Types which Comprise the SC

As previously stated, examining α3 expression in the tadpole SC was the primary focus of this project. The main analytical targets for this section included assessing whether α3 was present in the SC, where within the SC it was located, whether there was rostrocaudal variation of α3, whether expression was uniform within MNs, and identifiable RB sensory neurons within the SC. SC with positive α3 labelling (Figure 2.3 Ai) was contrasted to the CY3 negative control (Figure 2.3 Aii) which demonstrates that α3 expression is widely distributed within spinal cells comprising the SC.

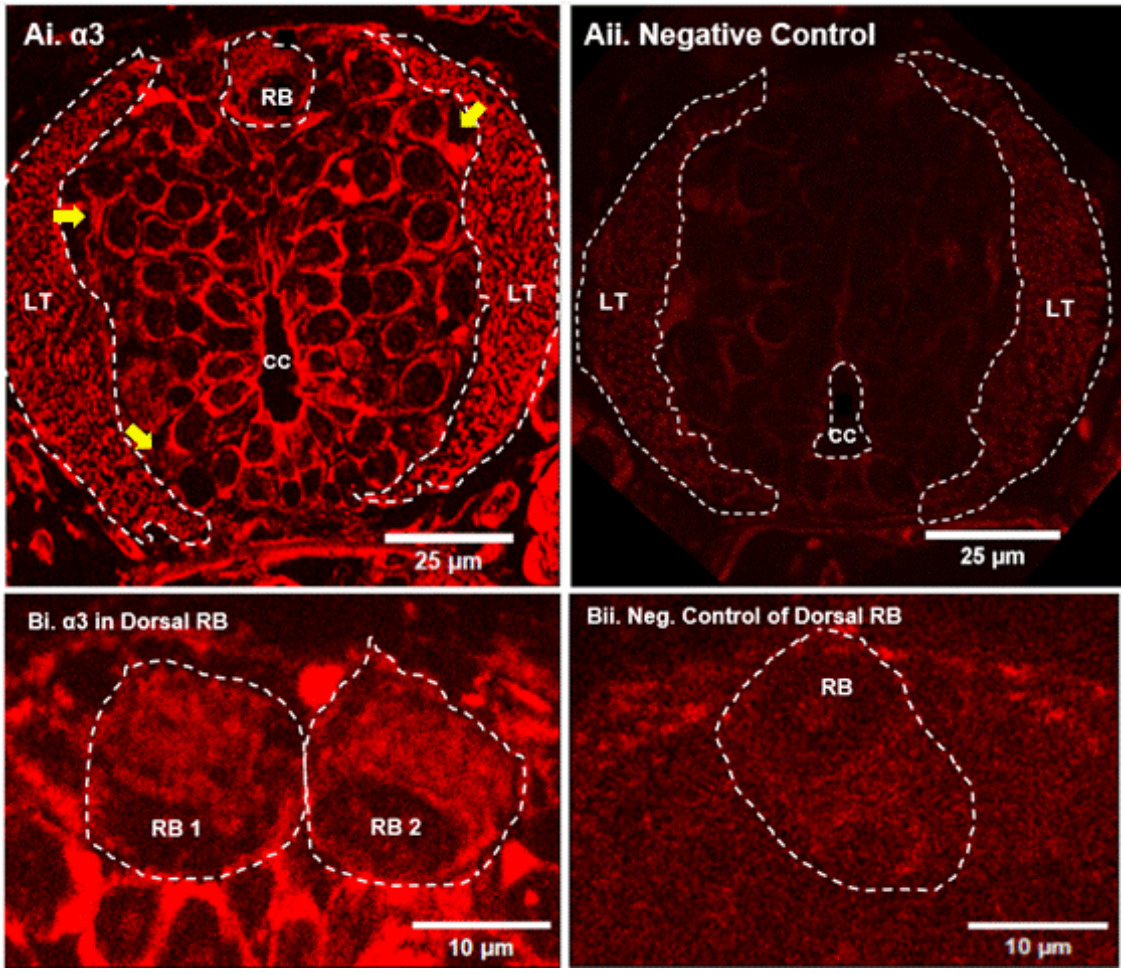

Figure 2.3: α3 is widely expressed within the spinal cell bodies comprising the SC. A. α3 expression was evaluated by comparing labelling on α3-labelled SC sections (Ai) to the negative control (Aii). α3 expression was assessed within notable anatomical regions including the LT (outlined by dashed line. B. Dorsal RB sensory neurons (outlined by dashed line) were also measured and compared between α3 labelled sections (Bi) and the negative control (Bii). (All images taken at 63X magnification).

There was visible variation in α3 expression which appears to differ across cell type and spatial region within the CNS.α3 expression is highly concentrated in the membrane of cells which border the CC (Figure 2.3 Ai). Based on their large size and spatial localization some of these strongly labelled cell types could be KA neurons which are CSF-contacting ciliated neurons (Dale et al., 1987; Yang, Wang and Strähle, 2020). A one sample t-test was conducted to compare whether fluorescence was higher in the positively labelled tadpole SC when normalized and compared to the negative control. Average fluorescence intensity was found to be significantly higher in the α3 labelled tadpoles ($t(21)=4.92$, $p\leq0.0001$, Mean ± SEM = 164.6 ± 13.14; N=22 tadpoles).

However, given the experimental constraints of this project, it is impossible to identify all specific cell types within the CNS accurately in sections where they are not specifically labelled. Identification of certain spinal cell types can still be done by assessing visible cues such as the cellular anatomy, soma size and spatial location within the SC. This method can be used fairly effectively to classify RB sensory cells, which are easily identifiable as they are located dorsally within the SC and possess a large soma (~20μm in diameter) (Figure 2.3 Ai labelled RB and outlined with dotted line)(Clarke et al., 1984). Analysis of α3 expression within RB neurons was conducted by comparing the normalized CTF values per cell. Fluorescence values were found to be significantly higher in the α3 labelled RB neurons ($t(31)=7.553$, $p\leq0.0001$, Mean ± SEM = 356.6 ± 32.2 %; N=30 RB neurons) when normalized and compared to the negative control (N=16 RB neurons). Furthermore, notably high fluorescence is also identifiable within the primary neurites of large neuronal cell bodies that project into the LT (Figure 2.3 Ai, yellow arrows bordering LT outlined by dotted line).

2.3.2 α3 Expression Does Not Vary Within Rostrocaudal SC Sections

Once α3 was affirmed to be present in the tadpole SC, I then measured the CTF of rostral and caudal SC sections to compare whether α3 varied in these regions. As tadpoles progress through larval developmental stages the tail lengthens, and the CNS is extended caudally (van Mier, Armstrong and Roberts, 1989a). This means that caudal SC regions

developed later than rostral regions and have previously demonstrated a developmental delay during mid to late larval development (Zhang et al., 2009a; Zhang, Issberner and Sillar, 2011).

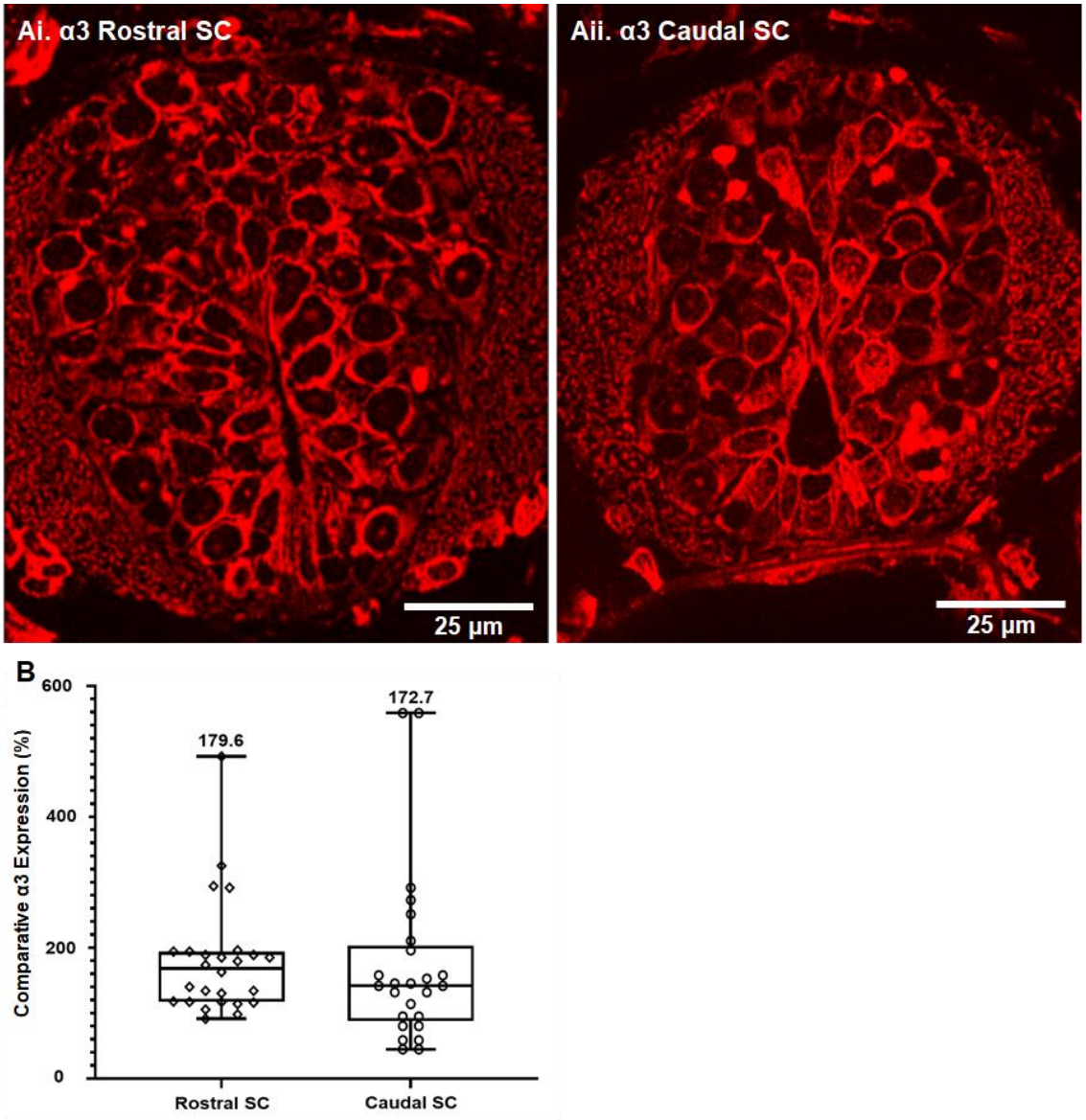

Figure 2.4: Expression of α3 is consistent across rostral and caudal SC sections. A. Expression of α3 was compared in rostral (Ai) and caudal (Aii) SC sections. B. Quantified values were averaged per tadpole (N=26) and found not to differ between the rostral and caudal data sets indicating that α3 was consistent along the length of the tadpole SC (Images in figure taken at 63X magnification).

To assess whether α3 differed between these two regions, sections from the previous data set were divided into rostral versus caudal data sets. Rostral sections were defined using the same parameters established in (Roberts and Clarke, 1982) which involved measuring the dorsoventral length and CC diameter of the SC (See Figure 1.4 Aii-Aiv in General Introduction). This length is longer in rostral SC (~150 μm) as is the CC diameter (~50-75 μm) (Figure 2.4 Ai) when compared to caudal sections which are dorsoventrally shorter (~100 μm) and feature a smaller CC diameter (~49-25 μm) (Figure 2.4 Aii). Neither data set passed the K-S normality test and so a non-parametric alternative was employed. A Mann-Whitney U test demonstrated that the CTF, and therefore amount of α3 measured, did not differ between the rostral (mean ± SEM = 179.6 ± 17.27 %, N = 26 tadpoles) and caudal SC sections (U = 269.5, n.s, caudal mean ± SEM = 172.7 ± 26.74 %, N = 26 tadpoles, Figure 2.4 B). This indicates that α3 is distributed equally across the rostrocaudal SC length.

2.3.3 α3 Expression is Prominent in Lateral versus Midline SC Cells

As noted, α3 expression was widely distributed across all spinal cells comprising the SC however in many sections there was notably higher fluorescence intensity observed in midline cells, which border the CC. The percent occurrence of this α3 expression pattern was noted in majority of tadpoles (N = 19/26) with expression in lateral cell populations appearing to be much lower by comparison (Figure 2.5 Ai). In the other tadpoles, α3 appeared equally distributed across all lateral and midline cell populations (Figure 2.5 Aii).

Importantly, this expression pattern was consistent across all sections taken from an individual tadpole and there was no rostrocaudal variation noted in this trend. To affirm whether this distribution was quantifiably identifiable, the fluorescence intensity was evaluated based upon spatial location within the SC. Tadpoles were first classified into two groups based upon where α3 expression was spatially distributed: SC sections with strong α3 expression in cells surrounding the CC (termed Midline α3; Figure 2.5 Ai) and sections where α3 was more equally distributed across the entire SC (termed Uniform α3; Figure 2.5 Ai).

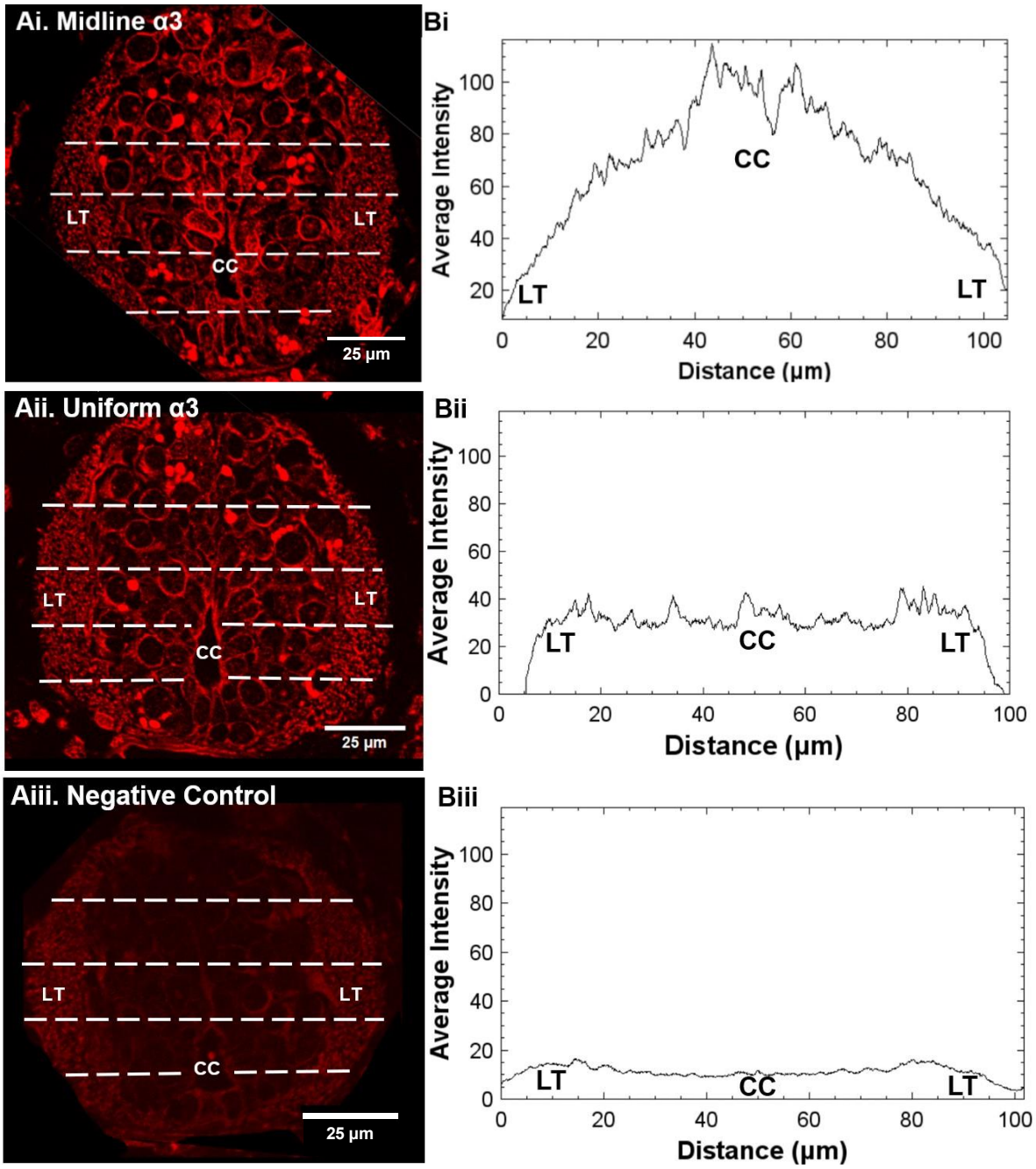

Figure 2.5: α3 is Highly Expressed in Cell Bodies Bordering the Central Canal. A. SC sections were categorized depending upon whether the highest intensity (representing α3) values were localized to cells bordering the central canal (Ai), α3 that was broadly and equally distributed (Aii) and compared to the negative control group, comprised of tadpole sections that were not incubated with α3 primary (Aiii). B. Line graphs corresponding to the representative SC images were graphed tracking CTF across the spatial SC regions: α3 concentration around midline (Bi), α3 distributed uniformly (Bii) and the negative control (Biii). (Images in figure taken at 63X magnification).

To quantify and measure α3 expression within the sections selected from each tadpole group, a line graph was drawn averaging cellular intensity over distance (μm) (Figure 2.5 Bi-Biii line graphs). The fluorescence intensity was calculated based off the averaged grey values taken from a series of horizontal measurements spanning the dorsoventral region of selected representative spinal cord sections, from lateral tract (LT) through cells bordering central canal (CC) and through to the opposite LT (distance measured indicated by dashed line and then plotted as a line graph across distance).

Due to a K-S test demonstrating that results were not normally distributed in the midline and distributed expression data sets, a Kruskal-Wallis test was run on the data sets from the three groups. The results demonstrated that the average fluorescence intensity did significantly vary between the negative control see (Figure 2.5Aii SC image for reference) and the two positively labelled α3 groups ($H(3)=2020$, $p\leq0.0001$) across the entirety of the SC, further validating that for α3 was present in the positively labelled groups. A multiple comparison Dunn's test also showed significant variance between the latter two α3 expression groups ($p\leq0.0001$). To further explore this difference, the values from the cellular region surrounding the CC were specifically compared between the three groups and again found to be significantly different ($H(3)=252.9$, $p\leq0.0001$). A Dunn's test also found significant difference in expression between the negative control group and the two positively labelled α3 groups ($p\leq0.0001$), and again between the latter two α3 expression groups ($p\leq0.0001$) with average intensity values indicating higher expression in the Midline group compared to the Uniform group. This expression distribution towards midline cells is worth further consideration though it could be due to the anatomy of this cell type. The cells expressed along the SC midline have been identified previously as ciliated ependymal cells which aid the CSF circulation through the tadpole ventricles (Roberts and Clarke, 1982).

2.3.4 α3 was Detected in All Backfilled MNs Within Tadpole SC

The previous quantification and analysis of α3 within cells that make up the spinal cord indicates that α3 is present to varying degrees within a majority, if not all, of cells comprising

the tadpole spinal cord (Figure 2.3 and Figure 2.5) and therefore demonstrates that α3 is likely expressed within all neuronal subtypes. Previous electrophysiological work has detected the presence of the usAHP in a subset of spinal populations (Picton et al., 2017; Picton, Sillar and Zhang, 2018; Hachoumi et al., 2022), with dINs initially being reported to not express the usAHP, and therefore likely not express α3. However, the usAHP has been shown to be masked in dINs which co-express a cationic Ih current that counterbalances the hyperpolarization induced by dynamic sodium pumps (Picton et al., 2017). Therefore, α3 is likely more broadly expressed across spinal cell populations than previously reported, including MNs.

To test this hypothesis directly, α3 was co-labelled (Figure 2.6 Ai) on the membrane of MNs that were backfilled with dextran-conjugated rhodamine dye (See Materials and Methodology). Backfilled MNs can be identified in the figure below by their red fluorescent labelling outlining large somata bordering the LT of the SC (Figure 2.6Aii). The bright red labelling in the torn portion of the right myotome is where the rhodamine-tipped needle was deposited, traveling through the ventral root to the MNs and even crossing over to the left ventral side of the section. When overlaid with the α3 labelling, the overlapping fluorescence on the MN membrane appears orange to yellow, indicating α3 is also expressed on the membrane of these cells (Figure 2.6 Aiii).

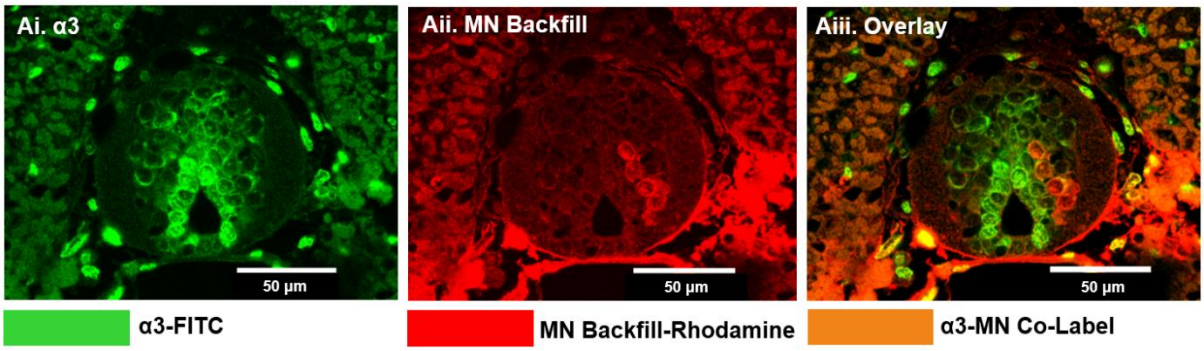

Figure 2.6: α3 Expression Amount is Variable in Backfilled MNs. A. α3 primary was co-labelled with FITC (Ai; green box indicates labelled α3 labelling) on MN backfilled spinal cord sections (Aii; red box indicates backfilled MN colour) and overlaid using FIJI Software to visualize overlapping fluorescence (Aiii; coloured orange in rhodamine backfilled MN membranes where α3 is co-labelled using FITC secondary). The CTCF of α3 labelled cells were cross compared to CY3 only incubated SC section MNs to demonstrate the positive labelling of α3 in MNs (all images were taken at 60X magnification).

To assess positive labelling of α3, the CTF each α3 labelled cell body of the corresponding backfilled MN cell body was calculated in images taken with exposure to green fluorescence only (Figure 2.6 Ai and Appendix D). The same was done for MN backfilled sections that were not labelled with α3, which therefore acted as the negative control for quantitative comparison (Appendix D, panel Biii). α3 labelled cells were then normalized to this negative control group. A one sample t-test demonstrated that the fluorescence intensity of MNs co-labelled with α3 primary was significantly higher than unlabelled cells from the negative control group ($t(5)=14.26$, $p \leq 0.001$, mean ± SEM = 372 ± 64 %, N=6/6 MNs, N=3 tadpoles). This quantitative analysis indicates that α3 is found to be expressed in the backfilled MNs from this experiment.

2.3.5 Expression of α3 Is Conserved in Albino and Wild Type Phenotypes

Another aim of this project was to compare whether α3 expression varied within the SC of WT (Figure 2.7 A) and albino (Figure 2.7 B) tadpoles. This was assessed by comparing the labelling patterns and CTF of α3 labelled SC sections from both tadpole phenotypes. From the images taken, α3 is noted to localize to the same spatial and anatomical regions within the SC in both groups. Mainly, there is widespread expression across all spinal soma comprising the SC with prominent labelling in midline cells bordering the CC.

Albino tadpoles also demonstrated notably higher α3 expression in spinal cells bordering the CC compared to lateral soma. Furthermore, while expression appears lower in cells border the LT of albino SC sections, this was also observable for many WT tadpoles (N = 10/26 tadpoles). As previous tests have demonstrated (Figure 2.5 B line graphs), while fluorescence appears comparably lower in the LT α3 is still quantifiably present.

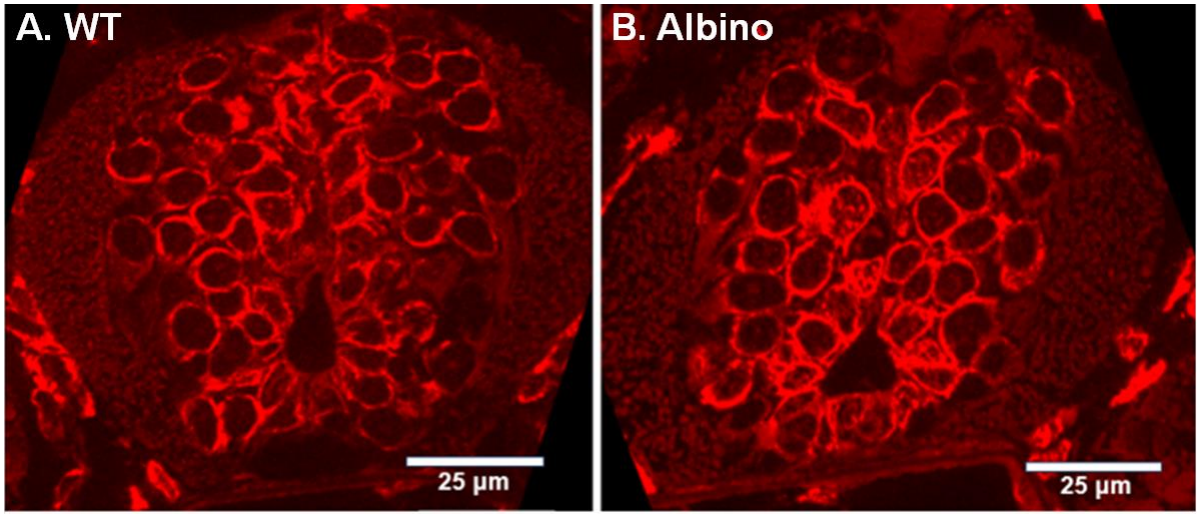

Figure 2.7: α3 Expression Did Not Differ Between WT and Albino Tadpoles. A. Positive α3 labelling on the SC of WT (A) compared to albino (B) NF stage 42 tadpoles. Spatial patterning of α3 is noted to be conserved between the two phenotypes. (Images in figure taken at 63X magnification).

The CTF of SC sections was also compared between the two phenotypes. The data was not found to be normally distributed in the WT data set (N = 26 tadpoles), a finding not shared in the albino data-set which was normally distributed (N = 4 tadpoles), a non-parametric Mann-Whitney U t-test was run to compare whether α3 expression significantly differed within the SC of WT (mean ± SEM=164.6 ± 8.53%) and albino (mean ± SEM= 129.4 ± 10 %) tadpoles. There was found to be no significant difference in average fluorescence intensity between the two groups (U=352, p=0.198, n.s). Though experimental repeats were low in the albino data set, the consistency of the measured CTF data set in that group (which passed the K-S normality test), demonstrates that α3 expression is not likely to differ between WT or albino tadpoles. This finding further indicates that α3 expression is likely conserved between the two phenotypes.

Overall, WT and albino phenotypes share observable overlap in α3 expression levels and in any spatially distributed variation in α3 expression within the same SC anatomical regions, mainly around midline cells bordering the CC. Considering that α3 function has been noted to be phylogenetically conserved across species (Picton et al., 2017), along with the above outlined similarities in α3 expression within the SC observed in the two groups, it is very

likely that α3 function is also conserved between both tadpole types, at least at this developmental stage.

2.3.6 α3 is Expressed in the Forebrain

Following analysis of α3 in the tadpole SC, the opportunity was also taken to assess expression of this subunit in the FB and rostral CNS regions such as the MB and HB. As done previously, all positively labelled forebrain sections were directly compared to a negative control in order to assess the spatial distribution of α3. It is important to note that α3 is expressed in similar cellular and anatomical regions within the FB as was noted within the tadpole SC (Figure 2.4). For example, α3 is expressed ubiquitously within the membrane of cell bodies that comprise the FB, with even distribution in cells bordering the lateral ventricle (LV) and LT (Figure 2.8 Ai). The FB contains two ipsilateral, symmetrical regions and distribution of α3 was noted to be ubiquitous across the cells comprising the two lobes of the FB.

The CTF of FB sections was also measured and compared to ensure that positively labelled sections showed accurate α3 expression within this region. Quantitative comparison of negative control (Figure 2.8 Aii) versus α3 (Figure 2.8 Ai) labelled FB sections was conducted to assess whether α3 was present in the FB. This was done by measuring the CTF of the FB region in each tadpole (N=3 tadpoles) and normalizing these values to the negative control. A one sample t-test was run to compare whether fluorescence intensity values were measurably higher in α3 labelled tadpoles versus in the CY3 negative control group. Fluorescence intensity in the α3 group was found to be over twice as high ($t(2)=7.48$, $p \leq 0.05$, N=3 tadpoles, mean ± SEM=237.4±18.36%) compared to the negative control group. This statistical test indicated that α3 is positively expressed in the forebrain.

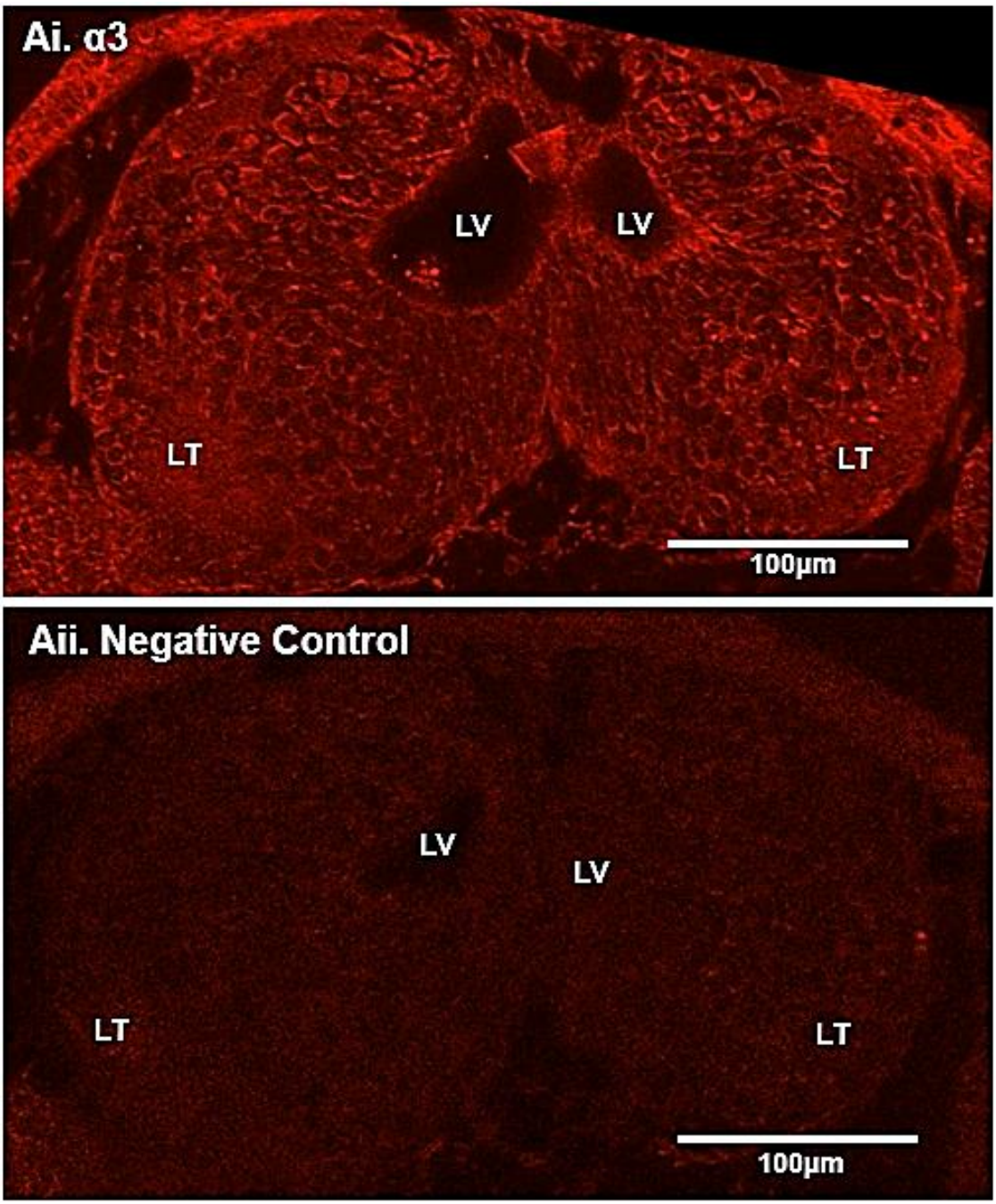

Figure 2.8: α3 is Present in the Forebrain. A. Visual comparison of α3 immunolabelled sections (Ai) to the negative control (Aii) of NF 42 tadpole FB sections indicates that α3 is present in the FB, with distribution across all soma comprising this region. (Images in figure taken at 40X magnification).

2.3.7 α3 is Expressed in the Midbrain

The next region evaluated was the MB, which is caudal to the FB. Sections were evaluated rostrocaudally (Figure 2.9 Ai-Aiv, labelled in order) and all demonstrated a comparable patterning of α3 within the same spatial regions, mainly in the distribution of α3 within cell bodies comprising the MB. a consistent feature of α3 expression across each section was the comparatively high fluorescence in cells bordering the 3rd ventricle (Figure 2.9 Ai-Aiv, white arrows). This area is not solely comprised of neurons and could indicate that α3 is likely positively expressed within the glial cells that border the tadpole ventricles.

The measured CTF again was used to assess whether α3 was quantifiable in the immunolabelled MB sections. A one sample t-test was run to compare whether fluorescence intensity values differed in α3 labelled tadpoles. Fluorescence intensity in the α3 group was found to be significantly higher compared to the CY3 group ($t(5)=2.88$, $p \leq 0.05$, N=6 tadpoles, Mean ± SEM=231.1±45.5%). Given that the normality test showed that fluorescence intensity values did not vary significantly it can be assumed that intensity is the same across all rostrocaudal MB sections, remaining consistent throughout rostrocaudal MB regions.

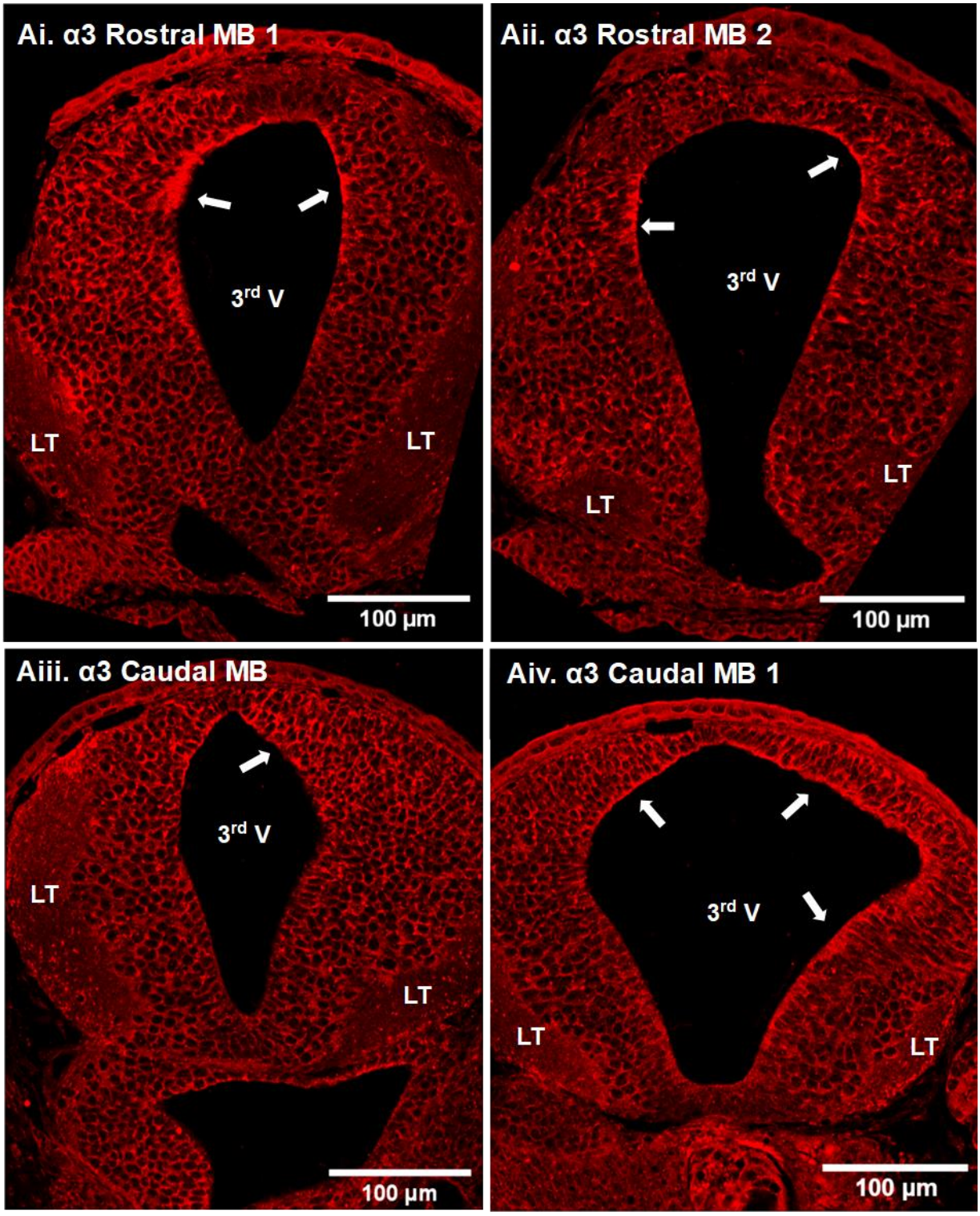

Figure 2.9: α3 is Present in the Midbrain. Positively α3 labelled midbrain sections demonstrating how the anatomical structure varies rostrocaudally (Ai-Aiv). Regions within each MB sections where there was comparably high α3 are indicated by white arrows. All images demonstrate positive labelling which is further demonstrated by comparison to negative control MB sections (Appendix E) (Images in figure taken at 40X magnification).

2.3.8 α3 is Expressed in the Hindbrain

The next CNS regions examined was the HB. Imaging of positively labelled HB sections show that α3 is widely expressed across all neurons comprising this region (Figure 2.10 Ai), which is consistent with the expression patterns noted in the SC (2.3.1-2.3.4), FB (2.3.6) and MB (2.3.7). At higher magnitude, and improved image resolution, α3 is shown to be ubiquitously expressed however there is a notable variation in the amount of α3 expressed in each region within the HB with the highest fluorescence visible in the (potentially glial) cells directly bordering the fourth ventricle and the cells directly bordering the LT as well as in the primary neurites projecting into the LT (Figure 2.10 Aii).

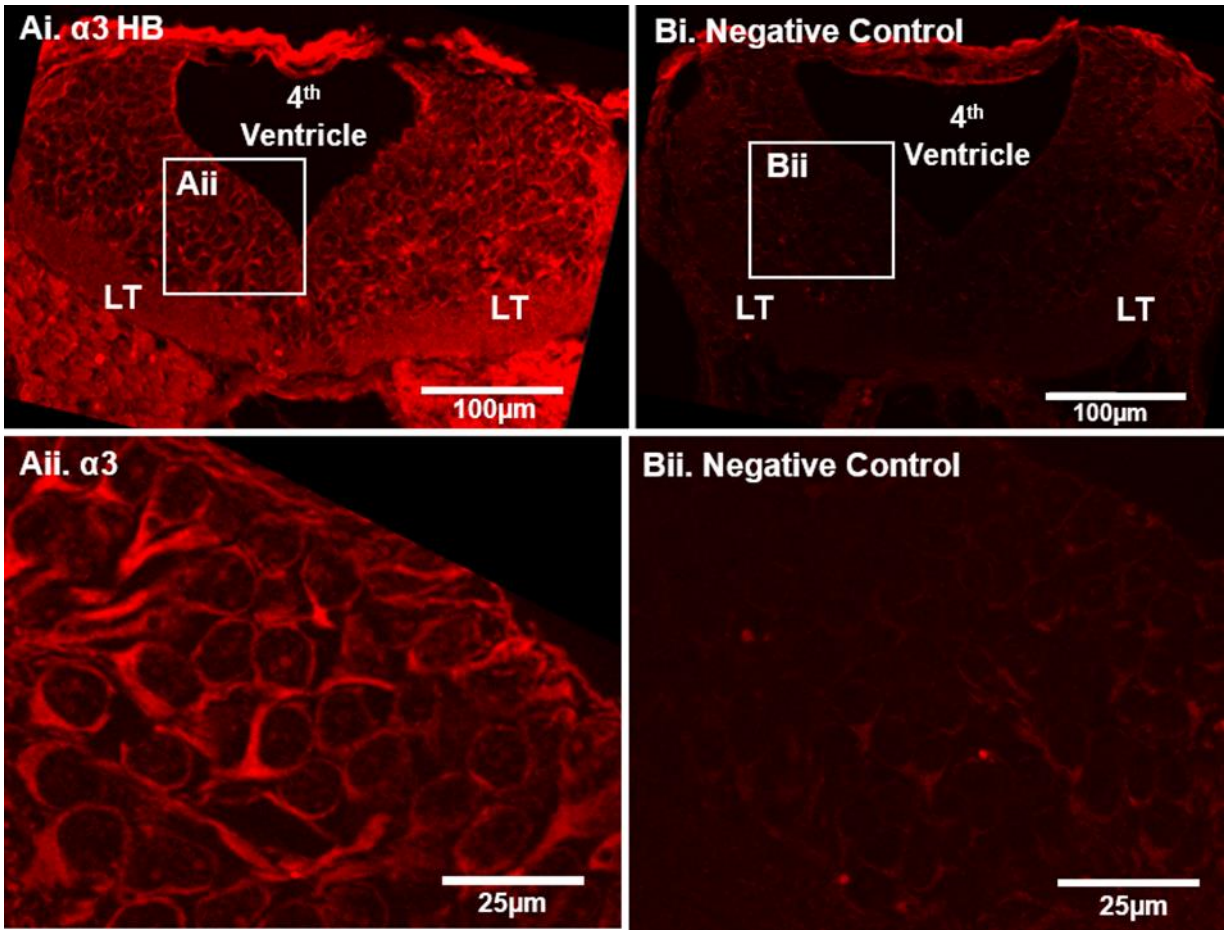

Figure 2.10: α3 is Widely Expressed Within the Hindbrain. A-B. Entire α3 labelled sections (A) were compared to the negative control HB sections (B). Higher magnification images (Aii & Bii) demonstrate labelling is fairly consistent between cells directly bordering the 4th ventricle and in more ventral cells in HB sections from the positive experimental condition (Aii). (Ai-Bi panels taken at 20X magnification; Aii-Bii panels taken at 63X magnification).

As in previous sections, the CTF of positively labelled sections was also compared to the HB of the negative control. The α3 data set was not found to be normally distributed, verified by a Kolmogorov-Smirnov test, and a Wilcoxon t-test was run to assess whether fluorescence intensity differed between the two group. CTF was found to be significantly higher in the HB of positively labelled tadpoles (W=118, p≤0.0001, N=15 tadpoles, mean ± SEM=248.6 ± 35.64%) compared to the negative control. This statistical significance therefore indicates that α3 is expressed within cells comprising the tadpole HB. Analysis of fluorescence intensity across cell layers between the fourth ventricle and the LT of tadpole hindbrain section was also conducted to see if an α3 expression gradient could be identified and expression was found to be quantifiably higher in cells bordering the fourth ventricle, as observed prior to measuring the CTF (p≤0.0001, N=12 tadpoles). Finally, to ascertain whether the level of α3 expression varied across the rostrocaudal tadpole CNS, the normalized CTF were compared across the MB (mean ± SEM = 231.1 ± 45.46%), the HB (mean ± SEM = 248.6 ± 35.6), and the SC (mean ± SEM = 164.6 ± 13.14%). Due to low experimental repeats, the FB was omitted. Neither the HB nor SC data sets were found to be normally distributed therefore a Kruskal-Wallis test was run and found no significant differences between the three groups (H=4.2, n.s). A follow up Dunn test demonstrated no quantifiable difference in α3 expression between any of these regions indicating that α3 did not significantly vary throughout the rostrocaudal CNS.

2.3.9 α3 is Expressed in the Myotomes

Myotomes are the segmented axial muscles on the left and right sides of the trunk and tail that the tadpole uses to generate propulsive swimming. Anatomically the myotomes are distributed along the tadpole CNS, beginning at the otic capsule where it is ventral to the CNS (See Chapter 1.4.2) before expanding to encapsulate the SC. As previous studies have found limited ATP1A3 expression in skeletal muscle therefore my project aimed to immunolabel and quantify α3 expression within myotome sections therefore indicating whether it is present within this tissue type.

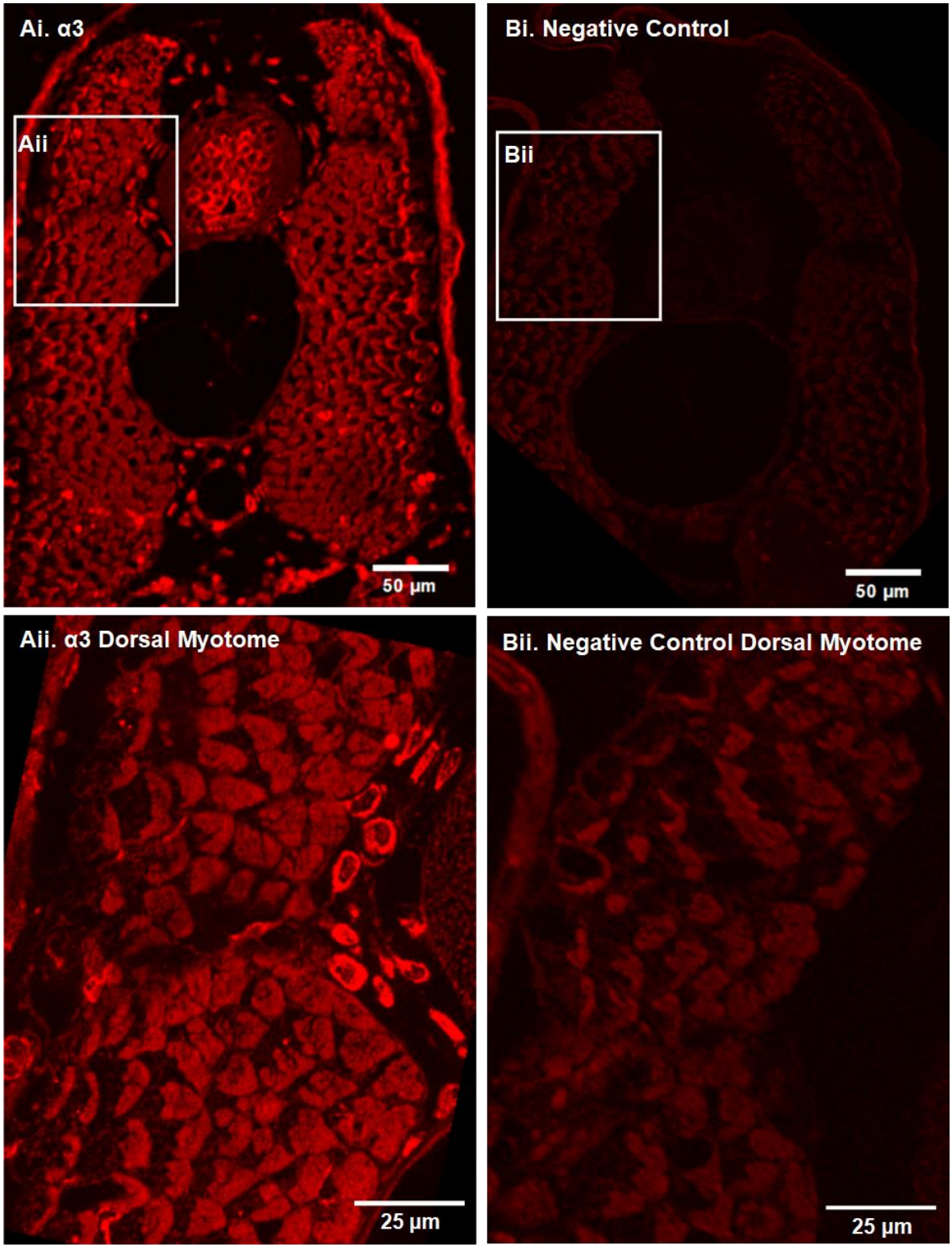

Figure 2.11: α3 is Present in the Myotomes. A. Positive expression of α3 was noted in the SC-level myotome of NF Stage 42 tadpole (Ai) when compared to the negative control (Aii). B. Higher magnification of outlined dorsal regions (enclosed in white box in Ai and Bi panels) demonstrate that α3 labelling is consistent throughout the myocytes comprising the myotome. Despite observable autofluorescence in both experimental and control myotome cross-sections, fluorescence is notably higher at greater magnification in positively labelled sections as observed in α3 labelled myotome (Aii) compared to the negative control indicating that α3 is present in tadpole myotomes (Bii). [Ai-Bi panels taken at 20X magnification, Aii-Bii panels taken at 63X magnification].

To quantify fluorescence intensity between the α3 labelled tadpoles and the CY3 only tadpoles, five sections from each tadpole, across the rostrocaudal CNS but mainly around the SC, were measured and normalized to a negative control. The average CTF from each individual tadpole was compared to the average CTF of negative control tadpoles. A Wilcoxon t-test found there to be a statistically significant difference between the two groups with higher fluorescence intensity measured in the α3 labelled tadpoles ($W=152$, $p \leq 0.001$, $N=24$ tadpoles; mean ± SEM=280.7 ± 38.3 %). This statistically higher fluorescence intensity indicates that α3 is present in the myotomes at this stage of development.

2.3.10 α3 is Expressed in Cells Comprising Skin Bilayer

Skin demonstrated notable fluorescence in most α3 incubated sections (Figure 2.12 Ai) indicating potential expression on the cells in this tissue type. Notably, the sections from the negative control group also tended to demonstrate some fluorescence (Figure 2.12 Aii) indicating that skin is auto fluorescent when exposed to high intensity light, as is used in fluorescent microscopes.

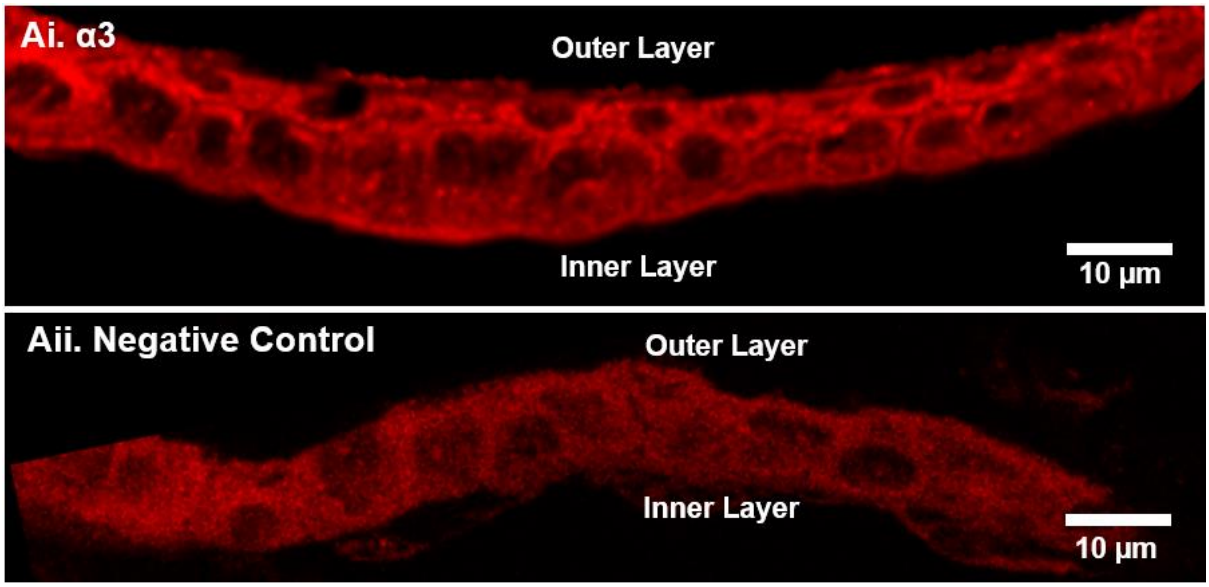

Figure 2.12: α3 is Highly Expressed in the Outer Bilayer of the Skin. A. Positive expression of α3 was noted in the skin cells of NF Stage 42 tadpole (Ai) after comparison to the negative control (Aii). There was a significant difference in the measured fluorescence intensity between the two experimental groups ($p \leq 0.001$) indicating that α3 was positively labelled by primary antibody [Images taken at 63X magnification].

To assess whether skin cells were expressing α3, as indicated in positively labelled sections (Figure 2.12 Ai) or auto fluorescent the CTF values of skin from α3 and negative control tadpoles were compared. A one sample t-test was run and found significantly higher fluorescence in the α3 labelled skin compared to the negative control ($t(19)=3.63$, $p\leq0.001$, mean ± SEM = 536 ± 138.6%, N=20 tadpoles, Figure 2.12). This notably high statistical significance indicates that, despite the skin's natural autofluorescence, it can be assumed that the measured fluorescence intensity measured is indicative of positive α3 expression in this tissue type.

2.3.11 α3 is Expressed in the Eye

When evaluating α3 expression the expectation is that this protein would be present in every retinal layer within the eye (Rahman et al., 2015; Liao et al., 2022a). To first quantify α3 expression in the eye, the fluorescence intensity of the whole eye (Figure 2.13 Ai) was measured and normalized to the CTF taken from the whole eye of the negative control (Figure 2.13 Aii). A one sample t-test found the average intensity between the retinal and lens regions were significantly different ($t(4)=4.38$, $p\leq0.05$, N=5 tadpoles, mean ± SEM=181.4±18.58%; Figure 2.13 B). These results lend confidence to the assessment that α3 is positively expressed within the retinal and photoreceptor cell types that comprise the NF stage 42 tadpole eye. To better ascertain which retinal layers were positively expressing α3, I selected and measured using ImageJ the fluorescence intensity of seven distinct regions of the eye: the ONL (comprised of photoreceptors such as rods and cones), the OPL, INL, IPL, the GCL, CMZ and the lens (See General Introduction: The Tadpole Eye).

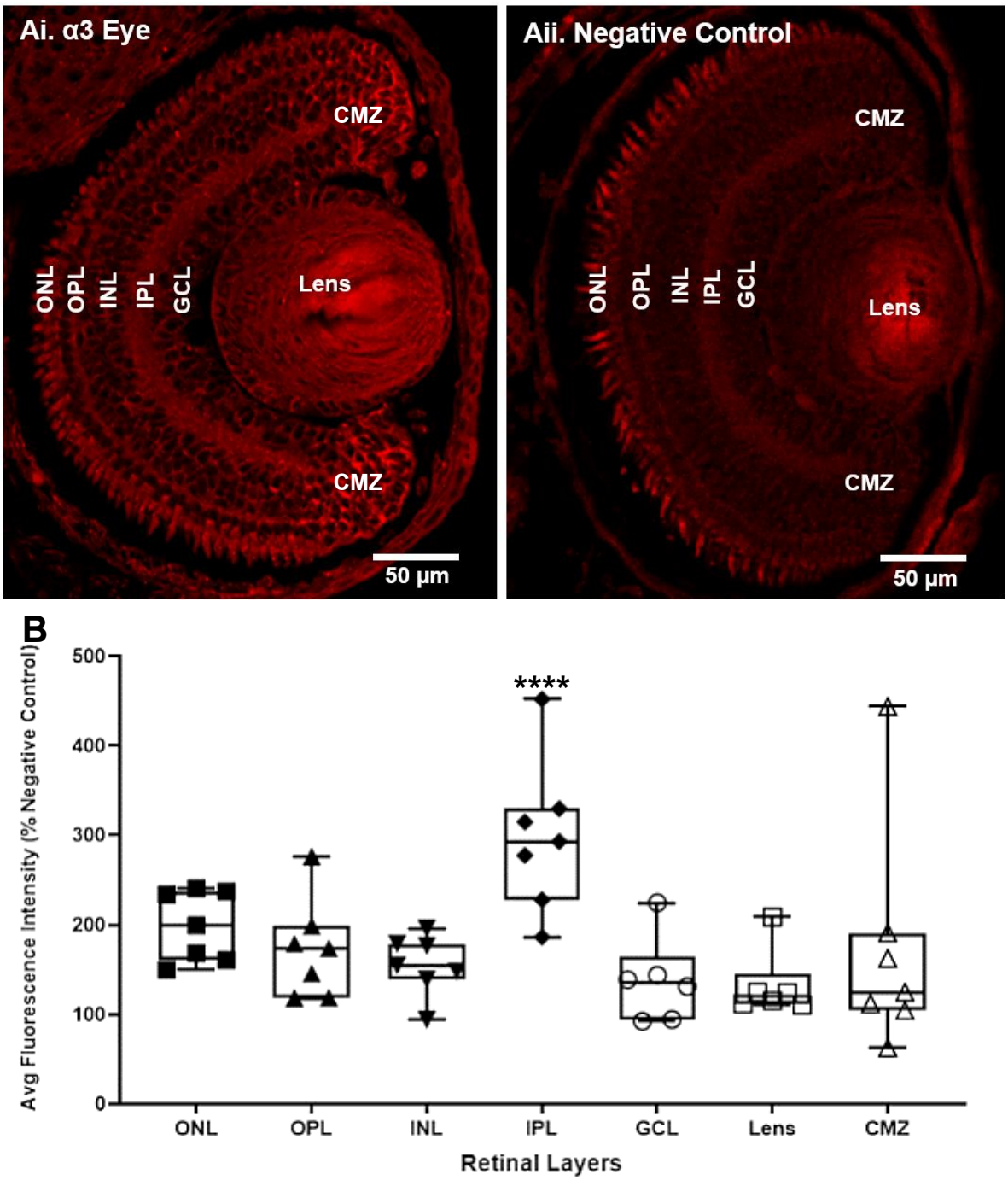

Figure 2.13: α3 is Variably Present in Eye Retinal Layers. A. Positive expression of α3 was found in the eye of NF Stage 42 tadpole (Ai) after comparison to CY3 only negative control (Aii). Each retinal layer was cross compared to fluorescent intensity measurements taken from a negative control and found to be present in each layer ($p \leq 0.05$) except for the GCL, Lens and CMZ. B. Box plot representing CTF values of retinal layers. A One-Way ANOVA found that α3 expression was highest in the IPL ($p \leq 0.0001$; represented by **** in panel B). (ONL: Outer Nuclear Layer, including rods and cones; OPL: Outer Plexiform Layer; INL: Inner Nuclear Layer; IPL: Inner Plexiform Layer; GCL: Ganglion Cell Layer; CMZ: Central Marginal Zone) (All images taken at 40X).

These findings almost completely fall in line with the expectations presented in Rahman et al., 2015 (Rahman et al., 2015). And while the quantitative comparison found no statistical difference between either the lens ($t(2)=7.48$, n.s, mean ± SEM = 132.5 ± 15.39%, N=3) or the GCL and the negative control, the mean fluorescent intensity in these regions of the α3 labelled tadpole group was measurably higher compared to the negative control (set to 100%). Aside from this, the main finding is that that α3 is positively expressed in the cell types that comprise the majority of retinal layers within the tadpole eye. Further experimental repeats could elucidate whether α3 is positively expressed in auto fluorescent regions such as the lens.

2.3.12 Expression Across Developmental Stages

To assess whether α3 labelling was consistent with prior mRNA measurements tracking expression across different stages of development (Session et al., 2016a), α3 was immunolabelled in the extracted protein taken from the whole body of *Xenopus* embryos and larvae from the following developmental stages: stage 20, stage 28, stage 32, stage 37/38, stage 42 and stage 45 (Figure 2.11). Since the data sets were not found to be normally distributed, a Kruskal-Wallis test was conducted to compare whether α3 expression varied across these stages. It was found that values did not vary significantly between developmental stages ($H(6)=4.025$, $p=0.55$, n.s.; Figure 2.11A) with a follow-up multiple comparison Dunn's test showing there was no significant difference between any single pair across the developmental stage data sets.

My findings did indicate that following NF stage 40, where Session et al., (2016) terminated their experiment, there is a very slight increase in α3 expression occurring between NF stage 42 and 45 although further experiments conducted on protein from later NF stage *Xenopus* tadpoles is still needed to verify this potential α3 increase as this difference was not found to be statistically significant when directly measuring variation in α3 expression via immunolabelling of the protein directly rather than from tracking changes in mRNA transcripts as was done by Session et al., (2016).

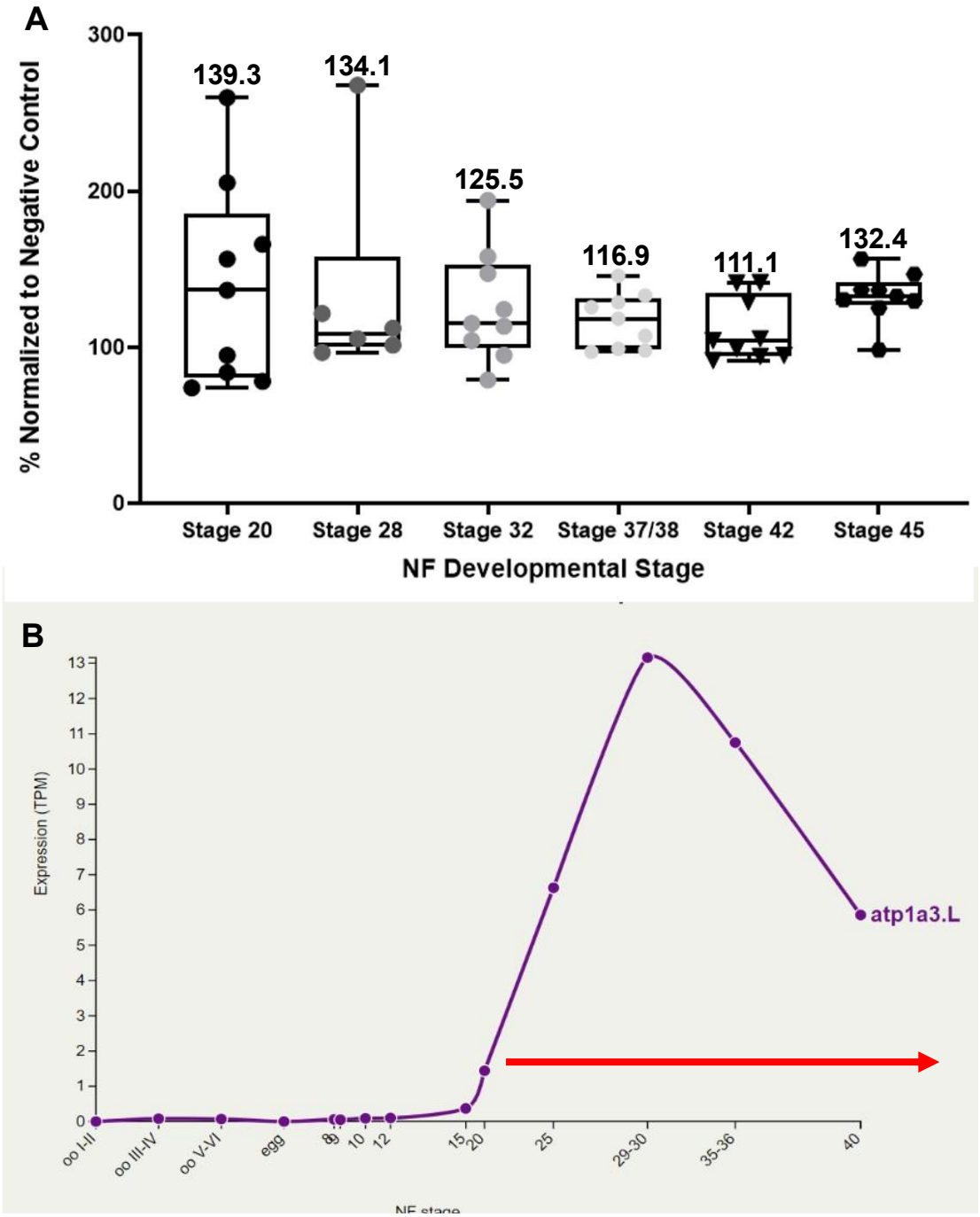

Figure 2.11: Average Expression of α3 Protein Across X. laevis NF Developmental Stages. A. In-lab testing for average α3 expression per developmental stage (A) from embryonic to larval stages in tadpoles. B. Line graph tracking ATP1A3 expression across a similar range of developmental stages, estimated by tracking *Xenopus* RNA. Expression levels were measured by mapping paired-end RNA-sequence reads to predicted full length cDNA, with TPM standing for transcripts per one million mapped reads [B, red arrow indicates stages tested and presented in panel A] (Bars represent Mean ± SEM).

Brief Summary of α3 Immunolabelling Experiments

1. Immunolabelling of α3 revealed broad expression of this catalytic subunit across spinal cells comprising the SC structure with particularly high fluorescence detected in midline cells bordering the CC. Within spinal cells, α3 immunolabelling was mainly restricted to the cell membrane and primary neurites.

2. Between the MB HB and SC regions, α3 expression was found to be measurably consistent indicating α3 did not form a rostrocaudal gradient within tadpoles. Furthermore, α3 was evenly distributed along rostral and caudal SC regions.

3. The backfilled MNs were shown to express α3 though fluorescence values were found to vary per co-labelled MN. This could indicate that while α3 is widely (potentially ubiquitously) expressed across cells within the CNS, it is likely restricted and variable per cell populations.

4. Non-CNS tissue was also found to express α3. Quantifiably higher expression values were noted in the myotomal and skin tissue in comparison to the negative control, indicating that α3 was present in these cell types.

5. Within the tadpole eye, α3 was found to be highly expressed in the IPL retinal layer but fluorescence values were not statistically significant in other regions. These findings indicate that α3 is not uniformly expressed across all cell types within the eye.

2.4 Discussion

2.4.1 α3 Expression Was Consistent Across CNS Regions

A series of IHC experiments were conducted to label the α3 subunit of the sodium pump in *Xenopus* tadpoles, identify the tissue, and cell types, in which α3 is present and finally investigate how α3 varies across neurons and in other tissue types. I was able to visualize expression of α3 within the tadpole CNS from the forebrain to the caudal spinal cord and cross-compare both the rostrocaudal and the dorsoventral expression patterns.

Previous research has found that in embryonic zebrafish (60 hpf) α3 expression was distributed across a rostrocaudal gradient within the CNS with higher α3 expression occurring in regions rostral to the SC such as the hindbrain (Doğanli et al., 2013). A similar rostrocaudal expression gradient has also been noted in other species, including humans (Smith et al., 2021). Considering the conserved function of tissue-specific sodium pumps across different species it was worthwhile to explore whether a similar rostrocaudal gradient in α3 expression also occurs in *Xenopus* tadpoles. When comparing across the entire CNS there were higher CSF values measured in rostral MB (mean ± SEM = 231.1 ± 45.46%), the HB (mean ± SEM = 248.6 ± 35.6%) regions compared to the SC (mean ± SEM = 164.6 ± 13.14%). However, no statistical significance was detected indicating that CTF values, and therefore α3, did not vary immensely across these three regions. When testing solely within the SC, rostrocaudal expression of α3 was also found not to vary along the entire SC length (Figure 2.4).

During early larval development (~NF stage 29/30) the tail begins to lengthen caudally forming myotomal segments which are innervated by newly differentiated SC spinal cell layers. Therefore prior to the advent of free swimming, larval spinal circuitry develops with a rostrocaudal delay along spinal circuits, which are repeated along myotomal segments (Huang and Hockaday, 1988; van Mier, Armstrong and Roberts, 1989a). Between NF stage 37/38 and NF stage 42 there is a notable maturation of caudal, newer SC sections that is

occurring with the segregation of neural circuits and the formation of distinct motor pools along the SC (Combes et al., 2004; Zhang, Issberner and Sillar, 2011). By NF stage 42, the maturity of neural circuits along the rostrocaudal CNS is more consistent. Therefore, the lack of variation in α3 expression across the entire SC of rostral and caudal regions would indicate that the α3-expressing dynamic sodium pumps underlie a phylogenetically conserved mechanism within these spinal cells. This underlying function is very likely the usAHP which confers an STMM on neural circuits (Zhang and Sillar, 2012) but has not previously been reported to be widely expressed in spinal cell populations (Zhang et al., 2015; Picton et al., 2017; Hachoumi et al., 2022). The variable detection of the usAHP in electrophysiological recordings is therefore a result endogenous modulation, such as by NO (Hachoumi et al., 2022), or masked by an inward cationic current such as the Ih current in dINs (Picton, Sillar and Zhang, 2018).

Another conserved consistency in α3 expression was noted in its distribution within each spinal section with comparably high α3 expression noted in midline spinal cells bordering the ventricles and CC (Figure 2.5 Ai). This strong labelling in regions directly in contact with CSF flow likely indicates the potential positive expression of α3 within KA and ependymal cells that are known to border this region (Roberts and Clarke, 1982; Dale et al., 1987; Yang, Wang and Strähle, 2020). These midline cells presented with unique expression patterns, with fluorescence often appearing “hairy” in comparison to more lateral spinal cells (Figure 2.6 Ai). This patterning could account for the measurably higher α3 population detected on these cell types with some SC sections fluorescing so brightly in this region that it visibly obscured the positive labelling of α3 in lateral cells, though high fluorescence was still measurable on these cells (Figure 2.5 Bii).

One explanation this difference in labelling could be due to the structure of the anatomical structure of ciliated ependymal cells. Ciliated ependymal cells possess a pear-shaped soma which tapers towards the CC. The ependymal surface of the soma project cilia into the CC although this is not always consistent with some cilia projecting from the soma. It is possible

that this “hairy” fluorescence patterning on these cells is due to α3 being present on cilia projecting from the soma as well as from the cell’s ependymal surface. Furthermore, these findings could indicate that α3 is present in these cell types. Another consideration was that α3 was instead expressed in the glial cells bordering the CSF, which would account for the measurably higher fluorescence detected in this spinal population (Figure 2.5). However, α3 expression is neuron-specific making this possibility unlikely (Session et al., 2016b; Liao et al., 2022b).

The ependymal layer is comprised of glial cells which utilize their cilia to drive the flow of CSF through the CNS (Brines and Robbins, 1992). This distinct expression patterning could therefore implicate α3 in regulating the flow of CSF. Sodium pumps are known to regulate brain ventricle dilation and control CSF secretion into cerebral ventricles by contributing to an osmotic gradient of Na+ that keeps the CSF consistently flowing through the spinal cord (Speake et al., 2001). It is possible that α3 sodium pumps are involved in maintaining these homeostatic conditions in the brain and spinal cord as a recent study on hydrocephalus in zebrafish demonstrated that knockdown of two ATP1A3 orthologues that code for α3 in the zebrafish, resulted in brain ventricle dilation believed to be caused by an immediate and subsequent build-up of CSF in the spinal and head regions which is symptomatic of hydrocephalus (Doğanli et al., 2013).

CSF has also been associated with contributing to neurogenesis throughout early development and into adulthood by helping to regulate neuronal migration and axonal pathfinding. One way in which it does so is by carrying diverse chemical signalling agents, such as ions and neurotransmitters which act on extrasynaptic receptors in CNS regions downstream of CSF flow, a process known as “volume transmission” (Dur et al., 2020). The presence of α3 in bordering regions could help to regulate ion flow by significantly lowering K+ and increasing Na+ extracellularly following periods of high cellular electrical activity. The flow of these ions through the ventricle could supply other bordering cells with Na+ ions which would lead to an increase intracellular excitability in these regions though pump

transport of these cations (Chang, Lowery and Sive, 2012). This could indicate the functional reasoning behind the quantifiably high α3 detected in CSF contacting cells.

2.4.2 α3 is Distributed Broadly Across CNS Cell Types

Within cells comprising the CNS, α3 was mainly confined to the cell membrane which is where the sodium pump is embedded once the heterotrimeric structure is assembled (Morth et al., 2007). This localization indicates that the labelled α3 subunit, part of the dynamic sodium pump heterotrimeric structure, could be adjoined to a formed pump complex. Another notable region of high α3 expression was in the axons, an expected morphological expression pattern that has been detailed in previous studies (Zahler et al., 1996; Borodinsky et al., 2017), This patterning indicates that α3 likely affects axonal conduction via hyperpolarizing the neuronal membrane potential, independent of synaptic transmission. That is not to say that synaptic transmission is unaffected; a byproduct of the usAHP is that neuronal firing is stalled for a prolonged period (~60 seconds) when dynamic sodium pumps are active (Zhang and Sillar, 2012; Hachoumi et al., 2022).

The comparative quantitative analysis of α3 labelled cell populations in the spinal cord indicated that α3 is expressed, to varying extents, ubiquitously across all cells, and thus neuronal subtypes, that comprise the spinal cord (Figure 2.7). This initial observation thus indicated that α3 is likely expressed to a higher degree within all four main CPG subtypes of the tadpole CPG: dINS, cINs, aINs and MNs (Miles and Sillar, 2011). As previously stated, the ubiquitous labelling of α3 in spinal cell bodies could indicate that the usAHP is present but either attenuated by neuromodulators or masked by a counteracting hyperpolarization-activated depolarizing current, as with Ih currents which are restricted to dINs and entirely mask the usAHP in these cells at NF stage 42 (Picton et al., 2017).

The functional presence of α3 within these cell types is likely to confer an STMM wherein neuronal firing is halted to prevent system fatigue. There is also substantial speculation that dynamic sodium pumps could interact with the Ih current to set the regularity of spontaneous swimming episodes, something that becomes more frequent in NF stage 42 tadpoles (Picton

et al., 2017; Currie and Sillar, 2018; Hachoumi et al., 2022). In the CPG, the α3 expressing sodium pump, termed the dynamic sodium pump, primarily functions to extrude intracellular Na+ following a period of neuronal excitation. During neuronal firing there is a substantial increase in intracellular Na+ which depolarizes the cell membrane. Prolonged depolarization can have negative effect on developing motor circuits as hyperexcitability in neuronal cells is linked to a variety of disorders characterized by parkinsonism (Hunanyan et al., 2018; Zúñiga-Ramírez et al., 2019).

Notably, my IHC findings did quantitatively demonstrate that α3 was positively co-labelled in all backfilled MNs (Figure 2.6). In the CPG, MNs are responsible for inducing muscle contraction through innervation of myotomes that surround the spinal cord via their ventral root. Strong α3 expression in MNs could act on multiple levels to halt swimming via hyperpolarizing the membrane potential of MNs, thus halting firing in the NMJ. Notably, prominent ATP1A3 expression has been noted in the regions bordering the NMJ, anticipated to be MNs. Further supporting this finding previous electrophysiological recordings documenting the presence of the usAHP within a subset of the MN population therefore the ubiquitous, if varied (Chapter 2.3.4), expression of α3 noted via immunolabelling is surprising (Zhang and Sillar, 2012). Though, as mentioned previously, this finding is not entirely unexpected as it could instead indicate that the usAHP is masked or attenuated by neuromodulators such as NO (Hachoumi et al., 2022).

Aside from MNs, there was also the presence of α3 noted in dorsally located RB neurons (Figure 2.3 Bi). Electrophysiological recordings of tadpoles in the Sillar lab have noted the presence of the usAHP in sensory neurons of NF stage 42 tadpoles (Hachoumi, personal communication) therefore this finding aligns with α3 expression in RB sensory neurons. Furthermore, in lamprey dorsal sensory cells there was an extended posttetanic hyperpolarization (PTH), also termed, slow afterhyperpolarization (sAHP, also lasting up to 30 sec). The amplitude and duration of this sAHP was also dependent on the stimulus duration and frequency suggesting that a STMM could occur in these sensory cells following

repeated stimulation, not unlike the usAHP (Christenson et al., 1988; Parker, Hill and Grillner, 1996). Given that these mechanosensory cells are similar to RB neurons in tadpoles, the presence of α3 in this cell type would indicate a similar function of conferring a short-term memory, or habituation, on RB sensory neurons resulting in decreased sensitivity to external stimuli. Therefore, α3 immunolabelling results are still entirely within expectations.

α3 was also noted to be present in the tadpole retina (Chapter 2.3.11). While findings from a previous study had noted that ATP1A3 is expressed in the retinal layers of *Xenopus* (Rahman et al., 2015), this project is the first to immunolabel and quantify α3 in retinal cell layers within the tadpole eye (Figure 2.14). This is further compounded by observed eye-related symptom pathology in ATP1A3 disorders with symptoms including rapid eye spasming and optic atrophy. This pathology has been associated with alternating childhood hemiplegia (AHC) and rapid onset dystonia parkinsonism (RDP) patients, disorders that have been related to identified ATP1A3 mutations (Heinzen et al., 2014; Hunanyan et al., 2018). The presence of α3 was detected through comparison to the negative control. This was unsurprising as the eye is comprised of electrically excitable cell types which mainly rely on Na+ to depolarize, are electrically excitable and include neurons and glial cells, all of which is compatible with the phenotype of α3-expressing cells (Rahman et al., 2015; Tranebjærg et al., 2018). This would further validate why the expression of α3 in retinal cells was expected (Rahman et al., 2015). Furthermore, the membrane potential of photoreceptors is light sensitive. When the environment is dark, and photons are restricted, photoreceptors express a “dark current” wherein an influx of Na+ ions transported by cGMP-gated Na+ channels depolarizes the photoreceptor (Yau, 1994). In light conditions, the membrane potential rapidly hyperpolarizes (-60 mV) due to inhibition of the Na+ channel by conversion of cGMP to GMP (Stryer, 1986). This rapid hyperpolarization is thought to be maintained by Na+/Ca2+ exchanger pump operating alongside active tonic sodium pumps however there is potential for α3 to contribute to the rapid hyperpolarization of the

membrane potential immediately following light exposure (Noguchi, Mutoh and Kawamura, 1994; Yau, 1994).

Given its kinetic properties entail it is activated by the presence of high intracellular Na+ it is possible that α3 could be present and tonically active under dark conditions and that the cessation of Na+ influx following exposure to light allows for its primary function (the usAHP) to be unmasked. Unexpectedly, my projected presented a lack of significantly detectable α3 expression in the tadpole photoreceptors given that this subtype has been found to be expressed in photoreceptors in rats (Schneider and Kraig, 1990). Though not statistically significant ($p=0.07$), the average fluorescence intensity was found to be higher than the negative control which could indicate that α3 was present in these cell types just to a comparatively lesser degree, likely because its contribution to membrane hyperpolarization could be supplemented by the presence of the Na+/Ca2+ exchanger pump (Yau, 1994) and tonic sodium pump. Further experimental repeats could help to establish whether this trend is consistent enough to be statistically significant.

While CTF was measurably higher in all measured retinal layers and lens compared to the negative control (Figure 2.14 B), α3 was only quantified as present in the INL ($p\leq0.01$), the IPL ($p\leq0.0001$), the ONL ($p\leq0.001$) and the OPL ($p\leq0.05$). In the retina, the IPL is comprised of synaptic connections between the bipolar cell axons and ganglion cell dendrites. This comparably high expression in the IPL region is consistent with previously observed α3 expression patterning since it has been observed in my project to also localize to the primary neurites of soma within the SC (Figure 2.3, 2.4, 2.5, 2.6) and the HB (Figure 2.10 Bi). Bipolar cells in zebrafish have demonstrated an ouabain-abolished, sustained AHP which presents in response to Na+ influx through ionotropic AMPA receptors activated by glutamatergic signalling. Immunolabelling for α3 ortholog, α5, in the zebrafish OPL did demonstrate that labelling was highest in the axons extending from bipolar cells (Nelson, Bender and Connaughton, 2003). Given this reasoning the α3 labelling in the IPL is likely strongest on

bipolar cell axons however labelling in these axons are impossible to differentiate at the magnification used for the α3 labelled eye images from this project.

2.4.3 α3 is Present in Electrogenic Tissue Types Adjoining or Neighbouring the CNS

Outside of the CNS, there was noted positive α3 expression noted in tissue neighbouring the CNS, as was discovered when quantifying expression of this subunit within the myotomes (see Figure 2.12). Expression in this tissue type has under-reported (Session et al., 2016a) however immunolabelling in my project revealed CTF intensity (mean ± SEM = 280.7 ± 38.25) was higher compared to the SC data set (mean ± SEM = 164.6 ± 13.14). This higher expression could be due to the broader, more even distribution of α3 throughout the myofibrils comprising the muscle cells. Unlike in muscle, α3 in neurons is membrane restricted and that could account for the difference in CTF intensity. This higher intensity, however, could also indicate a functional necessity for α3 in myotomes. α3 shares many structural and kinetic traits with the α2 isoform which is documented to be highly expressed in skeletal muscle where, when activated, it directly and indirectly contributes to the extrusion of intracellular cations following periods of high excitation (Rahman et al., 2015; Session et al., 2016a; Murata et al., 2020; Liao et al., 2022a). It is upregulated circumstantially in order to counteract periods of hyperexcitation in muscle which, if unregulated, can result in a loss of intracellular K+ and an increase in Na+ (Zahler et al., 1996; Clausen, 2003).

FXYD1 is thought to contribute to shuttling of α2-expressing pump complexes for this purpose (Stanley et al., 2015). Expression of α3 in myotomes could indicate this function conserved within the α subunit family in order to allow for regulation of cellular excitation under specific, or extreme, circumstances. The α3 subunit likely contributes to limiting muscle contractibility following intense locomotor activity by hyperpolarizing the myocyte membrane potential or by working in conjunction with cationic transmembrane ion channels to maintain a steady, tonic resting potential, as is identified in free swimming tadpoles (Currie

and Sillar, 2018). The latter scenario would result in the usAHP being masked and would account for the lower detectability in this tissue type.

Other tissue types also demonstrated prominent α3 expression which likely contributes to electrogenic function of the cells where it is expressed. One such tissue type was the skin where labelling was mainly noted in the outer epithelial layer. This outer layer is comprised of differentiated skin cell types whereas the inner layer is made up of undifferentiated cells . The disparity in α3 expression between these two layers would indicate that α3 is likely not essential to the development or differentiation of these inner cells. Instead, α3 localizing to the outer epithelia may indicate it has a functional role in managing the rate of skin impulse propagation, which demonstrates a fast rising phase that is Na+-dependent (Roberts, 1971).This skin impulse pathway is modulated by NO which increases the skin impulse duration in a skin cell while also decreasing the rate of propagation to successive skin cells along this pathway (Alpert et al., 2007).

NO directly inhibits the usAHP while unmasking a post-stimulus afterdepolarization in a majority (~60%) of CPG neurons (Therien and Blostein, 2000; Miles and Sillar, 2011; Hachoumi et al., 2022). NO is produced endogenously by a subset of skin cell populations and therefore relies upon its ability to diffuse across cell populations to modulate the skin impulse. It is possible that dynamic sodium pumps and NO contribute differentially to skin impulse propagation allowing for bimodal modulation of this pathway by relying solely on the presence or absence of NO given the observable widespread, possibly ubiquitous distribution of α3 across skin cells along the outer bilayer (Figure 2.12). Further experiments should track distribution of NO and α3 across cells comprising the epidermis bilayer by co-labelling NOS, DAF-2 (which labels NO itself) and α3. This could also be used in conjunction with tracking the propagation of the skin impulse pathway from tail to head and assessing whether α3 expression is consistent across all cells or potentially more highly expressed in cells to which the signal does not successfully propagate. If the latter instance is the case α3 could therefore aid in skin impulse path formation by diminishing the impulse duration, or

likelihood as during the usAHP, in these neighbouring cells as well as stabilizing the firing rate of skin cells comprising the skin impulse pathway. This feedback mechanism occurs in other electrogenic cell types where it is thought to stabilize firing rate and duration of neighbouring cells, including neurons where the usAHP has been shown to be present (Pellizzari et al., 2023). This purpose behind this function would therefore allow the main signal to propagate to skin cells where α3 is less expressed or where NO is more highly distributed. However, to date no current experiments have been conducted to test this hypothesis and so the above explanation is purely speculative reasoning as to why α3 is present in skin cells at this stage of tadpole development.

2.4.4 Presence of α3 in Embryonic to Prometamorphic Stages of Development

Another important step in this project was to investigate expression of each protein in the early stages of *Xenopus* development. A previous study measuring the presence of α3 via mRNA identified that α3 was upregulated between neurula stages, NF stage 11.5 to 20; ((Nieuwkoop and Faber, 1956) of *Xenopus* and remained present until stage 40 (Rahman et al., 2015). Between larval stages 29/30 to 40, α3 expression was expected to decrease (Session et al., 2016a; Peshkin et al., 2019). I also chose to measure α3 expression in protein extracted from early embryonic stages (NF stage 20) to free-swimming tadpole (NF stage 45) and while my findings for stage 20, which indicate α3 is highest at this stage, did not align with previous results (Figure 2.11B) (Session et al., 2016a), the expected trend for α3 expression levels at the other developmental stages remained broadly consistent (Figure 2.11A).

The rapid increase in α3 expression between stage 20 and stage 29/30 suggests that it could contribute to locomotor circuit formation during early development. This hypothesis is supported by studies on the link between loss of function ATP1A3 mutations and impaired motor control in a variety of neurological disorders with onset occurring as early on as infancy (Shrivastava, Triller and Melki, 2020). From previous research in spinal circuit formation we know that there is a switch in developing neurons, between NF stages 20 and

28, where action potentials go from being primarily calcium (Ca2+) driven to being primarily Na+ driven (O'Dowd, Ribera and Spitzer, 1988). This change is thought to be caused by an upregulation of delayed-rectifying K+ current (IKr) which itself is associated with the upregulation of Kv2 potassium channels (Burger and Ribera, 1996; Borodinsky et al., 2004). This induction of Na+ and K+ into the intracellular space could correlate with the rise in α3 expression over this same period as previous studies have demonstrated that sodium pumps, particularly heterozygous trimeric structures whose subunits confer varying ion affinities to each pump type, can establish unique spike frequencies which affects the transmitter phenotype of developing neuronal cells (Borodinsky et al., 2004). Thus, this substantial increase in α3 during early embryonic to larval stages potentially implicates it in establishing normal locomotor circuit function by stage 42.

There was also a recorded, but non-significant, increase in α3 between stage 42 and stage 45 measured in my project (Figure 2.5A). This trend could correspond functionally with the emergence of free-swimming behaviour in tadpoles, when significant functional changes occur in the tadpole nervous system such as a noted increase in the presence of the usAHP in spinal populations between NF stage 45 and 58 (Currie and Sillar, 2018). One noted change is the reduction in the likelihood of neurons firing if stimulated during their usAHP compared to earlier stages which corresponds with increased Ih expression that has also been noted at these stages (Currie and Sillar, 2018). This lower firing likelihood could be due to a corresponding increase in α3 insertion into the cellular membrane which would induce prolonged membrane potential hyperpolarization following Na+ influx and reduces firing potential. A possible explanation for how this could function at a cellular level could be due to some neurons having dynamic sodium pumps that are constantly activated if the intracellular Na+ concentration were kept consistently high enough to recruit these pump types. This activation would of course take into account the variation in Na+ affinity that can be conferred by an auxiliary FXYD subunit (Blanco, 2005a; Geering, 2006b; Bibert et al., 2008). This co-increase in Ih and dynamic sodium pump expression could work to regulate

locomotor function, such as free-swimming, seen in later NF developmental stages by raising the membrane potential but still protecting against toxic hyperexcitability via increased activation of dynamic sodium pumps (Picton, Sillar and Zhang, 2018). This dynamic relationship between the Ih current and dynamic sodium pumps can account for the increase in recruitment and de-recruitment of MNs activity that confers motor system flexibility seen in later stages of development (Currie and Sillar, 2018). The observed increase in α3 expression post-stage 42 likely continues into the prometamorphic period of development when limbs begin to develop. In the spinal cord, two CPGs can be detected, one for trunk-oriented swimming and versus for swimming via bipedal limb movement (Combes et al., 2004; Currie and Sillar, 2018). Further evidence of α3 expression levels potentially increasing from free swimming to prometamorphic stages remains to be concretely identified in future experiments but it seems very likely (given its activity-dependence) that α3 likely increases over the metamorphic period. Though yet unverified by personal research, I predict that further investigation into α3 expression between NF stage 45 and stage 62 will yield a similar rise and fall in expression as seen between NF stage 20 and 42 (See Figure 2.5).

2.4.5 Concluding Remarks

Dynamic sodium pumps, presumed to express the α3 subunit, are important regulators of neuronal function and CPGs that control locomotor output (Zhang and Sillar, 2012; Currie and Sillar, 2018; Picton, Sillar and Zhang, 2018) . My findings in this chapter demonstrate that α3 is widely expressed across neuronal cell types, and other tissue types. A broader explanation for this ubiquitous α3 expression, and indicative potential for varied function, is co-expression with varying FXYD subunit isoforms which have been shown to vary by tissue type and confer varying levels of Na+ affinity to sodium pumps (Blanco, 2005a; Geering, 2006b; Clausen, Hilbers and Poulsen, 2017). Thus, the presence of the usAHP could be masked either by modulation from an associate FXYD subtype or via a positive intrinsic ion current as identified with the presence, and co-upregulation, of Ih (Picton, Sillar and Zhang,

2018). The flexibility of dynamic sodium pump function also suggests that α3 could play an important role as motor behaviour emerges during development as shown by its upregulation during key periods of development for example from Stage 42 to 58 (Currie and Sillar, 2018).

In conclusion, the novel immunolabelling of α3 presented in this chapter, as well as the wealth of background data on motor system development in *Xenopus,* indicate that tadpole imaging provides a useful model in which to correlate α3 expression with known dynamic pump function. In the next chapters, I will further demonstrate how I used these IHC protocols developed in this chapter to investigate expression of the auxiliary FXYD subunit in conjunction with α3. I will then further expand upon the link between α3 expression and locomotor function: such as investigating how movement deprivation over the course of early development affects α3 expression in conjunction with altered swimming behaviour in *Xenopus.*

3. CHAPTER 3: TRACKING AND COMPARING FXYD1 AND FXYD6 IN THE TADPOLE CNS

3.1 Introduction

3.1.1 FXYDs: Tissue-Specific Regulators of Sodium Pumps

Until the latter half of the twentieth century, the sodium pump was thought to be a complex composed of only two proteins. The largest and most closely investigated protein component is the α subunit which is essential for the catalytic binding and transport of cations through the sodium pump (Blanco et al., 1994). The second protein is the β subunit which is thought to be the cornerstone in pump complex formation, affecting upregulation of α subunits and in anchoring the pump across the cellular membrane (McDonough, Geering and Farley, 1990). The existence of a potential third, auxiliary subunit in the complex was first postulated in 1978 when evidence showed that a small (~10 kDa) polypeptide, termed the 'proteolipid component', associated directly with sodium pumps purified from the renal tissue of pigs (Forbush, Kaplan and Hoffman, 1978). Subsequent studies continued to identify these small transmembrane proteins associated with renal sodium pumps of other species supporting the claim that the proteolipid component might be a previously overlooked auxiliary subunit in the sodium pump complex (Reeves, Collins and Schwartz, 1980; Hardwicke and Freytag, 1981; Collins et al., 1982).

Further evidence was provided in 1993 when Mercer et al successfully isolated the cDNA that coded for this protein, now termed the γ subunit, and showed that it coimmunoprecipitated with α and β subunits, colocalizing specifically with α1 sodium pump isozymes (Mercer et al., 1993). This evidence indicated that the γ subunit functioned as a previously undiscovered third component of the sodium pump complex. Around this time other small transmembrane proteins were also characterized by their co-expression with sodium pump α/β complexes as well as possessing an apparent regulatory effect on its kinetics and ion affinity (Palmer, Scott and Jones, 1991; Attali et al., 1995; Sweadner and Rael, 2000). After the sequences of four of these small regulatory proteins were characterized (defined as phospholemman, MAT-8, CHIF and Ric; See General Introduction for a previously outlined overview), Sweadner and Rael identified these proteins as

belonging to the same family which they named FXYD after the conserved FXYD motif, a signature sequence of six amino acids located in the extracellular domain (Sweadner and Rael, 2000; Geering, 2006b). Within the FXYD family, FXYD1 function (the protein initially termed as phospholemman) is the best characterized although FXYD2 was the first to be discovered in association with the α/β complex of the sodium pump (Forbush, Kaplan and Hoffman, 1978; Palmer, Scott and Jones, 1991).

The FXYD family comprises seven proteins: FXYD1 (phospholemman), FXYD2 (γ subunit), FXYD3 (mammary tumour marker 8 or "Mat-8"), FXYD4 (corticosteroid hormone induced factor or "CHIF"), FXYD5 (dysadherin or protein "related to ion channel/RIC"), FXYD6 (phosphohippolin), and FXYD7. Each FXYD type is expressed heterogeneously across different cell and tissue-types. Given this wide dispersal of expression across many cell types of varying electrical properties, the main function that this subtype may confer across a broad range of sodium pumps has become a recent topic of interest. It is important to note that while FXYD subunits were first investigated in conjunction with the sodium pump complex, it has been shown to induce intracellular pathway signalling, mainly PKA and PKC, which in turn affects the cation transport in various ways such as altering the membrane potential of the cell (Barbas et al., 2003; Meyer et al., 2020). This functional independence from the sodium pump could also provide the basis for the broad range of FXYD isoforms within this family and account for the tissue-restricted expression of these isoforms within vertebrates.

3.1.2 FXYD Subtypes Are Expressed in a Tissue-Specific Manner

While characterizing the expression pattern of different FXYD subtypes it was noted that different FXYD family members are distributed in a tissue-specific manner, with little to no overlap between cell types or regions where they are expressed (Sweadner and Rael, 2000; Crambert and Geering, 2003). FXYD1 is expressed in cells that are electrically excitable. It is found widely across the nervous system, in the brain and SC, and it is also located in cardiac and skeletal muscle (Palmer, Scott and Jones, 1991; Crambert et al., 2000, 2004). FXYD2

and FXYD4 are distributed differentially in the adult kidney with little to no overlap in expression. FXYD2 expression is highest in the inner stripe of the outer medulla in the thick ascending limb (TAL) (Zouzoulas et al., 2003), but its expression decreases in other regions, and it is sparsely expressed in the medullary and cortical portions of the collecting duct of the kidney. Instead, these regions are where FXYD4 expression becomes most prominent (Attali et al., 1995). The distinct expression patterns of FXYD2 and FXYD4, which show little to no overlap, correlates with their opposing regulatory effects on the kinetic properties of renal sodium pumps in these regions as FXYD2 is found to decrease Na^+ affinity whereas FXYD4 greatly increases Na^+ affinity (Crambert et al., 2005; Pavlovic, Fuller and Shattock, 2013).

Compared to FXYD2 and FXYD4, whose expression is restricted to the kidney, FXYD3 and FXYD5 are more widely expressed across different tissue types (Crambert et al., 2005; Nam, Hirohashi and Wakefield, 2007). While FXYD3 can act as a sodium pump regulator in healthy cells of mammalian tissue, both FXYD3 and FXYD5 show high upregulation in cancer cells and are thought to play a role in tumour growth and progression (Crambert et al., 2005; Geering, 2006a). FXYD1, FXYD6 and FXYD7 are all expressed in the nervous system. However, FXYD6 and FXYD7 are localized exclusively to the brain with FXYD7 being expressed mainly in neurons (and to a lesser extent glial cells) where it is believed to enhance neuronal excitability leading to a comparatively depolarized membrane potential and higher firing likelihood in these cell populations (Crambert et al., 2004). FXYD1 is more broadly expressed across different cell types compared to other FXYD isoforms. Because of this it is found to contribute to altering ion affinity in sodium pump complexes, often inducing differential short-term effects across different cell types. This unique function of FXYD1 to amend the cationic binding in sodium pump complexes has lead it to become the most investigated subunit of the FXYD family (Feschenko et al., 2003; Banine et al., 2011; Thomassen et al., 2016; Meyer et al., 2020; Yap et al., 2021b).

3.1.3 FXYD Isoform Structure Contribute to Its Broad Functional Capabilities

Unlike the much larger α subunit (>100 kDa), which consists of ten transmembrane domains, FXYD proteins are comparatively smaller (~>20 kDa), consisting of a single transmembrane segment that connects an extracellular N terminus and a cytoplasmic C terminus. The exception is FXYD3 which possesses two transmembrane domains (Sweadner and Rael, 2000; Geering, 2006a). All FXYD proteins share a FXYD motif of six conserved amino acids in the extracellular N terminus as well as two glycine residues and one serine residue in the transmembrane domain (Figure 3.1). The amino acids in the transmembrane domain are thought to mediate the important task of associating a FXYD isoform with the α subunit of the sodium pump complex. Two separate studies found that replacing either transmembrane glycine residue with arginine in FXYD2 and FXYD7 abolished all interactions between these proteins and their respective sodium pumps (Zouzoulas et al., 2003; Crambert et al., 2004).

These structural components are generally conserved across members of the FXYD family, however specific variations in protein structure between family members contributes to variations in the regulatory function of each FXYD. One example is in the conserved serine residues in the FXYD1 C terminus. Phosphorylation of these residues by either protein kinases A (PKA) or C (PKC) differentially impact FXYD1 modulation and downstream sodium pump function (Crambert et al., 2002; Bibert et al., 2008). For example, in heart and skeletal muscle, an unregulated increase in intracellular Na^+ can have a downstream effect that relies upon the phosphorylation of FXYD1, the increased transmembrane insertion of sodium pump complexes and a stall in sodium pump inhibition. In this case, for α1/β1/FXYD1 complexes, this can lead to an increase in K^+ affinity that is independent of Na^+ being present or absent (Crambert et al., 2002; Geering, 2006a; Meyer et al., 2020).

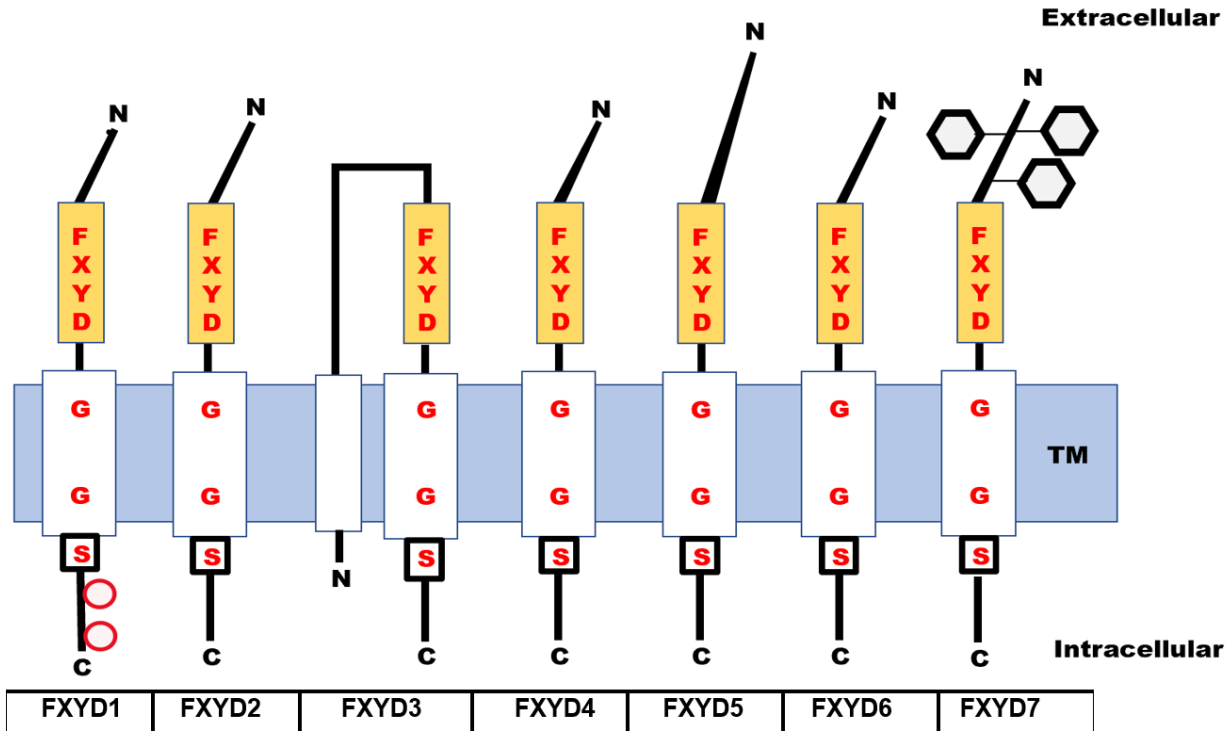

Figure 3.1: Structural Characteristics of FXYD1-FXYD7 Proteins. Conserved features such as the transmembrane (TM) amino acid residues and the extracellular FXYD motif are labelled in red font. Distinct structural differences are indicated on FXYD1 (phosphorylation sites at serine residues on the C terminus of FXYD1 are indicated by red circles), FXYD3 (second transmembrane domain), FXYD5 (an elongated N-terminus) and FXYD7 (O-glycosylation depicted by hexagons on the N terminus). (Figure adapted from Crambert and Geering (2003) (Crambert and Geering, 2003)).

Other distinctive differences in FXYD structures can be found in FXYD3 and FXYD5. FXYD3 possesses two transmembrane domains (Crambert et al., 2005), while FXYD5 is distinctive because of its elongated N terminus (Sweadner and Rael, 2000; Crambert and Geering, 2003), which is composed of 178 amino acids as opposed to the other FXYD proteins which contain between 61 to 95 amino acids (Nam, Hirohashi and Wakefield, 2007). It is uncertain how these structural variations have an impact on sodium pump function and this remains an important area for future research (Geering, 2006a). Unlike the other FXYDs, FXYD7 undergoes O-linked glycosylation where a sugar molecule is attached to the oxygen atom of three threonine residues in the protein's C terminus (Figure 3.1). This process is believed to stabilize FXYD7 and increase signalling within the endoplasmic reticulum of neurons, which could contribute to the role of FXYD7 in neuronal excitability (Crambert et al., 2004).

3.1.4 FXYD1 Regulates Pump Activity By Affecting The α Subunit

In its unphosphorylated state, FXYD1 binds to the α subunit, greatly reducing its affinity for $Na^{+,}$ and somewhat reducing its K^+ affinity, thus inhibiting sodium pump activity (Pavlovic, Fuller and Shattock, 2013). It has been suggested that FXYD1 indirectly controls the intracellular Ca^{2+} necessary for muscle contraction by reducing the amount of Na^+ that is transported out of the cell (Bibert et al., 2008). In skeletal and heart muscle, sodium pump activity is tightly coupled to the activity of a Na^+/Ca^{2+} exchanger that controls muscle contractility. If FXYD1 continuously restricts the transport of Na^+ out of the cell this will lead to a build-up of intracellular Ca^+, depolarizing the resting membrane potential and increasing the rate of muscle contraction. When phosphorylated by either PKA or PKC, FXYD1 disinhibits the α-subunit, allowing normal sodium pump function to resume (Gunnarsson et al., 2013; Thomassen et al., 2016). However, previous research has shown that phosphorylation of FXYD1 by either PKA or PKC can induce different effects on sodium pump kinetics (Teriete et al., 2009; Thomassen et al., 2016; Meyer et al., 2020). An example of this can be seen when investigating phosphorylation of FXYD1 expressed in muscle. When FXYD1 was phosphorylated by PKA an increase in Na^+ affinity within the associated sodium pump complex was noted but there appeared to be no significant effect on maximal pump rates (V_{max}) (Despa et al., 2005). Contrastingly, a separate study found that the V_{max} decreased following PKA phosphorylation of FXYD1 (Pavlovic, Fuller and Shattock, 2013). The variations in these effects have been attributed to the present ion affinity and V_{max} of different sodium pump α/β isoforms comprising these complexes, however there is some debate as to whether there are other factors affecting FXYD-modulation resulting in these observed contrasting effects (Bibert et al., 2008).

A yet less explored theory is that FXYDs affect sodium ion affinity intracellularly: either through directly affecting ion binding site access to intracellular Na^+ or affecting the E1↔E2 conformational change rate (Meyer et al., 2020). This is indicated by the Na^+ affinity of pump complexes becoming negligible in the absence of K^+ as well as some being voltage-

dependent for activation (Stanley *et al.*, 2015; Meyer *et al.*, 2020; Yap *et al.*, 2021). For comparison, externally located binding sites appear to be less affected by FXYD regulation with changes in K^+ affinity not being dependent upon presence or absence of Na^+ (Meyer et al., 2020). These studies demonstrate just one small facet of the broad effects FXYD modulation can have on sodium pump kinetic activity. By tracking and detailing FXYD1 and FXYD6 expression within the well-documented *Xenopus* CNS, this project could aid in clarifying these effects by inferring how FXYD localization likely affects pump function. Particularly when investigating this in conjunction with α3 expression.

3.1.5 Project Aims

Despite the biochemical evidence previously summarized, the exact distribution and function of FXYD isoforms expressed in the CNS (FXYD1, FXYD6 and FXYD7) remains largely unknown. This chapter will outline how I utilized carefully optimized immunohistochemical labelling protocols to label FXYD1 and FXYD6 expression in NF stage 42 *Xenopus* tissue and extracted protein. My results will primarily investigate the immunolabelling of FXYD1 and, more briefly, FXYD6 in transverse sections of the tadpole CNS, including the FB, MB and the eye, the HB and the SC. The data from this research will also provide the first detailed study of α3/FXYD1 expression within *Xenopus* by co-labelling the α3 and FXYD1 primary antibodies within the same cross-sections. Finally, I will detail the immunolabelling of non-neuronal tissue, particularly the skin and myotomes It is hypothesized, given the information presented above, that FXYD1 will be very strongly expressed by myotomes whereas FXYD6 will be more highly expressed in neuronal and eye tissue.

3.2 Materials and Methods

3.2.1 Experimental Animals

All experiments in this chapter were conducted on pre-feeding *Xenopus laevis* tadpoles at developmental stage 42, staged using the normal table of *Xenopus* development (Nieuwkoop and Faber, 1956). WT tadpoles were reared at room temperature (~18^{o}C) from fertilized ova obtained from an in-house adult *Xenopus* frog colony. Selected breeding pairs were given injections (by Home Office (HO) licenced personnel) of human chorionic gonadotropin (hCG, 1000U/ml, Sigma-Aldrich) into the dorsal lymph sac of the frogs to induce mating. All experimental procedures were approved by the Animal Welfare Ethics Committee (AWEC) of the University of St Andrews and conformed to United Kingdom Home Office regulations.

3.2.3 Primary Antibody Sequence Homology

Before experiments could begin, the sequence homology was calculated by comparing the epitopes of the selected primary antibodies to the respective *Xenopus* protein sequence of FXYD1 and FXYD6. The FXYD1 and FXYD6 protein sequence for *Xenopus* was obtained from Xenbase and GenBank (NCBI) databases and alignment was done using the NCBI BLASTP programme (Altschul et al., 1990). The FXYD1 antibody (Sigma, HPA026873) was compared against *Xenopus* and found to have 84% sequence homology (Figure 3.2B) while the FXYD6 antibody (Abcam, ab157196) was found to have 71% sequence homology (Figure 3.2B). The immunogen sequence of each primary antibody was compared to the tadpole proteome and the overlapping sequence homologies were outlined in red (Figure 3.2).

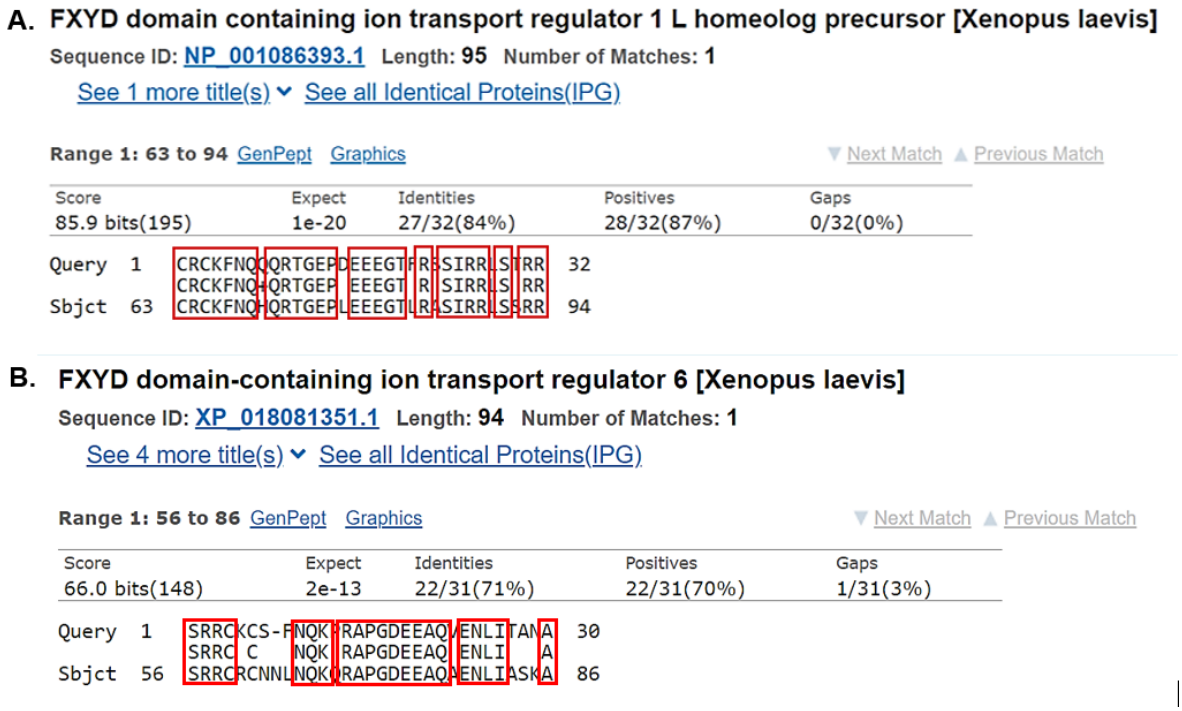

Figure 3.2: Alignment of Chosen FXYD1 Primary Antibody Against *X. laevis* Genome. A-B. Pairwise alignment of immunogen sequence corresponding to FXYD1 (A) and FXYD6 (B) within the human genome (gene id: 5348) against *X. laevis* genome (gene id: 8355). Positive identity between primary antibody and *X. laevis* genome outlined within red box.

3.2.4 Protein Extract Protocol

All protein extract obtained from *Xenopus* tadpoles were done using the protocol established in the Chapter 2.2.3.

3.2.5 Dot Blots

All Dot Blots were obtained using the protocol established in Chapter 2.2.4.

FXYD1 antibody showed reactivity across all concentrations (1:100, 1:250, 1:500, 1:1000; see Appendix Aii) with very little reactivity being detected in the latter 1:500 and 1:1000 concentration conditions. In comparison, FXYD6 antibody demonstrated notable reactivity across every concentration except 1:1000 (See Appendix Aiii). There was no detectable staining in the negative control conditions of either dot blot indicating reactivity was only recorded between *Xenopus* protein and the respective primary antibodies in each test.

3.2.6 Western Blot

To identify the molecular weight of the protein labelled by the chosen primary antibody, Western immunoblotting was performed on protein extracted from NF stage 42 tadpoles. First, the protein weight for FXYD1 (~10.8 kDa) and FXYD6 (~10.3 kDa) was estimated by entering the FASTA sequence into an online molecular weight calculator which takes into account the weight of each amino acid (Protein Molecular Weight Calculator (sciencegateway.org)). *Xenopus* protein was extracted using the method previously detailed in Protein Extract Protocol section (Chapter 2.2.5). The protein concentration was determined by running a Bradford Assay. Protein extract was prepared using the same method detailed in Chapter 2 with the exception that incubation was conducted with the FXYD1 primary antibody (Sigma Aldrich, HPA026873; 1:1000 concentration) at a lower concentration in order to determine antibody specificity to the FXYD1 protein. A positive control antibody α-tubulin (Santa Cruz Biotechnology, sc-32293; 1:1000 concentration) was also incubated separately for a period lasting overnight at 4°C. Blots were washed and incubated with anti-rabbit or anti-mouse horseradish peroxidase-conjugated secondary antibody (1:10,000), respectively, and positive bands were detected using the Pierce CL Plus Western Blotting Substrate kit (ThermoScientific, 32134). Though FXYD1 could be labelled, a delay in FXYD6 shipping combined with the time constraints for my experimental period meant that I could not complete my FXYD6 western blot and so only the FXYD1 results are presented in Appendix B. The weight of each protein band was calculated with an adjacent protein ladder (Thermoscientific, 26623) which was electrophoresed in the same gel as the protein extract. While banding was found to be faint there was reactivity in bands aligning to the 10kDa measurement on the protein ladder (Appendix Bii). As FXYD1 is estimated to be (~10.8 kDa) in tadpoles it was determined that I could proceed with IHC labelling with improved confidence in the accuracy of the chosen FXYD1 primary.

3.2.7 Tissue Preparation and Mounting

Xenopus tadpoles were S1K-ed, fixed in FAA and mounted using the same method detailed in Chapter 2.2.7.

3.2.8 Primary Antibody Concentration Optimization

Slides were immersed twice in histoclear to remove paraffin wax from sections, then taken through a series of rehydration steps in 100% alcohol, 96% alcohol and 70% alcohol before being washed once in TBS. They were then steamed in 0.1M citrate buffer for 25 minutes to retrieve cross-linked antigens, and cooled to room temperature and washed twice in TBS. A blocking solution of 5% MB was added for 20 minutes to block non-specific binding by the secondary antibody, followed by incubation in primary antibody overnight at 4°C. In FXYD1 optimisation experiments, FXYD1 primary antibody produced in rabbit (Sigma, HPA026873) was initially tested at the following concentrations: 1:25, 1:50, 1:100 and 1:200. All positively labelled images were compared to a negative control, where the primary antibody was omitted, and sections were solely incubated with fluorescent secondary antibody. Incubation of the primary and secondary antibodies were done using the same method detailed in Chapter 2.2.8.

FXYD1 labelled sections were incubated in fluorescein isothiocyanate (FITC; excitation at wavelength 495, peak emission at 515nm) conjugated goat anti-rabbit secondary antibody (Vector Labs, FI-1000) at 1:1000 dilution in TBS. After labelling with fluorescent secondary antibody, slides were then washed 5 times in TBS and mounted with a coverslip. It was determined that sections incubated with the 1:100 FXYD1 antibody concentration yielded the clearest images.

Optimization of the FXYD6 antibody (Abcam, ab157196) followed the above protocol however the chosen concentration range was broader: 1:100, 1:250, 1:500 and 1:1000. FXYD6 was also paired with the FITC secondary antibody. FXYD6 labelling was clearest at the 1:250 concentration and so a separate tadpole was incubated with the primary at this concentration to check whether the same cells and tissue types were consistently

immunolabelled between experiments. The two tadpoles were visually ascertained to possess similar labelling.

3.2.9 Co-Immunoabelling of α3 and FXYD1

For experiments where two primary antibodies were incubated in the same sections, a lengthened immunolabelling protocol was utilized. Following incubation with FXYD1 primary antibody (1:100 concentration) and FITC goat-anti-rabbit secondary antibody, the sections were then washed 4 times with TBS-T, five minutes per wash, and then incubated with the optimised α3 primary antibody (Alomone Labs, ANP-003, 1:250 concentration) and then with Cy3 goat anti-rabbit secondary antibody (Vector Labs CY-1300). Slides were then washed 5 times in TBS and mounted as detailed in the above sections.

The Cy3 secondary antibody was purchased as an appropriate antibody for co-labelling with FITC (Vector Labs, FI-1000) due to their excitation ranges not overlapping. Pairing the FXYD1 and α3 primary antibodies specifically with a chosen secondary, FITC and Cy3 respectively ensured that immunolabelling of FXYD1 would fluoresce under green light (FITC excitation is recorded at wavelength 495 with peak emission at 515nm) whereas α3 labelling would fluoresce under red light (Cy3 excitation at wavelength 550, peak emission at 570nm). Sections were imaged using different channels and overlaid afterwards using FIJI.

3.2.10 Fluorescent Microscopy and Image Processing

The same microscopes and image processing techniques detailed in Chapter 2.2.10 were also used in this set of experiments.

3.2.11 Fluorescence Intensity and Data Analysis

Fluorescence intensity, termed CTF, was quantified and analysed using the same methods detailed in Chapter 2.2.11.

3.3 Results

3.3.1 FXYD1 Localizes to Lateral Spinal Cells and The LT Within the SC

While, to the best of my knowledge, there have been no previous studies identifying FXYD1 expression within the CNS of *Xenopus* tadpoles, previous studies have detected FXYD1 expression within the SC of rats (Feschenko et al., 2003). To first ascertain the success of the immunolabelling, it was important to measure whether fluorescence intensity differed between SC sections that had been incubated with the prepared FXYD1 antibody (Figure 3.3 A) versus sections that had been incubated solely with fluorescent secondary, FITC (Figure 3.3 B; Negative Control). The CTF intensity of each FXYD1 labelled tadpole was calculated and then normalized to the CTF calculated from the negative control of each tadpole. A K-S normality test found an abnormal distribution of the data in the FXYD1 labelled groups therefore, a Wilcoxon signed rank test was run to compare CTF between the two groups. The average fluorescence intensity was found to be higher in the FXYD1 incubated group compared to the negative control ($W=71$, $p<0.05$, N=13 tadpoles, mean ± SEM=146.9 ± 29.35%). These findings indicate that the chosen primary antibody accurately labels FXYD1 in the SC.

The FXYD1 immunolabelling indicated membrane restricted perisomatic expression in neuronal cell bodies that extends into the membranes of primary neurites arising from the soma. Strong immunolabelling was also observed within the LT (Figure 3.3 Aii). FXYD1 expression in midline cells was notably attenuated in comparison to the lateral cells and higher resolution images indicated that FXYD1 might not even be present in this SC region. While FXYD1 expression was limited, detectable fluorescence was noted in the tissue directly bordering the CC (labelled CC, Figure3.3 Aii).

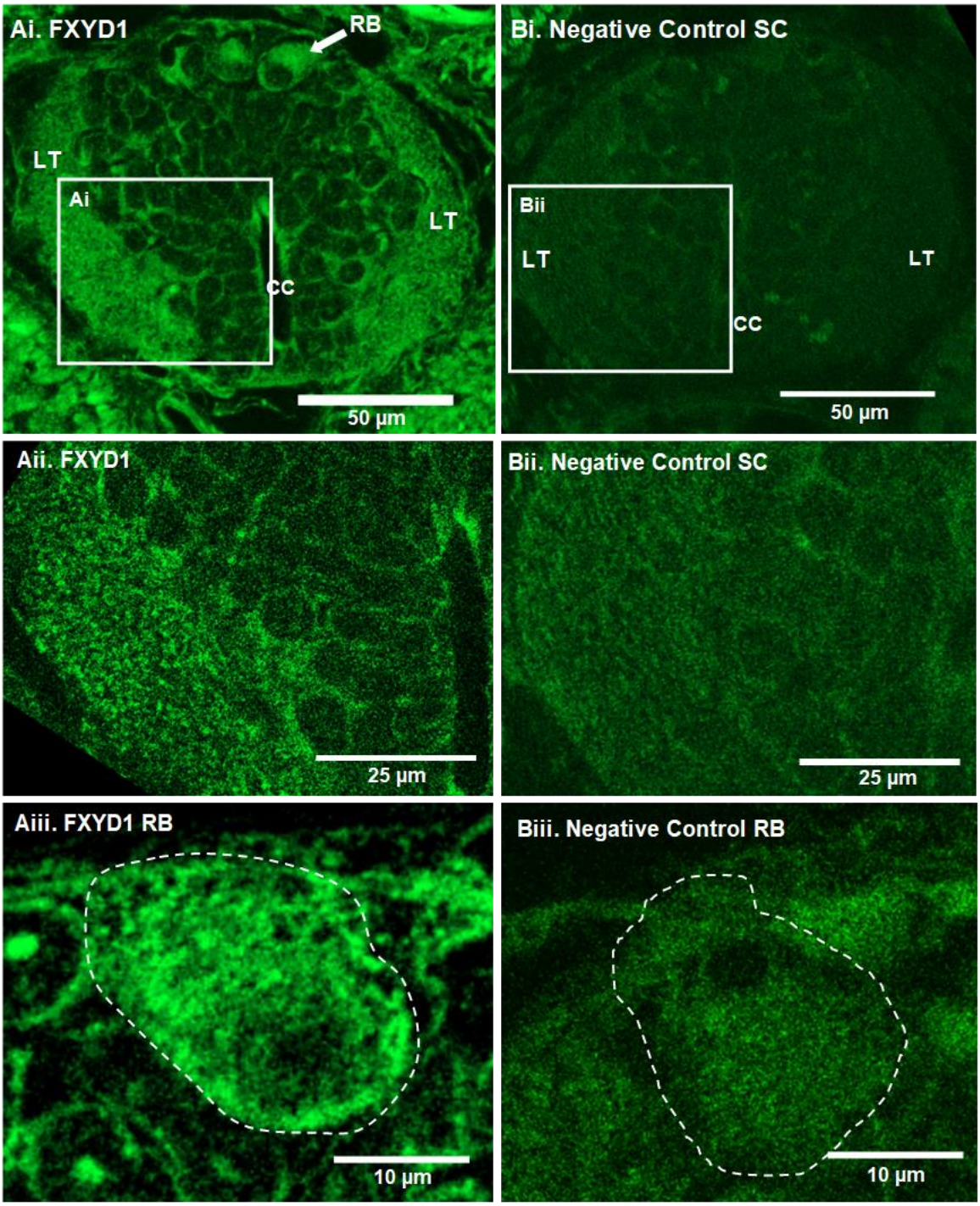

Figure 3.3: FXYD1 is Highly Expressed in Cells Bordering the LT Within the SC. A. FXYD1 labelled sections (Ai, 40X magnification; Aii-Aiii, 63X magnification) were compared to the negative control, Cy3 only incubated, SC sections (Bi, 40X magnification; Bii-Biii, 63X magnification). FXYD1 is shown to be expressed in lateral soma bordering the LT and within the CSF-contacting region of potential ciliated ependymal cells that border the CC (Aii). FXYD1 labelled SC, including RB neurons in the dorsal SC ($p \leq 0.0001$) (Ai, White Arrows; Aiii, outlined by dashed line), especially when compared to the negative control (Biii, outlined in white). [Note, Panels Aiii and Biii taken from separate SC section due to higher clarity observed in images]

As specific identification of these cells was not done in this project, the specific cell type expressed could not be identified. However, their location and their contact with the CC indicates that they could be ciliated ependymal cells though this observation has not been verified within the constraints of my project. Therefore, the labelling noted in the region directly bordering the CC could be the presence of FXYD1 restricted solely to the CSF contacting cilia processes not in the glial cell membrane (Figure 3.3 Bi).

Expression of FXYD1 in RB neurons, a uniquely identifiable spinal cell, was also assessed as there was notable fluorescence in the large, dorsally situated mechanosensory RB neurons in FXYD1 labelled SC sections (Figure 3.3 Ai, white arrow). Notable fluorescence was observable in this cell type (Figure 3.3 Aiii) based on visual comparison to the negative control (Figure 3.3 Biii). This was corroborated by quantifying the CTF and comparing to RB sensory neurons in the negative control group. In total, 28 RB neurons were identified from 12 tadpoles and identifiable fluorescence was confirmed in all of then (28/28 RB). Compared to RB neurons in the negative control groups, CTF was found to be consistently higher ($t_{(27)}$=5.27, p≤0.0001; Mean ± SEM = 160.7±11.56%).

3.3.2 Co-Labelling of α3 and FXYD1

Defining the SC regions where α3 and FXYD1 are distributed, the next step was to identify whether expression overlapped within the same spinal cells. This involved co-labelling the same SC sections with both antibodies but pairing with secondary antibodies that were excited by different wavelengths (See Chapter 3.2.11). This meant that FXYD1 fluorescence was green (Figure 3.4 Ai) while α3 labelling was red (Figure 3.4 Aii). This facilitated identification of differences in expression patterns, while areas of co-expression appear yellow. In the overlaid image (Figure 3.4 Aiii).

Since the previous part of my project established that α3 (Figure 3.4 Aii) is ubiquitously, but variably, expressed across all neuronal subtypes of the SC, this experiment focused on visualizing where in the SC α3 and FXYD1 are co-expressed (Figure 3.4 Ai). Co-expression

of α3 and FXYD1 was prominent in neurons bordering the LT with overlapping labelling (measured by CTF) also noted within the LT (Figure 3.4 B). This indicates that FXYD1, like α3, localizes prominently to axons which comprise the LT. Co-expression was also noted in dorsal, potentially RB, sensory neurons, which are distinguishable by their large soma (~20 αm diameter) (Figure 3.4, white arrows). FXYD1 expression diminished in cells along the spinal midline. Co-expression was detected in the region surrounding the CC however α3 was comparatively more highly expressed than FXYD1 in midline spinal cells within this spinal region. Both α3 and FXYD1 are detected as present in CSF-contacting region of the ependymal surface, where cilia are likely present though I was unable to accurately identify this structure within the parameters of my immunolabelling experiment.

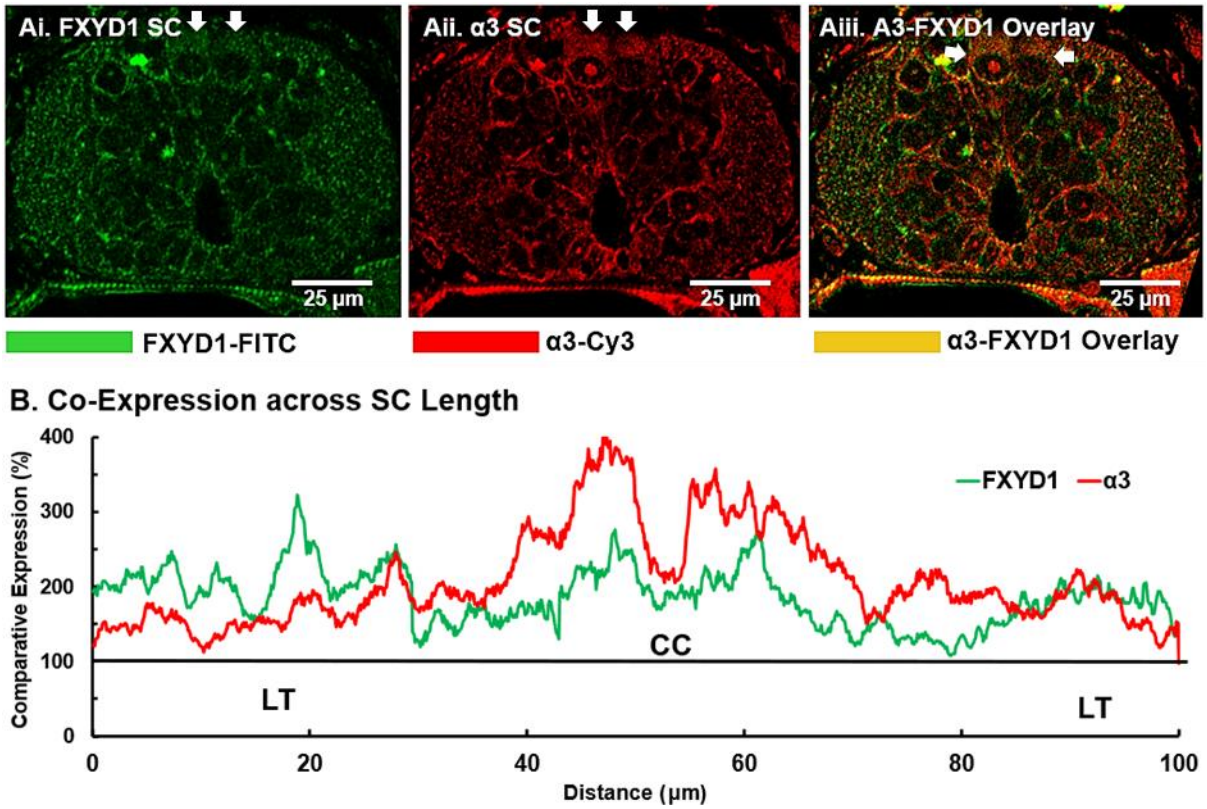

Figure 3.4: Co-labelling of FXYD1 and α3 Reveal Overlapping Expression in LT and Lateral Cells. A. FXYD1 was paired with green FITC secondary antibody (Ai) while α3 was paired with a red CY3 secondary antibody (Aii) and then images were overlaid using FIJI to visualize where FXYD1 and α3 were co-expressed (Aiii). B. Line graphs plotting the expression levels of FXYD1 (green) and α3 (red) within the co-labelled SC sections were plotted and overlaid. Values were normalized to the negative control which is represented on the graph as the threshold (blackline) below which the values are unlikely to indicate positive immunolabelling (All images represented were taken at 40X magnification).

3.3.3 FXYD1 is Present in the Hindbrain

Since previous research has noted the presence of FXYD1 in the cerebellum of rats and mice (Feschenko et al., 2003; Banine et al., 2011), it was expected that FXYD1 would also be present in similarly rostral CNS regions within tadpoles, mainly the hindbrain. Visual analysis revealed that there was labelling present in the FXYD1 incubated transverse sections of the hindbrain (Figure 3.5 Ai) and this was further corroborated by calculating the CTF and comparing to the CTF of the negative control group (Figure 3.5 Aii).

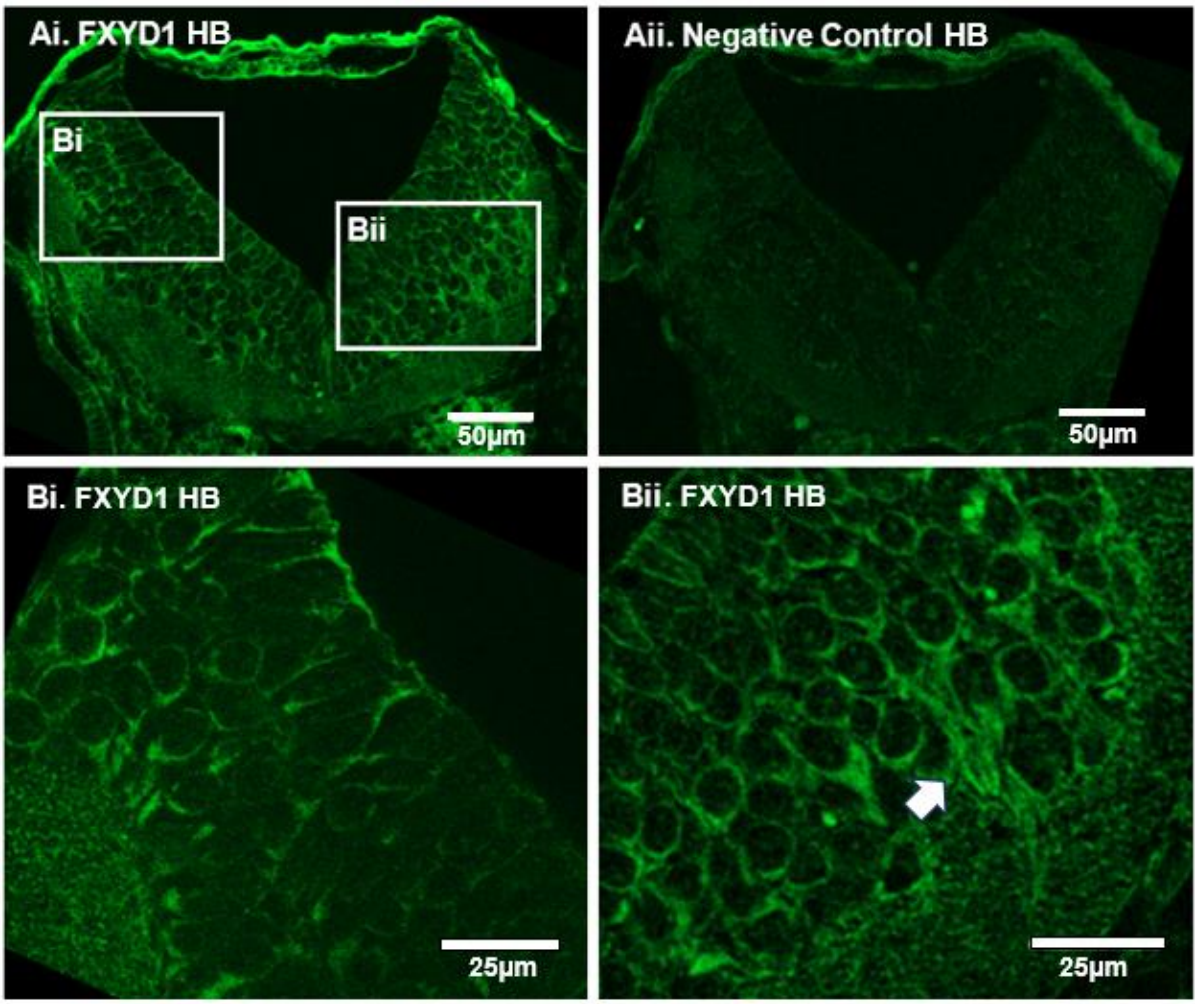

Figure 3.5: FXYD1 In Highly Expressed in Lateral Hindbrain Cells. A. **FXYD1 labelled** HB sections illustrate the distribution of FXYD1 across neuronal and non-neuronal tissue (Ai), particularly in comparison to the lack of prominent labelling in the FITC negative control (Aii). At a higher magnification (Bi, 40X, areas magnified outlined by white box in Ai), FXYD1 is shown to distributed across a lateral to median gradient (Bi) with most prominent expression of FXYD1 found in the soma and primary neurites (indicated by white arrow) bordering the LT (Bii).

Fluorescence intensity was found to be significantly higher in the FXYD1 group compared to the negative control ($t_{(6)}$=2.94, p≤0.05, N= 7 tadpoles; mean ± SEM = 117.8±11.9%; Figure 3.5 Ai, Bi-Bii). Thus, the data support the conclusion that FXYD1 is expressed in the *Xenopus* hindbrain. Similar to the expression patterning observed in other CNS regions, SC (Figure 3.3), FXYD1 is not found to be ubiquitously expressed by all cell types within the hindbrain (see Figure 3.5 Bi for representative image). Instead FXYD1 was prominently expressed in cells bordering the LT and particularly in the primary neurites projecting from the soma into the adjoining LT (Figure 3.5 Bii, white arrow).

There was also a noted demarcation of fluorescence between these neurons and the tissue directly bordering the 4th ventricle where FXYD1 appeared to be expressed by non-neuronal cells in this region. As noted in the previous chapter, the cells that make up this layer are unidentified but likely ciliated ependymal cells based on the pear-shaped soma and spatial abutment to the CC, allowing for a tapered surface of their membrane to be CSF-contacting (Roberts and Clarke, 1982; Dale et al., 1987).

3.3.4 FXYD1 Is Expressed in the Midbrain

An initial qualitative assessment of the FXYD1 labelled images demonstrated that there was visibly higher fluorescence in the FXYD1 MB sections (Figure 3.5 Ai-Aiv) compared to the negative control (See Appendix E), indicating FXYD1 expression is found in the tadpole MB. To quantify this, the average fluorescence intensity (CTF) of the MB sections in each tadpole was quantified and compared against the CTF of FITC only negative control MB sections. The data set was demonstrated to be non-parametric through a K-S test and so a Wilcoxon t-test was run. The average CTF was significantly higher in positively labelled sections (W=0, p<0.05, N=6 tadpoles, mean ± SEM = 431.19±182.4%) indicating that FXYD1 protein is present in the *Xenopus* MB.

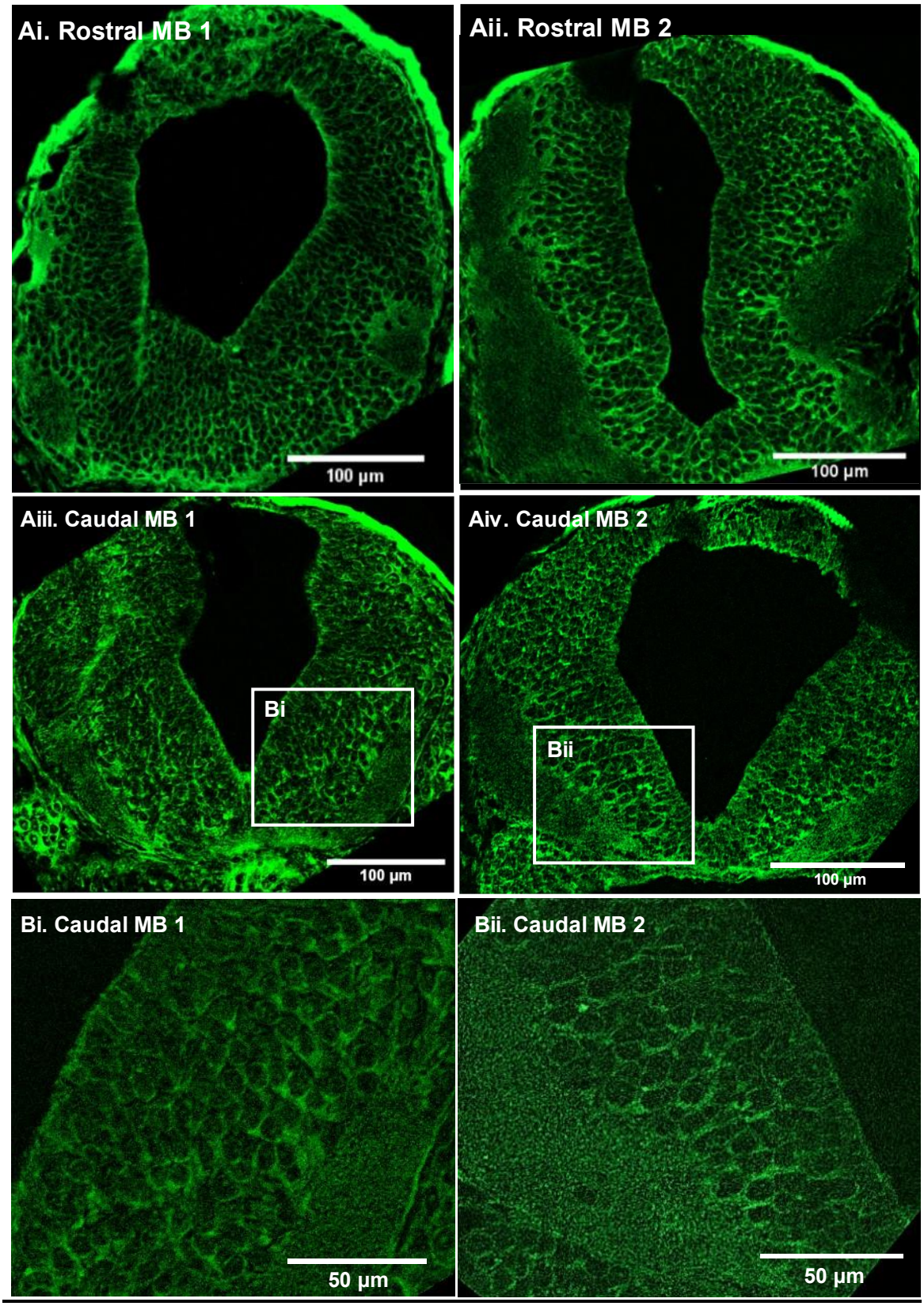

Figure 3.6: FXYD1 is Present in the MB. A. Positive FXYD1 labelled MB sections demonstrate how FXYD1 expression patterning is consistent across rostrocaudal sections (represented Ai-Aiv). B. MB images at a higher magnification, 40X, demonstrates at the cellular level that FXYD1 localizes to the LT and cells bordering this region (Bi-Bii). [Ai-Aiv panels taken at 20X magnification, Bi-Bii images taken at 40X].

An important feature to note is that the pattern of FXYD1 expression within each MB region paralleled the same patterning identified in the tadpole SC. Namely that there was notable labelling present in cells bordering the lateral margins, particularly in the axons projecting into the ventral lateral tract (Figure 3.6 Bi-Bii). There was a notable lack of FXYD1 expression in cells oriented closer to the 3rd ventricle (most notable in Figure 3.6 Bii) however some labelling was apparent in the CSF-contacting region of the MB that directly bordered the 3rd ventricle (Figure 3.6 Bi).

3.3.5 FXYD1 Immunolabelling Within the Myotome

In my project, FXYD1 is demonstrated to be highly expressed in the myotome tissue of *Xenopus* tadpoles (Figure 3.7 Ai) particularly when compared to the negative control (Figure 3.7 Aii). FXYD1 expression was evenly distributed within the myocyte leading to uniform distribution of FXYD1 throughout the dorsoventral myotome. As previously stated, (Chapter 2.3.9) myotome tissue is auto fluorescent when exposed to high intensity light emitted during fluorescent imaging. This results in myocytes within the negative control appearing labelled despite the absence of the primary antibody in this experimental set. Visually, FXYD1 does appear present in the positively labelled myotome segment based upon the higher intensity of fluorescence present FXYD1-incubated myotomes.

However, the degree to which FXYD1 is present in the myotome was worth assessing. The CTF of the FXYD1 labelled tissue (Figure 3.7 Ai) was measured and compared to the negative control (Figure 3.7 Aii) to identify the exact degree to which fluorescence intensity was influenced by the auto fluorescing properties of the myotome. As expected, the CTF significantly higher in the FXYD1 labelled myotomal muscle surrounding the SC by an almost two-fold degree compared to the negative control ($t_{(10)}$=3.59, p≤0.01, N=11 tadpoles; Mean ± SEM = 178.3 ± 21.82%; Figure 3.7Ai). This further supports that FXYD1 is positively immunolabelled in the *Xenopus* myotome.

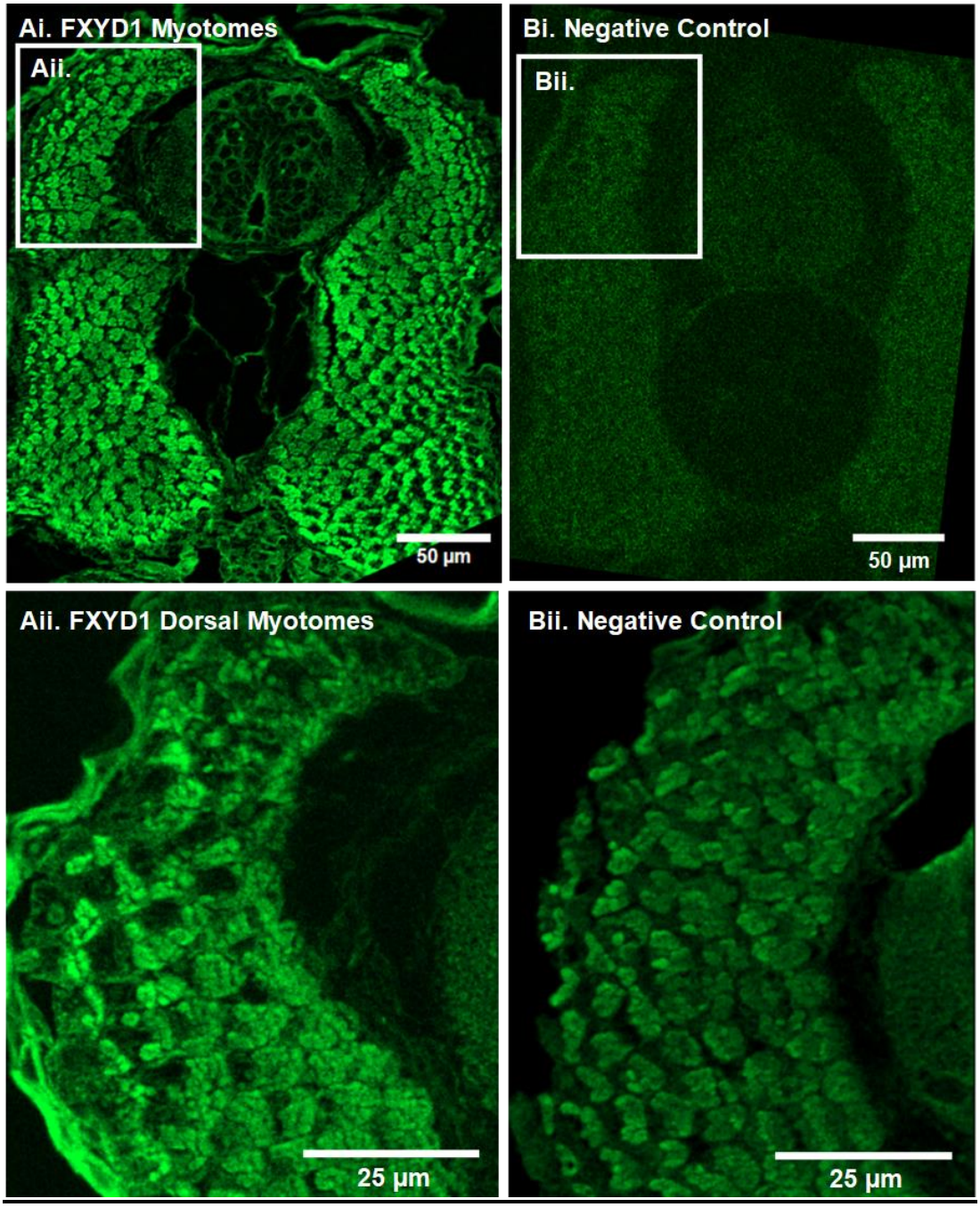

Figure 3.7: FXYD1 Is Highly Expressed in Myotomes. A. Immunolabelling demonstrates consistent, positive FXYD1 expression in SC-level myotome of NF Stage 42 tadpole (Ai) particularly when compared to the negative control (Aii). B. Higher magnification of outlined dorsal regions (enclosed in white box in Ai and Bi panels) demonstrate that FXYD1 labelling is ubiquitously distributed within each myocyte comprising the myotome. The difference in fluorescence is also notable in higher magnifications with α3 labelled myotomes (Aii) demonstrating that fluorescence is significantly higher compared to the negative control indicating that α3 is present in tadpole myotomes (Bii). [Ai-Bi panels taken at 20X magnification, Aii-Bii panels taken at 63X magnification].

3.3.6 FXYD1 Expression Was Evenly Distributed Across the Skin Bilayer

During imaging of FXYD1 immunolabelling in tadpole cross-sections, high fluorescence was noted in the skin cell bilayer outlining each CNS cross-section (Figure 3.9 Ai-Aii). While skin cells do autofluoresce brightly when exposed the high intensity light during fluorescent imaging, FXYD1 labelling still appeared to enhance this intensity (Figure 3.8 Ai), particularly when sections were directly compared to the skin of negative control cross-sections (Figure 3.8 Aii). This provided a viable basis for analysing whether FXYD1 was expressed in these skin cells. FXYD1 labelling of skin cells also revealed that the expression was limited to the epithelial cell membrane, enabling the skin bilayer to be discernible at higher magnitude images.

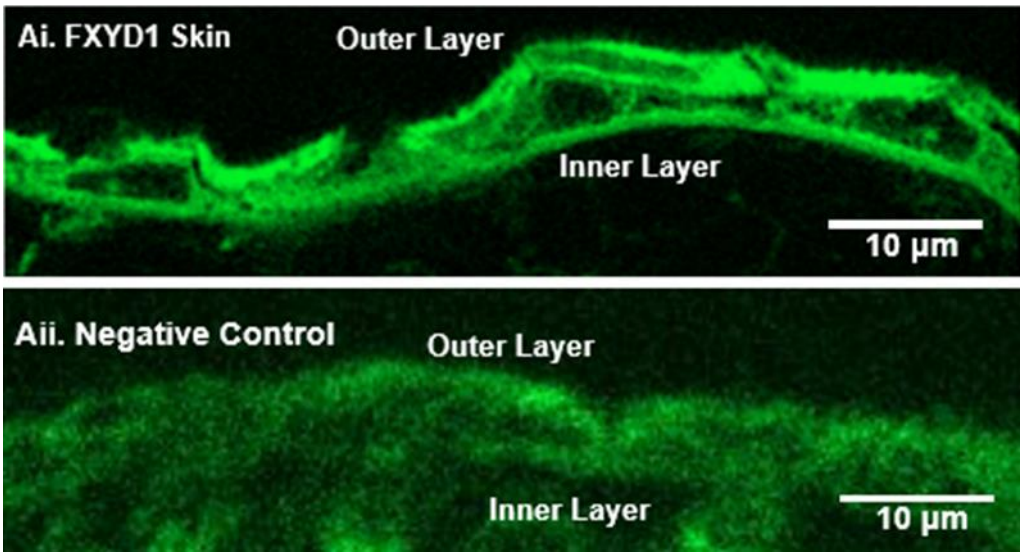

Figure 3.8: FXYD1 is Broadly Expressed Across Skin Cells. The presence of FXYD1 in skin was identified via visual and quantitative comparison between sections incubated with FXYD1 primary antibody (Ai) and the negative control sections incubated solely with FITC secondary antibody (Aii). FXYD1 is localized within the skin cell membrane and demonstrated no discernible variation in expression levels between the inner and outer epithelial cells comprising the skin bilayer [All images taken at 40X magnification, skin was imaged at the rostral to mid-caudal SC level).

Measuring and normalizing the CTF values of skin cells from the FXYD1 and the negative control tadpoles allowed me to test whether the this observed difference in fluorescence intensity was due to positive labelling of FXYD1 within skin cells. These measurements were then compared to see whether CTF was higher in the experimental group versus the control.

A one sample t-test was run and found significantly higher fluorescence in the FXYD labelled skin compared to the negative control ($t_{(8)}$=3.266, p ≤ 0.05, N=9 tadpoles; mean ± SEM = 282.4 ± 18.6%). This statistically higher fluorescent value indicates that, despite the skin's natural autofluorescence, it can be asserted that FXYD1 is expressed in this tissue type.

3.3.7 FXYD1 Is Expressed Within the Tadpole Retina

Expression of FXYD1 within the tadpole eye was examined in a small tadpole population (N=4) with the main aim being to assess whether FXYD1 was present within the eye and whether distribution across retinal layers formed any identifiable patterns or gradients, as was identified in the SC (Chapter 3.3.1-3.3.2). To quantify whether FXYD1 was present within the eye, the average CTF of the FXYD1 labelled eye (Figure 3.9Ai) was measured and normalized to the whole eye of the negative control (Figure 3.9Aii) tadpole. A K-S test showed that, when eye CTF values were normalized by tadpole (N=4 tadpoles), there were too few fluorescence intensity measurements to verify normality therefore the data set was treated as being non-parametrically distributed due to the high variation across retinal layer data sets. A Mann-Whitney U test found that intensity values were significantly higher in comparison the FXYD1 labelled tadpole eyes to the negative control (p≤0.05, mean ± SEM = 164.2 ± 18.43%) indicating that FXYD1 is measurably present within the tadpole eye.

Next, the CTF of each retinal layer was quantified and cross-compared to the negative control as well as to each other using a Kruskal-Wallis test and a follow-up Dunn's multiple comparison test. Variation across retinal layers was found to be significant (H(7) = 19.53, p≤0.01) and retinal layers demonstrating the highest detectable fluorescence were measured to be the OPL (p≤0.001), the INL (p≤0.05), the IPL (p≤0.01) and the GCL (p≤0.05) compared to the negative control. Despite the high fluorescence visible within the lens, the CTF was not found to be high enough to indicate FXYD1 is expressed in this region (mean ± SEM = 131.1 ± 47.59%; *n.s.*). Intensity values were also not statistically significant in the ONL (mean ± SEM = 132.7 ± 13.27%; *n.s.*) despite every tadpole recording a higher CTF values on average compared to the negative control (Figure 3.9 B).

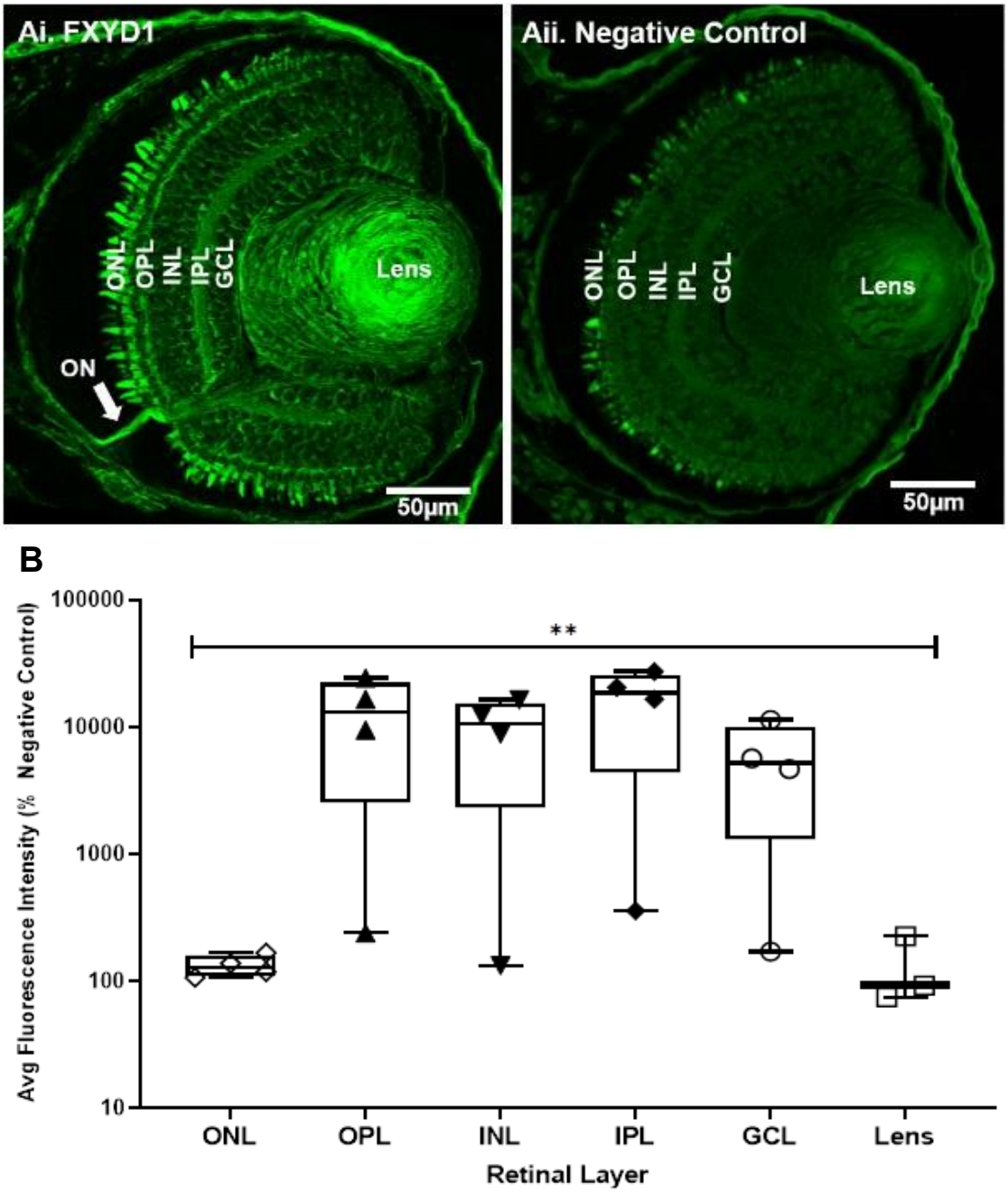

Figure 3.9: FXYD1 Demonstrated Expression Across Retinal Layers Within the Eye. A. FXYD1 expression was variably distributed across the retinal layers of the tadpole eye (Ai) The optic nerve (ON) is revealed within a tadpole eye cross-section and FXYD1 immunolabelling revealed differential fluorescence between the nerve length located within the neural retina and length spanning between the ONL and the pigmented epithelium where fluorescence is visibly higher (denoted by white arrow). All FXYD1 retinal layers were compared to respective retinal layers taken from eyes of tadpoles in the negative control group (Ai). B. Box plot demonstrating CTF values across retinal layers. A Kruskal-Wallace test demonstrated that FXYD1 expression was highest in the OPL and IPL ($p \leq 0.005$; represented by ** in panel B) (panel A images captured at 60X magnification).

According to the CTF values, FXYD1 was most strongly expressed within the inner (Mean ± SEM = 12304.53 ± 4462.98; IPL) and outer (mean ± SEM = 8753.76 ± 3332.33%; OPL) plexiform layers and along the optic nerve (O.N., white arrow; Figure 3.9 Ai). These regions, excluding the optic nerve, are comprised of dendritic projections from the cells in the INL and ONL, respectively. It is important to note that the comparatively higher intensity values in this region is likely due to FXYD1 being more closely distributed across the dendritic structure resulting in immunolabelling that appears to indicate higher expression in this region. By comparison, FXYD1 was also detected in the GCL and INL where it was found but intensity was measured to be lower due to FXYD1 expression being distributed across membrane rings making expression appear less concentrated in these regions.

3.3.8 Preliminary Assessment of FXYD6 Immunolabelling

The time constraints for my experimental period, combined with a delivery delay for the FXYD6 primary antibody (Sigma, HPA041334) meant that there was only enough time to test antibody reactivity with *Xenopus* protein extract (See Appendix Aiii) and run an initial set of preliminary IHC labelling experiments for assessing the presence of FXYD6 within the tadpole SC. However, despite these set-backs I was still able to identify an optimal primary antibody concentration (1:250) and note some consistent immunolabelling patterns shared by FXYD1 and FXYD6 within the tadpole SC.

Within the SC, FXYD6 was found to be most prominent in the soma of lateral neurons that bordered the LT. Immunolabelling of FXYD6 also found that expression was more prominent in dorsally oriented neurons and less apparent in ventral neurons, indicating that only a subset of motoneurons likely express FXYD6. These observations provided a basis upon which to conduct a more quantitative analysis.

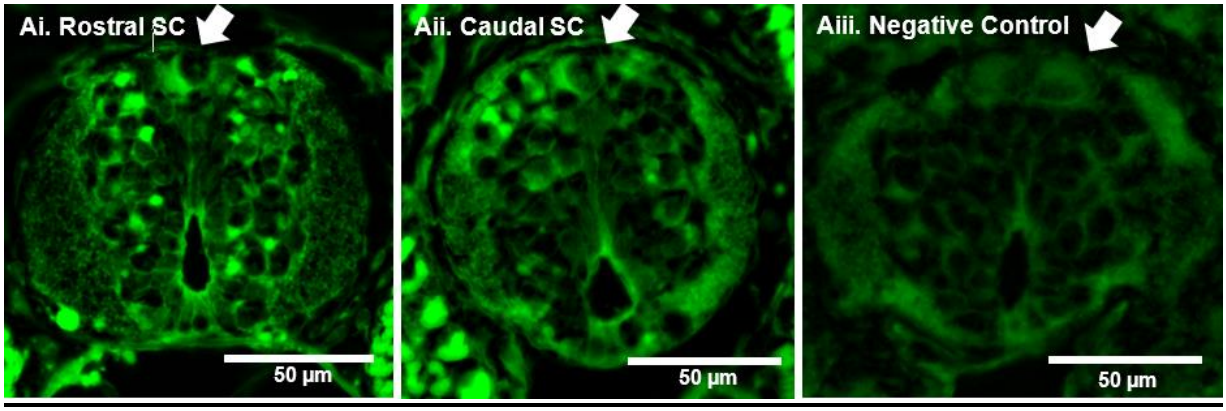

Figure 3.10: FXYD6 Immunolabelling in the SC.A. Optimization experiments with FXYD6 antibody proved most successful at a 1:250 antibody concentration (Ai-Aii) compared to the negative control (Aiii). Immunolabelled FXYD6 sections demonstrated notable expression in the large soma of neurons bordering the LT and within the LT itself. Prominent dorsal labelling was also noted in RB neurons within rostral (Ai, white arrow) and caudal (Aii, white arrow) SC sections, particularly in comparison to RB soma within the negative control (Aiii, white arrow). There is also indication of a rostrocaudal variation with rostral SC sections (Ai) demonstrating higher fluorescence intensity values.

The CTF values of each FXYD6 labelled section was first calculated and then a K-S test was run to determine normality. Once the data set was found to not differ from normal distribution, the values were compared to the CTF of the negative control group to which they were normalized. These values were found to be above the normalized value (set as 100) (mean ± SEM=165.78 ± 23.56%; N=2 tadpoles) further indicating that FXYD6 was likely present in the SC. There was rostrocaudal variation in fluorescence intensity with higher values being found in more rostral (Mean ± SEM = 189.35 ± 28.5 %; Figure 3.10Ai) SC sections compared to caudal (mean ± SEM = 142.2 ± 32.6%; Figure 3.10Aii) SC sections, however this value could not be analysed statistically due to the small sample size. A notable similarity between rostrocaudal sections was consistent FXYD6 labelling of identified RB neurons in the dorsal SC region (Figure 3.10 Ai-Aii, white arrows). The CTF of these cells were measured, normalized and compared to unlabelled RB neurons from the negative control (Figure 3.10 Aiii, white arrow). Due to the data set being larger (N=7 measured RB neurons) and normally distributed, a t-test was run and found that CTF was significantly higher in FXYD6 labelled RB neurons ($t_{(6)}$=4.44, $p \leq 0.01$, mean ± SEM = 166.78 ±15.03%). This indicates that FXYD6 is expressed in RB neurons.

3.3.9 Brief Summary of FXYD Immunolabelling Results

1. FXYD1 is positively immunolabelled in the SC as well as rostral CNS regions such as the MB and HB where the distribution pattern of FXYD1 expression was found to be conserved within the LT and proximal cell bodies.

2. FXYD1 forms a mediolateral gradient between the midline cells abutting the CC and lateral cells lining the LT. Labelling consistently found FXYD1 was more concentrated in lateral cells. FXYD1 was prominently expressed in the membrane and in ventrolateral projections of these cells as well as in the LT itself which is comprised of ascending and descending axons and dendrites.

3. FXYD1 is present in other tissue types including the myotomes, the skin and in the eye. In the myotomes and skin, FXYD1 was distributed uniformly across myocytes and epithelial cells within the inner and outer skin bilayer. In the eye FXYD1 was strongly detected in both plexiform layers and measurably present in the GCL and the INL.

4. Preliminary labelling of FXYD6 within the SC revealed prominent overlap with FXYD1 expression within FXYD6 expression detected within the LT, lateral cells and dorsal RB sensory neurons. FXYD6 also demonstrated a mediolateral gradient with limited fluorescence observed in midline cells compared to cells bordering the LT.

3.4 Discussion

3.4.1 FXYD1 Labelling Follows a Mediolateral Gradient Within The CNS

The main aim of this experiment was to track FXYD1, and preliminarily FXYD6, expression within the tadpole CNS and neighbouring tissue types. Assessments of FXYD1 immunolabelling were mainly focussed within the SC where it was found to positively immunolabel spinal cell bodies. While FXYD1 has been previously found in Purkinje neurons in the cerebellum (Feschenko et al., 2003), expression of FXYD1 in spinal cells within the *Xenopus* SC has, to the best of my knowledge, not been reported until now making this experimental data set a novel contribution to the growing literature investigating FXYDs expression within the *Xenopus* CNS.

Within the SC, FXYD1 expression presented a medio-lateral gradient wherein it was prevalent in cells bordering the LT and less present in midline populations. Within these cells FXYD1 immunolabelling was conserved to the membrane and to primary neurites which projected ventro-laterally (Figure 3.3). Notably, FXYD1 was conserved within rostral CNS regions being found to be expressed along comparable spatial regions within the MB (Figure 3.5) and HB (Figure 3.6) where labelling was noted to be prominent in neuronal populations bordering the rostral LT however expression diminished in cells bordering the ventricle (Figure 3.6Bi), mimicking the medio-lateral expression gradient noted in the SC. This distinct expression gradient was repeatable across independent experiments, lending further confidence that labelling was specific to the FXYD1 subunit. Consistent FXYD1 expression was also identified in the LT of the CNS which is a region comprised of ascending and descending axons projected from lateral neurons (Roberts and Clarke, 1982). This expression gradient could be functional, with FXYD1 likely contributing to attenuating pump function specifically in lateral cells which is a spinal population primarily comprised of cINs, aINs as well as ventral dINs and MNs (Roberts and Clarke, 1982).

Additionally, within the CNS FXYD1 expression was detected in CSF-contacting regions abutting the CC but not in the cells directly bordering it (Figure 3.4B). The cell bodies which border the CC are very likely to be ciliated ependymal cells (Roberts and Clarke, 1982; Dale et al., 1987). The cilia are primarily expressed in the CSF-contacting region of the ependymal cell body which was where FXYD1 was noted to be strongly expressed (Figure 3.1Aii). indicating that FXYD1 could be involved in mediating CSF flow-a function that FXYD1 has been implicated in owing to previous analysis of FXYD1 expression in ependymal cells in the choroid plexus, the organ that secretes CSF in ventricles (Feschenko et al., 2003). The flow of CSF through the ventricles through the cilia on the ependymal cells that line these ventricles (Date et al., 2019; Dur et al., 2020). The main driver in *Xenopus* tadpoles are the cilia, which are found on the ependymal cells that line the ventricle and central canal (Roberts and Clarke, 1982; Dur et al., 2020). Within the CNS, the cilia protrude into the ventricle and beat unidirectionally to drive the flow of CSF caudally. In other tissue, such as the heart, FXYD1 regulates sodium pumps expression, regulates ionic exchange all in order to prevent cellular hyperexcitation (Rasmussen, Kristensen and Juel, 2008; Teriete *et al.*, 2009). As CSF is an intermediary for Na^+ transport through caudal CNS regions it is possible that FXYD1 expression in abutting cells lining the ventricle could be functionally expressed for the same purpose.

It is entirely possible that the functional role that FXYD6 possesses in the regions bordering the ventricles and central canal is similar to FXYD1. Prior to being termed “FXYD6”, this protein was known as ‘phospholemman-like protein’ due to its structural similarity to FXYD1 (Yamaguchi et al., 2001; Feschenko et al., 2003; Kadowaki et al., 2004). Within the SC itself, FXYD6 expression patterns were similar to FXYD1 findings: expression within neuronal populations bordering the LT, expression within RB neurons and, notably, expression in CSF-contacting tissue which bordered the CC (Figure 3.10). The latter results are interesting as neither FXYD1 nor FXYD6 was expressed in the cell bodies of the midline cells directly bordering the CC. This raises some questions as to what tissue type is demonstrating this

immunolabelling. The first option is that FXYD1 and FXYD6 are expressed in cilia extended from the CSF-contacting region of ciliated ependymal cells. However, FXYD6 is not expressed in glia (Kadowaki et al., 2004) unlike FXYD1 (Feschenko et al., 2003). If FXYD1 and FXYD6 co-labelling is indicative of co-expression within the same cells it therefore makes it unlikely that either are expressed by ciliated ependymal cells.

The second tissue type is the epithelium lining the tadpole ventricle and is the most likely cell type in which these subunits overlap. The functional purpose of FXYD1 and FXYD6 is currently unknown however they likely contribute to regulating the ion concentration of CSF. In the inner ear of rats, FXYD6 is expressed in the epithelial cells that border the endolymph space where it is believed to contribute to maintaining the ionic composition of this space, low Na^+ (~3mM) to high K^+ (~150 mM), by actively and continuously transporting Na^+ out of the fluid via the ionic exchange of the sodium pump (Kuijpers and Bonting, 1970; Kvljrmcs and Bonting, 1970; Delprat et al., 2007a). This ionic ratio is reversed in CSF which maintains a high Na^+ and low K^+ ionic composition. FXYD6 likely inhibits functional α1/β1 expression, allowing for the high extracellular Na^+ concentration to be maintained within the CSF (Meyer et al., 2020). FXYD1, when phosphorylated by PKA, could serve in conjunction with α2/β and α1/β complexes to replenish any decrease in extracellular Na^+ by increasing the transmembrane insertion of sodium pump complexes and allowing for further extrusion of Na^+ (Crambert et al., 2002; Ingwersen et al., 2011). A notable feature of FXYD1 is that this increased pump activity has been found to occur regardless of the presence or absence of extracellular Na^+ concentrations indicating that the extrusion of Na^+ is likely persistent thus the presence of FXYD1 could work in conjunction with α1/β to continuously maintain the ionic composition of CSF (Crambert et al., 2002; Lifshitz et al., 2006; Delprat et al., 2007a; Meyer et al., 2020).

Co-expression of FXYD1 and FXYD6 was also notable in the dorsal RB sensory neurons. While FXYD1 expression has not been closely examined in sensory neurons, FXYD6 has been found in the dorsal root ganglion in the SC of mice where it is first expressed in the

soma and migrates to the afferent fibres in the superficial laminae (Luo et al., 2021). In these cells, FXYD6 enhances the transient receptor potential channel V1 (TRPV1) by increasing TRPV1-mediated Ca^{2+} currents resulting in a lowered thermal threshold and increased firing threshold in DRG sensory neurons. In comparison, FXYD6 is shown to decrease sodium pump activity indicating that it might also function to lower firing threshold in sensory neurons. Assuming that FXYD1 and FXYD6 structural similarities predicate overlapping function then we can infer that FXYD1 and FXYD6 increase RB firing threshold, likely by enhancing TRPV1 which is also expressed in this sensory cell type (Session et al., 2016a; Dong et al., 2018).

3.4.2 α3 and FXYD1 Expression overlapped in the SC

Another aim of this project was to develop IHC protocols to accurately co-label α3 and FXYD1 within the hindbrain and SC of stage 42 *Xenopus* tadpoles. Following this, a secondary aim was to evaluate distribution, and potential functional significance, of α3 and FXYD1 across different cell types in rostral and caudal regions of the CNS. The preliminary data has outlined α3 and FXYD1 expression occurring on a variety of cell types ranging from neurons within the CNS to neighboring structures including skin cells (Figure 2.12; Figure 3.8), retinal layers within the eye (Figure 2.13; Figure 3.9) and myotomal muscle fibres (Figure 2.11; Figure 3.7). It should be noted that these proteins were independently labelled with separate primary antibodies and thus it can't be immediately assumed that they reside within the same heterotrimeric sodium pump complex (Crambert et al., 2002).

FXYD1 was found to be uniformly expressed within the myocytes comprising the myotomal segments and consistently present in myotome tissue across rostrocaudal SC transverse sections. This expression overlapped entirely with observed α3 expression in the tadpole myotome, indicating that their expression overlapped in this region. However, while FXYD1 has been shown to associate to α1 and α2 pump complexes it has not been shown to interact with α3 (Crambert et al., 2002). Instead, this finding likely exhibits overlapping expression of these subunits in myocytes but not within the same complex.

In vertebrates, FXYD1 is expressed abundantly in skeletal muscle where it regulates the Na^+ affinity of sodium pumps differentially in response to phosphorylation by PKA and PKC (Crambert et al., 2002; Lifshitz et al., 2006; Floyd et al., 2010). FXYD1 also has a well-characterized functional role in regulating sodium pump-mediated muscle contractions (Palmer, Scott and Jones, 1991). My immunolabelling for FXYD1 in *Xenopus* demonstrated a similar trend of high expression within myotomal muscle fibres (Figure 3.7). Within a range of vertebrate species such as rats, mice and humans, FXYD1 has been noted to be preferentially expressed within skeletal muscle where it is upregulated in response to exercise (Crambert and Geering, 2003; Murphy et al., 2004; Ingwersen et al., 2011). The high FXYD1 expression observed in the myotomal muscles presented in this study for *Xenopus* is consistent with these findings. Functionally, unphosphorylated FXYD1 can exert an inhibitory effect on sodium pump activity and is necessary for regulating intracellular Na^+ and, as a downstream effect, Ca^+ concentrations (Lifshitz et al., 2006; Mishra et al., 2011). Previous studies investigating the effects of exercise on FXYD1 have found that increased sodium pump activity (possibly expression levels as well) upregulated FXYD1 in rat and human skeletal muscle (Rasmussen, Kristensen and Juel, 2008). This has been suggested to be a downstream effect of phosphorylated FXYD1 initiating the trafficking and insertion of intracellular sodium pump complexes within the membranes of muscle cells.

The observed overlap in α3 and FXYD1 expression is interesting as these subunits induce opposite effects to the cell membrane potential. Whereas α3 is responsible for shuttling out Na+ and hyperpolarizing the membrane potential FXYD1 is primarily noted to inhibit pump function by diminishing Na^+ affinity in sodium pumps. In skeletal muscle, FXYD1 maintains a high intracellular Na^+ by limiting the Na^+ affinity of α/β complexes, preferentially associating to the α2/β complexes, but is downregulated following PKA activation (Meyer et al., 2020). This shuttling of FXYD1 in and out of the cell membrane in response to endogenous pathways highlight its transient, activity-dependent presence within this cell type (Meyer et al., 2020). Assuming α3-expressing complexes are retained in myocytes and are less

subject to activity-dependent regulation of their expression, it is possible that the presence of FXYD1 could influence usAHP expression by masking or limiting detection of the usAHP, to a degree, via FXYD1 upregulation. The primary manner with which it might mask usAHP expression is by inhibiting α2/β sodium pumps, an isoform which functions much like α3 in terms of extruding Na^+ concentrations in a depolarized cell (Blanco and Mercer, 1998).

Labelling of FXYD1 in neuronal cell types was less ubiquitous, unlike α3 which was present in every neuronal cell type measured in my project, albeit to varying degrees. therefore attenuating expression of the usAHP. This is apparent from the overlapping expression seen within the LT of the SC as well as in the neuronal soma and primary neurites projecting ventro-laterally towards the LT (Figure 3.4Aiii, blue arrows). Within SC sections, neurons expressing FXYD1 were distributed broadly between the central canal and the marginal zone, including in regions where α3 was found to be prominently expressed. This overlap would suggest that many spinal neurons co-express FXYD1 and α3 subunits, though as mentioned before these subunits likely associate to pump complexes. Given the paucity of information available on the distribution of FXYD1 in the vertebrate nervous system, the data gathered from my study demonstrates for the first time that expression of FXYD1 and α3 across the whole tadpole CNS.

3.4.3 Concluding Remarks

This chapter provides the first evidence for FXYD1 expression within the *Xenopus* CNS, and other tissues, using immunohistochemical labelling techniques I have developed for this project. Although research is still in early stages, the preliminary results indicate that further experiments in this field could expand current knowledge on the functional range of each protein in electrically excitable cells. Though this experiment could not directly evaluate what these functions could be, FXYD1 and FXYD6 underlie similar functions within the cells of regions where immunolabelling was noted to overlap. FXYD1 and FXYD6 both contribute to reducing sodium pump function by affecting the Na^+ affinity therefore often reducing Na+ extrusion from a cell, which could contribute to depolarizing the membrane potential and

increasing firing threshold. In contrast, α3-expressing sodium pumps function to shuttle out the intracellular Na^+. As all three subunits were found to overlap within the same spinal cell populations, based upon where they were observed to be spatially distributed within the SC, I hypothesized that α3 is potentially masked in instances when FXYD1 is upregulated in the same cell. In the next chapter, I will present how depriving tadpole embryos of movement over the early course of development can affect locomotor function, structural anatomy of myotomes and α3 expression in larval tadpoles.

4. CHAPTER 4: LA REARING ALTERS TADPOLE SWIMMING & SODIUM PUMP SUBUNIT EXPRESSION

4.1 Introduction

4.1.1 Pre-Programmed and Externally Induced Changes in Tadpole Development

As this project has tracked and established the expression patterns of selected sodium pump subunits, α3 (Chapter 2.4) and FXYD1 (Chapter 3.4), within the tadpole CNS it now becomes important to ascertain how movement deprivation over the course of development impacts tadpole swimming behaviour.

The work presented in this chapter builds on previous research presented by Franziska Bender (Bender, 2012). Bender's work evaluated the behaviour and CPG output of tadpoles reared from an early embryonic stage to larval stage NF stage 42 under two experimental conditions: a High Activity (HA) rearing condition where tadpole swimming was mechanically stimulated repeatedly throughout development and a Low Activity (LA) rearing condition where movement was suppressed using the anaesthetic MS-222. Both experimental conditions were compared to a control group where tadpoles were reared normally. While Bender documented changes in spinal neuron output and swimming function fairly extensively, the main focus of her project was on tadpoles reared under high activity conditions, wherein swimming was mechanically stimulated over the course of development. Furthermore, there was limited examination into potential alterations to internal anatomy within LA tadpoles, nor did she do any immunolabelling of the sodium pump subunits. As such, my project seeks to expand upon research presented by Bender by focusing on correlating any changes in internal anatomy to swim behaviour. Furthermore, my project seeks to identify whether movement deprivation induces changes in α3 and FXYD1 expression and to explore potential correlative effects on tadpole swimming induced from any changes in expression of these subunits.

During development, neuron differentiation and CPG circuit output rely upon sensory feedback from tadpole movement as the animal progresses from the embryonic to the larval stage and begins swimming (Roberts and Clarke, 1982; Roberts et al., 1987; Hachoumi and

Sillar, 2019). Sensory and motor system development relies on, and is influenced in turn, by signalling which varies depending upon the neuronal subtypes underlying these sensory pathways and the strength of their synaptic interconnections which increases with repeated interactions between cells. Neuronal differentiation and cell fate relies upon a complex interaction of multiple influencers including but not limited to transcription factors, Ca^{2+} signalling cascades (Borodinsky et al., 2004), membrane potential of neighbouring cells (Pai et al., 2012) and mechanical cues (Paulus et al., 2009; Gangatharan, Schneider-Maunoury and Breau, 2018). In *Xenopus*, these signals affect many aspects of neuronal development including delineation of spinal neurons into lateral and midline-oriented cells (Borodinsky et al., 2004) and intercellular signalling within spinal circuits (Roberts, Li and Soffe, 2012).

While Franziska did identify that MNs were differentiated and present in her LA tadpole population, she noted that movement deprivation over the course of development had induced changes to MN firing threshold, and by extension the MN output by NF stage 42 which could indicate an altered or less mature MN population by this stage the latter of which being measured using VR recordings (Bender, 2012). Given this information, another aim of this project was to identify if SC structure was preserved within tadpoles and how LA rearing might have impacted the spinal neurons comprising the SC. This involves understanding how early on neural fate is established in *Xenopus*. Spinal neuron subtypes are distributed spatially and typically following a dorsoventral gradient when differentiating where these populations are differentiated within the SC (Roberts and Clarke, 1982).

Bender's project noted that tadpoles developed normally in the LA conditions and that CPG output, even with limited sensory input and mechanical cues, resulted in swim behaviour and ventral root output that did not differ from control animals (Bender, 2012). These data indicate that the locomotor system likely follows an innate, pre-established cell fate in tadpoles, at least up to NF stage 42. Transcription factors also play an important role in determining cell fate very early on in tadpole embryogenesis, as can be seen for example when tracking the differentiation in the developing *Xenopus* SC through using SOX3 as a

marker in neural cells (Figure 4.1B). In this experiment, the induction of transcription factor signaling relied upon external signalling cues such as sensory signals (Thuret, Auger and Papalopulu, 2015). This was also observed to occur in differentiating KA cells (Yang, Wang and Strähle, 2020), therefore there is the potential that movement deprivation could affect transcription factor signalling, therefore altering spinal cell differentiation and development.

Differentiation of ependymal cells occurs very early on in tadpole development, with cell fate for this cell type established between fertilization and gastrulation stages (NF stage 10.5) of embryogenesis (Nieuwkoop and Faber, 1956). As a result, stage 22 embryos have almost closed their neural tube and are already beginning to differentiate their spinal neurons (Thuret, Auger and Papalopulu, 2015) by the time they are placed into MS-222. The previous study by Thuret et al., (2015) tracking stage dependent differentiation of spinal cells in *Xenopus* noted that cells are organized into 2 neuroepithelial layers extending dorsoventrally along the SC midline during early development that begins to occur at NF stage 14 and will continue until larval NF stage 45, past the target NF stage 42 established in this project. These epithelial layers will form the lateral spinal cells, which will directly border the LT, and the midline spinal cells which directly border the CC. The cells mature from the midline towards the lateral region demonstrating a spatiotemporal delineation for cell population maturity. The implication of this paper is that the shape and cell size within the SC structure will need to be examined in this chapter to identify whether motor output inhibition affected spinal cell distribution in LA tadpoles. Notably, Bender did not study whether changes occurred within internal SC anatomy, and it is therefore worthwhile to investigate this aspect. My experiment uses a slightly earlier stage embryo, stage 20, for rearing in MS-222 therefore this alteration could also affect the neural fate in the SC of LA tadpoles.

The previous study did note that movement deprived animals appeared less excitable, indicating that the sensory systems which underlie stimulus-induced motor activity require external input during early development in order for tadpole to remain responsive by later stages of development (Bender, 2012). This lower sensitivity could be due to Hebbian

principles of plasticity which establishes that synaptic connectivity between neighbouring neurons strengthens or weakens depending upon whether pre and post-synaptic activities are time-locked (Bailey et al., 2000). Given that there will also be an influence of pre-predictive plasticity influencing cell fate and neural connection formation, it would be interesting to investigate whether any observed breakdown in sensory path function is solely due to lack of signalling over the course of development.

4.1.2 Mechanosensory Inhibition: The Cement Gland Pathway

Previous research has noted that swimming is inhibited when *Xenopus* sensory neurons located in the head and CG is activated (Figure 4.1 Ai). It is important to highlight that both the CG and head skin are essential for initiating the stopping response in tadpoles although only one is sufficient for initiating the pathway which underlies stopping response in tadpoles. This was demonstrated when Boothby and Roberts (1992) removed the CG and tested the stopping response by applying gentle pressure to only the head skin. This was found to be sufficient for initiating the stopping response, and similarly when the head skin was removed applying light pressure to the in-tact CG (Figure 4.1) is sufficient for halting swimming (Boothby and Roberts, 1992).

The CG is mucous secreting which enables tadpoles to suspend their bodies vertically from the water surface during early stages of development (Jamieson and Roberts, 2000). The stopping response induced through innervation of the head skin and CG by unmyelinated neurites (≤1μm diameter) projecting from TG neurons. Stimulation of these sensory neurons can also occur when a weight is hung from the CG (Boothby and Roberts, 1995). The TG are located bilaterally along the rostral tadpole head and while both TG innervate the CG, the severing of one TG was insufficient for abolishing stopping in response to head skin and CG stimulation (Boothby and Roberts, 1992). It was only after both TG were severed that stopping could not be initiated.

Once activated, either by mechanical pressure or pulling of the mucous secreted from the CG, the TG neurons are activated (Figure 4.1 Aiii) to excite mhr neurons through

glutamatergic signalling. The excitation of mhr neurons is continuous so long as TG firing is maintained demonstrating that the TG neurons can maintain a very regulated period of consistent and prolonged depolarization in response to stimulation to the head skin and GC. In the hindbrain, excited mhrs then GABA-ergically inhibit CPG neurons, therefore halting swim circuit output continuously until contact to the TG-innervated head skin and CG ceases (Roberts et al., 1987; Boothby and Roberts, 1992; Li, Wagner and Porter, 2014) (Figure 4.1 B).

Triggering the TG pathway can occur frequently in the tadpole's natural environment as when a tadpole bumps into an obstacle while swimming, such as natural vegetation, then swimming will cease almost immediately (Figure 4.1 Ai). Stopping behaviour like this provides an evolutionary advantage during early larval stages when swimming function is not yet fast or complex enough to ensure successful predator evasion (Kahn and Roberts, 1982; van Mier, Armstrong and Roberts, 1989a; Boothby and Roberts, 1995) (Figure 4.1 Ai). An example of CG-stimulated stopping behaviour can also be seen during larval stages when tadpoles will adhere themselves to the water meniscus by the mucous secreted from their CG (van Mier, Armstrong and Roberts, 1989a). Tadpoles hang sessile from this position as stimulation of these TG neurons occurs when a weight is hung from the CG. Activation of the TG pathway immobilizes the tadpole for the duration that they are tethered to the water's surface. (Boothby and Roberts, 1995).

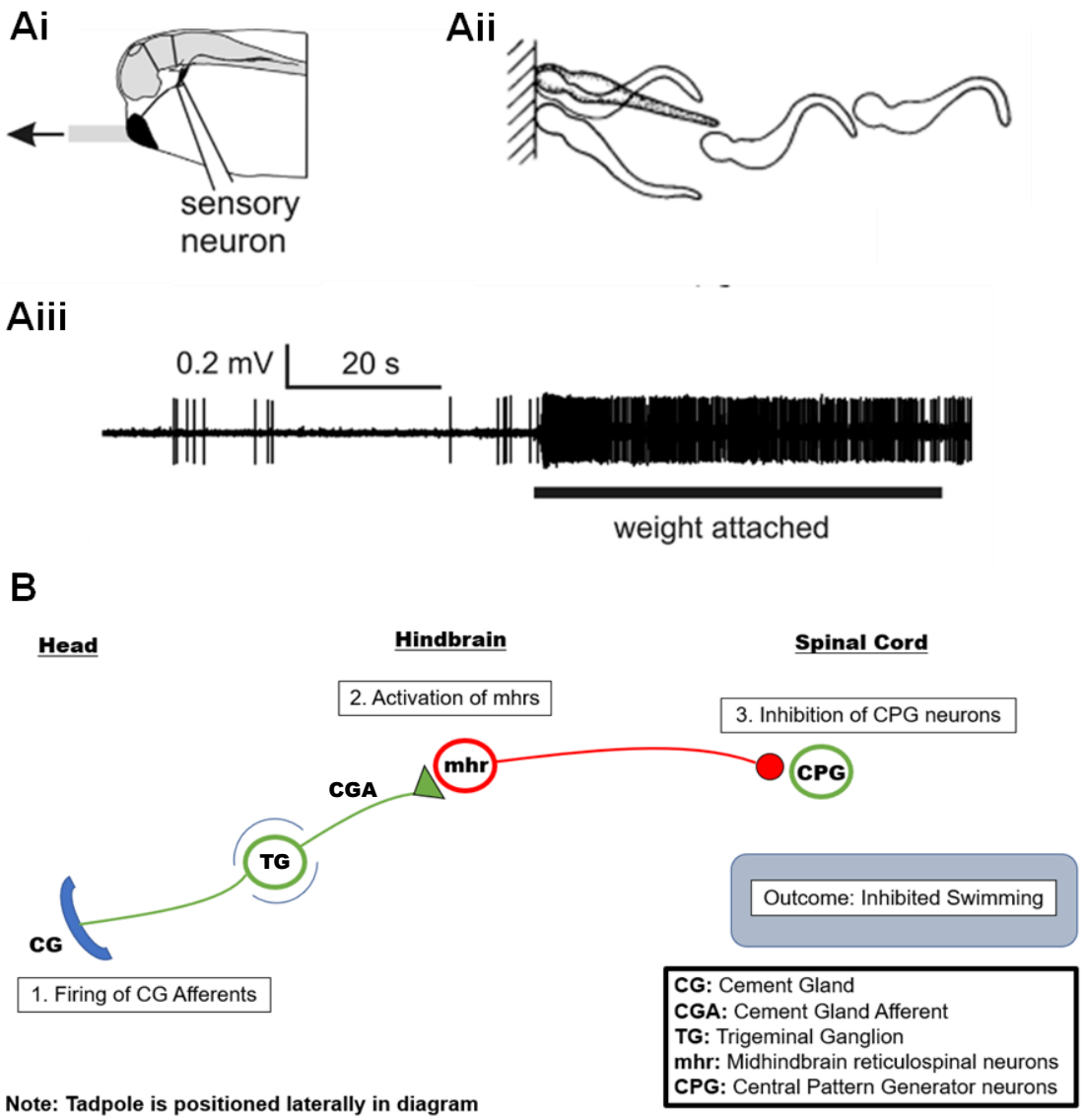

Figure 4.1: Activation of TG Pathway Via Applied Mechanical Pressure to the CG. A. Illustration of laterally oriented tadpole head with labelled CG. Caudal brainstem and CNS are outlined (light gray) demonstrating that this stopping mechanism is initiated outside of the CPG (Ai). Vertical head collision with wall stimulates tadpole to stop swimming within 1.5 swim cycles due to direct pressure applied to CG by this barrier (Aii). Action potentials recorded extracellularly from the TG nerve when activated via weight suspension attached to mucosal secretion from CG which is enervated by TG neurons (Aiii). B. Diagram of TG Pathway following CG stimulation and the ensuing swimming inhibition through inhibition of CPG neurons (B). (Ai & Aiii Panels adapted from Lambert et al., 2004a & reviewed in Roberts et al., 2010; Aii Panel adapted from Boothby & Roberts, 1992).

Mechanosensory pressure to the tadpole head skin also induces a stopping response however the underlying inhibitory pathway differs from the TG pathway. This pathway is activated only when a “fast” mechanical tap, or prod, (2.5-10 Hz) is applied to the tadpole

forehead (Li, Zhu and Ritson, 2017). This fast tap induces a concussion-like response in tadpoles wherein movement ceases for almost a minute following this impact. Swimming is theorized by Li et al. (2017) to be halted by the activation of G protein-coupled inward-rectifying potassium channels (GIRKs) which are opened by M_2 muscarinic receptors expressed on cholinergic interneurons in the brainstem. Once opened, GIRK channels then halt, and inhibit, further swimming by suppressing the excitability of dINs located in the hindbrain. Most concussion responses are fast (~343 ms) though in tadpoles some swimming cycles will persist for several seconds following a quickly applied, “fast,” pressure to the head skin. This inhibitory pathway will also be considered when tracking stopping response in LA tadpoles though this investigation will primarily be done by monitoring tadpole behaviour (including swimming duration) rather than tracking fictive swimming, as was done by Li et al (2017).

4.1.3 Anticipated Swim Behaviour Changes from Prolonged Movement Deprivation

Another facet of this rearing experiment that must be considered is the prolonged period during which myotomes will be inhibited from contracting. This has the potential to significantly impact neuronal development in the tadpole CNS as guidance of projections from sensory neurons is facilitated by these muscle contracts (Gangatharan, Schneider-Maunoury and Breau, 2018). For example, muscle contractions influence skin innervation by peripheral RB sensory neurons during early development (Roberts and Hayes, 1977; Clarke et al., 1984). During early development, movement in embryos (NF stage 32) is limited to tail twitches and spasms that provide minimal propulsion for locomotion (van Mier, Armstrong and Roberts, 1989a). This erratic motor function is thought to influence development in two main ways. First, muscle contractions can induce a calcium release from intracellular stores. In early development, this function has been implicated in affecting the structural development and differentiation of the myocytes comprising the myotome (Huang and Hockaday, 1988; Ferrari et al., 1998). Second, muscle contractions have been implicated in axon guidance as many nerves, reactive to a variety of sensory pathways including

nociception and mechanoreception, project through the myotome in order to innervate the skin (Roberts and Hayes, 1977; Ossipov, Dussor and Porreca, 2010; Winlow, Gillette and Walters, 2018; Luo et al., 2021). There is evidence that during early zebrafish development the repeated alternating contraction of the bilateral muscle (Paulus et al., 2009), through which RB periphery axons travel towards the skin (Clarke et al., 1984), is imperative for ensuring localization of their free nerve ending projections. In zebrafish mutants where little to no muscle contractions occurred during early development, RB periphery axons grew longitudinally instead of ventrally and failed to repel one another on contact leading to dysregulated axonal overlap amongst these projections (Paulus et al., 2009).

As previously mentioned (Chapter 1.2.1), α3, coded by *ATP1A3*, is primarily found in neurons within the brain and spinal cord and has been implicated in affecting motor circuit output by limiting the duration and intensity of consecutive locomotor episodes (Zhang and Sillar, 2012). *ATP1A3* mutations have long been implicated in movement disorders and are induced following a dysregulation in α3 expression. The disorders vary in severity, however all pathologies appear to affect movement regulation and motor control as is seen in *ATP1A3* related diseases such as rapid onset dystonia parkinsonism, alternating childhood hemiplegia and epilepsy (Heinzen et al., 2014; Paciorkowski et al., 2015; Arystarkhova et al., 2019, 2021). The symptom severity of many *ATP1A3* disorders can also vary broadly however a shared pathology of these disorders is that they can result in dysregulated intracellular sodium levels (Oblak et al., 2014; Tranebjærg et al., 2018; Shrivastava, Triller and Melki, 2020). These findings therefore implicate dynamic sodium pumps in moderating normal locomotor function in developing vertebrates, potentially by impacting CPG development (Doğanli et al., 2013; Smith et al., 2021; Zou et al., 2023). If motor deprivation results in changes to tadpole behaviour, as has been noted in previous LA experiments (Bender, 2012), it is therefore worthwhile to explore whether there is any change in the regulation of two sodium pump subunits, α3 (Hachoumi et al., 2022) and FXYD1 (Meyer et

al., 2020), which have independently been demonstrated to influence neural circuit output through altering the cationic exchange rate within a cell.

There have so far been few definitive links between FXYD dysregulation and motor disorders, with many studies instead drawing largely correlative results rather than supporting a causal relationship (Clausen, Hilbers and Poulsen, 2017; Yap et al., 2021b). However, there is an established relationship between FXYD1 expression and movement. In particular, FXYD1 regulation has been closely tied to exercise in humans (Gunnarsson et al., 2013; Thomassen et al., 2016; Christiansen et al., 2017) and rats (Lifshitz et al., 2006; Rasmussen, Kristensen and Juel, 2008). Following prolonged periods of muscle disuse FXYD1 has been found to be downregulated in skeletal muscle by a large degree (52%) (Boon et al., 2012) indicating that its expression is dependent upon physical activity. Notably, if exercise was limited to a short period of time (a matter of two weeks in human) there was little change in FXYD1 expression (Thomassen et al., 2010) indicating that any substantial decrease in FXYD1 would have to be attributed to long-term disuse. This downregulation of FXYD1 is therefore a likely outcome in this project which entails prolonged movement deprivation over the course of development in *Xenopus* embryos. Therefore, by tracking expression of α3 and FXYD1 in tadpoles that have been deprived of movement throughout development, this project seeks to heighten the current understanding of how these proteins potentially contribute to mature tadpole behaviour.

4.1.4 Project Aims

The main aim of the project presented in this chapter was to track how movement deprivation over the course of embryonic and early larval development affected tadpole anatomy and swimming behaviour. This was done by optimizing and monitoring the LA rearing protocol, limiting the potential for confounding variables conferred by experimental conditions. The rearing protocol reported in this chapter has been exhaustively amended to mitigate any environmental effects on tadpole development. The next aim of this project was to track any changes to swimming demonstrated by LA tadpoles and denote whether this

change was induced by endogenous changes in tadpole anatomy or whether changes in neural circuit function was a more likely possibility. Cellular recordings were not conducted in this experiment and so this aim focussed on documenting the observable changes in tadpole anatomy. Alongside this investigation, I also documented whether expression of α3 and FXYD1 differed in LA tadpoles. It is important to highlight that any altered expression noted with either subunit could not be directly attributed to changes in tadpole swimming behaviour within the experimental limitations of my project, however a correlative relationship was still open to investigation within the experimental parameters. As discussed in my previous results chapter (Chapter 2.4), the widespread distribution of α3 across spinal cells could indicate that it underlies a conserved functional role in these cells either in conferring an STMM on motor networks or in contributing to managing intracellular concentration of Na^+ and K^+ in the instances when usAHP is masked or counterbalanced by a cationic current, as observed with Ih in dINs (Picton et al., 2017). The following project aim is to correlate, but not definitely state, whether movement deprivation over the course of development affects α3 distribution within the SC. Similarly, as FXYD1 expression is directly influenced by exercise and movement (Rasmussen, Kristensen and Juel, 2008; Wyckelsma et al., 2019) this project also sought to investigate how LA-rearing affected expression of this subunit within the SC and myotomes.

4.2 Materials and Methods

4.2.1 Experimental Animals

All movement deprivation experiments in this chapter were conducted on *Xenopus* embryos which had reached NF developmental stage 20 (Nieuwkoop and Faber, 1956). Behavioural assessments and IHC experiments were conducted using pre-feeding *Xenopus laevis* tadpoles at developmental stage 42. WT tadpoles were reared at a stable room temperature (~20^{o}C) from fertilized ova obtained from in-house adult *Xenopus* frog colony. Selected breeding pairs were given injections (by HO licenced personnel) of human chorionic gonadotropin (hCG, 1000U/ml, Sigma-Aldrich) into the dorsal lymph sac of the frogs to induce mating. All experimental procedures were approved by the Animal Welfare Ethics Committee (AWEC) of the University of St Andrews and conformed to United Kingdom Home Office regulations.

4.2.2 LA Rearing Conditions

NF stage 20 embryos and animal environment was kept consistent within their assigned experimental condition until NF stage 42. NF stage 20 was selected as this is post-closure of the neural tube and the scaffolding for the developing nervous system is more established. Furthermore, the animal is immobile therefore ensuring that the first occurrence of swimming in LA tadpoles is at NF stage 42, post-recovery from MS-222 immersion. In relation to previous research on movement deprivation over the course of development (Bender, 2012), embryos were divided into two rearing conditions: a “Low Activity/LA” group (also termed “LA” in this project) where animals were reared in a low MS-222 concentration (0.015%) and a control group where no drugs were administered. To determine an optimal MS-222 concentration, animals were reared to target NF stage 42 in a broad range of solutions: 0.02% (0.76mM), 0.01% (0.38mM), 0.005% (0.19mM) and 0.0025% (~0.1mM). Preparation of these concentrations involved dissolving the MS-222 in de-ionised water (pH=7), which is the same medium in which the control tadpoles were reared. This also allowed my project to use the water as a vehicle control for the LA rearing experiment as the only difference in the

solution in which these two experimental groups were reared was the presence or omission of MS-222. During the initial two optimization trials, embryos reared in the 0.005% and 0.0025% MS-222 conditions were insufficiently anesthetized as was demonstrated by NF stage 32 when they began moving when lightly prodded with a pipette. As no movement was observed in the 0.01% and 0.02% MS-222 concentrations, only these two concentrations were subsequently omitted from any further experiments. Until this point, tadpole development rate was normal across all four tested concentrations. In final set of optimization trials, tadpole development was compared closely for any measurable differences noted between the 0.01% and 0.02% tadpole groups to discern whether physical aberrations or lower survival rates were affected by MS-222.

Tadpole development in the LA rearing conditions was assessed by comparing the occurrence of malformations (such as presence of edemas, crooked tail structure and stunted growth) as well as the rate of survival between the two MS-222 concentrations and tadpoles from the control rearing condition (where development was deemed to be normal). Average development and survival rate were determined to be comparatively better in the 0.01% MS-222 concentration and so this was set as the optimal LA rearing condition for all further movement deprivation experiments and all further analyses were conducted using only tadpoles reared at this concentration. Rearing experiments were repeated across multiple trials, each one using the offspring of different frog breeding pairs from within the in-house breeding colony in order to ensure experimental repeatability in the movement deprivation experiment. As such, 21 total LA trials were conducted.

4.2.3 Developmental Differences Between Experimental Conditions

Tadpoles from both conditions were assessed for any significant morphological and anatomical differences during development: occurrence of malformations, survival rate, development rate and anatomy were the parameters compared across experimental conditions. Tadpoles with malformations, or a failure to recover post-rearing, were S1K-ed prior to IHC experiments which were conducted using only tadpoles that presented with

normal external features. The frequency of occurrence for the above conditions were attributed to either rearing in MS-222 or to animals being deprived of movement over the course of early development. To investigate internal structural development, tadpoles were sectioned to assess whether internal anatomy differed. Differences in myotome morphology were assessed and compared to control tadpole myotomes.

The myocyte structures were then compared between the rearing conditions by measuring the total dorsoventral length (μm) and the diameter (μm) of individual myocytes comprising the myotomes of mid-rostral level SC sections (N=5 sections per tadpole) and averaging across individual tadpoles (N=8 control tadpoles and N=14 LA tadpoles). Measuring the myocyte diameter also allowed for the structural geometry to be assessed. The rounded formation of these myocytes was initially assessed by drawing a line across the cell, bisecting the structure at several points, and then measuring and comparing the various diameters from a single cell and then later across the cells of myotomes in LA tadpoles to establish if there were consistencies in its morphology within this experimental group. Variation within each set of measured myocyte diameters was assessed by quantifying the standard deviation and standard error and running a K-S normality test and assessing whether the skewness was above 0. To measure the average occurrence of these round myocytes within each myotome segment, each myocyte was tallied from the same SC-level sections and compared across rearing conditions (N=14 tadpoles from each condition).

4.2.4 Imaging Tools and Behaviour Analysis Software

Videos and images of the developing tadpoles from each rearing condition were taken using a Canon EOS 250D camera. Videos of swimming behaviour were recorded at 30 fps. Tadpole swimming was recorded from above. Videos were converted to avi format before the swimming trajectory and path were tracked using Animal Tracker API Plugin in ImageJ (Gulyás et al., 2021). The generated swim path was visualized by a yellow line and the start and end points of the tadpole swim path were established. The stopping point was denoted by an oval therefore enabling swim direction to be portrayed on this software.

4.2.5 Cataloguing Tadpole Swim Behaviour

Once tadpoles from each rearing condition reached NF stage 42, swim behaviour was assessed between control and LA animals using an Animal Tracker API and Excel. Each tadpole was manually stimulated to swim by pipetting the tadpole into the petri dish and recording swimming using the Canon EOS 250d camera mounted to a tripod and positioned directly above a petri dish filled with deionised water. Control tadpole swimming was recorded immediately upon confirming tadpoles had reached the target NF stage 42. LA tadpoles were briefly washed in deionised tap water (2X at RT) to rinse off any residual MS-222 before being placed into a final petri dish also filled with water and allowed to recover for half an hour. During this initial recovery time tail twitching and spontaneous swimming was noted and compared between rearing conditions. Tadpoles were then individually placed into a petri dish with a pipette and their swimming behaviour was documented through recorded videos. All catalogued swim behaviour is derived from the first evoked swim episode. The following swim behaviour was assessed: swim episode duration (s), total distance travelled (mm), average swim velocity (mm/s) and average swim frequency (swim cycle/s, Hz).

Swimming trajectory was tracked using an Animal Tracker API, which outlined the path travelled through the petri dish, and raw values were then logged into Excel. The size (diameter and circumference, mm) of the dish where swimming took place was also measured and the API path trajectory values were confined to these parameters to accurately quantify tadpole swimming distance (mm) and velocity (mm/s). All converted values were copied and pasted into Excel spreadsheets and from them the remaining swim behaviour was catalogued. The tracked swim trajectory that was plotted using the Animal Tracker API allowed path intersections to be plotted by counting the number of overlaps in the traced swim path. This also allowed for any observation of direction preference and quantification of mid-episode turning during swimming.

4.2.6 Documenting Stopping Behaviour

Bender (2012) previously noted that sensitivity to sensory stimulation was more limited in LA tadpoles. This was investigated in the current project by measuring and comparing stopping response in tadpoles from both conditions following impact with a barrier, in this case the wall of the petri dish in which they were placed. As in the previously detailed experiment (Chapter 4.2.5) tadpoles were placed into a petri dish filled with deionised water and allowed to swim freely. Stopping responses were analysed during episodes where tadpole's head collided with the petri dish wall, all of which was recorded on video. Recorded episodes were restricted only to instances where tadpoles came into direct, head-on collision with the wall and that CG stimulation was more likely to have occurred, as previously detailed by Boothby & Roberts (1992) (Figure 1.2 Aii). Under these conditions, it was also considered that a fast (2.5-10 Hz) forehead collision could also have occurred inducing a stopping response known as knockout (or KO) (Li, Zhu and Ritson, 2017). If impact of tadpole forehead with wall was "fast" similar to the tapping executed in Li et al. (2017) then cessation of swimming was attributed to KO response and was disregarded from the study. Finally, swimming duration following CG/head collision was only counted towards this portion of the experiment if head collision was clearly identifiable in the video. From these documented events, the swim duration (s) and swim frequency (Hz) were calculated from time of collision (termed post-CG Stimulation in the experiment) and cessation of swimming (illustrated in Figure 4.1 Aii).

4.2.7 Induced Swim Fatigue and Recovery

A series of swim episodes were induced, filmed and analysed to further categorize swimming normality in LA tadpoles compared to the control. This experiment aim was to whether the relationship between ISI and swim episode duration differed between the two experimental groups by testing the duration of each subsequent swim episode following an ISI <5 s intervals. After the first evoked swim episode, from which swim behaviour was analysed, a succession of further episodes was also induced with the ultimate goal to fatigue the tadpole. This was done by repeatedly pipetting the tadpole into a petri dish and allowing

the ensuing swim episode to begin and end without interruption. This stimulation was continued until swimming ceased entirely and then the tadpole was left to recover (30 s). Following the initial recovery period, the tadpole was again pipetted into the petri dish to induce swimming. If swimming could not be stimulated post the initial recovery period, then the tadpole was granted another recovery period (30 s). This protocol was repeated until tadpole swimming recovered. The number of completed swim episodes and the cumulative recovery time required for resumption of swimming was then compared between the control and LA tadpole groups.

4.2.8 Tissue Preparation and Mounting

All tadpoles were S1K-ed, fixed overnight, embedded in paraffin and then sectioned using the same techniques outlined previously (See Chapter 2.2.7). Prior to anatomical staining or immunolabelling, slides mounted with tadpole sections were then stripped of paraffin by also using these aforementioned methods.

4.2.9 H&E Staining

SC level cross-sections taken from control and LA tadpoles were stained with Harris haematoxylin (Sigma-Aldrich, HHS32) and eosin (5g eosin Y and 500ml dH_2O) (H&E) to visualize morphological differences between the two rearing experiments. Staining solutions were filtered beforehand to avoid potentially obscuring the tissue sections with dye sediment from the prepared solution. Slides were immersed first in haematoxylin for four minutes and then washed in gently running tap water for five minutes until sections turned blue. Slides were then immersed in eosin for another four minutes then washed three times in dH_2O, five minutes each time, to remove residual solution from the tissue. Sections were then placed through a series of dehydration baths ranging from 70% (once), 96% (once) to 100% (twice) ethanol for two minutes each wash. Sections were then washed twice in xylene, five minutes each time, and slides were mounted in DPX (Thermo-Fisher, 06522). Post-staining H&E shows up nuclei and nissl as blue while cytoplasm and yolk platelets show up as pink.

4.2.10 Sequence homology of α3 and FXYD1 primary antibodies

Sequence homology for each antibody, α3 and FXYD1**,** were presented in the α3 (Chapter 2.2.8) and FXYD1 (Chapter 3.2.3) results chapters.

4.2.11 Protein Extract Protocol

All protein extract obtained from *Xenopus* tadpoles were done using the protocol established in the α3 Materials and Methods section from the previous chapter (See Chapter 2.2.3).

4.2.12 Antibody Reactivity and Binding Accuracy

The reactivity of each primary antibody, α3 and FXYD1, to *Xenopus* protein was tested via dot blot (Findings presented in Chapter 2.2.4). The dot blot showed reactivity for α3 primary with *Xenopus* protein (see Appendix Ai) in higher concentration conditions (1:100 and 1:250 being ideal) while FXYD1 also demonstrated reactivity with *Xenopus* protein but to a lesser extent, indicating that 1:100 was an optimal concentration in proceeding IHC experiments. Separate Western Blots were also run with each primary antibody to ensure that antibody likely was binding accurately to target proteins (See Appendix B for results).

4.2.13 ELISAs

A series of ELISAs were run (N=6) to measure whether α3 expression differed within the entire body[3] of tadpoles (through the PE extracted from N = 25-50 tadpole bodies from each rearing condition). ELISA protocols and subsequent analyses were performed according to previously detailed experimental protocol (see Chapter 2.2.6).

4.2.14 Immunolabelling with α3 and FXYD1 Primary Antibodies

Labelling of tadpole cross sections with α3 and FXYD1 primary antibodies was carried out as detailed previously (See Chapter 2.2.8 and 3.2.8). All sections were labelled individually with either α3 or FXYD1 primary antibody and all analyses of the results were also kept separated. It should be noted that due to a delay in a new order of FITC all α3 and FXYD1 were labelled with CY3 secondary antibody however to visually differentiate the results

[3] Except the yolk sac which was excised from tadpole prior to beginning Protein Extraction protocol.

between the two primaries, the FXYD1 incubated sections were changed to green using ImageJ LUT function. No other photo-editing was applied.

4.2.15 Fluorescent Microscopy and Image Processing

Unless otherwise specified, all images were mainly acquired using Zeiss Axio Imager M2 fluorescence microscope equipped with Apotome2 or a Leica DM IRE2 confocal microscope. All comparative analyses were restricted to images taken from the same camera. All image processing and analysis was done using the same method detailed in Chapter 2 (see Chapter 2.2.10).

4.2.16 Data Analysis

CTF was measured from fluorescent labelled image with FIJI (ImageJ) software using the same method detailed in Chapter 2 (see Chapter 2.2.11). Any potential variations in α3 and FXYD1 expression were evaluated by measuring the average CTF of selected tissue types (SC and Myotome) from individual tadpoles in each rearing condition: Control and LA. These values were normalized to a shared negative control beforehand to directly assess the average percent (%) difference in α3 or FXYD1 present within the tadpoles from each rearing condition.

All statistical analysis was carried out using GraphPad Prism (v9.0, GraphPad Software) and the same statistical tests also outlined in Chapter 2.2.11 with the omission that a one sample t-test was not relevant in this experiment as the main comparisons made were between two experimental rearing conditions. Therefore statistical significance was tested using either an unpaired t-test or a Mann-Whitney U test, depending upon data set normality. For comparison of swim episodes completed by the same tadpole a paired t-test, or Wilcoxon signed rank test was run if data was not normally distributed.

4.3 Results

4.3.1 Anatomical Differences in LA Tadpoles

When the movement deprivation experiment was initially optimized there were two main aims. First, to identify which low MS-222 concentration would anaesthetize animals in the experimental condition through the course of development from NF stage 20 to NF stage 42 without significantly impacting tadpole development. Second, to ensure that the MS-222 concentration was minimal so that any detected developmental variations between experimental groups could be attributed solely to movement deprivation reduce the possibility of MS-222 becoming a confounding variable in this rearing experiment.

Initially four MS-222 concentrations were selected (0.02%, 0.01%, 0.005% and 0.0025%) because commonly the concentration range used in tadpoles for short-term experiments is 0.01-0.1% (Jamieson and Roberts, 2000; Li, Soffe and Roberts, 2004; Roberts et al., 2009a; Mogi et al., 2012; Ramlochansingh et al., 2014; Hunt, Bruno and Pratt, 2020; Butler et al., 2022). I selected 0.02% and 0.01% from this range as they are the lowest concentrations. I then included the two lowest MS-222 concentrations in order to test whether tadpoles are successfully anaesthetized in solutions that were <0.01% MS-222. However, the latter two lowest concentrations (0.005% and 0.0025%) did not fully anaesthetize the animals as movements is possible by NF stage 32 (N=10 in each condition), and swimming was observed to occur by day 2 of rearing in LA condition.

Tadpole development progressed at a normal rate across all four MS-222 concentrations however by larval stages the anaesthetic was less effective at the two lowest MS-222 concentrations (0.005% and 0.0025%). Due to this, the two lower concentrations were omitted from the rearing experiment, further experimental repeats were conducted to compare tadpole development between the 0.01% and 0.02% concentrations, which were both termed the LA conditions. The next step in this experiment was to determine which of the remaining MS-222 concentration conditions was ideal for LA rearing.

It was also noted that tadpoles reared in both the LA and control conditions would present with malformations including edema (characterized by excess fluid retention in the head and yolk sac; Figure 4.2 Ai), tail malformations (characterized by otherwise normal tadpole growth except for warping identified within the tail; Figure 4.2 Aii) and stunted growth (characterized by shorter tail length; Figure 4.2 Aiii). During the MS-222 concentration optimization trials, the occurrence of these malformations was higher in the 0.01% and 0.02%% MS-222/LA groups compared to the control ($F_{(2, 43)}$ = 33.43, $p \leq 0.0001$) with a follow-up multiple comparison between the three groups demonstrating that the number of malformations in the 0.02% MS-222 experimental condition was significantly higher ($p \leq 0.0001$, N=57/123 malformed tadpoles) compared to both the control (N=7/117 malformed tadpoles) and 0.01% MS-222 tadpoles (N=22/93 malformed tadpoles)[4]. This trend continued throughout the remainder of the LA optimization experiments. By the end, malformations continued to be slightly higher in tadpoles reared in 0.01% MS-222 (p=0.0017, N=59/347 total tadpoles documented as being malformed by end of LA rearing experiment, 17% occurrence in total). However, the occurrence rate of malformations was not found to statistically differ from the control group (N=15/370 total tadpoles by end of the entire LA rearing experiment, 4% occurrence in total; See Figure 4.3 Bi). This further validated that the 0.01% MS-222 concentration was ideal for LA rearing.

[4] The number of available stage 20 embryos did vary in each trial during the rearing experiment optimization, but population was kept consistent across all experimental groups in each trial (e.g., if there were 15 embryos available, five were placed in each condition). By the second day if there were animals (across all rearing conditions) that did not develop past stage 20 (likely due to low batch fertility or other factors unrelated to the experiment) they were omitted from the experiment since MS-222 rearing was not considered a factor in this death rate. Therefore, the total number of tadpoles varied across experimental groups.

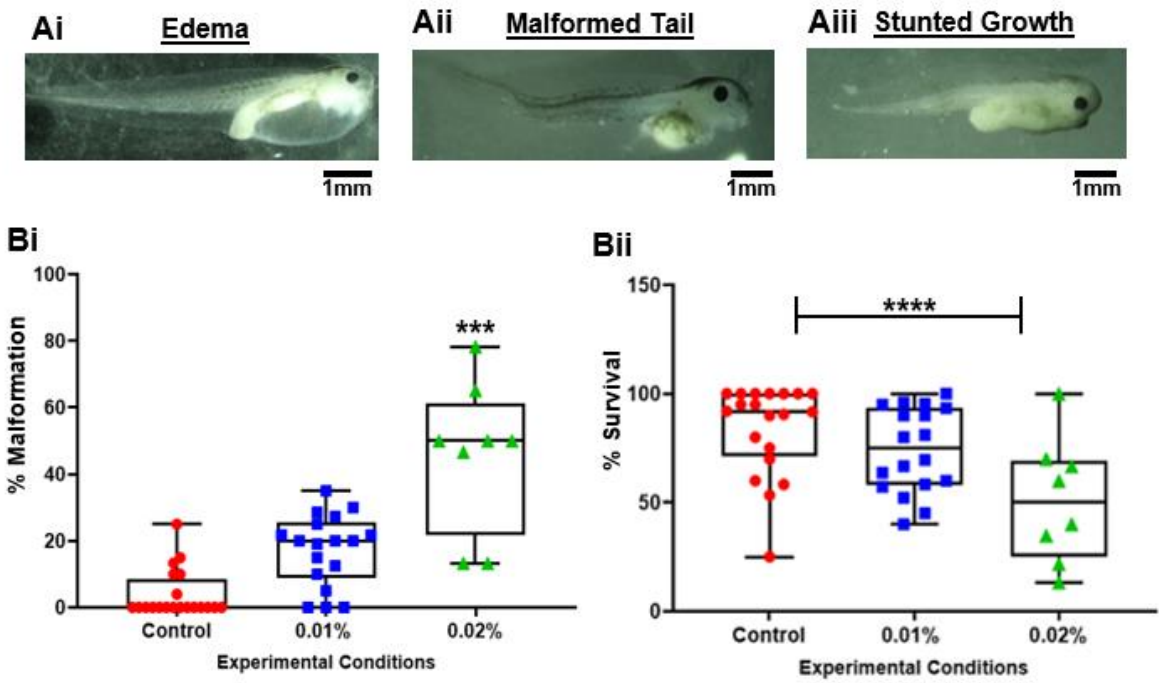

Figure 4.2: Rate of Developmental Malformations and Survival Are Concentration-Dependent in the LA Condition. A. In both experimental conditions, morphological differences such as (Ai) edema, (Aii) a malformed tail shape and (Aiii) stunted growth were observed to occur more frequently in LA tadpoles compared to control tadpoles. B. The average occurrence for these malformations was calculated per rearing experiment trial[5] and was highest in tadpoles reared in 0.02% MS-222 (Bi). Tadpole survival was found to be significantly lower in tadpoles reared in both LA condition concentrations compared to the control with lowest survival rate occurring in the 0.02% MS-222 condition. [Scale bar represents 1mm, *** indicates a statistical significance of p≤0.001, **** indicates a statistical significance of p≤0.0001.]

Next, tadpole mortality (termed the survival rate) was assessed across MS-222 concentrations in comparison to the control. A one-way ANOVA demonstrated that the survival rate varied significantly across rearing conditions ($F_{(2, 43)} = 6.568$, $p=0.0032$) and a follow up multiple comparisons test found survival to be significantly lower among tadpoles reared in 0.02% MS-222 (N=33/77 tadpoles died, 57.14% survival rate; Figure 4.2 Bii) compared to the control (N=23/117 tadpoles died during optimization trials, 80% survival rate). Survival was also lower among tadpoles reared in 0.01% MS-222 (N=22/93 died

[5] Rearing in LA was repeated across tadpole populations with repeat trials including embryos from different frog breeding pairs each time. As fertility varied across produced embryos the statistical occurrence was calculated per repeat trial. Data points in both graphs represent the malformation rate and survival rate of each tadpole populations sorted by rearing trial in order to account for issues across tadpole batches bred from the in-house from colony.

during optimization trials, 76% survival rate) compared to the control but the difference was found by the post-hoc test to be non-significant (*n.s.*) between these two rearing conditions.

By the end of the entire rearing experiment, the same multiple comparisons test did not find any difference between the two conditions: N=55/370 total tadpoles died in the control condition (85.1% survival rate) and N=85/347 total tadpoles died in the 0.01% MS-222 condition (75.5% survival rate; *n.s*; See Figure 4.2 Bii). Following the optimization trials, these findings indicated that the occurrence of malformations and the survival rate were affected by MS-222 in a dose-dependent manner and so to lessen the impact of MS-222 on the activity deprivation experiment the 0.02% condition was omitted from future trials, and all LA rearing was subsequently conducted in 0.01% MS-222 (now termed the “LA” experimental condition in proceeding sections and figures).

4.3.2 Myotomes in LA Tadpoles Demonstrated Differences in Myocyte Morphology

Following documentation of external differences in tadpole anatomy, rostrocaudal cross-sections were taken from tadpoles in both rearing conditions to compare internal anatomy. The anatomy appeared unaltered in LA tadpoles and the overall structure and orientation was preserved. This was done by evaluating and comparing the structure of the myotomes by measuring the length of each myotome cross-section (μm; taken from the total area) ($t_{(26)}$ = 2.05, *n.s.*; control mean ± SEM = 316.52 ± 8.11 μm; N = 14 control tadpoles; LA mean ± SEM = 341.52 ± 11.66 μm; N = 14 LA tadpoles) and average area (μm) of the structure within tadpole mid to rostral SC sections ($t_{(26)}$ = 0.81, *n.s.*; control mean ± SEM = 47317.57 ± 222.8 μm; N = 14 control tadpoles; LA mean ± SEM = 45119.31 ± 1572.5 μm; N = 14 LA tadpoles).

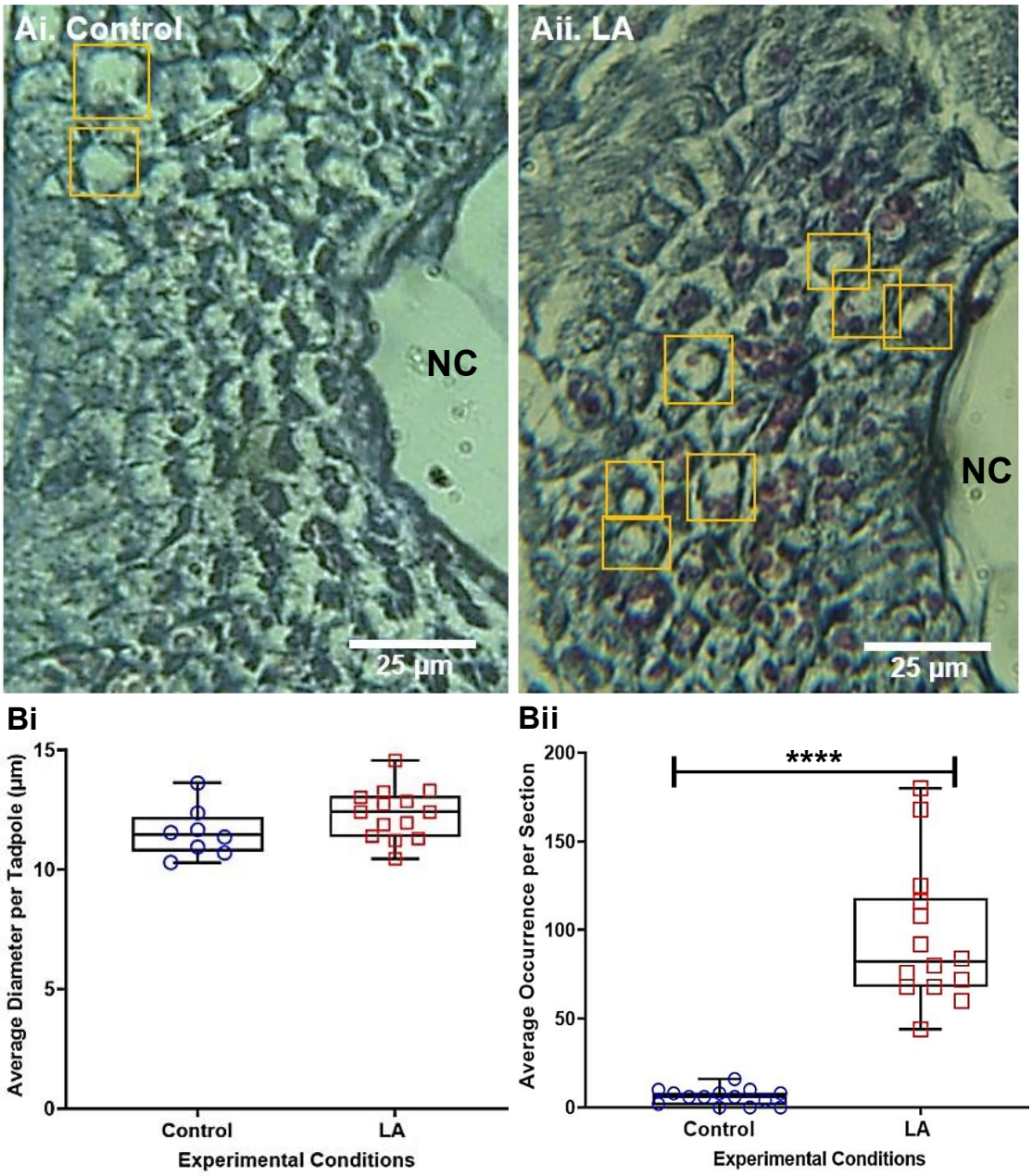

Figure 4.3: Increased Occurrence of Round Myocyte Morphology Within Myotome of LA Tadpoles. A. Comparison of morphological differences in myotome structure between (Ai) control and LA tadpoles (Aii). Images feature the ventral right myotome region, bordering the NC, were taken from a section at the mid-rostral SC level of LA and control tadpoles and stained with H&E. A myocyte structure that was widely occurring in LA tadpole featured with rounded morphology (structure outlined by orange box). The myocyte structure and diameter is similar between rearing conditions (Bi). There is instead a significantly higher occurrence of myocytes exhibiting this structure across LA tadpole myotomes compared to control (Bii). [**** indicates a statistical significance of $p \leq 0.0001$.]

While no structural difference were detected in LA myotomes, individual myocytes comprising this tissue type demonstrated a round morphology in cross section: characterized by a thick outer membrane layer (Figure 4.3 Aii, orange box). This round morphology has also been noted in some myocytes within control tadpole sections (Figure 4.5 Ai, orange box). The diameter of the myocyte did not significantly vary between control and LA tadpoles (Bi) however the average dorsoventral distribution of this round morphology per myotome section was notably widespread in LA tadpoles compared to the control as there was a measurably higher population of round myocytes within the myotome sections of LA tadpoles ($t_{(26)}$ = 2.06, p ≤ 0.0001; N = 14 tadpoles; LA mean ± SEM = 95.78 ± 10.63 round myocyte per myotome cross-section) compared to in the control (control mean ± SEM = 6.57 ± 1.41 round myocyte per myotome cross-section, N = 14 tadpoles).

The myocytes observed in the LA tadpole myotome were also identified in the myotome of control tadpole cross-sections. These myocytes shared a similar morphology and size ($t_{(20)}$ = 1.65, *n.s.*; Figure 4.3 Bii), which was compared by measuring the myocyte diameter in myotome cross-sections from tadpoles in the LA condition (mean ± SEM = 12.34 ± 0.29 mm) to tadpoles in the control condition (mean ± SEM = 11.56 ± 0.37 mm). This indicates that the round myocyte in LA tadpoles is structurally equivalent to the round noted in control myotomes.

4.3.4 Expression of α3 in the SC and Myotome Increased in LA Tadpoles

Previous studies tracking α3 expression across *Xenopus* development have recorded an increase between NF stage 32 and stage 40 (Rahman et al., 2015) which is notable for developmental range when the occurrence, and complexity, of tadpole swimming gradually increases (van Mier, Armstrong and Roberts, 1989a; Sillar, Wedderburn and Simmers, 1991; Sillar and Li, 2020). Whether this increase is attributable to the advent of movement in tadpoles is unknown however measuring expression in tadpoles that have been deprived of movement provided a relevant avenue of research into this potential upregulation.

A series of ELISAs were run (N = 6 independent experimental repeats) to measure whether α3 expression differed within the entire body[6] of tadpoles from each rearing condition. Notably, a K-S normality test did demonstrate that variation was normal within the control data set however the LA dataset distribution was found to be not normally distributed by the same test. Average colorimetric intensity was similar in the LA condition (mean ± SEM = 187.4 ± 50.55%) and the control (mean ± SEM = 139.2 ± 54.1%). Therefore the results were not found to be statistically significant (U = 13, p = 0.485, *n.s*) between the two groups. These findings indicated that movement deprivation over the course of development did not significantly increase α3 expression within the body of LA tadpoles, although variation in α3 within exact tissue types within LA tadpoles was not assessed in this experiment.

4.3.5 Expression of α3 Increased in SC of LA Tadpoles

Differences in α3 expression within specific tissue types of NF stage 42 tadpoles was evaluated by measuring the CTF of specific anatomical structures within SC-level sections taken from individual tadpoles in the control (Figure 4.4 Ai-Aii) and LA (Figure 4.5 Bi-Bii) rearing conditions. All tadpole sections were compared to a shared negative control (Figure 4.4 Ci-Cii) to directly assess the difference in positive α3 labelling present within the SC sections of tadpoles from each rearing condition (see Chapter 2.2.11).

Further analysis revealed that expression of α3 within the SC was significantly higher in LA tadpoles (N = 11 tadpoles; mean ± SEM = 375.4 ± 49.9%) compared to control tadpoles (N = 12 tadpoles; mean ± SEM = 167.1 ± 11.2%; $t_{(21)}$ = 4.24, p≤0.001; Figure 4.4 Dii). The overall pattern of α3 expression did not vary in the SC from LA tadpoles and overlapped consistently with the SC of control tadpoles (detailed noted in Chapter 2.3.1): broadly expressed, peri-somatic labelling across midline spinal neurons comprising the SC with comparatively high labelling noted within midline cells that directly bordered tadpole CC (Figure 4.4 Bii).

[6] Except the yolk sac which was cut from tadpole prior to commencing Protein Extraction protocol.

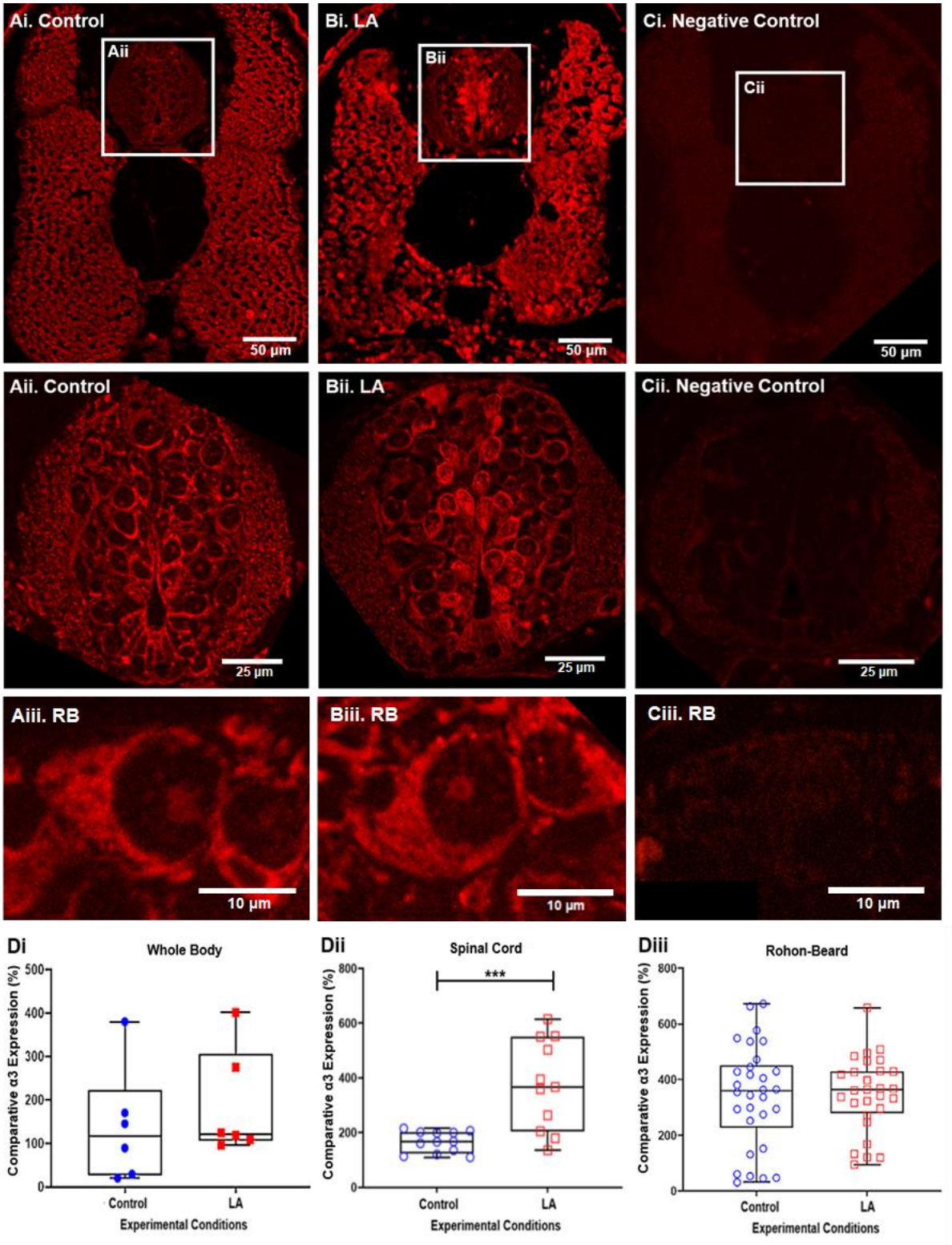

Figure 4.4: α3 Expression is Higher in SC of LA versus Control Tadpoles. A-B. Positive α3 labelling on SC level sections from control (Ai-Aii) compared to LA (Bi-Bii) tadpoles. C. All α3 labelled sections were compared to a negative control SC section (Ci-Cii). Labelling on RB neurons were also compared (Aiii, Biii, Ciii). D. α3 expression was quantified and compared across groups. α3 expression was not globally change in the tadpole body following LA rearing (Di). α3 expression did increase within the SC LA tadpoles compared to control tadpoles ($p \leq 0.001$) (Dii) however α3 expression did not change in RB sensory neurons (*n.s*) [Panels Ai, Bi, and Ci were taken at 20X magnification. Panels Aii, Bii and Cii were taken at 63X magnification; *** indicates significance of $p \leq 0.001$].

To assess whether α3 expression differed between specific spinal neuron subtypes due to movement deprivation, the CTF of individual RB neurons was measured and it was demonstrated that there was no statistically significant difference found between control (mean ± SEM = 341 ± 33.48%) and LA RB neurons (mean ± SEM = 348.7 ± 25.35%; $t_{(56)}$ = 0.18, *n.s* ; Figure 4.4 Diii) indicating that it was not upregulated in LA tadpoles.

4.3.6 α3 Expression Increased in Myotomes of LA Tadpoles

Like the SC, the surrounding myotomes were also visibly brighter in LA tadpole sections (Figure 4.5 Aii) compared to their control counterparts (Figure 4.5 Ai). Furthermore, the lack of fluorescent labelling in LA negative control sections further confirmed that this visual difference was not solely attributable to the altered myotome cell structure (Figure 4.5 Ai-Aiii;).

The average CTF of the tadpole myotome, measured per cross-section, was then calculated there was measurably higher expression in most LA tadpoles (N = 7/11 tadpoles) the average overall expression was measured to be higher in this group (mean ± SEM = 229.7 ± 18.36%) compared to tadpoles in the control ($t_{(20)}$ = 3.42, p ≤ 0.01; N = 11 tadpoles; control mean ± SEM = 146.5 ± 16%; Figure 1.7 Bi).

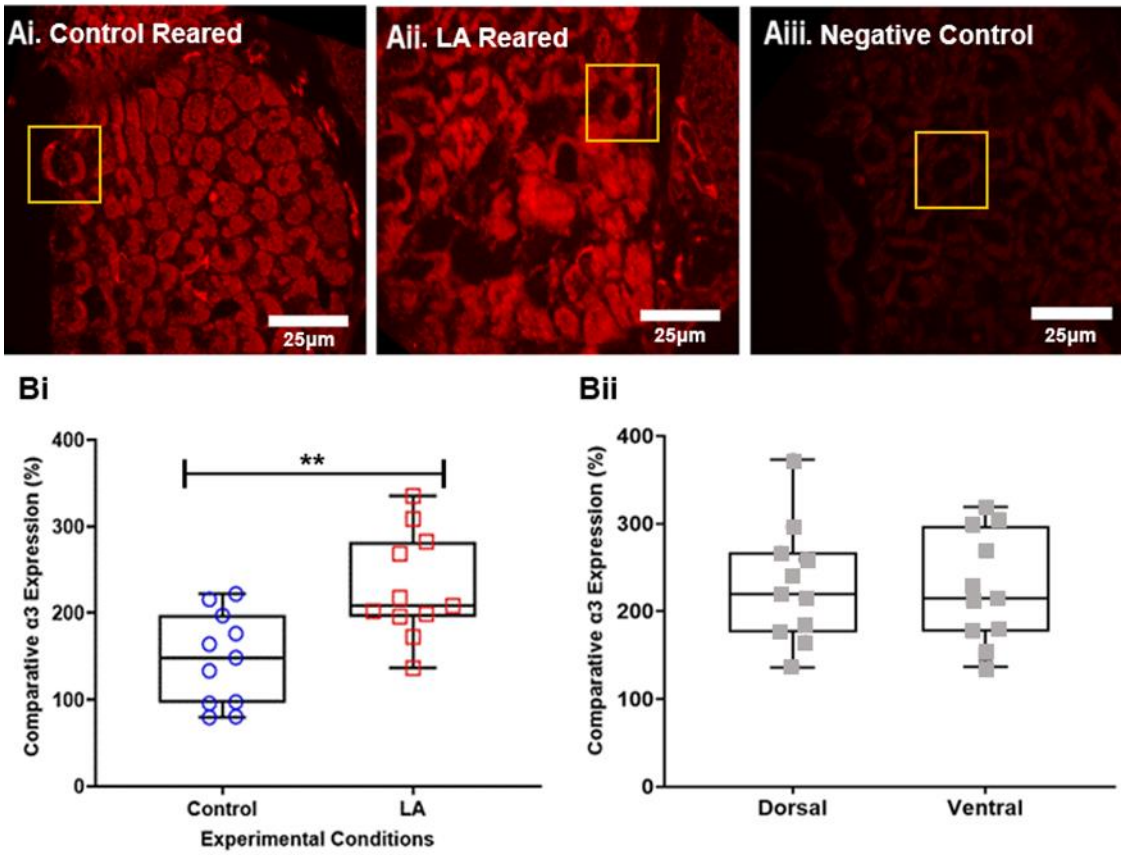

Figure 4.5: α3 Expression Increased in Myotomes of Control versus LA Tadpoles. A. Positive α3 labelling in right ventral myotome of SC level sections from control (Ai) compared to LA (Aii) tadpole myotome section. All positively labelled α3 sections were normalized to a negative control (Aiii). B. The CTF of α3 labelled myotome sections were averaged and compared between control and LA tadpoles and the found to be higher in LA tadpoles (Bi). The CTF of the dorsal and ventral myotome regions from LA tadpoles were also calculated, and no statistically significant difference was measured between the two (Bii). [Panel Ai-Aiii taken at 63X magnification, '**' indicates significance of p≤0.01].

The α3 expression level in dorsal (mean ± SEM = 230.3 ± 20.4) versus ventral myotome regions (mean ± SEM = 226 ± 19.13) was also assessed to measure whether this increase in α3 within the LA group myotome was evenly distributed across the entire section. As there was no statistical difference between the two regions it was determined that expression increased evenly across the entire myotome ($t_{(20)} = 0.13$, *n.s.*; Figure 4.7 Bii).

4.3.7 FXYD1 Expression Was Downregulated In the LA Tadpole SC

In contrast to the increase in α3 noted in LA tadpole SC, FXYD1 was measurably lower in the SC of LA tadpoles (N = 2; mean ± SEM = 169.6 ± 8.55%; Figure 4.7 Bi-Bii) compared to control tadpoles (N= 2; mean ± SEM = 299.8 ± 26.37%; Figure 4.7 Ai-Aii; $t_{(2)} = 4.6$, $p \leq 0.05$; Figure 4.7 Ci). Notably, cell populations that still demonstrated comparatively stronger expression of FXYD1 were consistently more dorsal in LA tadpoles sections (Figure 4.7 Bii) compared to in the SC of control tadpoles (Figure 4.7 Bi). The regions where fluorescence intensity was lower compared to the control was in the ventral cells bordering the LT indicating that FXYD1 was downregulated in the LA tadpole SC. This downregulation appeared restricted to these ventral spinal cells (Figure 4.6 Bii). FXYD1 labelling was also present in the membrane of these LT adjoining cells although fluorescence was weaker compared to the control (Figure 4.6 Bi).

Labelling was also bright enough to outline the primary neurites of lateral spinal neurons that projected into the LT of LA SC sections. There was still notable expression FXYD1 observed in the CSF-contacting tissue bordering the CC. As noted in the previous chapter (see Chapter 3.3.1 and 3.3.5) This labelling was not present on the membrane of midline cells bordering the CC. These findings indicate that movement deprivation induced two possible effects: either FXYD1 was diminished in spinal neurons, or it was not upregulated over the course of development.

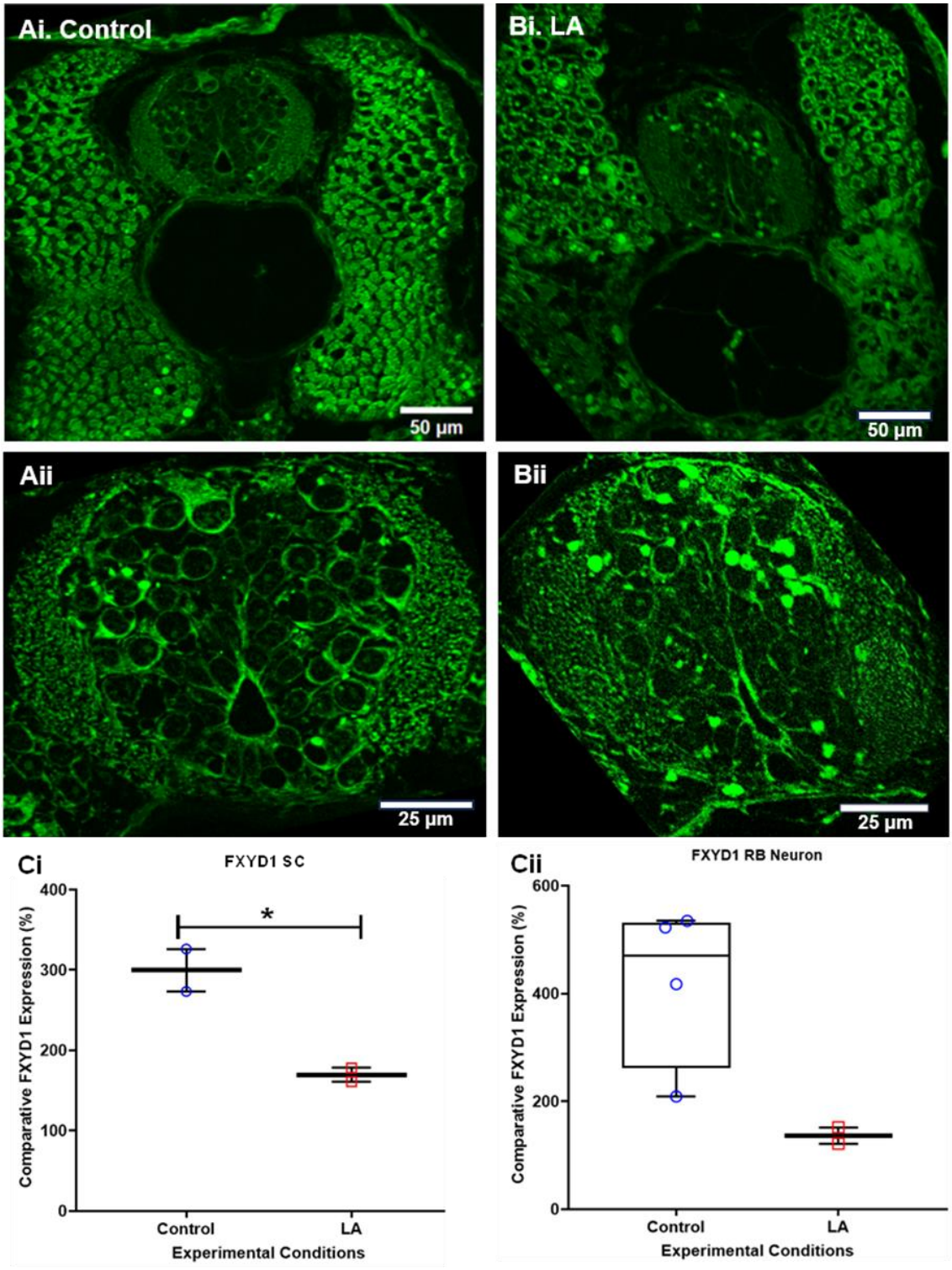

Figure 4.6: FXYD1 Expression Did Not Vary Within the SC of Control Compared to LA Tadpoles. A-B. Immunolabelling visualizes FXYD1 expression within the SC of control (Ai-Aii) versus LA tadpoles (Bi-Bii) tadpoles. C. FXYD1 expression (represented as CTF normalized to the negative control, %) was comparatively lower across the entire SC of LA tadpoles compared to the control (Ci). FXYD1 expression was not measurably different in dorsal RB sensory neurons between control and LA conditions (Cii). [Panels Ai and Bi were taken at 20X magnification. Panels Aii and Bii were taken at 63X magnification; * indicates significance of $p \leq 0.05$].

Alhough FXYD1 expression was diminished overall within the SC of LA tadpoles, this downregulation appeared restricted to ventral cells bordering the LT but did not occur to the same extent iin dorsal spinal neurons. Indeed, the RB sensory neurons situated in this region did not exhibit any statistical difference in CTF between the two rearing conditions ($t_{(2)}$ = 2.5, *n.s.;* Figure 4.6 Cii), which indicates that FXYD1 expression likely was not downregulated within this neuron type in the SC of LA tadpoles. Ultimately, FXYD1 was downregulated within the SC of LA tadpoles but expression remained consistent in the dorsal neurons of LA tadpoles.

4.3.8 Expression of FXYD1 in LA Tadpole Myotome

FXYD1 expression has been previously detected in the tadpole myotome of control tadpoles (See Chapter 3: Results; Figure 4.7 Ai) and was similarly observed in the myotome of LA tadpoles (Figure 4.7 Aii) when sections were assessed. The quantified FXYD1 expression was measured ($t_{(2)}$ = 2.5, *n.s.;* Figure 4.7 Bi) but was not found to differ significantly between the two rearing conditions (control mean ± SEM = 828.3 ± 60.4%; N= 2 tadpoles, 10 sections total, LA mean ± SEM = 677.4 ± 102.5%). FXYD1 expression was also compared between the dorsal and ventral myotome of LA tadpoles in order to account for the variation in myocyte structure within this condition. Ventral CTF was lower on average (dorsal mean ± SEM = 910.2 ± 61.7 compared to ventral mean ± SEM = 769 ± 36.6) however there was no statistical difference measured between these two spatial regions ($t_{(2)}$ = 1.97, *n.s.;* Figure 4.7 Bii). Overall, these statistical findings do indicate that FXYD1 expression in the myotome was not influenced by the abolishment of swimming during development of LA tadpoles, further scrutiny is required to ascertain repeatability of this suggested trend in LA tadpoles.

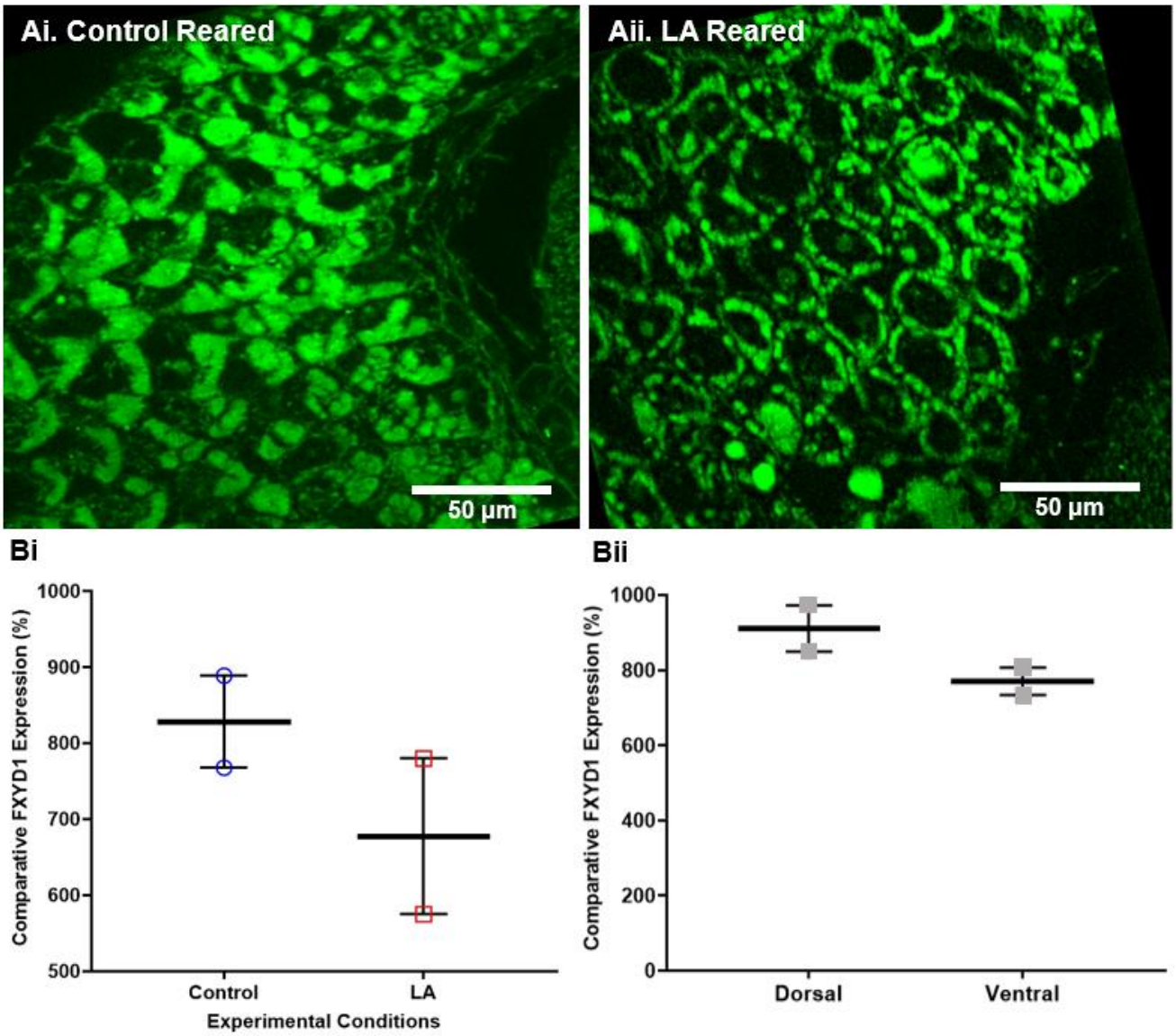

Figure 4.7: FXYD1 Expression Was Consistent Within the Myotome of Control and LA Tadpoles. A. Positive FXYD1 labelling in right dorsal myotome of SC level sections from control (Ai) compared to LA tadpole myotome section (Aii). B. The CTF of FXYD1 labelled myotome sections was found to be lower in LA tadpoles though this difference was not statistically significant (Bi). The CTF of the dorsal and ventral myotome regions from LA tadpoles were also calculated, and no statistically significant difference was measured between the two regions indicating consistent dorsoventral expression of FXYD1 within each myotome (Bii). [Panels Ai-Aii were imaged at 63X magnification].

4.3.9 How Movement Deprivation Influences Tadpole Swimming Behaviour

Another aim of this experiment was to expand on observations made in previous research into the effect of movement deprivation on swimming which documented that, upon removal from MS-222 (0.015% concentration throughout LA rearing) the tadpole gradually began to swim, demonstrating “normal” swim behaviour in the process (Bender, 2012). In my project it was confirmed that within the first five minutes almost full recovery from MS-222 was observed in LA tadpoles. Recovered tadpoles demonstrated motor output, all in the absence of externally applied stimulus, first through tail twitching that evolved rapidly into tail-based swimming. It was determined that even though swimming behaviour was demonstrated by LA tadpoles within the first five minutes of recovery, analysis of tail based swimming activity would be restricted to tadpoles that were allocated approximately 30 minutes recovery time in order to diminish the potential influence of the MS-222 as residual drug effects have been pinpointed as a confounding factor in a similar previous drug-induced movement deprivation study (Haverkamp and Oppenheim, 1986).

4.3.10 Tail-Based Swimming Varied Between Rearing Conditions

Swim episode duration of tadpoles from each rearing condition was tracked through videos and documentation of tail-based swimming was investigated by tracking their swimming dynamics over the course of each swimming episode. Since the myotomes of LA tadpoles underwent a notable shift in myocyte structure development (see above) it was deemed important to deduce whether previously observed “normal” swimming (Bender, 2012) could be subtly different due to uncharacterized changes in swimming behaviour. An immediate difference in body movement during swimming was apparent with control tadpoles relying upon their entire body, undulating from their trunk through their tail, (Figure 4.8 Ai panels 1-4) as opposed to LA tadpoles relying almost entirely on their tail (Figure 4.8 Aii panels 1-4).

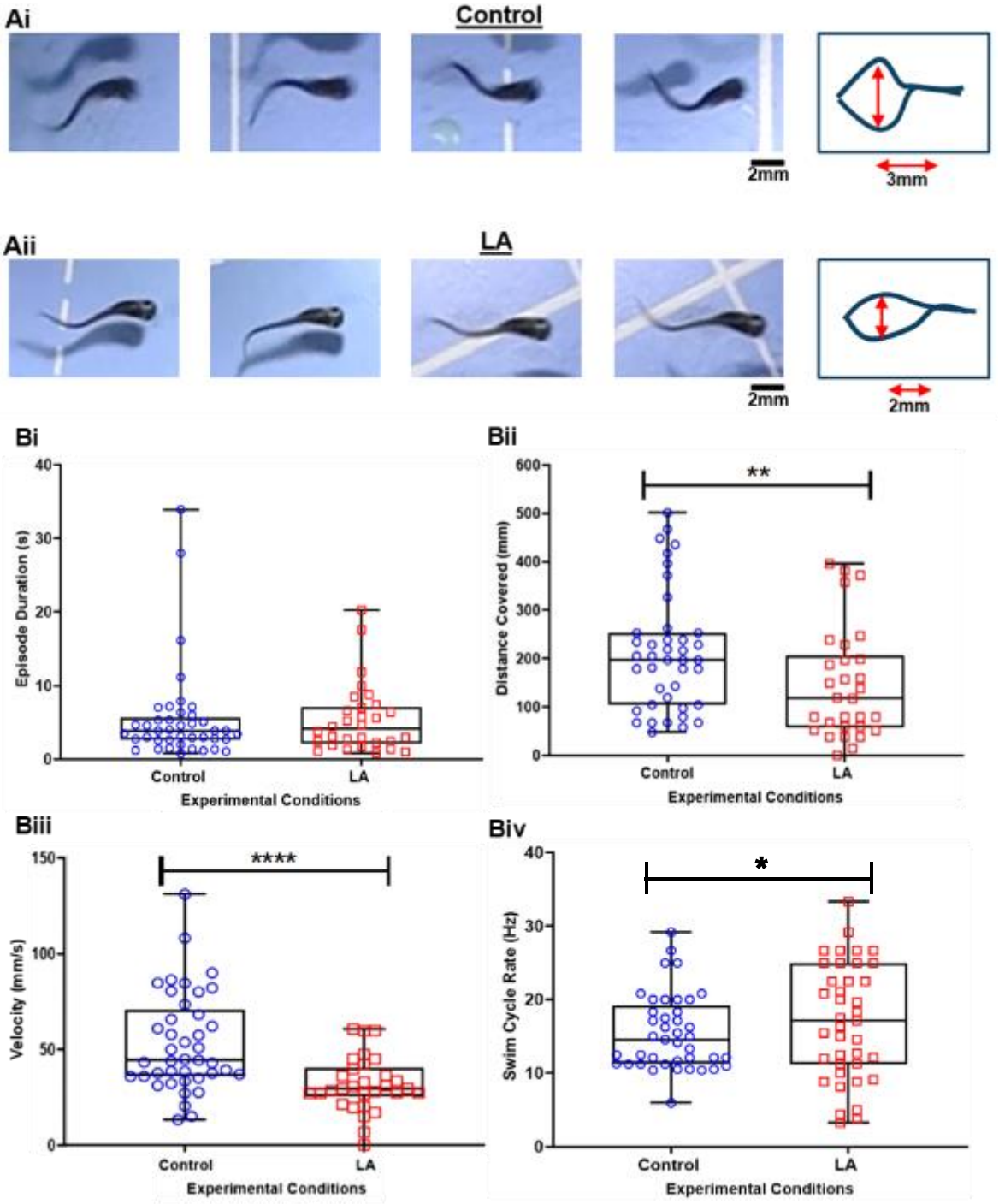

Figure 4.8: Tail-Based Swimming Differed in Control versus LA Tadpoles. A. Frames of tadpole swimming taken at ~5 ms intervals. Tail arc was measured (red arrow) and an overlay was made to compare average diameter between tadpoles from the control (Ai) and LA (Aii) rearing conditions. B. Average swim episode duration (s) was evaluated for tadpoles who stopped swimming spontaneously rather than through activation of the TG pathway (Bi). The average swim distance per episode was also calculated (mm) and control condition tadpoles covered a greater distance compared to the LA condition (Bii). Velocity (mm/s) was calculated using the prior two measured values and was calculated to be higher in control tadpoles (Biii). Swimming frequency (Hz) was calculated by measuring the duration of each tadpole's swim cycle and there was no measurable difference noted between the two rearing conditions (Biv). [* indicates significance of p≤0.05, ** indicates significance of p≤0.01, **** indicates significance of p≤0.0001].

Swimming mainly relies upon tail undulations for propulsion and so the tail arc of tadpoles from each rearing condition was measured (Figure 4.9 Ai-Aii, panel 5). A K-S normality demonstrated that tail arc (measured at point of maximum bend angle where rostral the rostral body aligned closest to the caudal tail; Figure 4.8 Ai-Aii, red line) significantly varied between the two tadpole populations as there was found to be higher variability in the control data set (N = 56[7] tadpoles, p = 0.01) compared to the LA data set (N = 38 tadpoles, p = 0.0001). There was furthermore a statistically measurable decrease (U = 307.5, p ≤ 0.0001) in arc diameter (mm) documented in LA tadpoles (mean ± SD = 1.67 ± 2.66 mm) when compared to control tadpoles (mean ± SD = 2.49 ± 4.48 mm).

Swim episode duration data did not pass K-S normality test in either condition but overall, the mean episode duration was not comparatively different (U = 49.5, *n.s.*) between control tadpoles (N = 41 tadpoles, mean ± SD = 5.05 ± 41.82 s) compared to LA tadpoles (N = 30 tadpoles, mean ± SD = 5.4 ± 25.5 s; Figure 4.8 Bi). Despite this, the average total distance (mm) travelled during each episode was found to be larger in control tadpoles (mean ± SD = 240.2 ± 22.04 mm) compared to LA tadpoles (mean ± St Dev = 128.5 ± 15.17 mm; U = 392, p ≤ 0.01).

To assess whether the difference in distance covered during swimming was due to the noted difference in tail arc between the tadpoles influencing tadpole speed, the velocity (Figure 4.9 Biii) and swim frequency (Hz) (Figure 4.8 Biv) of each swim episode was also measured. Average velocity was higher in the control group (mean ± SD = 52.95 ± 3.98 mm/s; U = 276, p ≤ 0.0001) indicating that they swam at a higher speed compared to LA tadpoles (mean ± SD = 33.89 ± 2.69 mm/s; Figure 4.8 Biii). A similar observation was also noted in the previous study where the fastest recorded LA tadpole did not exceed 93 mm/s (Bender, 2012). By comparison the fastest speed attained by an LA tadpole in this study was 71.9 mm/s in comparison to the fastest control tadpole speed of 130.3 mm/s. The swim frequency

[7] Tadpole tail arc was measured based upon clarity of video footage at higher magnification and so included tadpole swim episodes that were halted by CG stimulation rather than spontaneously.

(Hz) was also measurably higher on average in LA tadpoles (mean ± SD = 19.52 ± 0.26 Hz) compared to in the control (mean ± SD = 15.5 ± 0.8 Hz; U = 394, $p \leq 0.05$, Figure 4.9 Biv). All of this indicates that while the diminished tail arc diameter may have allowed more swim cycles to be completed per second in LA tadpoles this did not enhance their overall speed.

The consistent variability across the control tadpole swimming data sets demonstrated that swimming behaviour was more adaptable in control tadpoles compared to LA tadpoles (data sets which did not pass the K-S test include: recorded tail arc, swim duration (s), swim distance (mm), swim frequency and average velocity (mm/s). LA swim data was more consistent with the only data sets that did not demonstrate normal distribution being duration and swim distance. These tests indicated that control tadpole swimming could potentially be more complex than LA tadpoles by NF stage 42 if the tadpoles are capable of altering their speed and swim duration more in response to external stimuli. This was considered when assessing the variability in swim path trajectory between rearing conditions.

4.3.11 LA Rearing Induced Changes in Swimming Trajectory

The trajectories of tadpole swimming were tracked using an Animal Tracker API plugin in ImageJ on video files. The plugin illustrated the complete trajectory of the tadpole to be traced (Figure 4.9 Ai-Aii, red line) with the starting point (Figure 4.9, green circle) and end point (not illustrated) demarcated by the program. Any overlapping swim trajectories (categorized as swim path intersection) were compared across tadpoles and categorized. Tadpole path intersection was tracked blindly, tallied and set as percent occurrence per tadpole swimming episode (%). Next, I tracked the number of times that these path intersections were repeated within a single swim episode of each tadpole.

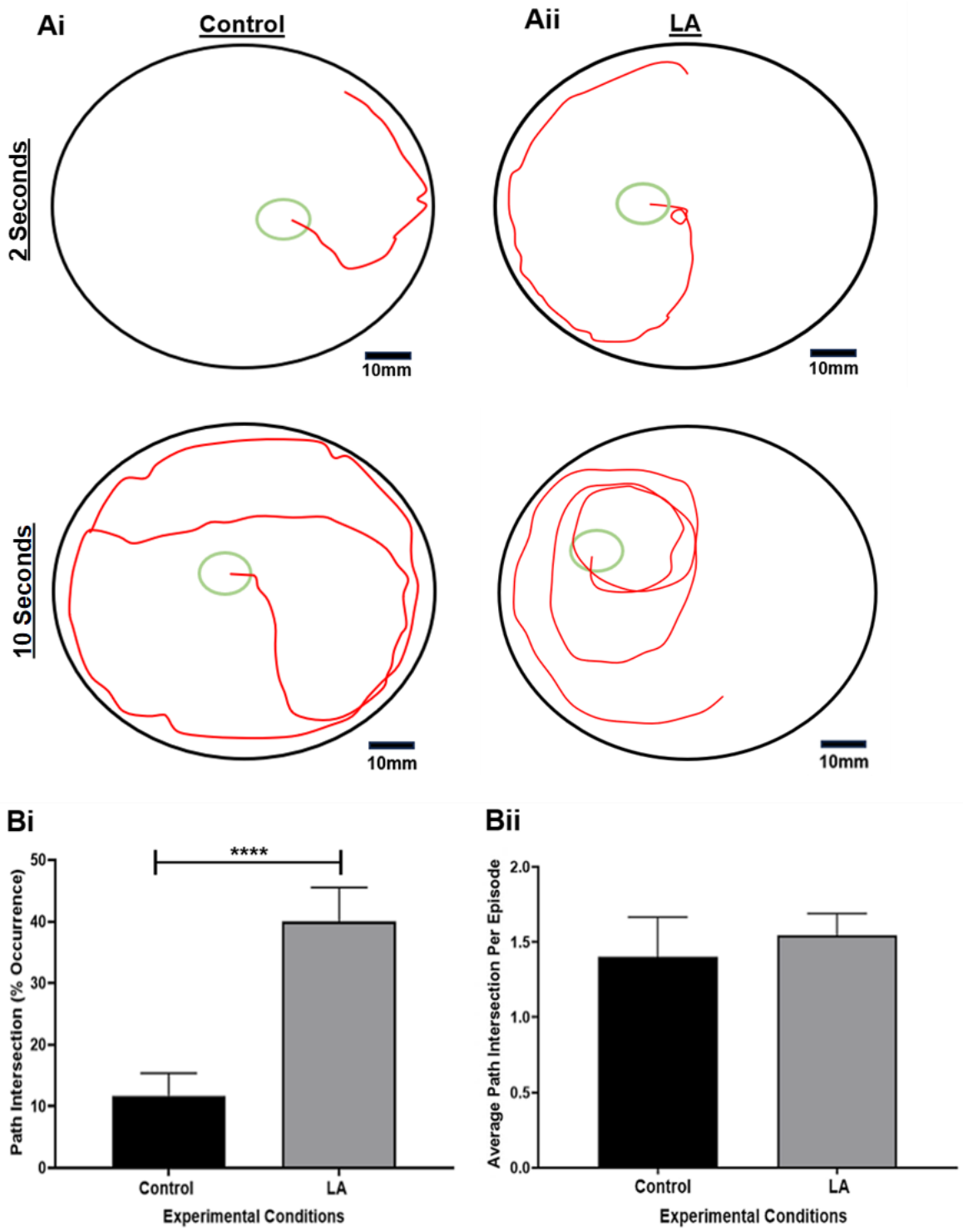

Figure 4.9: Comparative Analysis of Swim Paths Trajectory Between Experimental Groups. A. Overlay of tracked (using Animal Tracker API) swim paths of (Ai) control and (Aii) LA tadpoles based on swim duration: 2 s and 10 s. Swim paths were traced (red line) and the starting point outlined (green). B. Swim path intersection was also compared between the two experimental groups (Bi). Across all measured swim episodes, the percent occurrence of swim path intersection was calculated and found to be more frequent in the LA rearing group (40%) compared to the control group (12.9%). The average number of times a tadpole intersected their own swim path within a swim episode was also calculated but there not found to be significantly different between groups (Bii). [Error bars represent SEM; **** indicates significance of p≤0.0001].

Swim paths were first compared by measuring where in the petri dish tadpoles tended to swim. This was assessed by measuring how frequently tadpoles crossed their own path while swimming, represented as an intersection in the line tracing this path. Path intersection occurred more frequently amongst LA tadpoles (LA mean ± SD = 40 ± 5.51% of tadpoles per rearing trial; U = 2222; Figure 4.9 Bi) compared to their control counterparts (control mean ± SD = 12.99 ± 3.86% of tadpoles per rearing trial). However, the average number of path intersections per swim episode did not vary between populations indicating that while LA tadpoles were more likely to cross their own path during swimming, they were unlikely to cross their swim path any more frequently than the control tadpoles (Control mean ± SD = 1.5 ± 0.86%, LA mean ± SD = 1.65 ± 0.66%; $t_{(35)} = 2.03$, *n.s.*; Figure 4.9 Bii). However, the increased occurrence of path intersections amongst LA tadpoles could be attributed to their altered swim path within the petri dish.

A common area frequented by tadpoles from both rearing conditions was near the petri dish wall. Many swimming episodes tracking the animal demonstrated a path that skirted the border of the petri dish in which they were placed (represented most clearly in Figure 4.9 Ai-Aii, 2 Seconds). This preference was more frequently observed (U = 637, $p \leq 0.001$) amongst control tadpoles (87.5%) compared to LA tadpoles (47.4%) though it did still occur in this population. The left-right preference of tadpoles was assessed by measuring the number of times a tadpole changed their swimming direction mid-episode. Since most control tadpoles tend to skirt the petri dish wall during swimming any potential direction preference was also assessed by using the petri dish to delineate travel as being either clockwise or counterclockwise. Tadpoles did not display a preferred direction during swimming as left versus right turning was found to be entirely random with majority of tadpoles from both populations swimming in the same direction as they started in for the duration of the episode. Sudden turning (orienting body in opposite direction of original swim path) was also tracked using the animal API tracker. Turning did not occur significantly more

frequently in LA tadpoles (18.4% occurrence per swim episode) compared to control tadpoles (7.4% occurrence; U = 944, *n.s.*).

4.3.12 LA-Induced Changes in Stopping Behaviour

In contrast to control tadpoles which were largely sessile by hanging from the water surface by CG-secreted mucous (Figure 4.10 Ai), LA tadpoles were observed to remain supine at the bottom of the petri dish in which they were kept (Figure 4.10 Aii). For control tadpoles this consistent pulling exerted to their CG by their hanging promoted sessile behaviour through continuous sensory stimulation to the TG neurons innervating this gland. Comparably, the CG gland appeared anatomically indistinct from tadpoles in either group (Figure 4.10Bi-Bii) indicating that diminished stimulus to this gland did not impact its structural development in LA tadpoles (Figure 4.10 Bii).

As noted in previous work LA tadpoles presented with a decrease in sensitivity to external stimulus applied to their CG (Bender, 2012). This was noted in instances when tadpoles would swim directly into the petri dish, placing pressure on the CG and continue to swim for periods exceeding previously documented stopping response in tadpoles (~75 ms). (Boothby and Roberts, 1992; Li, Wagner and Porter, 2014). In my project, I found that the LA tadpoles continued swimming into the barrier for more swim cycles than previously reported (Figure 4.10 Ci). To identify if this effect differed significantly from their control counterparts, tadpoles from each condition were placed in a petri dish and allowed to swim freely until contacting the wall of the dish. Collision required direct contact of the head to the barrier to ensure CG was stimulated during this impact. Conditions were also considered in the event that stopping behaviour was GIRK-mediated (Li, Zhu and Ritson, 2017) and stopping behaviour that featured a sudden increased swim frequency post-collision and ceased within 0.3 seconds was determined to possibly be due to activation of this pathway rather than the CG.

The anticipated time post-CG stimulation for stopping to occur was previously recorded as approximately 0.15 s (Boothby and Roberts, 1992; Li, Wagner and Porter, 2014). Tadpoles in

both rearing conditions swam for longer than this expected time though data was very largely dispersed, as indicated by a K-S normality test. While swim time was unexpectedly prolonged in both conditions, including the control (mean ± SD = 0.9 ± 1.4 s), the average duration was significantly longer amongst LA tadpoles (mean ± SD = 17.75 ± 62.9s; U = 1664, $p \leq 0.05$; Figure 4.10 Ci). In a portion of LA tadpoles (N = 8/57 tadpoles) swimming would continue for minutes at a time post-collision with the wall (Figure 4.11 Ci).

Swim frequency post CG stimulation was also compared between the two rearing conditions and both rearing condition data sets were not found to be normally distributed. Swim frequency was found to be higher amongst LA tadpoles (mean ± SD = 11.57 ± 4.5 Hz) compared to in the control (mean ± SD = 9.67 ± 4.86 Hz, U = 1469, $p \leq 0.01$) following CG-stimulation. This change was noted as a significant decrease from the previously reported control (control Pre-CG mean ± SD = 15.5 ± 2.9 Hz) and LA (LA Pre-CG mean ± SD = 19.52 ± 5.2 Hz) swim rates.

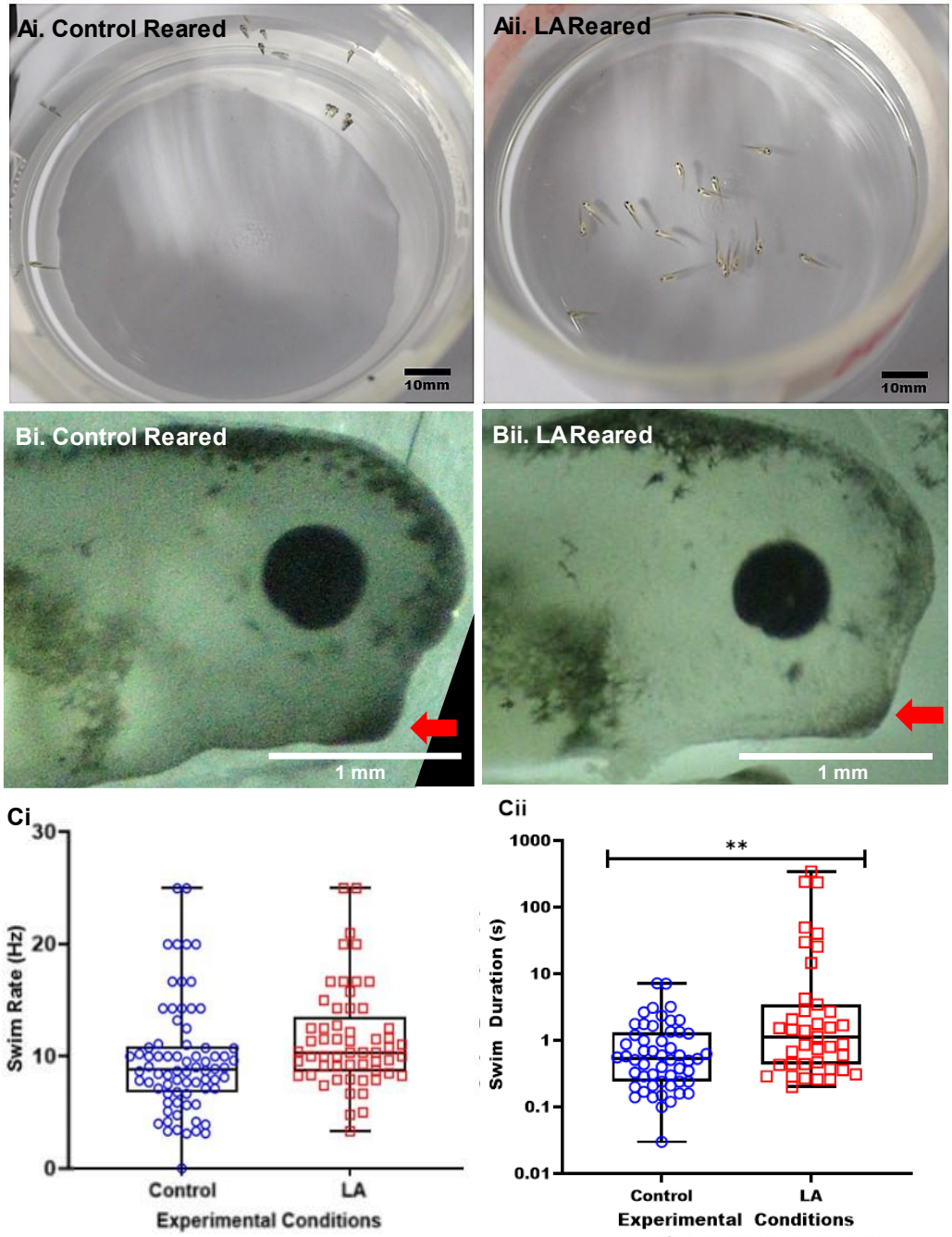

Figure 4.10: CG-Stimulated Stopping Behaviour is Altered in LA Tadpoles. A. Larval tadpoles under control conditions (NF stage 39-40) will suspend vertically from the water surface through mucous secreted from their cement gland (Ai) while LA tadpoles remain supine at the petri dish bottom (Aii). B. Comparison of CG structure (indicated by red arrow) from control (Bi) and LA (Bii) NF stage 42 tadpoles demonstrated no obvious anatomical difference. C. Swim cycle frequency (Hz) post CG contact did not differ between groups (Ci). Average swim duration (s) was significantly longer in LA tadpoles versus control tadpoles post-CG stimulation induced by direct vertical contact with barrier (petri dish wall) during swimming (Cii). Duration was highly variable amongst LA tadpoles with N=6 swimming episodes duration exceeding 1 minute[8]. [** indicates significance of p≤0.01].

[8] Removal of outliers identified through a Grubb's test (N=8/57 LA tadpoles) demonstrates that post-CG swim duration is still comparatively longer on average in LA tadpoles compared to their control counterparts ($p < 0.05$).

LA swimming frequency decreased the most following CG-stimulation ($U = 337$, $p \leq 0.05$) although the difference was noted to be equivalently significant amongst control tadpoles, which also swam at a higher frequency prior to collision with wall ($U = 665$, $p \leq 0.05$). In summary, the responses of LA tadpoles to contact with a barrier in their swim path are consistent with a decrease in the efficiency of the CG stopping pathway.

To ascertain if the difference in stopping behaviour was due to anatomical differences in head and CG formation, the structure was compared between tadpoles. The size and shape of the head and CG did not differ noticeably between the animals from both groups (Figure 4.10 C, CG indicated by red arrow). Therefore, the diminished stopping response following CG stimulation likely was attributable to changes in the underlying neuronal pathway from the CG to the motor circuits of the SC (Figure 4.2B).

4.3.13 Movement Deprivation Leads to Increased Fatigue

Following the first swimming episode, from which the measurements in the above sections were taken, tadpole fatigue was then assessed by repeatedly pipetting the tadpole into the petri dish until swimming ceased entirely even with further pipetting. Fatigue was then assessed by measuring the number of total episodes completed. While the average number of episodes completed before fatigue was consistent among control tadpoles there was measurably higher variation amongst LA tadpoles ($p < 0.0001$). Control tadpoles completed more episodes on average ($N = 54$ tadpoles; mean ± SD= 7.65 ± 2.3 episodes) compared to LA tadpoles ($N = 50$ tadpoles; mean ± SD = 4 ± 2.2 episodes; $U = 305.5$, $p \leq 0.0001$) indicating that control tadpoles are more fatigue-resistant while LA tadpoles fatigued more easily by comparison (Figure 4.11 Ai)

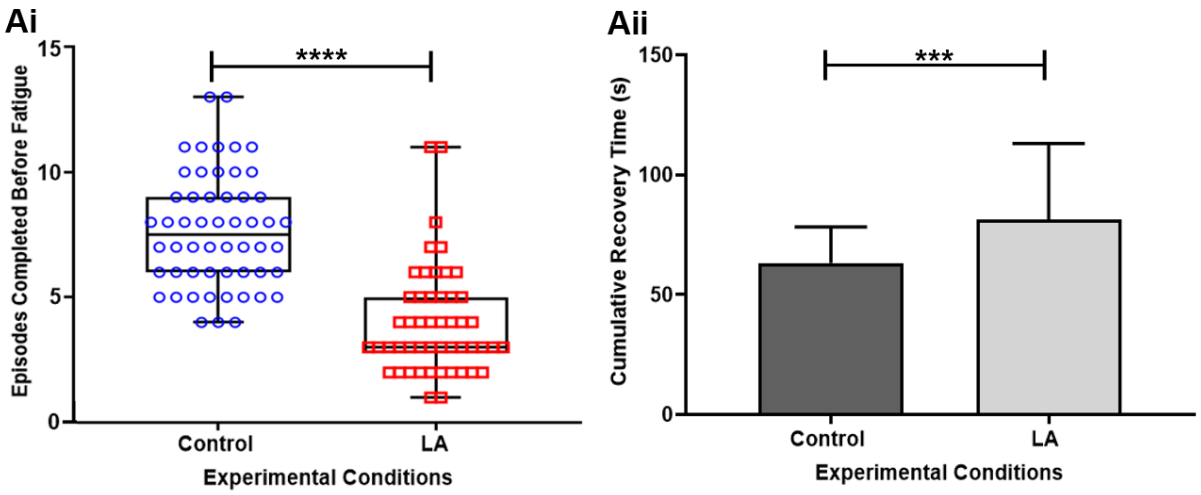

Figure 4.11: LA Tadpoles Were More Easily Fatigued and Required More Time to Recover Swimming. A. Tadpole swimming was stimulated repeatedly, initiating swim episodes in quick succession (<5 s) until swimming ceased entirely (Ai). Control tadpoles completed a higher number of episodes compared to the LA tadpoles (Ai). Following fatigue induction, tadpoles were given a period to recover (30 s) in which to recover. Control tadpoles also required less time to recover compared to LA tadpoles indicating that control animals recovered more easily from fatigue (Aii). [** indicates significance of p≤0.01, *** indicates significance of p≤0.001].

Following fatigue induction, tadpoles were given an interval period in which to recover, during which time each tadpole could rest in untreated water without being subjected to any external stimulus or intervention. If tadpole swimming did not resume following this period, the animal was assigned more time to recover. The cumulative recovery time was dispersed similarly between both groups ($p < 0.0001$) as noted by a K-S test. On average, control tadpoles required less time to recover (mean ± SD = 63.24 ± 14.8 s, N=54 tadpoles) compared to their LA counterparts (N=50 LA tadpoles, mean ± SD = 81.3 ± 31.8 s; $U = 972.5$, $p \leq 0.001$; Figure 4.11 Aii). The swim episode duration was compared within rearing conditions to track any decrease in CPG output following repeated stimulation. In the majority of tadpoles, the first swim episode was longer than the final episode preceding cessation of swimming (termed the pre-recovery episode) in both the control (N = 25/33 tadpoles, first episode duration, mean ± SD = 7.155 ± 11.55 s, pre-recovery episode duration mean ± SD = 3.82 ± 3.96 s; $W = 131$, $p \leq 0.01$) and LA conditions (N = 28/43 tadpoles, first episode duration, mean ± SD = 5.2 ± 4.2 s, pre-recovery episode duration, mean ± SD =

2.68 ± 1.72 s; W = 224.5, p ≤ 0.01) indicating that by the final swim episode, the swim duration decreased by approximately half of the first swim episode in both groups.

To compare whether swim episode durations following the recovery period (termed the post-recovery episode) returned to normal, a Wilcoxon Signed rank test was run comparing any difference to the first swimming episode for each tadpole. In a majority of the control population (N = 23/33 tadpoles), the post-recovery swim episode duration was found not to statistically differ from the first episode duration (post-recovery mean ± SD = 6.6 ± 11.29 s; W = 224.5, *n.s.*) indicating successful swimming recovery following fatigue. While swim duration also increased by the post-recovery episode in LA tadpoles (N = 39/43 tadpoles, post-recovery mean ± SD = 4 ± 8.17 s) this was still found to be significantly lower compared to the first swimming episode duration (W = 253, p ≤ 0.01) indicating that LA tadpoles did not fully recover from fatigue, despite having a longer cumulative rest time on average compared to control tadpoles (Figure 4.11 Aii).

4.3.14 Brief Summary of Low Activity Rearing Experiment

1. Tadpoles reared in a higher MS-222 concentration (≥0.02%) had a higher occurrence of anatomical malformations and had a lower survival rate compared to control tadpoles. At a lower concentration (≤0.005%) tadpole larvae demonstrated a significantly higher tolerance for the anaesthetic and would resume moving by NF stage 32 during the rearing period.

2. In transverse cross-sections, the internal anatomy of the LA tadpole CNS retained a similar superficial structure to their control counterparts. In the myotome, a subset of individual myocytes presented with a round morphology which might indicate that movement plays a key role in structural development.

3. Sodium pump subunits demonstrated differential changes in expression within the LA tadpole SC in response to movement deprivation experiments: α3 was upregulated whereas FXYD1 was downregulated. This trend was also noted in the myotome of LA tadpoles however only the difference in α3 expression was found to be statistically significant.

4. LA tadpoles swam at a lower speed compared to control tadpoles, however their swim cycle frequency was comparatively higher owing to mechanical changes in their tail-based swimming.

5. During swimming, the LA tadpole swim path was less likely to border the petri dish wall leading to a higher occurrence of path intersection, possibly due to the smaller area in which they swam. LA tadpoles were fatigued more quickly and required a comparatively longer recovery period for swimming to return.

6. LA tadpoles took longer to stop swimming upon collision of their head with a barrier and a subset of tadpoles would continue to swim into the side of the petri dish for upwards of a minute. Given the experimental constraints, it is difficult to determine which underlying pathway (CG or GIRK) is mediating the stopping response in both tadpole conditions, but this response is noticeably less sensitive in LA tadpoles.

7. There was no visible structural difference in the head or CG of LA tadpoles. Tadpoles also hung from the water meniscus less often in the LA condition.

4.4 Discussion

4.4.1 LA Rearing Induced Variable Structural Changes in Tadpoles

As stated previously, this project sought to expand upon work presented by Bender (2012) and optimize the LA rearing protocol for future, specific experiments. This was done by first evaluating if MS-222 affected tadpole development across concentrations, measuring whether MS-222 induced concentration-dependent alterations in tadpole development and identify a low, effective concentration at which swimming did not occur over the course of development. Following this, the next aim involved tracking expression of α3 and FXYD1 within the tadpole CNS and myotomes in control and LA tadpoles. The final aim focussed on tracking tadpole swimming function by evaluating the tadpole swim path, mechanics of tadpole swim function and relationship between ISI and swim episode duration.

Before evaluating swim behaviour, it was important to assess any changes that LA rearing conditions may have induced in tadpole anatomy. While Bender (2012) did not note any major anatomical aberrations due to LA rearing she did not investigate this at the internal level nor observe any changes in cell size or shape. Furthermore, the present project sought to establish whether there were any baseline physical changes within the CNS and surrounding tissue potentially as a direct result of movement deprivation over the course of embryonic and larval development. This was investigated by observing the external tadpole morphology (Figures 4.2) and then by evaluating internal structures by imaging CNS cross-sections. Structural changes were subtle and there were minimal noted differences in LA tadpole size (tail length) or in the shape and orientation of their internal anatomy, particularly their CNS. Furthermore, at the optimized MS-222 concentration the occurrence of observable malformations were statistically no different from control tadpoles indicating that MS-222 was applied at a low enough concentration that effects outside of movement restriction were negligible and unlikely to directly impact tadpole behaviour.

The SC structure was unaffected by LA rearing, retaining the previously outlined structural dimensions and dorsoventral cell alignment including the CC location, midline cells, dorsal RB sensory neurons and cells bordering the LT (See General Introduction Figure 1.4 and Figure 4.5 Ai-Aii and Bi-Bii) (Kahn and Roberts, 1982; Clarke and Roberts, 1984). This finding aligns with previous research which indicated that cell fate and the spatial mapping of spinal neurons in *Xenopus* (Thuret, Auger and Papalopulu, 2015) occurred early enough in development (NF stage 10.5) to be independent of environmental influences such as anaesthetic-induced movement deprivation. There was no observable effect on cellular differentiation in the SC of LA tadpoles (Figure 4.5 Bii); for example, RB sensory neurons developed apparently normally and the cellular structures of other spinal neurons were indistinguishable from the control (Figure 4.5 Aii) (Roberts and Clarke, 1982).

4.4.2 Altered LA Tadpole Myocyte Structure Is Due to Blocking Muscle Contractions

When view externally, the size and overall appearances of the myotomes were not obviously impacted in LA tadpoles compared to control animals. However, when viewed in cross section, the myotome of LA tadpoles were comprised of myocytes with distinct round morphology (Figure 4.3 Aii & 4.5 Aii). Round myocytes were also noted in control animals but less frequently, suggesting an upregulation of myocytes expressing this structure was linked directly to movement deprivation (Figure 4.5 Bi). This latter explanation could also help to account for the structural variation within the LA myotome (Figure 4.6 Bi).

Myocyte differentiation occurs between NF stage 22 and 28 with the appearance of myocytes identified as early as NF stage 24 (Huang and Hockaday, 1988). The construction of myocytes relies upon careful organization of their myofilaments which in turn receives essential feedback from a series of calcium cascades released from intracellular stores (Ferrari et al., 1998). During muscle contraction the electrical activity begins on the surface membrane and is conducted to the cell interior to regulate sarcoplasmic reticular calcium release (Franzini-Armstrong, 2018). This is referred to as excitation-contraction coupling. When LA animals were exposed to the hydrophilic anaesthetic MS-222, motor function was

abolished due to specific block of voltage-dependent Na^+ channels in neurons and myocytes thereby preventing depolarization of these cell membranes (Ramlochansingh et al., 2014). MS-222 therefore operates by suppressing motoneuronal activity and preventing muscle contractions throughout LA tadpole development. It is likely that in LA tadpoles, the blocked muscle contractions means that no electrical activity can be conducted to the cell interior could have led to the round morphology of these myocytes.

4.4.3 Altered Myocyte Structure Likely Affected LA Tadpole Swimming

This change in myocyte structure did not translate into any immediately obvious changes in swimming behaviour in LA tadpoles. A possible impact of this structural change was a diminished tail arc during tail-based swimming (i.e., the maximum angle of left-right bending measured at the junction between the head and trunk) which appeared to affect swimming kinetics and propulsion. Another potential impact of this changed myocyte structure was also noted in the tracked LA tadpole swim paths. As was noted by Bender (2012), I found that LA tadpoles more frequently exhibited turning behaviour and path intersection compared to their control counterparts (Figure 4.10 Ci), although there was no left or right directional preference exhibited in this turning behaviour. There were instances where tadpoles would swim in a tight circular motion of varying circumferences (Figure 4.9 Aii, 2 second and 10 second panels), however these instances were infrequent.

Bender (2012) previously observed that LA tadpoles exhibited preferential turning behaviour, continuous circuitous turning during swimming, and hypothesized that this behaviour was potential structural changes such as a “crooked” or warped NC. These structural changes were believed to be linked the LA tadpole spending the majority of their development lying on their side as lack of movement affected their ability to adhere to the water surface and hang from the mucus secreted by their CG, an occurrence which was also observed in my experiment (Figure 4.10 Aii) (Bender, 2012).This turning phenomenon could therefore more likely be attributed to the anatomical variation noted in the myocytes comprising the myotome (Figure 4.5). Aside from the myocytes, myotome tissue was irregular with notable

gaps across the dorsoventral length of a single lateral myotome, an anatomical feature which was not typically repeated symmetrically on the opposing side (Figure 4.5 Aii). This irregularity along each lateral side could likely have led to higher contractibility on one side versus the other which could have affecting the swim path of LA tadpoles (Figure 4.4 Aii-Aiii & 4.5 Aii).

In my project it was noted that LA tadpoles did lie on their sides rather than adhere to the water surface (Figure 4.10 Aii) suggesting that the CG gland may have been impaired or functionally altered in the tadpoles in the LA rearing condition. The CG structure itself appeared to be normal in LA compared to control (Figure 4.10Bii) and as detritus was observed attached to the cement gland of LA tadpoles (Appendix F), it can be assumed that mucus secretion was still occurring. Therefore, the supine position is likely due to the tadpole being unable to swim, therefore lacking the opportunity to make contact with the water surface and attach themselves there. When investigated further, notochord structures were not observed to be uneven within LA tadpole cross-sections (Figure 4.3 Aii).

4.4.4 Reduced Sensory Activation Indicates Reduced Connectivity Within the TG Pathway

Another noted difference of LA tadpoles from control tadpoles was the reduced sensitivity following impact with head skin/CG, which occurred following collision with petri dish wall in LA tadpoles (Figure 4.10). Following head impact with a barrier (the side of the petri dish), tadpoles often failed to stop and continued to swim despite being met with a direct barrier (the wall), indicating a potential breakdown in either the TG sensory pathway (Boothby and Roberts, 1992) or GIRK-mediated inhibition swim circuits (Li, Zhu and Ritson, 2017). They also continued swimming for much longer durations as though the wall in front of them was not even present though their swimming frequency did decrease following collision ($p < 0.05$). This breakdown in mechanosensory sensitivity could, in part, be attributed to prolonged bath application of MS-222 during development. While MS-222 functions by blocking depolarization of neuron and myocytes, it also impacts the electrical activity of

sensory afferents (Ramlochansingh et al., 2014). It is therefore conceivable that diminished activation of sensory pathways, including the TG afferent which underlies both stopping pathways, is due to chronic exposure to MS-222 interfering in the firing of certain sensory afferents leading to weaker signalling between sensory neurons within these pathways, even with short term exposure (Ramlochansingh et al., 2014; Félix et al., 2018b).

Movement deprivation could therefore directly impact the CG pathways due to Hebbian plasticity and the lack of established signaling between any of the neurons comprising the CG pathway (Halvagal and Zenke, 2023) in LA tadpoles, however there is evidence to suggest that this sensory pathway breakdown was variable across different pathway types, and even within the same pathway of different animals. For example, stopping behaviour was comparatively prolonged but also highly varied within LA tadpoles indicating there was some retention of TG pathway connectivity in certain animals despite this pathway never once being activated across embryonic development. There has been evidence that sensory-induced CPG activation can be unaffected by limited sensory input during development which suggests that sensory pathways are still highly adaptable following prolonged sensory deprivation, as noted in *Drosophila* (Suster and Bate, 2002). Furthermore, mechanosensory pathways are differentially modulated across development in tadpoles by neuromodulators like NO which can switch from being net inhibitory to excitatory as the tadpole develops, as has been documented in motor circuits between NF stages 37/38 to 54/55 (Currie and Sillar, 2016). This indicates that plasticity within these systems could account for the variable stimulus-induced response noted in LA tadpoles (Halvagal and Zenke, 2023).

Another example of variable sensitivity within certain sensory pathways can also be seen in how swim behaviour was evoked across LA animals. Tadpoles were pipetted into the petri dish and their subsequent swim path was tracked by video recording and Animal Tracker API in ImageJ (Gulyás et al., 2021).. This act of pipetting a tadpole into the petri dish creates a current which pushes into and past the tadpole's head as the animal is propelled forwards

into the water. This pressure can induce swimming by activating a variety of sensory pathways including skin cell pathways or mechanical stimulus to RB axons in between the skin bilayer. Swimming is more likely induced by this same water current pressure stimulating the lateral line pathway which is activated by neuromasts on the skin of the dorsolateral regions on the head and rostral tail (Roberts *et al.*, 2009; Saccomanno *et al.*, 2021). Bath application of MS-222 has been shown to significantly reduce the spontaneous and sensory stimulus-evoked firing of the posterior lateral line nerve in older (NF stage 52-57) *Xenopus* (Ramlochansingh et al., 2014) which could result in diminished excitation of this pathway in LA tadpoles when pipetted, leading to variable occurrence of swimming in response. However, this effect was not observed in LA tadpoles therefore indicating that different sensory pathways were affected variably in LA rearing and that prolonged MS-222 exposure on sensory pathways (particularly over the course of development) is worth further consideration in future replicated work. As the tadpoles from Ramlochansingh's study were much older than the NF stage 42 tadpoles investigated in my project, it is difficult to infer that MS-222 had the same effect on tadpoles reared from early embryogenesis.

The study does highlight that MS-222 could directly, or indirectly, disrupt the firing of sensory nerves which could directly impede the spike-timing dependent plasticity which underlies Hebbian learning. However, in the absence of external stimulus to the CG or head skin of developing tadpoles, Hebbian learning would also be impeded and the synaptic connection between the TG nerve and the mhrs could fail to be properly established. Therefore, in order to establish whether MS-222 is a confounding factor in the breakdown the CG stimulated stopping behaviour future work should consider extending the recovery time of LA tadpole beyond the 30-60 minute range employed in this project to ensure that MS-222 retained within tadpole tissue is not interfering with CG pathway sensitivity (Ramlochansingh et al., 2014). My project therefore highlights another viable aim for future research into LA rearing: establishing whether the reduced sensitivity observed in the CG pathway is environmental or or a result of prolonged exposure to an anaesthetic over the course of development.

4.4.5 Movement Deprivation During Development Altered α3 Subunit Expression

Movement deprivation during development induced notable effects on sodium pump subunit expression that was especially apparent within the tadpole SC and myotome. The effect of movement deprivation in expression of α3 was of particular interest in this project since changes to *ATP1A3* expression has been closely aligned with disorders that present with motor dysfunction (Bøttger et al., 2011a; Arystarkhova et al., 2019; Zúñiga-Ramírez et al., 2019). As previously noted, symptom pathologies occur fairly early in movement development within human infants and children (Brashear et al., 2012; Rosewich et al., 2012; Zou et al., 2023). Since α3 is associated with dynamic sodium pumps, the absence of movement induced STMM (characterized by the usAHP) (Zhang and Sillar, 2012) over the course of tadpole development was liable to result in changes to expression of this catalytic subunit in spinal neurons.

Measured expression across the entire tadpole body revealed that there was no difference in global expression of α3 (Figure 4.4 Di). However a significant change in expression was detected at the SC-level in immunolabelled transverse cross-sections by increase in α3 within the cells comprising the SC (Figure 4.4) and myotome (Figure 4.5). This was further demonstrated by measuring the CTF of these regions that α3 had increased by over 150% in the SC (Figure 4.5 Dii) and had doubled in the myotomes (Figure 4.6 Bi). These findings indicate that α3 was likely upregulated as a direct result of movement deprivation and hints that it's previously measured upregulation during the onset of swimming (Session *et al.*, 2016) could be due to dynamic sodium pumps contributing to swim development.

This change in α3 expression was not consistent across all cell types within the SC. For example, the measured RB neurons from LA tadpole sections were not measured to have significantly higher α3 compared to the RB neurons in their control counterparts however considering the fairly small number of tadpoles measured in this specific immunolabelling experiment it is worthwhile to investigate whether this trend is repeated across future experiments (Figure 4.5 Diii). The finding that α3 expression increased in the SC of LA

tadpoles when movement was restricted suggests that the STMM induced in CPG neurons by the usAHP (Zhang and Sillar, 2012) is an important component of motor circuit maturation. This is particularly consistent with work noting the relation of α3 expression to development of motor control as α3 expression has been found to be consistently high within neurons in brain regions such as the substantia nigra (Bøttger et al., 2011a). It is therefore reasonable to propose a similar importance for α3 within spinal neurons of other vertebrates.

4.4.6 Upregulation of α3 Produced a Potential Effect on Swimming Recovery

The protocols underlying my project involved immunolabelling and subsequent fluorescence analysis of positively labelled CNS tissue. The upregulation of α3 could not feasibly be linked to reducing swim duration in LA tadpoles. Similarly, changes in swimming behaviour function were investigated separately and mainly correlated to observable changes in tadpole anatomy. Due to the constraints of this experiment, no direct comparison can be made between the altered swimming function in LA tadpoles and the noted α3 upregulation within the SC and myotomes of LA tadpoles. However, there are some influences linked to this change in expression that would benefit from further analysis in the future. One notable change in swimming behaviour was that LA tadpoles fatigued more quickly compared to control tadpoles, completing fewer swim episodes before ceasing to swim entirely (Figure 4.11 Ai). Tadpoles from both conditions could resume swimming after ~ 1 minute at rest following induced fatigue, though LA tadpoles did require comparatively more time compared to their control counterparts (Figure 4.11 Aii). The results from this fatigue experiment therefore demonstrated that LA tadpoles will fatigue more easily and require more time to resume swimming, an effect reminiscent of the reduced circuit output that occurs during the usAHP of tadpoles (Zhang and Sillar, 2012; Hachoumi et al., 2022). It is therefore plausible that this increased sensitivity to fatigue is due to underlying changes in spinal neuron function due to increased α3 expression within these cells. Bender (2012) noted that the RMP of LA spinal neurons (assumed to be MNs) was comparatively hyperpolarized which could certainly contribute to fatigue sensitivity (Figure 4.11 Ai) as well as the measurably

lower post-recovery swim episode despite the cumulatively longer recovery period in this group (Figure 4.13 Aii). This result does not necessarily implicate dynamic sodium pumps and could instead indicate a potential upregulation of tonic α1-containing pumps in the membrane of spinal neurons.

Alternatively, the potential that this fatigue sensitivity is linked to the measured upregulation of α3 in LA tadpoles (Figure 4.5 Dii) can be noted through their changed recovery response. In tadpoles, the usAHP confers STMM on the motor system by limiting the duration of subsequent swimming episodes, which was found to occur in both conditions (Zhang and Sillar, 2012; Hachoumi et al., 2022). In the fatigue experiment, LA tadpoles completed fewer episodes before becoming fatigued which could be indicative of the increased α3 expression also representing an increase in the dynamic pump population in the cell membrane. When the membrane potential is consistently depolarized (e.g., during sustained neuronal firing), this pump population was recruited more quickly inducing hyperpolarization at a faster rate compared to in the CPG cells of control tadpoles. Similarly, once hyperpolarized it would have taken comparatively longer to restore the RMP as this larger population would need to be de-recruited. While a plausible hypothesis, this specific relationship would need to be examined more directly in future experiments by measuring how ventral root output changes during fictive swimming when fatigue is induced in LA animals through repeated stimulation. This method would ensure a cell-specific investigation into how α3 upregulation affects the usAHP across repeated swimming episodes, including post-recovery.

4.4.7 Downregulated FXYD1 Expression Is Likely Directly Related to Movement Deprivation

In contrast to α3 expression, FXYD1 expression was noted to be downregulated in the SC of LA tadpoles. Within the SC, decreased FXYD1 expression was particularly in ventral spinal neurons in the LA group (Figure 4.6). Since MNs are located in this region (Roberts and Clarke, 1982) it is likely that FXYD1 is diminished, or was never highly expressed, in this neuron subtype in LA tadpoles due to them being deprived of movement over the course of

development. Unfortunately, there exists little information on FXYD1 expression in neurons (Feschenko et al., 2003; Meyer et al., 2020) making it difficult to determine its potential function in the SC. However, extrapolations can be made by tracking whether changes in FXYD1 expression alter sodium pump-mediated neuronal output. In the brain of mice, an excess of FXYD1 is thought to reduce sodium pump activity, resulting in the deregulation of endogenous K^+ conductance and leading to stunted neuronal growth (Matagne et al., 2018). By comparison, a decreased expression of FXYD1 results in an increase in NKA activity which would be expected as previous studies on FXYD1 upregulation documented it augmenting sodium pump function in a similar manner in neurons (Meyer et al., 2020). These findings would align with expectations from the LA rearing experiment where NKA activity is implied to be increased resulting in hyperpolarized RMPs in certain spinal neurons (Bender, 2012). Due to this, further expansion within this rearing experiment should also consider backfilling MNs and co-labelling with FXYD1 to assess how FXYD1 expression may have changed in this neuron population by NF stage 42. It is worth detailing that the above interpretation is based upon an observable trend demonstrated by a fairly small population of LA tadpoles (N=2). Despite the consistency demonstrated by these tadpoles any further research should account for small sample size and determine whether this observed trend persists across experimental repeats.

FXYD1 expression did not significantly vary within the myocytes of LA tadpoles though there was some indication it may have decreased on average. The expectation was that there would be a significant decrease of FXYD1 within the tadpole myotome, as that would align with previous studies which noted a downregulation in FXYD1 in skeletal muscle in response to decreased exercise (Figure 4.7) (Boon et al., 2012). This was an unexpected finding as there has always been a well-established relationship between FXYD1 expression and exercise in adult vertebrates such as humans and rats (Rasmussen, Kristensen and Juel, 2008; Thomassen et al., 2016). However, the lack of significant change in FXYD1 expression within myotomes could be due to the intervention of MS-222, which blocks

muscle contraction (Ramlochansingh et al., 2014), in early development. Under normal conditions, increased FXYD1 expression during development is potentially not solely contingent on the increased motility associated with increased movement (Thomassen et al., 2016) like swimming in tadpoles (van Mier, Armstrong and Roberts, 1989). Again, given the small sample size tested in this experiment set (N=2), future experiments should determine the reproducibility of this result across a larger population.

While the evidence that FXYD1 regulation is movement dependent can be seen when tracking its expression following changes to exercise in adult rats and humans, the FXYD1 expression in tadpoles could be more predetermined. Protein transcript levels within the entire animal across developmental stages show a trend not entirely consistent with the advent of movement according to developmental stage. A steep upregulation of FXYD1 occurs between embryonic to early larval stages (~stage 15-20 until stage 35/36) however by NF stage 40 FXYD1 drops to the same level as detected by NF stage 32, midway through the steep climb (Session et al., 2016). It is therefore possible that FXYD1 expression in muscle remained fairly normal initially, when embryonic and young larval tadpoles remain largely sessile (van Mier, Armstrong and Roberts, 1989). FXYD1 would have been downregulated by the tadpole larval stage (such as NF stage 37/38 and later) resulting in the comparably lower FXYD1 noted by NF stage 42 in my experiment (Chapter 4.3.7) in contrast to their control counterparts. Nevertheless, the impact would have been tissue dependent given the larger decrease noted in the tadpole SC.

Many of the inferences I have discussed rely upon establishing a more solid cause and effect relationship between movement deprivation and FXYD1 expression within tadpoles. Therefore a potential follow-up experiment should consider identifying whether resumption of movement following recovery led to an upregulation of FXYD1 in the SC and myotome tissue. This could be investigated by removing LA tadpoles from the movement deprivation experiment at an earlier stage (such as NF stage 40) and allowing tadpole to swim normally until reaching NF stage 42. If FXYD1 is downregulated due to a lack of movement then there

should be some measurable upregulation of FXYD1 in these tadpoles compared to LA tadpoles from this experiment.

4.4.8 Concluding Remarks

The rearing experiment outlined in this chapter provides a suitable protocol for the practical application of MS-222 as a motor inhibitor during embryo and larval tadpole stages. At a higher concentration (0.02%; Figure 4.2), MS-222 was found to increase the likelihood of tadpole developing malformed or tadpole death. At half this concentration (0.01%), these occurrences were significantly lower and the trends in the LA tadpole populations aligned more closely, statistically, to control tadpoles therefore enabling my project to provide a successful and repeatable framework for future experiments in movement deprivation over the course of development. Results from this project also highlighted subtle but noteworthy changes in tadpole swimming behaviour which are correlated to observed changes in tadpole anatomy, mainly the myotomes. Furthermore, the measurable upregulation of α3 within the SC and myotomes bear further scrutiny due to the potential influence this altered expression pattern could have on spinal circuit output, such as the increased incidence of network fatigue following successive swimming episodes with short ISI (<5 s) between stimuli. Furthermore, the possibility that FXYD1 is functionally downregulated compared to control tadpoles as a result of movement deprivation is worth future scrutiny with the potential to elucidate whether FXYD1 downregulation is influenced by tadpole development or due to decreased motor function. Perhaps even both having variable influence over the presence of FXYD1 in the tadpole CNS. Overall, my experiments present a well-scrutinized, repeatable framework for future investigations into the relationship between decreased or inhibited motor function, altered sodium pump subunit expression and tadpole swimming behaviour.

5. GENERAL DISCUSSION

Sodium pumps are essential for maintaining the cellular membrane potential through the active transport of Na^+ and K^+ against their cationic concentration gradients. This accounts for their wide expression across different cell types and their conserved function across vertebrate and invertebrate species (Pivovarov, Calahorro and Walker, 2019). The ubiquitously expressed sodium pump subtype possesses an α1 catalytic subunit within its heterotrimeric complex (McGrail, Phillips and Sweadner, 1991; Sweadner et al., 1994; Zahler et al., 1997; De Carvalho Aguiar et al., 2004). It is constitutively active owing to its ability to maintain the RMP, which is arguably essential for regulating the rapid depolarization that underlies neuronal firing (Zahler et al., 1997). Owing to this function, it has been termed the tonic sodium pump (See Chapter 1.1) (Hachoumi et al., 2022). In contrast to this, a substantial amount of literature has highlighted another pump subtype which is activity-dependent and will remain largely inactive at the RMP (Zahler et al., 1996; Zhang and Sillar, 2012; Picton et al., 2017; Hachoumi et al., 2022).

Though largely silent, this pump will activate once a high enough intracellular Na^+ concentration has been reached (Zahler et al., 1996, 1997). This pump type, defined as the dynamic sodium pump and presumed to contain the α3 subunit (Zhang et al., 2015), generates a prolonged usAHP and limits the cell firing threshold as the membrane potential hyperpolarizes following the increased extrusion rate of intracellular Na^+ by this recruited pump (Zhang and Sillar, 2012; Zhang et al., 2015; Picton, Sillar and Zhang, 2018). While α3 has been immunolabelled in the SC of neonatal mice (Picton et al., 2017), it has not previously been immunolabelled in the tadpole CNS. It is important to highlight that numerous studies have tracked *ATP1A3* localization through quantifying and localizing mRNA transcripts and while this method can elucidate which tissue types are anticipated to express α3 (Rahman et al., 2015; Session et al., 2016; Liao et al., 2022) there are expected variations in protein amount across cell types which require direct investigation by immunolabelling the tadpole CNS in transverse cross-sections. This was relevant within my own project as tracking α3 across extracted protein taken from the *Xenopus* tissue of

selected NF stages (Nieuwkoop and Faber, 1956) demonstrated that there was no significant variation in α3 amount across development (see 2.3.12) which is not in line with previous work tracking α3 expression through *ATP1A3* mRNA transcriptions (see Figure 2.11B) (Session et al., 2016). Therefore, my first result chapter focussed on tracking the expression of α3 within the tadpole CNS by identifying positive immunolabeling in the cells comprising the SC (see Chapter 2.3.1 to 2.3.4).

A notable observation from my first chapter was the widespread expression of α3 in the majority of, if not all, spinal cells comprising the SC, with particularly strong fluorescence measured in medial cells adjacent to the CC (Chapter 2.3.3). Though α3 is quantifiably higher in these medial spinal cells, α3 was also detected in spinal cells bordering the LT, including backfilled MNs (see Chapter 2.3.4) indicating that expression was widespread but varied within this cell population. The comparatively higher α3 expression in cell bodies bordering the CC is worth further investigation as it could indicate that the usAHP is functionally relevant in the cell types comprising this specific region within the SC, though not every spinal cell type was identified in my project outside of backfilled MNs. When quantifying and comparing the fluorescently labelled sections to a consistent negative control, α3 was measured as present in all backfilled MNs from my experiment (N=6/6 MNs, N=3 stage 42 tadpoles; Chapter 2.3.4).

While this sample size is small, the consistent and detectable presence of α3 in this neuron subtype belies previous electrophysiological recordings which detected the usAHP in only a subset of MNs (~42%) (Picton et al., 2017). Furthermore, there is evidence to suggest that α3 expression is conserved across development, both from across stages of development (Chapter 2.3.12) and from the consistent expression levels in rostrocaudal SC cross-sections (Chapter 2.3.3). The upregulation of α3 across all spinal cells of LA tadpoles (Chapter 4.3.5) further implicates the functional importance of conserved dynamic sodium pump expression in development, especially when contrasted to the downregulation of FXYD1 in the SC of LA tadpoles (Chapter 4.3.7). Therefore the variation in usAHP

expression across spinal cell populations (Picton, Sillar and Zhang, 2018), and across tadpole developmental stages (Currie and Sillar, 2018), could indicate that this functional output by dynamic sodium pumps is attenuated by neuromodulation (Hachoumi et al., 2022), or masked by both intrinsic and extrinsic factors. The neuromodulators NO and 5-HT have been demonstrated to attenuate, even completely inhibit the usAHP in neurons (Hachoumi et al., 2022). 5-HT can bimodally affect neuronal firing depending upon which receptor subtype it is acting upon in spinal neurons. In tadpoles, 5-HT2aR activation has been shown to increase network excitability particularly by acting on MNs and premotor cells. This results in the usAHP being attenuated. Meanwhile 5-HT7R has the opposite effect and the usAHP remains present, even enhanced in cell expressing this receptor subtype (Hachoumi et al., 2022). Therefore, the variable presence of the usAHP in MNs (Picton et al., 2017; Picton, Sillar and Zhang, 2018) could be dependent upon which 5-HT receptor subtype is expressed within this cell type.

NO was also found to inhibit the usAHP and diminish the STMM conferred on the motor circuit by the usAHP (Hachoumi et al., 2022). During early larval stages NO slows the frequency and duration of sensory-evoked swimming, demonstrating a net inhibitory effect on locomotor activity (McLean and Sillar, 2004). By NF stage 45, there is a stage-dependent switch in the modulatory outcome with NO having a net excitatory effect on swimming however it is still noted to decrease the usAHP (Currie and Sillar, 2018). While NOS is not expressed in MNs, KA neurons bordering the CC are a possible source of endogenous NO in zebrafish (Bradley et al., 2010; Hachoumi and Sillar, 2019), allowing this neuromodulator to act on cells within the proximal vicinity such as ventral MNs. It is therefore possible that the comparably high α3 expression quantified in spinal cells bordering the CC could aid in countering attenuation of the usAHP by NO allowing the usAHP to be variably detectable in cells within this region. A future experiment exploring this correlation would involve co-labelling neuronal NOS (nNOS) and α3 within the tadpole SC, then measuring whether α3 was higher in nNOS-expressing spinal cell populations.

While the intrinsic mechanisms by which NO and 5-HT attenuate the usAHP have not been investigated, there is evidence to suggest that modulation of usAHP expression occurs through PKC-phosphorylation of the dynamic sodium pump (Hachoumi et al., 2022). The protein kinase pathways are another area worth further investigation as they have been demonstrated to affect pump function by influencing sodium pump cation affinity and even in altering pump transport into the cell membrane. Protein kinase pathways can act on different subunits within the sodium pump complex to induce a diverse range of alterations to pump function. For example, PKA-mediated phosphorylation of α3 can induce long-term inhibition of dynamic sodium pumps (Wu et al., 2007). Inhibition of α3 in turn inhibits the usAHP leading to increased neuronal output in response to increased intracellular Na^+ (Azarias et al., 2013). By comparison, PKA or PKC phosphorylation of FXYD1 primarily affects the Na^+ affinity of α1/β and α2/β sodium pump complexes, usually increasing cationic affinity (Bibert et al., 2008) though this effect can vary depending upon tissue type (Meyer et al., 2020), cellular activity (Thomassen et al., 2016) and neuromodulator signalling (Pavlovic et al., 2013). Any relationship between FXYD1 and α3 would likely occur indirectly as the formation of α3/β/FXYD1 pump complexes has been debated previously, though α3/β/FXYD6 complexes can occur in neuronal cells (Delprat et al., 2007b).

An example of neuromodulation operating through the protein kinase pathways can be found in cardiomyocytes where NO modulation instigated PKC phosphorylation of FXYD1. This increased sodium pump affinity for intracellular Na^+ leading to increased sodium pump activity (Pavlovic et al., 2013) and increased extrusion of Na^+. Therefore, NO modulation likely indirectly affected dynamic sodium pump recruitment as intracellular Na^+ would have been kept below the high intracellular threshold for the comparably Na^+ insensitive α3 isoform (Zahler et al., 1996, 1997) located in this pump type. This theoretical relationship also highlights the potential that FXYD1 indirectly affects the presence of the usAHP in cell types by altering the ion affinity of complexes where it is co-expressed, therefore affecting dynamic sodium pump activity through managing the intracellular Na^+ available.

Furthermore, PKA phosphorylation also affects the trafficking of FXYD1-containing pump complexes which in turn could induce a downregulation in the population of tonic sodium pumps in neurons, as is what likely occurred in the SC of LA tadpoles. This in turn could have facilitated the upregulation of α3 in the spinal cells of LA tadpoles to compensate for the absence of a constitutively active pump continuously shuttling out intracellular Na^+.

In my second results chapter (See Chapter 3.3), FXYD1 and FXYD6 labelling showed prominent overlap within the SC with prominent subunit expression noted in lateral spinal cells and reduced, but absent expression of these FXYD subtypes in medial spinal cells. This indicates that α3 overlapped with FXYD1, and likely by extension with FXYD6, primarily in lateral cells (see Chapter 2.3.3). The overlap in FXYD1 and FXYD6 expression within lateral spinal regions was consistent and could indicate that both subtypes share an overlapping function. This is further supported by the prominent structural similarities shared by these two subunits, leading to FXYD6 being termed the "phospholemman-like protein[9]" upon its discovery (Yamaguchi et al., 2001). While there is overlap in FXYD1 and FXYD6 expression in my immunolabelling results, this experiment would still benefit from further scrutiny. The findings from my FXYD6 immunolabelling experiment did demonstrate that FXYD6 expression was consistent within the tadpole SC, however these sections were taken from only two tadpoles. Though this consistency is promising, these tadpoles all came from the same adult frog breeding pair and it would therefore be beneficial for further experimental repeats to be conducted to see if findings are consistent across breeding pairs as well as across repeat immunolabelling experiments.

Following my α3 and FXYD1 immunolabelling experiments, the final aim of my thesis was to outline the relationship between α3 and FXYD1 expression and tadpole locomotion more closely. Therefore, in Chapter 4 I began by investigating how movement deprivation over the course of development affects tadpole anatomy and swimming. I expanded upon this

[9] Phospholemman (PLM) was the original term for FXYD1 before the discovery of the conserved FXYD domain shared by the sodium pump's auxiliary γ subunit enabled these isoforms to be grouped into the same family, FXYD (Reviewed in Yap et al., 2021).

experiment by correlating identified changes in swimming behaviour to observed changes in the expression of α3 and FXYD1. As mentioned above, there was a marked increase in α3 within the SC of LA tadpoles (Chapter 4.3.5). In retrospect, this was expected as in the absence in activity-dependent activation of a protein can leads to a compensatory upregulation of this protein in response. Notably, this did not appear to be the case with FXYD1 which was shown to be measurably decreased in the SC (Chapter 4.3.7) and myotome (Chapter 4.3.8) of LA tadpoles. In humans and rats there is a close link between exercise, subsequent increased sodium pump activity and FXYD1 upregulation in different tissue types, such as skeletal tissue (Rasmussen, Kristensen and Juel, 2008; Wyckelsma et al., 2019; Yap et al., 2021a). Therefore, an absence in exercise-induced sodium pump upregulation in LA tadpoles could also have resulted in FXYD1 never being upregulated during development. As mentioned above, this downregulation of FXYD1 following LA rearing could also have been due to increased trafficking from the cell membrane which would have been cause by a decrease in PKA-phosphorylation of FXYD1 (Meyer et al., 2020). If the injection of PKA's catalytic subunit rescues this decreased FXYD1 expression by increasing FXYD1 trafficking into the cell membrane, then this could be shown to be the underlying cause for this change in FXYD1 expression in LA tadpoles. However, if no rescue occurs then it could instead be inferred that FXYD1 expression was downregulated intracellularly, and that there is no FXYD1 available for transport to the cell membrane.

Closing Remarks

With this project, I have developed and optimized IHC protocols for immunolabelling α3, FXYD1 and FXYD6 within *Xenopus* tissue. The results presented in this thesis also provide a foundation for which cell and tissue types express these subunit isoforms which will form the basis for future experiments going forward. I have also demonstrated how these techniques can allow for correlative analysis of α3 and FXYD1 expression to tadpole movement. Beyond basic research conducted in the relatively simple and amenable tadpole model, further research into this field could also include investigating the role of these subunits in disease pathology. Both α3 and FXYD1 have been strongly implicated motor dysfunction as demonstrated by the movement disorders which are directly linked to missense gene mutations (Arystarkhova et al., 2019, 2021; Cuomo et al., 2022). These diseases encompass a large pathological range with α3 being directly linked to RDP (Zúñiga-Ramírez et al., 2019), AHC (Capuano et al., 2020) and CAPOS (Dard et al., 2015) while FXYD1 has been directly linked Rett syndrome (Cuomo et al., 2022). Given the fact that all these conditions begin in early childhood there is also a strong basis for investigating the role of α3 and FXYD1 in locomotor development, another field where tadpoles are an ideal vertebrate model given the relatively short time span required for them to advance from the embryonic to larval stages (~2 days). With all of this in mind I predict that my research project provides a solid gateway for a range of future IHC experiments which will further advance our understanding of how dynamic sodium pumps and neuromodulation contribute to locomotor function, dysfunction and development.

APPENDIX

Appendix A: Dot Blot Experiments

Appendix Ai: α3 Dot Blot

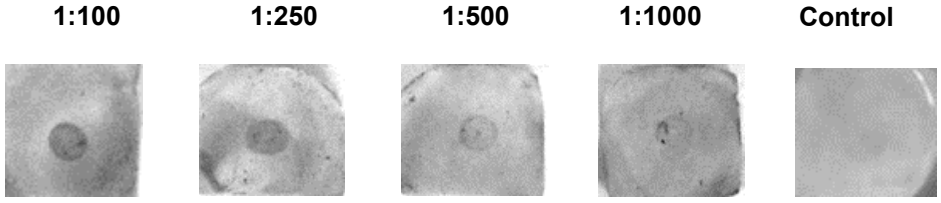

Dot Blot featuring nitrocellulose membrane in which the chosen primary α3 antibody was incubated with extracted *Xenopus laevis* protein. At every concentration reactivity was visualized by labelling with DAB.

Appendix Aii: FXYD1 Dot Blot

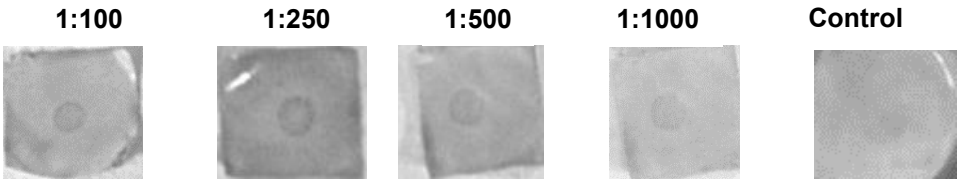

Dot Blot demonstrating reactivity between FXYD1 primary antibody incubated with extracted *Xenopus laevis* protein. At every concentration reactivity was visualized by labelling with DAB.

Appendix Aiii: FXYD6 Dot Blot

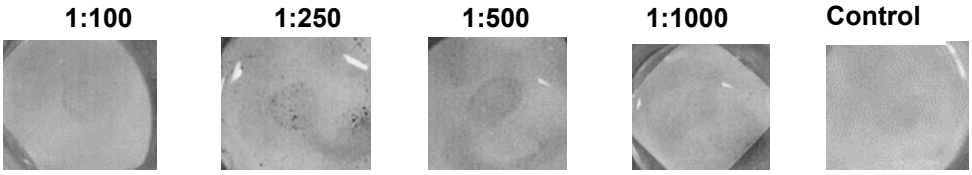

Dot Blot demonstrating reactivity between FXYD6 primary antibody incubated with extracted *Xenopus laevis* protein. At every concentration except 1:1000, reactivity was visualized by labelling with DAB.

Appendix B: Western Blot Results

Appendix Bi: α3 Western Blot

α3 Western Blot

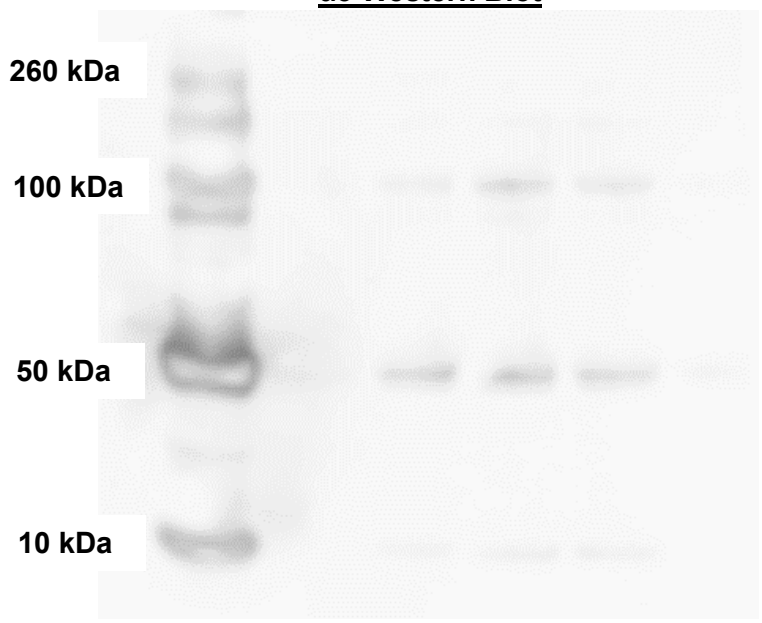

Western blot demonstrating α3 and α-tubulin labelling, calculated to be ~112 kDa and ~48.9 kDa respectively in *Xenopus laevis* by chosen primary antibodies.

Appendix Bii: FXYD1 Western Blot

FXYD1 Western Blot

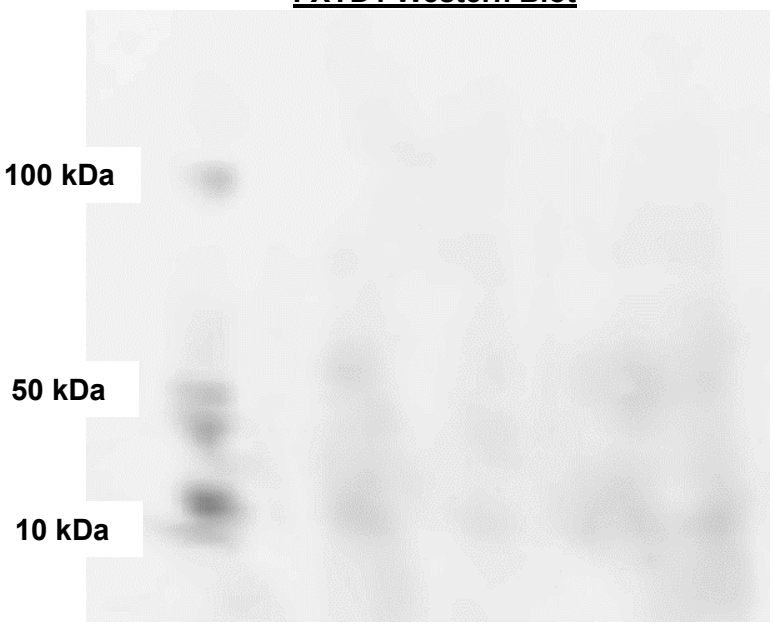

Western blot demonstrating FXYD1 and α-tubulin labelling, calculated to be ~10.8 kDa and ~48.9 kDa respectively in *Xenopus laevis,* by chosen primary antibodies.

Appendix C: MN Backfilling Protocol and MN Labelling in Transverse SC Sections.

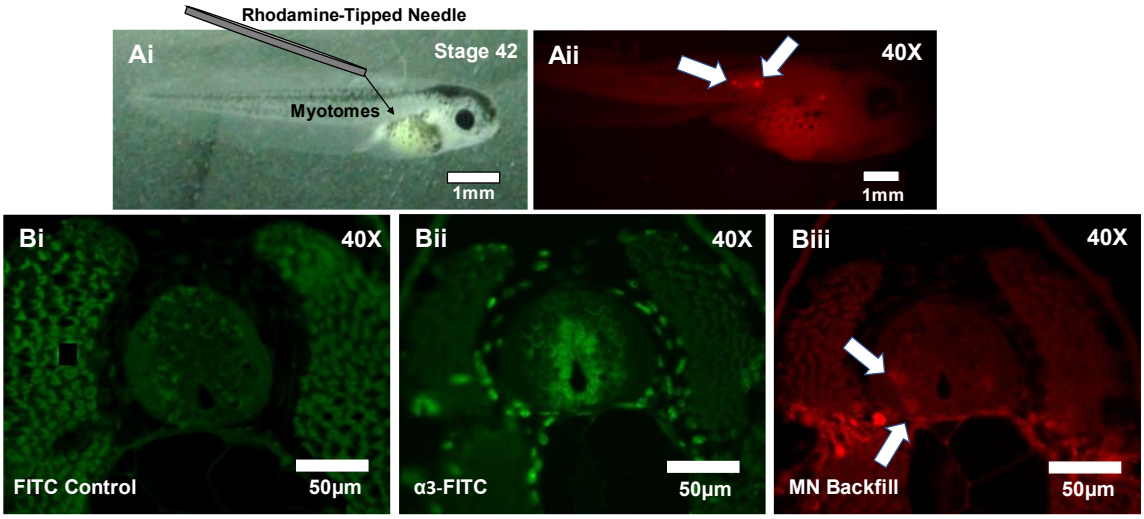

Protocol Illustrating MN Backfilling and Co-Labelling with α3. A. Dextran-conjugated rhodamine dye was deposited into myotomes of stage 42 tadpole using a needle (Ai). Post fixation period, rhodamine could be visualized using a fluorescent microscope to ensure higher possibility of successful MN backfilling (Aii, white arrows). B. FITC only incubated tadpole sections (Bi) were compared to α3-FITC labelled SC sections (Bii). Backfilled MNs are visualized separately using Texas Red filter (Centre Wavelength 559nm) on the Photometrics Moment Camera (Biii, MNs indicated by white arrows).

Appendix D: MN Staining Cross-Compared To α3-Fluorescence Intensity

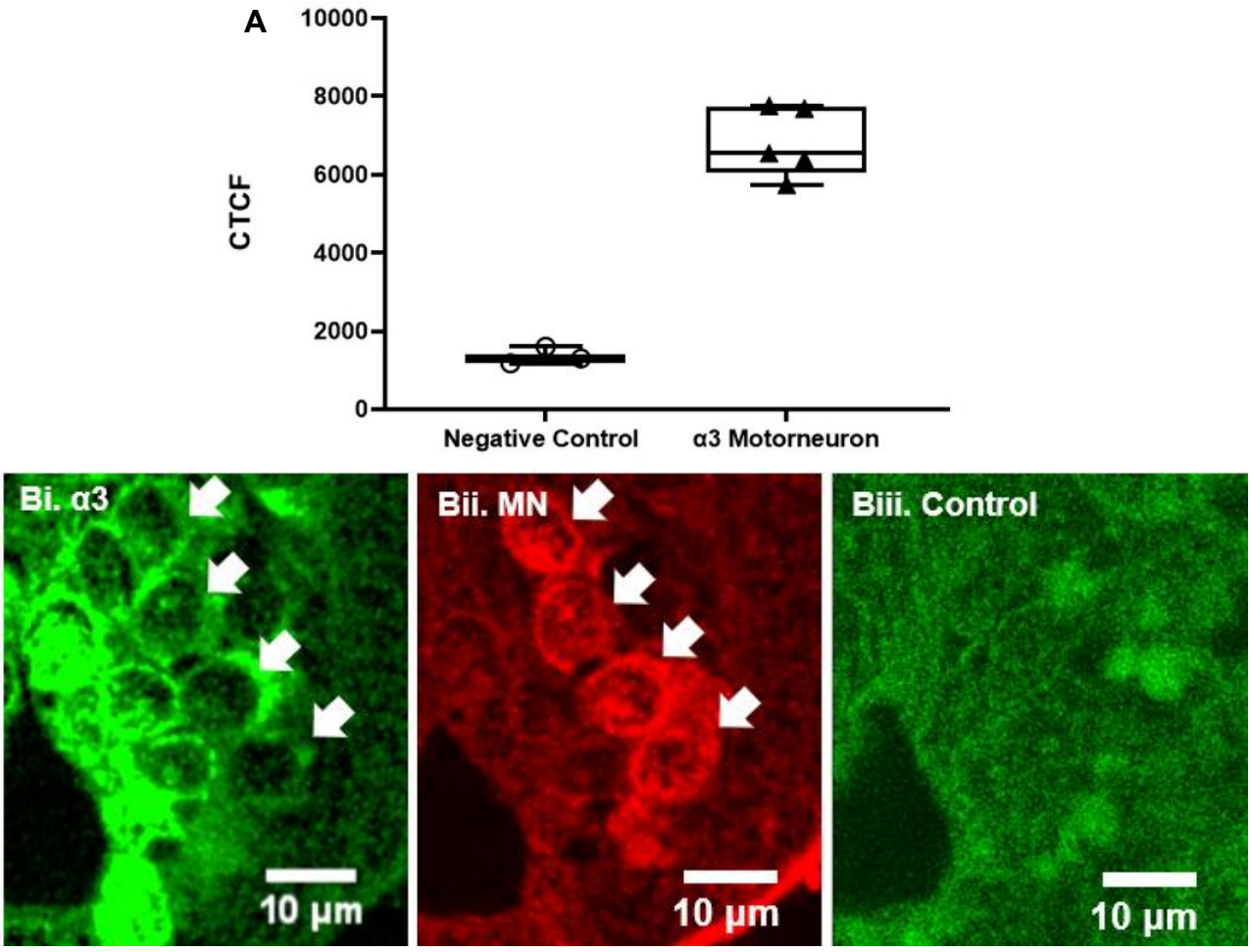

Quantitative measurements of co-labelled α3 and MN cell bodies. A. Comparison of CTCF intensity from α3 labelled backfilled MNs. B. Comparisons were made between co-labelled (white arrows) α3 (Bi) and backfilled MN (Bii) cell bodies. These values were compared to a negative control, section which was incubated solely with FITC (visualised in panel Biii).

Appendix E: CY3 and FITC Midbrain Negative Control Images

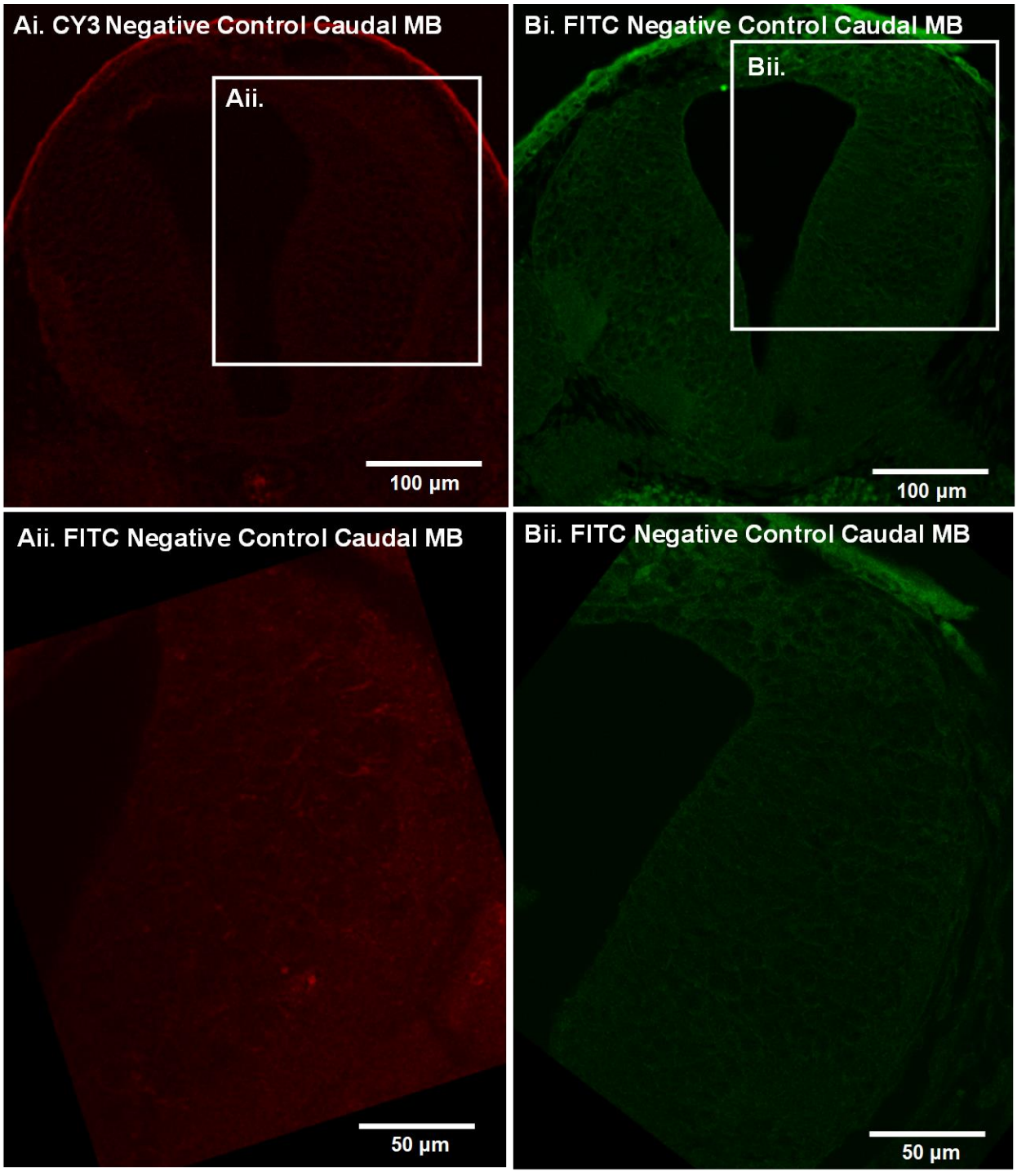

Negative control MB for CY3 and FITC. Ai-Bi. CY3 and FITC were incubated in separate MB tadpole cross-sections in the absence of a primary antibody. Aii-Bii. Higher magnification reveals that the resultant images show no fluorescence in MB cells upon exposure to light microscopy, therefore allowing sections to provide a viable comparison for positively labelled MB sections from my immunolabelling experiments.

Appendix F: Detritus Adhered to CG of LA Tadpoles Indicates Preserved Mucous Secretion

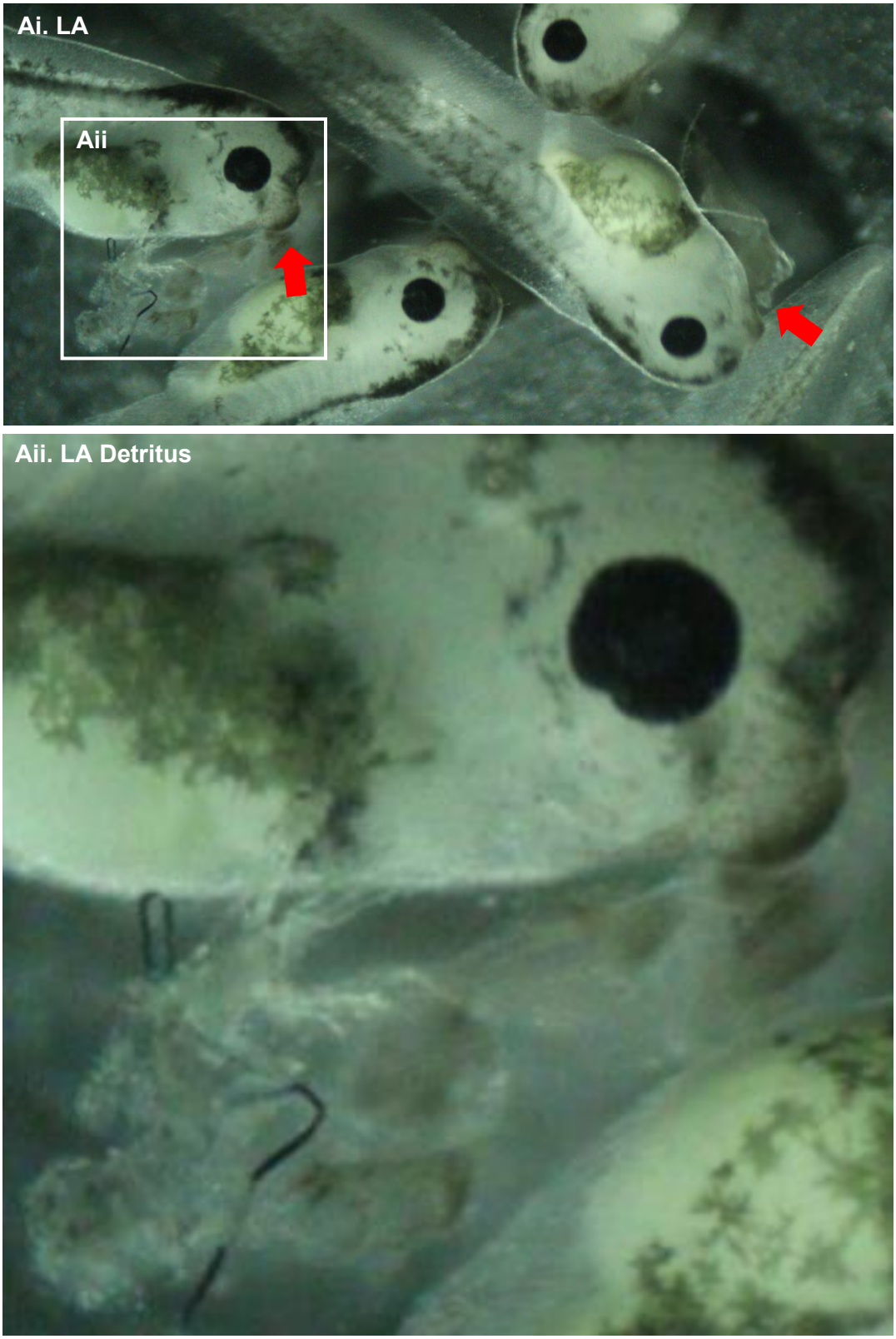

Detritus Adhered to the CG of LA Tadpoles. A. During the rearing trial NF stage 42 tadpole developed normally in comparison to control tadpoles. This included the CG structure (red arrow) which often had detritus attached (close-up image outlined by white box; Aii) indicating that mucous was likely still secreted by this gland and that this function was therefore not impaired by LA rearing.

REFERENCES

Adebogun, G.T. *et al.* (2023) 'Albino *Xenopus* laevis tadpoles prefer dark environments compared to wild type', *microPublication Biology* [Preprint].

Albers, R.W. (1967) 'Biochemical aspects of active transport.', *Annual review of biochemistry*. Annual Reviews 4139 El Camino Way, P.O. Box 10139, Palo Alto, CA 94303-0139, USA, pp. 727–756. Available at: https://doi.org/10.1146/annurev.bi.36.070167.003455.

Allocco, A.A. *et al.* (2019) 'Recessive Inheritance of Congenital Hydrocephalus With Other Structural Brain Abnormalities Caused by Compound Heterozygous Mutations in ATP1A3', *Frontiers in Cellular Neuroscience*, 13, p. 425. Available at: https://doi.org/10.3389/fncel.2019.00425.

Alpert, M.H. *et al.* (2007) 'Nitric oxide modulation of the electrically excitable skin of *Xenopus* laevis frog tadpoles', *Journal of Experimental Biology*, 210(22), pp. 3910–3918. Available at: https://doi.org/10.1242/jeb.009662.

Altschul, S.F. *et al.* (1990) 'Basic local alignment search tool', *Journal of Molecular Biology*, 215(3), pp. 403–410. Available at: https://doi.org/10.1016/S0022-2836(05)80360-2.

Antonicek, H., Persohn, E. and Schachner, M. (1987) 'Biochemical and functional characterization of a novel neuron-glia adhesion molecule that is involved in neuronal migration', *Journal of Cell Biology*, 104(6), pp. 1587–1595. Available at: https://doi.org/10.1083/jcb.104.6.1587.

Arystarkhova, E. *et al.* (2019) 'Factors in the disease severity of ATP1A3 mutations: impairment, misfolding, and allele competition', *Neurobiology of disease*, 132, p. 104577. Available at: https://doi.org/10.1016/J.NBD.2019.104577.

Arystarkhova, E. *et al.* (2021) 'Misfolding, altered membrane distributions, and the unfolded protein response contribute to pathogenicity differences in Na,K-ATPase ATP1A3 mutations', *The Journal of biological chemistry*, 296. Available at: https://doi.org/10.1074/JBC.RA120.015271.

Attali, B. *et al.* (1995) 'A corticosteroid-induced gene expressing an "IsK-like" K+ channel activity in *Xenopus* oocytes', *Proceedings of the National Academy of Sciences of the United States of America*, 92(13), pp. 6092–6096. Available at: https://doi.org/10.1073/pnas.92.13.6092.

Azarias, G. *et al.* (2013) ‘A specific and essential role for Na,K-ATPase α3 in neurons co-expressing α1 and α3’, *Journal of Biological Chemistry*, 288(4), pp. 2734–2743. Available at: https://doi.org/10.1074/jbc.M112.425785.

Baccaglini, P.I. and Spitzer, N.C. (1977) ‘Developmental changes in the inward current of the action potential of Rohon-Beard neurones’, *The Journal of Physiology*, 271(1), p. 93. Available at: https://doi.org/10.1113/JPHYSIOL.1977.SP011992.

Bailey, C.H. *et al.* (2000) ‘Is Heterosynaptic modulation essential for stabilizing hebbian plasiticity and memory’, *Nature Reviews Neuroscience 2000 1:1*, 1(1), pp. 11–20. Available at: https://doi.org/10.1038/35036191.

Balestrini, S. *et al.* (2020) ‘Cardiac phenotype in ATP1A3 -related syndromes: A multicenter cohort study’, *Neurology*, 95(21), pp. E2866–E2879. Available at: https://doi.org/10.1212/WNL.0000000000010794.

Banine, F. *et al.* (2011) ‘Brain region-specific expression of Fxyd1, an Mecp2 target gene, is regulated by epigenetic mechanisms’, *Journal of Neuroscience Research*, 89(6), pp. 840–851. Available at: https://doi.org/10.1002/jnr.22608.

Barbas, D. *et al.* (2003) ‘Multiple serotonergic mechanisms contributing to sensitization in aplysia: evidence of diverse serotonin receptor subtypes.’, *Learning & memory (Cold Spring Harbor, N.Y.)*, 10(5), pp. 373–86. Available at: https://doi.org/10.1101/lm.66103.

Barwe, S.P. *et al.* (2009) ‘Dysfunction of ouabain-induced cardiac contractility in mice with heart-specific ablation of Na,K-ATPase β1-subunit’, *Journal of Molecular and Cellular Cardiology*, 47(4), pp. 552–560. Available at: https://doi.org/10.1016/J.YJMCC.2009.07.018.

Beard, J. (1890) ‘On the early development of Lepidosteus osseus’, *Royal Society*, 46(280–285), pp. 108–118. Available at: https://doi.org/10.1098/rspl.1889.0015.

Becker, H.E. and Cone, R.A. (1966) ‘Light-stimulated electrical responses from skin’, *Science (New York, N.Y.)*, 154(3752), pp. 1051–1053. Available at: https://doi.org/10.1126/SCIENCE.154.3752.1051.

Béguin, P. *et al.* (1997) ‘The γ subunit is a specific component of the Na,K-ATPase and modulates its transport function’, *EMBO Journal*, 16(14), pp. 4250–4260. Available at: https://doi.org/10.1093/emboj/16.14.4250.

Béguin, P. *et al.* (2002) ‘FXYD7 is a brain-specific regulator of Na, K-ATPase α1-β isozymes’, *EMBO Journal*, 21(13), pp. 3264–3273. Available at: https://doi.org/10.1093/emboj/cdf330.

Bender, F. (2012) *Activity-dependent development of the locomotor network in Xenopus laevis larvae*. University of St Andrews.

Bernhardt, R.R. *et al.* (1990) ‘Identification of spinal neurons in the embryonic and larval zebrafish’, *Journal of Comparative Neurology*, 302(3), pp. 603–616. Available at: https://doi.org/10.1002/CNE.903020315.

Bertolesi, G.E. *et al.* (2021) ‘Type II Opsins in the Eye, the Pineal Complex and the Skin of *Xenopus* laevis: Using Changes in Skin Pigmentation as a Readout of Visual and Circadian Activity’, *Frontiers in Neuroanatomy*, 15. Available at: https://doi.org/10.3389/FNANA.2021.784478.

Bibert, S. *et al.* (2008) ‘Phosphorylation of phospholemman (FXYD1) by protein kinases A and C modulates distinct Na,K-ATPase isozymes’, *Journal of Biological Chemistry*, 283(1), pp. 476–486. Available at: https://doi.org/10.1074/jbc.M705830200.

Biel, M. *et al.* (2009) ‘Hyperpolarization-Activated Cation Channels: From Genes to Function’, *Physiological Reviews*, 89, pp. 847–885. Available at: https://doi.org/10.1152/physrev.00029.2008.

Binkley, S. *et al.* (1988) ‘*Xenopus* Tadpole Melanophores Are Controlled by Dark and Light and Melatonin Without Influence of Time of Day’, *Journal of Pineal Research*, 5(1), pp. 87–97. Available at: https://doi.org/10.1111/J.1600-079X.1988.TB00771.X.

Blanco, G. *et al.* (1994) *The a-Subunit of the Na,K-ATPase Has Catalytic Activity Independent of the α-Subunit**, *THE JOURNAL OF BIOLOGICAL CHEMISTRY*.

Blanco, G. (2005a) ‘Na,K-ATPase Subunit Heterogeneity as a Mechanism for Tissue-Specific Ion Regulation’. Available at: https://doi.org/10.1016/j.semnephrol.2005.03.004.

Blanco, G. (2005b) ‘Na,K-ATPase Subunit Heterogeneity as a Mechanism for Tissue-Specific Ion Regulation’. Available at: https://doi.org/10.1016/j.semnephrol.2005.03.004.

Blanco, G. and Mercer, R.W. (1998) ‘Isozymes of the Na-K-ATPase: Heterogeneity in structure, diversity in function’, *American Journal of Physiology - Renal Physiology*.

American Physiological SocietyBethesda, MD. Available at: https://doi.org/10.1152/ajprenal.1998.275.5.f633.

Boon, H. *et al.* (2012) 'Influence of chronic and acute spinal cord injury on skeletal muscle Na +-K +-ATPase and phospholemman expression in humans', *American Journal of Physiology - Endocrinology and Metabolism*, 302(7), pp. 864–871. Available at: https://doi.org/10.1152/AJPENDO.00625.2011/ASSET/IMAGES/LARGE/ZH1007126493000 5.JPEG.

Boothby, K.M. and Roberts, A. (1992) 'The stopping response of *Xenopus* laevis embryos: behaviour, development and physiology', *Journal of comparative physiology. A, Sensory, neural, and behavioral physiology*, 170(2), pp. 171–180. Available at: https://doi.org/10.1007/BF00196899.

Boothby, K.M. and Roberts, A. (1995) 'Effects of site of tactile stimulation on the escape swimming responses of hatchling *Xenopus* laevis embryos', *Journal of Zoology*, 235(1), pp. 113–125. Available at: https://doi.org/10.1111/j.1469-7998.1995.tb05132.x.

Borodinsky, L.N. *et al.* (2004) 'Activity-dependent homeostatic specification of transmitter expression in embryonic neurons', *Nature*, 429(6991), pp. 523–530. Available at: https://doi.org/10.1038/NATURE02518.

Borodinsky, L.N. *et al.* (2017) '*Xenopus* laevis as a Model Organism for the Study of Spinal Cord Formation, Development, Function and Regeneration'. Available at: https://doi.org/10.3389/fncir.2017.00090.

Bøttger, P. *et al.* (2011a) 'Distribution of Na/K-ATPase alpha 3 isoform, a sodium-potassium P-type pump associated with rapid-onset of dystonia parkinsonism (RDP) in the adult mouse brain', *The Journal of Comparative Neurology*, 519(2), pp. 376–404. Available at: https://doi.org/10.1002/cne.22524.

Bøttger, P. *et al.* (2011b) 'Distribution of Na/K-ATPase alpha 3 isoform, a sodium-potassium P-type pump associated with rapid-onset of dystonia parkinsonism (RDP) in the adult mouse brain', *Journal of Comparative Neurology*, 519(2), pp. 376–404. Available at: https://doi.org/10.1002/cne.22524.

Boudjelida, H. and Muntz, L. (1987) 'Multinucleation during myogenesis of the myotome of *Xenopus* laevis: a qualitative study', *Development*, 101, pp. 583–590.

Bradley, S. *et al.* (2010) ‘Nitric oxide synthase regulates morphogenesis of zebrafish spinal cord motoneurons’, *Journal of Neuroscience*, 30(50), pp. 16818–16831. Available at: https://doi.org/10.1523/JNEUROSCI.4456-10.2010.

Brashear, A. *et al.* (2012) ‘ATP1A3 mutations in infants: A new rapid-onset dystonia-Parkinsonism phenotype characterized by motor delay and ataxia’, *Developmental Medicine and Child Neurology*, 54(11), pp. 1065–1067. Available at: https://doi.org/10.1111/j.1469-8749.2012.04421.x.

Brines, M.L. and Robbins, R.J. (1992) ‘Inhibition of α2/α3 sodium pump isoforms potentiates glutamate neurotoxicity’, *Brain Research*, 591(1), pp. 94–102. Available at: https://doi.org/10.1016/0006-8993(92)90982-F.

Burger, C. and Ribera, A.B. (1996) ‘*Xenopus* spinal neurons express Kv2 potassium channel transcripts during embryonic development’, *Journal of Neuroscience*, 16(4), pp. 1412–1421. Available at: https://doi.org/10.1523/jneurosci.16-04-01412.1996.

Butler, J.M. *et al.* (2022) ‘Development of the visual system in social poison frog tadpoles’, *bioRxiv preprint*, 10(18), pp. 512–729.

Capuano, A. *et al.* (2020) ‘Alternating hemiplegia of childhood: Understanding the genotype–phenotype relationship of ATP1A3 variations’, *Application of Clinical Genetics*. Dove Medical Press Ltd., pp. 71–81. Available at: https://doi.org/10.2147/TACG.S210325.

De Carvalho Aguiar, P. *et al.* (2004) ‘Mutations in the Na+/K+-ATPase α3 gene ATP1A3 are associated with rapid-onset dystonia parkinsonism’, *Neuron*, 43(2), pp. 169–175. Available at: https://doi.org/10.1016/j.neuron.2004.06.028.

Chang, J.T., Lowery, L.A. and Sive, H. (2012) ‘Multiple roles for the Na,K-ATPase subunits, Atp1a1 and Fxyd1, during brain ventricle development’, *Developmental Biology*, 368(2), pp. 312–322. Available at: https://doi.org/10.1016/j.ydbio.2012.05.034.

Christenson, J. *et al.* (1988) ‘The dorsal cell, one class of primary sensory neuron in the lamprey spinal cord. I. Touch, pressure but no nociception — a physiological study’, *Brain Research*, 440(1), pp. 1–8. Available at: https://doi.org/10.1016/0006-8993(88)91152-3.

Christiansen, D. *et al.* (2017) ‘Regulation of Na+,K+-ATPase isoforms and phospholemman (FXYD1) in skeletal muscle fibre types by exercise training and cold-water immersion in men’, *bioRxiv*, p. 151035. Available at: https://doi.org/10.1101/151035.

Clarke, J.D. *et al.* (1984) ‘Sensory physiology, anatomy and immunohistochemistry of Rohon-Beard neurones in embryos of *Xenopus* laevis.’, *The Journal of Physiology*, 348(1), pp. 511–525. Available at: https://doi.org/10.1113/jphysiol.1984.sp015122.

Clarke, J.D. and Roberts, A. (1984) ‘Interneurones in the *Xenopus* embryo spinal cord: sensory excitation and activity during swimming.’, *The Journal of Physiology*, 354(1), pp. 345–362. Available at: https://doi.org/10.1113/JPHYSIOL.1984.SP015380.

Clausen, M. V., Hilbers, F. and Poulsen, H. (2017) ‘The structure and function of the Na,K-ATPase isoforms in health and disease’, *Frontiers in Physiology*. Frontiers Media S.A., p. 371. Available at: https://doi.org/10.3389/fphys.2017.00371.

Clausen, T. (2003) ‘Na+-K+ pump regulation and skeletal muscle contractility’, *Physiological Reviews*. American Physiological Society, pp. 1269–1324. Available at: https://doi.org/10.1152/physrev.00011.2003.

Collins, J.H. *et al.* (1982) ‘Purification and characterization of an (Na++K+)-ATPase proteolipid labeled with a photoaffinity derivative of ouabain’, *BBA - Biomembranes*, 686(1), pp. 7–12. Available at: https://doi.org/10.1016/0005-2736(82)90145-6.

Combes, D. *et al.* (2004) ‘Developmental segregation of spinal networks driving axial- and hindlimb-based locomotion in metamorphosing *Xenopus* laevis’, *Journal of Physiology*, 559(1), pp. 17–24. Available at: https://doi.org/10.1113/jphysiol.2004.069542.

Combes, D., Sillar, K.T. and Simmers, J. (2020a) ‘*Xenopus* frog metamorphosis: A model for studying locomotor network development and neuromodulation’, *The Neural Control of Movement: Model Systems and Tools to Study Locomotor Function*, pp. 175–203. Available at: https://doi.org/10.1016/B978-0-12-816477-8.00008-9.

Combes, D., Sillar, K.T. and Simmers, J. (2020b) ‘*Xenopus* frog metamorphosis: A model for studying locomotor network development and neuromodulation’, *The Neural Control of Movement*, pp. 175–203. Available at: https://doi.org/10.1016/B978-0-12-816477-8.00008-9.

Cornelius, F. and Mahmmoud, Y.A. (2003) ‘Functional Modulation of the Sodium Pump: The Regulatory Proteins “Fixit”’, *Physiology*, 18(3), pp. 119–124. Available at: https://doi.org/10.1152/nips.01434.2003.

Couto, N.F. do *et al.* (2020) ‘Measuring Intracellular Vesicle Density and Dispersion Using Fluorescence Microscopy and ImageJ/FIJI’, *Bio-protocol*, 10(15). Available at: https://doi.org/10.21769/BIOPROTOC.3703.

Crambert, G. *et al.* (2000) ‘Transport and pharmacological properties of nine different human Na,K- ATPase isozymes’, *Journal of Biological Chemistry*, 275(3), pp. 1976–1986. Available at: https://doi.org/10.1074/jbc.275.3.1976.

Crambert, G. *et al.* (2002) ‘Phospholemman (FXYD1) associates with Na,K-ATpase and regulates its transport properties’, *Proceedings of the National Academy of Sciences of the United States of America*, 99(17), pp. 11476–11481. Available at: https://doi.org/10.1073/pnas.182267299.

Crambert, G. *et al.* (2004) ‘FXYD7, mapping of functional sites involved in endoplasmic reticulum export, association with and regulation of Na,K-ATPase’, *Journal of Biological Chemistry*, 279(29), pp. 30888–30895. Available at: https://doi.org/10.1074/jbc.M313494200.

Crambert, G. *et al.* (2005) ‘FXYD3 (Mat-8), a new regulator of Na,K-ATPase’, *Molecular Biology of the Cell*, 16(5), pp. 2363–2371. Available at: https://doi.org/10.1091/mbc.E04-10-0878.

Crambert, G. and Geering, K. (2003) ‘FXYD proteins: new tissue-specific regulators of the ubiquitous Na,K-ATPase.’, *Science’s STKE : signal transduction knowledge environment*. Science Signaling, pp. re1–re1. Available at: https://doi.org/10.1126/stke.2003.166.re1.

Cuomo, M. *et al.* (2022) ‘Epigenetic remodelling of Fxyd1 promoters in developing heart and brain tissues’, *Scientific Reports*, 12(1), pp. 1–11. Available at: https://doi.org/10.1038/s41598-022-10365-y.

Currie, S.P. *et al.* (2016) ‘A behaviorally related developmental switch in nitrergic modulation of locomotor rhythmogenesis in larval *Xenopus* tadpoles’, *Journal of Neurophysiology*, 115(3), pp. 1446–1457. Available at: https://doi.org/10.1152/JN.00283.2015.

Currie, S.P. and Sillar, K.T. (2018) ‘Developmental changes in spinal neuronal properties, motor network configuration, and neuromodulation at free-swimming stages of *Xenopus* tadpoles’, *Journal of Neurophysiology*, 119(3), pp. 786–795. Available at: https://doi.org/10.1152/jn.00219.2017.

Dale, N. *et al.* (1987) ‘The morphology and distribution of “Kolmer–Agduhr cells”, a class of cerebrospinal-fluid-contacting neurons revealed in the frog embryo spinal cord by GABA immunocytochemistry’, *Proceedings of the Royal Society of London. Series B. Biological Sciences*, 232(1267), pp. 193–203. Available at: https://doi.org/10.1098/RSPB.1987.0068.

Dard, R. *et al.* (2015) ‘Relapsing encephalopathy with cerebellar ataxia related to an *ATP1A3* mutation’, *Developmental Medicine & Child Neurology*, 57(12), pp. 1183–1186. Available at: https://doi.org/10.1111/dmcn.12927.

Date, P. *et al.* (2019) ‘Visualizing flow in an intact CSF network using optical coherence tomography: implications for human congenital hydrocephalus’, *Scientific Reports*, 9(1), pp. 1–15. Available at: https://doi.org/10.1038/s41598-019-42549-4.

Delprat, B. *et al.* (2007a) ‘FXYD6 is a novel regulator of Na,K-ATPase expressed in the inner ear’, *Journal of Biological Chemistry*, 282(10), pp. 7450–7456. Available at: https://doi.org/10.1074/jbc.M609872200.

Delprat, B. *et al.* (2007b) ‘FXYD6 Is a Novel Regulator of Na,K-ATPase Expressed in the Inner Ear’, *Journal of Biological Chemistry*, 282(10), pp. 7450–7456. Available at: https://doi.org/10.1074/JBC.M609872200.

Despa, S. *et al.* (2005) ‘Phospholemman-phosphorylation mediates the β-adrenergic effects on Na/K pump function in cardiac myocytes’, *Circulation Research*, 97(3), pp. 252–259. Available at: https://doi.org/10.1161/01.RES.0000176532.97731.e5.

Dobretsov, M. and Stimers, J.R. (2005) ‘Neuronal function and alpha3 isoform of the Na/K-ATPase’, *Frontiers in Bioscience*, 10(SUPPL. 1), pp. 2373–2396. Available at: https://doi.org/10.2741/1704/PDF.

Dobyns, W.B. *et al.* (1993) ‘Rapid-onset dystonia-parkinsonism’, *Neurology*, 43(12).

Doğanli, C. *et al.* (2013) ‘α3Na+/K+-ATPase deficiency causes brain ventricle dilation and abrupt embryonic motility in zebrafish’, *Journal of Biological Chemistry*, 288(13), pp. 8862–8874. Available at: https://doi.org/10.1074/jbc.M112.421529.

Dong, C. *et al.* (2018) ‘Expression of trpv channels during *Xenopus* laevis embryogenesis’, *Gene Expression Patterns*, 30, pp. 64–70. Available at: https://doi.org/10.1016/j.gep.2018.10.001.

Dur, A.H. *et al.* (2020) ‘In *Xenopus* ependymal cilia drive embryonic CSF circulation and brain development independently of cardiac pulsatile forces’, *Fluids and Barriers of the CNS*, 17(1), pp. 1–22. Available at: https://doi.org/10.1186/s12987-020-00234-z.

Félix, L.M. *et al.* (2018a) ‘MS-222 short exposure induces developmental and behavioural alterations in zebrafish embryos’, *Reproductive Toxicology*, 81, pp. 122–131. Available at: https://doi.org/10.1016/j.reprotox.2018.07.086.

Félix, L.M. *et al.* (2018b) ‘MS-222 short exposure induces developmental and behavioural alterations in zebrafish embryos’, *Reproductive Toxicology*, 81, pp. 122–131. Available at: https://doi.org/10.1016/j.reprotox.2018.07.086.

Ferrari, M.B. *et al.* (1998) ‘A calcium signaling cascade essential for myosin thick filament assembly in *Xenopus* myocytes’, *Journal of Cell Biology*, 141(6), pp. 1349–1356. Available at: https://doi.org/10.1083/jcb.141.6.1349.

Feschenko, M.S. *et al.* (2003) ‘Phospholemman, a single-span membrane protein, is an accessory protein of Na,K-ATPase in cerebellum and choroid plexus’, *Journal of Neuroscience*, 23(6), pp. 2161–2169. Available at: https://doi.org/10.1523/jneurosci.23-06-02161.2003.

Floyd, R. V. *et al.* (2010) ‘Differential cellular expression of FXYD1 (phospholemman) and FXYD2 (gamma subunit of Na, K-ATPase) in normal human tissues: A study using high density human tissue microarrays’, *Annals of Anatomy*, 192(1), pp. 7–16. Available at: https://doi.org/10.1016/j.aanat.2009.09.003.

Forbush, B., Kaplan, J.H. and Hoffman, J.F. (1978) ‘Characterization of a New Photoaffinity Derivative of Ouabain: Labeling of the Large Polypeptide and of a Proteolipid Component of the Na,K-ATPaset’, *Biochemistry*, 17(17), pp. 3667–3676. Available at: https://doi.org/10.1021/bi00610a037.

Franzini-Armstrong, C. (2018) ‘The relationship between form and function throughout the history of excitation-contraction coupling’, *Journal of General Physiology*, 150(2), pp. 189–210. Available at: https://doi.org/10.1085/jgp.201711889.

Fukuzawa, T. (2021) ‘Periodic albinism of a widely used albino mutant of *Xenopus* laevis caused by deletion of two exons in the Hermansky–Pudlak syndrome type 4 gene’, *Genes to Cells*, 26(1), pp. 31–39. Available at: https://doi.org/10.1111/GTC.12818.

Gangatharan, G., Schneider-Maunoury, S. and Breau, M.A. (2018) ‘Role of mechanical cues in shaping neuronal morphology and connectivity’, *Biology of the Cell*, 110(6), pp. 125–136. Available at: https://doi.org/10.1111/BOC.201800003.

Geering, K. (2006a) ‘FXYD proteins: New regulators of Na-K-ATPase’, *American Journal of Physiology - Renal Physiology*. American Physiological Society. Available at: https://doi.org/10.1152/ajprenal.00126.2005.

Geering, K. (2006b) ‘FXYD proteins: New regulators of Na-K-ATPase’, *American Journal of Physiology - Renal Physiology*. American Physiological Society. Available at: https://doi.org/10.1152/ajprenal.00126.2005.

Gulyás, M. *et al.* (2021) ‘AnimalTracker: An ImageJ-Based Tracking API to Create a Customized Behaviour Analyser Program’, *Neuroinformatics* [Preprint]. Available at: https://doi.org/10.1007/s12021-016-9303-z.

Gunnarsson, T.P. *et al.* (2013) ‘Effect of intensified training on muscle ion kinetics, fatigue development, and repeated short-term performance in endurance-trained cyclists’, *American Journal of Physiology - Regulatory Integrative and Comparative Physiology*, 305(7), pp. R811-21. Available at: https://doi.org/10.1152/ajpregu.00467.2012.

Guo, Y. *et al.* (2022) ‘Cryo-EM structures of recombinant human sodium-potassium pump determined in three different states’, *Nature Communications*, 13(1), pp. 1–9. Available at: https://doi.org/10.1038/s41467-022-31602-y.

Hachoumi, L. *et al.* (2022) ‘Bimodal modulation of short-term motor memory via dynamic sodium pumps in a vertebrate spinal cord’, *Current Biology*, 32(5), pp. 1038-1048.e2. Available at: https://doi.org/10.1016/j.cub.2022.01.012.

Hachoumi, L. and Sillar, K.T. (2019) ‘Developmental stage-dependent switching in the neuromodulation of vertebrate locomotor central pattern generator networks’, *Developmental Neurobiology*, p. dneu.22725. Available at: https://doi.org/10.1002/dneu.22725.

Halberstadt, A.L., Powell, S.B. and Geyer, M.A. (2013) ‘Role of the 5-HT_2A receptor in the locomotor hyperactivity produced by phenylalkylamine hallucinogens in mice’, *Neuropharmacology*, 70, pp. 218–227. Available at: https://doi.org/10.1016/J.NEUROPHARM.2013.01.014.

Halvagal, M.S. and Zenke, F. (2023) ‘The combination of Hebbian and predictive plasticity learns invariant object representations in deep sensory networks’, *Nature Neuroscience*, 26(11), pp. 1906–1915. Available at: https://doi.org/10.1038/s41593-023-01460-y.

Hardwicke, P.M.D. and Freytag, J.W. (1981) ‘A proteolipid associated with Na,K-ATPase is not essential for ATPase activity’, *Biochemical and Biophysical Research Communications*, 102(1), pp. 250–257. Available at: https://doi.org/10.1016/0006-291X(81)91514-X.

Harris-Warrick, R.M. and Marder, E. (1991) ‘Modulation of Neural Networks for Behavior’, *Annual Review of Neuroscience*, 14(1), pp. 39–57. Available at: https://doi.org/10.1146/annurev.ne.14.030191.000351.

Hatakeyama, J. and Kageyama, R. (2004) ‘Retinal cell fate determination and bHLH factors’, *Seminars in Cell & Developmental Biology*, 15(1), pp. 83–89. Available at: https://doi.org/10.1016/J.SEMCDB.2003.09.005.

Haverkamp, L.J. and Oppenheim, R.W. (1986) ‘Behavioral development in the absence of neural activity: effects of chronic immobilization on amphibian embryos’, *Journal of Neuroscience*, 6(5), pp. 1332–1337. Available at: https://doi.org/10.1523/JNEUROSCI.06-05-01332.1986.

Heinzen, E.L. *et al.* (2012) ‘De novo mutations in ATP1A3 cause alternating hemiplegia of childhood’, *Nature Genetics*, 44(9), pp. 1030–1034. Available at: https://doi.org/10.1038/ng.2358.

Heinzen, E.L. *et al.* (2014) ‘Distinct neurological disorders with ATP1A3 mutations’, *The Lancet Neurology*. Lancet Publishing Group, pp. 503–514. Available at: https://doi.org/10.1016/S1474-4422(14)70011-0.

Hewapathirane, D.S. and Haas, K. (2009) ‘The albino *Xenopus* laevis tadpole as a novel model of developmental seizures’, *Neuromethods*. Humana Press, pp. 45–57. Available at: https://doi.org/10.1007/978-1-60327-263-6_3.

Hoperskaya, O.A. (1975) ‘The development of animals homozygous for a mutation causing periodic albinism (ap) in *Xenopus* laevis’, *Development*, 34(1), pp. 253–264. Available at: https://doi.org/10.1242/DEV.34.1.253.

Horisberger, J.D. (2004) ‘Recent Insights into the Structure and The Sodium Pump in the P-ATPase’, *Physiology*, 19, pp. 377–387.

Huang, C.L. and Hockaday, a R. (1988) ‘Development of myotomal cells in *Xenopus* laevis larvae.’, *Journal of anatomy*, 159, pp. 129–36.

Hunanyan, A.S. *et al.* (2018) ‘Mechanisms of increased hippocampal excitability in the Mashl+/- mouse model of Na+/K+ -ATPase dysfunction’, *Epilepsia*, 59(7), pp. 1455–1468. Available at: https://doi.org/10.1111/epi.14441.

Hundal, H.S. *et al.* (1994) ‘Subcellular distribution and immunocytochemical localization of Na,K-ATPase subunit isoforms in human skeletal muscle’, *Molecular Membrane Biology*, 11(4), pp. 255–262. Available at: https://doi.org/10.3109/09687689409160435.

Hunt, J.E., Bruno, J.R. and Pratt, K.G. (2020) ‘An Innate Color Preference Displayed by *Xenopus* Tadpoles Is Persistent and Requires the Tegmentum’, *Frontiers in Behavioral Neuroscience*, 14(May), pp. 1–11. Available at: https://doi.org/10.3389/fnbeh.2020.00071.

Ingwersen, M.S. *et al.* (2011) ‘Na,K-ATPase activity in mouse muscle is regulated by AMPK and PGC-1α’, *Journal of Membrane Biology*, 242(1), pp. 1–10. Available at: https://doi.org/10.1007/s00232-011-9365-7.

Jaffer, F. *et al.* (2015) ‘Faulty cardiac repolarization reserve in alternating hemiplegia of childhood broadens the phenotype’, *Brain*, 138(10), pp. 2859–2874. Available at: https://doi.org/10.1093/brain/awv243.

James, P.F. *et al.* (1999) ‘Identification of a Specific Role for the Na,K-ATPase α2 Isoform as a Regulator of Calcium in the Heart’, *Molecular Cell*, 3(5), pp. 555–563. Available at: https://doi.org/10.1016/S1097-2765(00)80349-4.

Jamieson, D. and Roberts, A. (2000) ‘Responses of young *Xenopus* laevis tadpoles to light dimming: Possible roles for the pineal eye’, *Journal of Experimental Biology*, 203(12), pp. 1857–1867. Available at: https://doi.org/10.1242/jeb.203.12.1857.

Jorgensen, P.L., Håkansson, K.O. and Karlish, S.J.D. (2003) ‘Structure and Mechanism of Na,K-ATPase: Functional Sites and Their Interactions’, *Annual Review of Physiology*, 65(1), pp. 817–849. Available at: https://doi.org/10.1146/annurev.physiol.65.092101.142558.

Kadowaki, K. *et al.* (2004) ‘Phosphohippolin expression in the rat central nervous system’, *Molecular Brain Research*, 125(1–2), pp. 105–112. Available at: https://doi.org/10.1016/j.molbrainres.2004.03.021.

Kahn, J.A. and Roberts, A. (1982) ‘The central nervous origin of the swimming motor pattern in embryos of *Xenopus* laevis.’, *Journal of Experimental Biology*, 99, pp. 185–196.

Kaplan, J.H. (2002) ‘Biochemistry of Na,K-ATPase’, *Annual Review of Biochemistry*, 71(1), pp. 511–535. Available at: https://doi.org/10.1146/annurev.biochem.71.102201.141218.

Kuijpers, W. and Bonting, S.L. (1970) ‘The cochlear potentials. I. The effect of ouabain on the cochlear potentials of the guinea pig’, *Pflugers Archiv : European journal of physiology*, 320(4), pp. 348–358. Available at: https://doi.org/10.1007/BF00588213.

Kvljrmcs, W. and Bonting, S.L. (1970) ‘The Cochlear Potentials II. The Nature of the Cochlear Endolymphatic Resting Potential’, *Pflfigers Arch*, 320, pp. 359–372.

Larsen, B.R. *et al.* (2014) ‘Contributions of the Na+/K+-ATPase, NKCC1, and Kir4.1 to hippocampal K+ clearance and volume responses’, *GLIA*, 62(4), pp. 608–622. Available at: https://doi.org/10.1002/GLIA.22629.

Laursen, M. *et al.* (2013) ‘Crystal structure of the high-affinity Na+,K+-ATPase- ouabain complex with Mg2+ bound in the ca tion binding site’, *Proceedings of the National Academy of Sciences of the United States of America*, 110(27), pp. 10958–10963. Available at: https://doi.org/10.1073/PNAS.1222308110/-/DCSUPPLEMENTAL.

Laursen, M. *et al.* (2015) ‘Structures and characterization of digoxin- And bufalin-bound Na+,K+-ATPase compared with the ouabain-bound complex’, *Proceedings of the National Academy of Sciences of the United States of America*, 112(6), pp. 1755–1760. Available at: https://doi.org/10.1073/PNAS.1422997112/-/DCSUPPLEMENTAL.

Li, W.C. *et al.* (2003) ‘The neuronal targets for GABAergic reticulospinal inhibition that stops swimming in hatchling frog tadpoles’, *Journal of Comparative Physiology A: Neuroethology, Sensory, Neural, and Behavioral Physiology*, 189(1), pp. 29–37. Available at: https://doi.org/10.1007/s00359-002-0372-0.

Li, W.C. *et al.* (2004) ‘Primitive roles for inhibitory interneurons in developing frog spinal cord’, *Journal of Neuroscience*, 24(25), pp. 5840–5848. Available at: https://doi.org/10.1523/JNEUROSCI.1633-04.2004.

Li, W.C. *et al.* (2006) ‘Persistent responses to brief stimuli: Feedback excitation among brainstem neurons’, *Journal of Neuroscience*, 26(15), pp. 4026–4035. Available at: https://doi.org/10.1523/JNEUROSCI.4727-05.2006.

Li, W.C. and Moult, P.R. (2012) ‘The control of locomotor frequency by excitation and inhibition.’, *The Journal of neuroscience : the official journal of the Society for Neuroscience*, 32(18), pp. 6220–30. Available at: https://doi.org/10.1523/JNEUROSCI.6289-11.2012.

Li, W.C., Roberts, A. and Soffe, S.R. (2009) ‘Locomotor rhythm maintenance: Electrical coupling among premotor excitatory interneurons in the brainstem and spinal cord of young *Xenopus* tadpoles’, *Journal of Physiology*, 587(8), pp. 1677–1693. Available at: https://doi.org/10.1113/jphysiol.2008.166942.

Li, W.C., Roberts, A. and Soffe, S.R. (2010) ‘Specific brainstem neurons switch each other into pacemaker mode to drive movement by activating NMDA receptors.’, *The Journal of neuroscience : the official journal of the Society for Neuroscience*, 30(49), pp. 16609–20. Available at: https://doi.org/10.1523/JNEUROSCI.3695-10.2010.

Li, W.C., Soffe, S.R. and Roberts, A. (2002) ‘Spinal Inhibitory Neurons that Modulate Cutaneous Sensory Pathways during Locomotion in a Simple Vertebrate’.

Li, W.C., Soffe, S.R. and Roberts, A. (2004) ‘Glutamate and acetylcholine corelease at developing synapses.’, *Proceedings of the National Academy of Sciences of the United States of America*, 101(43), pp. 15488–93. Available at: https://doi.org/10.1073/pnas.0404864101.

Li, W.C., Wagner, M. and Porter, N.J. (2014) ‘Behavioral Observation of *Xenopus* Tadpole Swimming for Neuroscience Labs’, *Journal of Undergraduate Neuroscience Education*, 12(2), p. A107.

Li, W.C., Zhu, X.Y. and Ritson, E. (2017) ‘Mechanosensory stimulation evokes acute concussion-like behavior by activating girks coupled to muscarinic receptors in a simple vertebrate’, *eNeuro*, 4(2), pp. 1–17. Available at: https://doi.org/10.1523/ENEURO.0073-17.2017.

Meyer, D.J. *et al.* (2020) ‘FXYD protein isoforms differentially modulate human Na/K pump function’, *Journal of General Physiology*, 152(12). Available at: https://doi.org/10.1085/JGP.202012660.

Rasmussen, M.K., Kristensen, M. and Juel, C. (2008) ‘Exercise-induced regulation of phospholemman (FXYD1) in rat skeletal muscle: implications for Na^+/K^+-ATPase activity’, *Acta Physiologica*, 194(1), pp. 67–79. Available at: https://doi.org/10.1111/j.1748-1716.2008.01857.x.

Roberts, A. *et al.* (2009) ‘Responses of hatchling Xenopus tadpoles to water currents: First function of lateral line receptors without cupulae’, *Journal of Experimental Biology*, 212(7), pp. 914–921. Available at: https://doi.org/10.1242/jeb.027250.

Saccomanno, V. *et al.* (2021) ‘The early development and physiology of Xenopus laevis tadpole lateral line system’, *Journal of Neurophysiology*, 126(5), pp. 1814–1830. Available at: https://doi.org/10.1152/jn.00618.2020.

Session, A.M. *et al.* (2016) ‘Genome evolution in the allotetraploid frog Xenopus laevis’, *Nature*, 538(7625), pp. 336–343. Available at: https://doi.org/10.1038/nature19840.

Stanley, C.M. *et al.* (2015) ‘Article Importance of the Voltage Dependence of Cardiac Na/K ATPase Isozymes’. Available at: https://doi.org/10.1016/j.bpj.2015.09.015.

Teriete, P. *et al.* (2009) ‘Effects of PKA phosphorylation on the conformation of the Na,K-ATPase regulatory protein FXYD1’, *Biochimica et Biophysica Acta - Biomembranes*, 1788(11), pp. 2462–2470. Available at: https://doi.org/10.1016/j.bbamem.2009.09.001.

Yap, J.Q. *et al.* (2021) ‘FXYD proteins and sodium pump regulatory mechanisms’. Available at: https://doi.org/10.1085/jgp.202012633.

Liao, Y. *et al.* (2022a) ‘Cell landscape of larval and adult *Xenopus* laevis at single-cell resolution’, *Nature Communications 2022 13:1*, 13(1), pp. 1–15. Available at: https://doi.org/10.1038/s41467-022-31949-2.

Liao, Y. *et al.* (2022b) ‘Cell landscape of larval and adult *Xenopus* laevis at single-cell resolution’, *Nature Communications 2022 13:1*, 13(1), pp. 1–15. Available at: https://doi.org/10.1038/s41467-022-31949-2.

Liedtke, H.C. *et al.* (2023) ‘Background matching through fast and reversible melanin-based pigmentation plasticity in tadpoles comes with morphological and antioxidant changes’, *Scientific Reports*, 13(1). Available at: https://doi.org/10.1038/s41598-023-39107-4.

Lifshitz, Y. *et al.* (2006) ‘Functional interactions of phospholemman (PLM) (FXYD1) with Na +,K +-ATPase: Purification of α1/α1/PLM complexes expressed in pichia pastoris’, *Journal of Biological Chemistry*, 281(23), pp. 15790–15799. Available at: https://doi.org/10.1074/jbc.M601993200.

Lingrel, J.B. *et al.* (2007) ‘Na,K-ATPase and the role of α isoforms in behavior’, *Journal of Bioenergetics and Biomembranes*. Springer, pp. 385–389. Available at: https://doi.org/10.1007/s10863-007-9107-9.

Liu, J. and Jordan, L.M. (2005) ‘Stimulation of the Parapyramidal Region of the Neonatal Rat Brain Stem Produces Locomotor-Like Activity Involving Spinal 5-HT 7 and 5-HT 2A Receptors’, *J Neurophysiol*, 94, pp. 1392–1404. Available at: https://doi.org/10.1152/jn.00136.2005.

Luo, H. *et al.* (2021) ‘FXYD6 promotes thermal nociception by regulating TRPV1’, *Molecular Pain*, 17. Available at: https://doi.org/10.1177/1744806921992249.

Matagne, V. *et al.* (2018) ‘Correcting deregulated Fxyd1 expression rescues deficits in neuronal arborization and potassium homeostasis in MeCP2 deficient male mice HHS Public Access’, *Brain Res*, 1697, pp. 45–52. Available at: https://doi.org/10.1016/j.brainres.2018.06.013.

McDonough, A.A., Geering, K. and Farley, R.A. (1990) ‘The sodium pump needs its β subunit’, *The FASEB Journal*, 4(6), pp. 1598–1605. Available at: https://doi.org/10.1096/fasebj.4.6.2156741.

McGrail, K.M., Phillips, J.M. and Sweadner, K.J. (1991) *Immunofluorescent Localization of Three Na,K-ATPase Isozymes in the Rat Central Nervous System: Both Neurons and Glia Can Express More Than One Na,K-ATPase*.

McLean, D.L. and Sillar, K.T. (2000) ‘The distribution of NADPH-diaphorase-labelled interneurons and the role of nitric oxide in the swimming system of *Xenopus* laevis larvae’, *Journal of Experimental Biology*, 203(4).

McLean, D.L. and Sillar, K.T. (2002) ‘Nitric Oxide Selectively Tunes Inhibitory Synapses to Modulate Vertebrate Locomotion’, *Journal of Neuroscience*, 22(10), pp. 4175–4184. Available at: https://doi.org/10.1523/JNEUROSCI.22-10-04175.2002.

McLean, D.L. and Sillar, K.T. (2004) ‘Metamodulation of a spinal locomotor network by nitric oxide’, *Journal of Neuroscience*, 24(43), pp. 9561–9571. Available at: https://doi.org/10.1523/JNEUROSCI.1817-04.2004.

Mercer, R.W. *et al.* (1993) ‘Molecular cloning and immunological characterization of the γ polypeptide, a small protein associated with the Na,K-ATPase’, *Journal of Cell Biology*, 121(3), pp. 579–586. Available at: https://doi.org/10.1083/jcb.121.3.579.

Meyer, D.J. *et al.* (2020) ‘FXYD protein isoforms differentially modulate human Na/K pump function’, *Journal of General Physiology*, 152(12). Available at: https://doi.org/10.1085/JGP.202012660.

van Mier, P., Armstrong, J. and Roberts, A. (1989) ‘Development of early swimming in *Xenopus* laevis embryos: Myotomal musculature, its innervation and activation’, *Neuroscience*, 32(1), pp. 113–126. Available at: https://doi.org/10.1016/0306-4522(89)90111-5.

Miles, G.B. and Sillar, K.T. (2011) ‘Neuromodulation of vertebrate locomotor control networks’, *Physiology*. American Physiological Society Bethesda, MD, pp. 393–411. Available at: https://doi.org/10.1152/physiol.00013.2011.

Mishra, N.K. *et al.* (2011) 'FXYD proteins stabilize Na,K-ATpase: Amplification of specific phosphatidylserine-protein interactions', *Journal of Biological Chemistry*, 286(11), pp. 9699–9712. Available at: https://doi.org/10.1074/jbc.M110.184234.

Mogi, K. *et al.* (2012) 'Visualisation of cerebrospinal fluid flow patterns in albino *Xenopus* larvae in vivo', *Fluids and Barriers of the CNS*, 9(1), p. 9. Available at: https://doi.org/10.1186/2045-8118-9-9.

Morth, J.P. *et al.* (2007) 'Crystal structure of the sodium-potassium pump', *Nature*, 450(7172), pp. 1043–1049. Available at: https://doi.org/10.1038/nature06419.

Moult, P.R., Cottrell, G.A. and Li, W.-C. (2013) 'Fast silencing reveals a lost role for reciprocal inhibition in locomotion.', *Neuron*, 77(1), pp. 129–40. Available at: https://doi.org/10.1016/j.neuron.2012.10.040.

Murata, K. *et al.* (2020) 'Region- and neuronal-subtype-specific expression of Na,K-ATPase alpha and beta subunit isoforms in the mouse brain', *Journal of Comparative Neurology*, 528(16), pp. 2654–2678. Available at: https://doi.org/10.1002/cne.24924.

Murphy, K.T. *et al.* (2004) 'Intense exercise up-regulates Na+, K+-ATPase isoform mRNA, but not protein expression in human skeletal muscle', *Journal of Physiology*, 556(2), pp. 507–519. Available at: https://doi.org/10.1113/jphysiol.2003.054981.

Nam, J.S., Hirohashi, S. and Wakefield, L.M. (2007) 'Dysadherin: A new player in cancer progression', *Cancer Letters*. Elsevier, pp. 161–169. Available at: https://doi.org/10.1016/j.canlet.2007.02.018.

Nelson, R., Bender, A.M. and Connaughton, V.P. (2003) 'Stimulation of sodium pump restores membrane potential to neurons excited by glutamate in zebrafish distal retina', *Journal of Physiology*, 549(3), pp. 787–800. Available at: https://doi.org/10.1113/JPHYSIOL.2003.042051.

Nieuwkoop, P.D. and Faber, J. (1956) *Normal table of Xenopus laevis (Daudin). A systematical and chronological survey of the development from the fertilized egg till the end of metamorphosis.* North-Holland, Amsterdam: Garland Pub.,.

Noguchi, S., Mutoh, Y. and Kawamura, M. (1994) 'The functional roles of disulfide bonds in the β-subunit of (Na,K)ATPase as studied by site-directed mutagenesis', *FEBS Letters*, 341(2–3), pp. 233–238. Available at: https://doi.org/10.1016/0014-5793(94)80463-X.

Oblak, A.L. *et al.* (2014) ‘Rapid-onset dystonia-parkinsonism associated with the I758S mutation of the ATP1A3 gene: A neuropathologic and neuroanatomical study of four siblings’, *Acta Neuropathologica*, 128(1), pp. 81–98. Available at: https://doi.org/10.1007/s00401-014-1279-x.

O’Dowd, D.K., Ribera, A.B. and Spitzer, N.C. (1988) ‘Development of voltage-dependent calcium, sodium and potassium currents in *Xenopus* spinal neurons’, *Journal of Neuroscience*, 8(3), pp. 792–805. Available at: https://doi.org/10.1523/jneurosci.08-03-00792.1988.

Orlowski, J. and Lingrel, J.B. (1988) ‘Tissue-specific and developmental regulation of rat Na,K-ATPase catalytic α isoform and β subunit mRNAs’, *Journal of Biological Chemistry*, 263(21), pp. 10436–10442. Available at: https://doi.org/10.1016/S0021-9258(19)81535-1.

Ossipov, M.H., Dussor, G.O. and Porreca, F. (2010) ‘Central modulation of pain.’, *The Journal of clinical investigation*, 120(11), pp. 3779–87. Available at: https://doi.org/10.1172/JCI43766.

P, van M., J, A. and A, R. (1989) ‘Development of early swimming in *Xenopus* laevis embryos: myotomal musculature, its innervation and activation’, *Neuroscience*, 32(1), pp. 113–126. Available at: https://doi.org/10.1016/0306-4522(89)90111-5.

Paciorkowski, A.R. *et al.* (2015) ‘Novel mutations in ATP1A3 associated with catastrophic early life epilepsy, episodic prolonged apnea, and postnatal microcephaly’, *Epilepsia*, 56(3), pp. 422–430. Available at: https://doi.org/10.1111/epi.12914.

Pai, V.P. *et al.* (2012) ‘Transmembrane voltage potential controls embryonic eye patterning in *Xenopus* laevis’, *Development*, 139(2), pp. 313–323. Available at: https://doi.org/10.1242/dev.073759.

Palmer, C.J., Scott, B.T. and Jones, L.R. (1991) ‘Purification and complete sequence determination of the major plasma membrane substrate for cAMP-dependent protein kinase and protein kinase C in myocardium.’, *undefined* [Preprint].

Parker, D., Hill, R. and Grillner, S. (1996) ‘Electrogenic pump and a Ca2+-dependent K+ conductance contribute to a posttetanic hyperpolarization in lamprey sensory neurons’, *Journal of Neurophysiology*, 76(1), pp. 540–553. Available at: https://doi.org/10.1152/JN.1996.76.1.540.

Paulus, J.D. *et al.* (2009) ‘Muscle contractions guide Rohon-Beard peripheral sensory axons’, *Journal of Neuroscience*, 29(42), pp. 13190–13201. Available at: https://doi.org/10.1523/JNEUROSCI.2179-09.2009.

Pavlovic, D. *et al.* (2013) ‘Nitric oxide regulates cardiac intracellular Na+ and Ca2+ by modulating Na/K ATPase via PKCε and phospholemman-dependent mechanism’, *Journal of Molecular and Cellular Cardiology*, 61(0022), pp. 164–171. Available at: https://doi.org/10.1016/j.yjmcc.2013.04.013.

Pavlovic, D., Fuller, W. and Shattock, M.J. (2013) ‘Novel regulation of cardiac Na pump via phospholemman’, *Journal of Molecular and Cellular Cardiology*. Academic Press, pp. 83–93. Available at: https://doi.org/10.1016/j.yjmcc.2013.05.002.

Pellizzari, S. *et al.* (2023) ‘Neuron populations use variable combinations of short-term feedback mechanisms to stabilize firing rate’, *PLoS Biology*, 21(1), pp. 1–17. Available at: https://doi.org/10.1371/journal.pbio.3001971.

Peshkin, L. *et al.* (2019) ‘The protein repertoire in early vertebrate embryogenesis’, *bioRxiv*, p. 571174. Available at: https://doi.org/10.1101/571174.

Picton, L.D. *et al.* (2017) ‘Sodium pumps mediate activity-dependent changes in mammalian motor networks’, *Journal of Neuroscience*, 37(4), pp. 906–921. Available at: https://doi.org/10.1523/JNEUROSCI.2005-16.2016.

Picton, L.D., Sillar, K.T. and Zhang, H.Y. (2018) ‘Control of *Xenopus* Tadpole Locomotion via Selective Expression of Ih in Excitatory Interneurons’, *Current Biology*, 28(24), pp. 3911-3923.e2. Available at: https://doi.org/10.1016/j.cub.2018.10.048.

Pivovarov, A.S., Calahorro, F. and Walker, R.J. (2019) ‘Na+/K+-pump and neurotransmitter membrane receptors’, *Invertebrate Neuroscience*, 19(1), p. 1. Available at: https://doi.org/10.1007/S10158-018-0221-7.

Post, R.L., Hegyvahy, C. and Kume, S. (1972) *Activation by Adenosine Triphosphate in the Phosphorylation Kinetics of Sodium and Potassium Ion Transport Adenosine Triphosphatase*.

Pulver, S.R. and Griffith, L.C. (2009) ‘Spike integration and cellular memory in a rhythmic network from Na+/K+ pump current dynamics’, *Nature Neuroscience 2009 13:1*, 13(1), pp. 53–59. Available at: https://doi.org/10.1038/nn.2444.

Rahman, M.M. *et al.* (2015) 'Developmental expression analysis of Na, K-ATPase α subunits in *Xenopus*', *Development Genes and Evolution*, 225(2), pp. 105–111. Available at: https://doi.org/10.1007/s00427-015-0497-0.

Ramlochansingh, C. *et al.* (2014) 'Efficacy of tricaine methanesulfonate (MS-222) as an anesthetic agent for blocking sensory-motor responses in *Xenopus* laevis tadpoles', *PLoS ONE*, 9(7), p. e101606. Available at: https://doi.org/10.1371/journal.pone.0101606.

Ramola, B. *et al.* (2019) 'Evaluation, comparison of different solvent extraction, cell disruption methods and hydrothermal liquefaction of Oedogonium macroalgae for biofuel production', *Biotechnology Reports*, 22, p. e00340. Available at: https://doi.org/10.1016/J.BTRE.2019.E00340.

Rasmussen, M.K., Kristensen, M. and Juel, C. (2008) 'Exercise-induced regulation of phospholemman (FXYD1) in rat skeletal muscle: implications for Na^+/K^+-ATPase activity', *Acta Physiologica*, 194(1), pp. 67–79. Available at: https://doi.org/10.1111/j.1748-1716.2008.01857.x.

Reeves, A.S., Collins, J.H. and Schwartz, A. (1980) 'Isolation and characterization of (Na,K)-ATPase proteolipid', *Topics in Catalysis*, 95(4), pp. 1591–1598. Available at: https://doi.org/10.1016/S0006-291X(80)80080-5.

Reis, J. *et al.* (2005) 'Expression of phospholemman and its association with Na+-K +-ATPase in skeletal muscle: Effects of aging and exercise training', *Journal of Applied Physiology*, 99(4), pp. 1508–1515. Available at: https://doi.org/10.1152/japplphysiol.00375.2005.

Roberts, A. (1971) 'The role of propagated skin impulses in the sensory system of young tadpoles', *Zeitschrift für Vergleichende Physiologie*, 75(4), pp. 388–401. Available at: https://doi.org/10.1007/BF00630559.

Roberts, A. *et al.* (1987) 'The early development of neurons with GABA immunoreactivity in the CNS of *Xenopus* laevis embryos', *Journal of Comparative Neurology*, 261(3), pp. 435–449. Available at: https://doi.org/10.1002/cne.902610308.

Roberts, A. *et al.* (1998) 'Central circuits controlling locomotion in young frog tadpoles', in *Annals of the New York Academy of Sciences*. New York Academy of Sciences, pp. 19–34. Available at: https://doi.org/10.1111/j.1749-6632.1998.tb09036.x.

Roberts, A. *et al.* (2009a) ‘Responses of hatchling *Xenopus* tadpoles to water currents: First function of lateral line receptors without cupulae’, *Journal of Experimental Biology*, 212(7), pp. 914–921. Available at: https://doi.org/10.1242/jeb.027250.

Roberts, A. *et al.* (2009b) ‘Responses of hatchling *Xenopus* tadpoles to water currents: First function of lateral line receptors without cupulae’, *Journal of Experimental Biology*, 212(7), pp. 914–921. Available at: https://doi.org/10.1242/jeb.027250.

Roberts, A. and Clarke, J.D. (1982) ‘The neuroanatomy of an amphibian embryo spinal cord.’, *Philosophical transactions of the Royal Society of London. Series B, Biological sciences*, 296(1081), pp. 195–212. Available at: https://doi.org/10.1098/rstb.1982.0002.

Roberts, A. and Hayes, B.P. (1977) ‘The anatomy and function of “free” nerve endings in an amphibian skin sensory system’, *Proceedings of the Royal Society of London - Biological Sciences*, 196(1125), pp. 415–429. Available at: https://doi.org/10.1098/rspb.1977.0048.

Roberts, A., Li, W.-C. and Soffe, S.R. (2010) ‘How Neurons Generate Behavior in A Hatchling Amphibian Tadpole: An Outline’, *Frontiers in Behavioral Neuroscience*, 4(JUN). Available at: https://doi.org/10.3389/FNBEH.2010.00016.

Roberts, A., Li, W.C. and Soffe, S.R. (2012) ‘A functional scaffold of CNS neurons for the vertebrates: The developing *Xenopus* laevis spinal cord’, *Developmental Neurobiology*, 72(4), pp. 575–584. Available at: https://doi.org/10.1002/dneu.20889.

Robinson, J.D. and Pratap, P.R. (1993) ‘Indicators of conformational changes in the Na+/K+-ATPase and their interpretation’, *Biochimica et Biophysica Acta (BBA) - Reviews on Biomembranes*, 1154(1), pp. 83–104. Available at: https://doi.org/10.1016/0304-4157(93)90018-J.

Rohon, V. (1885) ‘Zur histogenese des riickenmarkes der forelle, S.B. bayer’, *Denkschriften der Kaiserlichen Akademie der Wissenschaften / Mathematisch-Naturwissenschaftliche Classe*, 14, pp. 39–57.

Rosewich, H. *et al.* (2012) ‘Heterozygous de-novo mutations in ATP1A3 in patients with alternating hemiplegia of childhood: A whole-exome sequencing gene-identification study’, *The Lancet Neurology*, 11(9), pp. 764–773. Available at: https://doi.org/10.1016/S1474-4422(12)70182-5.

Saccomanno, V. *et al.* (2021) ‘The early development and physiology of Xenopus laevis tadpole lateral line system’, *Journal of Neurophysiology*, 126(5), pp. 1814–1830. Available at: https://doi.org/10.1152/jn.00618.2020.

Saito, S. *et al.* (2001) ‘Expression of a novel member of the ATP1G1/PLM/MAT8 family, phospholemman-like protein (PLP) gene, in the developmental process of mouse cerebellum’, *Gene*, 279(2), pp. 149–155. Available at: https://doi.org/10.1016/S0378-1119(01)00745-4.

Sautois, B. *et al.* (2007) ‘Role of type-specific neuron properties in a spinal cord motor network’, *Journal of Computational Neuroscience*, 23(1), pp. 59–77. Available at: https://doi.org/10.1007/s10827-006-0019-1.

Schneider, B.G. and Kraig, E. (1990) ‘Na+,K+-ATPase of the photoreceptor: Selective expression of α3 and β2 isoforms’, *Experimental Eye Research*, 51(5), pp. 553–564. Available at: https://doi.org/10.1016/0014-4835(90)90086-A.

Session, A.M. *et al.* (2016a) ‘Genome evolution in the allotetraploid frog *Xenopus* laevis’, *Nature*, 538(7625), pp. 336–343. Available at: https://doi.org/10.1038/nature19840.

Session, A.M. *et al.* (2016b) ‘Genome evolution in the allotetraploid frog *Xenopus* laevis’, *Nature*, 538(7625), pp. 336–343. Available at: https://doi.org/10.1038/nature19840.

Shamraj, O.I. and Lingrel, J.B. (1994) ‘A putative fourth Na+,K+-ATPase α-subunit gene is expressed in testis’, *Proceedings of the National Academy of Sciences of the United States of America*, 91(26), pp. 12952–12956. Available at: https://doi.org/10.1073/pnas.91.26.12952.

Shan, Z. *et al.* (2023) ‘Embryonic and skeletal development of the albino African clawed frog (*Xenopus* laevis)’, *Journal of Anatomy*, 242(6), pp. 1051–1066. Available at: https://doi.org/10.1111/joa.13835.

Shrivastava, A.N., Triller, A. and Melki, R. (2020) ‘Cell biology and dynamics of Neuronal Na+/K+-ATPase in health and diseases’, *Neuropharmacology*. Elsevier Ltd. Available at: https://doi.org/10.1016/j.neuropharm.2018.12.008.

Shull, G.E., Greeb, J. and Lingrel, J.B. (1986) ‘Molecular Cloning of Three Distinct Forms of the Na+,K+-ATPase a-Subunit from Rat Brain’, *Biochemistry*, 25(25), pp. 8125–8132. Available at: https://doi.org/10.1021/bi00373a001.

Sillar, K.T. and Li, W.-C. (2020) ‘The Neural Control of Movement Historical perspectives Neural control of swimming in hatchling *Xenopus* frog tadpoles’. Available at: https://doi.org/10.1016/B978-0-12-816477-8.00007-7.

Sillar, K.T. and Roberts, A. (1988) ‘A neuronal mechanism for sensory gating during locomotion in a vertebrate’, *Nature*, 331(6153), pp. 262–265. Available at: https://doi.org/10.1038/331262A0.

Sillar, K.T., Wedderburn, J.F.S. and Simmers, A.J. (1991) ‘The development of swimming rhythmicity in post-embryonic *Xenopus* laevis’, *Proceedings of the Royal Society B: Biological Sciences*, 246(1316), pp. 147–153. Available at: https://doi.org/10.1098/rspb.1991.0137.

Smith, R.S. *et al.* (2021) ‘Early role for a Na+,K+-ATPase (ATP1A3) in brain development’, *Proceedings of the National Academy of Sciences*, 118(25). Available at: https://doi.org/10.1073/PNAS.2023333118.

Speake, T. *et al.* (2001) ‘Mechanisms of CSF secretion by the choroid plexus.’, *Microscopy research and technique*, 52(1), pp. 49–59. Available at: https://doi.org/10.1002/1097-0029(20010101)52:1<49::AID-JEMT7>3.0.CO;2-C.

Stanley, C.M. *et al.* (2015) ‘Article Importance of the Voltage Dependence of Cardiac Na/K ATPase Isozymes’. Available at: https://doi.org/10.1016/j.bpj.2015.09.015.

Stehouwer, D.J. and Farel, P.B. (1985) ‘Development of locomotor mechanisms in the frog’, *Journal of Neurophysiology*, 53(6), pp. 1453–1466. Available at: https://doi.org/10.1152/jn.1985.53.6.1453.

Stryer, L. (1986) ‘Cyclic GMP cascade of vision’, *Annual Review of Neuroscience*, VOL. 9, pp. 87–119. Available at: https://doi.org/10.1146/annurev.ne.09.030186.000511.

Suhail, M. (2010) ‘Na+, K+-ATPase: Ubiquitous Multifunctional Transmembrane Protein and its Relevance to Various Pathophysiological Conditions’, *Journal of Clinical Medicine Research*, 2(1), p. 1. Available at: https://doi.org/10.4021/jocmr2010.02.263w.

Suster, M.L. and Bate, M. (2002) ‘Embryonic assembly of a central pattern generator without sensory input’, *Nature 2002 416:6877*, 416(6877), pp. 174–178. Available at: https://doi.org/10.1038/416174a.

Sweadner, K.J. *et al.* (1994) 'Immunologic identification of Na+,K(+)-ATPase isoforms in myocardium. Isoform change in deoxycorticosterone acetate-salt hypertension', *Circulation research*, 74(4), pp. 669–678. Available at: https://doi.org/10.1161/01.RES.74.4.669.

Sweadner, K.J. *et al.* (2019) 'Genotype-structure-phenotype relationships diverge in paralogs ATP1A1, ATP1A2, and ATP1A3', *Neurology: Genetics*. Lippincott Williams and Wilkins. Available at: https://doi.org/10.1212/NXG.0000000000000303.

Sweadner, K.J. and Rael, E. (2000) 'The FXYD gene family of small ion transport regulators or channels: cDNA sequence, protein signature sequence, and expression', *Genomics*, 68(1), pp. 41–56. Available at: https://doi.org/10.1006/geno.2000.6274.

Teriete, P. *et al.* (2009) 'Effects of PKA phosphorylation on the conformation of the Na,K-ATPase regulatory protein FXYD1', *Biochimica et Biophysica Acta - Biomembranes*, 1788(11), pp. 2462–2470. Available at: https://doi.org/10.1016/j.bbamem.2009.09.001.

Therien, A.G. and Blostein, R. (2000) 'Mechanisms of sodium pump regulation', *American Journal of Physiology - Cell Physiology*. American Physiological SocietyBethesda, MD. Available at: https://doi.org/10.1152/ajpcell.2000.279.3.c541.

Thomassen, M. *et al.* (2010) 'Effect of 2-wk intensified training and inactivity on muscle Na +-K+ pump expression, phospholemman (FXYDI) phosphorylation, and performance in soccer players', *Journal of Applied Physiology*, 108(4), pp. 898–905. Available at: https://doi.org/10.1152/JAPPLPHYSIOL.01015.2009/ASSET/IMAGES/LARGE/ZDG0041089910005.JPEG.

Thomassen, M. *et al.* (2016) 'Intensive training and reduced volume increases muscle FXYD1 expression and phosphorylation at rest and during exercise in athletes', *American Journal of Physiology - Regulatory Integrative and Comparative Physiology*, 310(7), pp. R659–R669. Available at: https://doi.org/10.1152/ajpregu.00081.2015.

Thuret, R., Auger, H. and Papalopulu, N. (2015) 'Analysis of neural progenitors from embryogenesis to juvenile adult in *Xenopus* laevis reveals biphasic neurogenesis and continuous lengthening of the cell cycle', *Biology Open*, 4(12), pp. 1772–1781. Available at: https://doi.org/10.1242/bio.013391.

Tokhtaeva, E. *et al.* (2010) 'N-Glycan-Dependent Quality Control of the Na,K-ATPase β2 Subunit', *Biochemistry*, 49(14), pp. 3116–3128. Available at: https://doi.org/10.1021/BI100115A.

Tokhtaeva, E. *et al.* (2012) ‘Subunit isoform selectivity in assembly of Na,K-ATPase α-β heterodimers’, *Journal of Biological Chemistry*, 287(31), pp. 26115–26125. Available at: https://doi.org/10.1074/jbc.M112.370734.

Tranebjærg, L. *et al.* (2018) ‘The CAPOS mutation in ATP1A3 alters Na/K-ATPase function and results in auditory neuropathy which has implications for management’, *Human Genetics*, 137(2), pp. 111–127. Available at: https://doi.org/10.1007/s00439-017-1862-z.

Wasser, C.R. and Kavalali, E.T. (2009) ‘Leaky synapses: Regulation of spontaneous neurotransmission in central synapses’, *Neuroscience*, pp. 177–188. Available at: https://doi.org/10.1016/j.neuroscience.2008.03.028.

Wilson, D.M. and Wyman, R.J. (1965) ‘Motor Output Patterns during Random and Rhythmic Stimulation of Locust Thoracic Ganglia’, *Biophysical Journal*, 5(2), pp. 121–143. Available at: https://doi.org/10.1016/S0006-3495(65)86706-6.

Winlow, W., Gillette, R. and Walters, E.T. (2018) ‘Nociceptive Biology of Molluscs and Arthropods: Evolutionary Clues About Functions and Mechanisms Potentially Related to Pain’. Available at: https://doi.org/10.3389/fphys.2018.01049.

Wu, Z.Q. *et al.* (2007) ‘Involvement of Dopamine System in Regulation of Na+,K+-ATPase in the Striatum upon Activation of Opioid Receptors by Morphine’, *Molecular Pharmacology*, 71(2), pp. 519–530. Available at: https://doi.org/10.1124/MOL.106.029561.

Wyckelsma, V.L. *et al.* (2019) ‘Inactivity and exercise training differentially regulate abundance of Na+-K+-ATPase in human skeletal muscle’, *Journal of Applied Physiology*. American Physiological Society, pp. 905–920. Available at: https://doi.org/10.1152/japplphysiol.01076.2018.

Yamaguchi, F. *et al.* (2001) ‘Molecular cloning and characterization of a novel phospholemman-like protein from rat hippocampus’, *Molecular Brain Research*, 86(1–2), pp. 189–192. Available at: https://doi.org/10.1016/S0169-328X(00)00213-8.

Yang, L., Wang, F. and Strähle, U. (2020) ‘The Genetic Programs Specifying Kolmer–Agduhr Interneurons’, *Frontiers in Neuroscience*. Available at: https://doi.org/10.3389/fnins.2020.577879.

Yap, J.Q. *et al.* (2021a) ‘FXYD proteins and sodium pump regulatory mechanisms’. Available at: https://doi.org/10.1085/jgp.202012633.

Yap, J.Q. *et al.* (2021b) ‘FXYD proteins and sodium pump regulatory mechanisms’. Available at: https://doi.org/10.1085/jgp.202012633.

Yau, K.-W. (1994) ‘Phototransduction mechanism in retinal rods and cones. The Friedenwald Lecture.’, *Investigative Ophthalmology & Visual Science*, 35(1), pp. 9–32.

Zahler, R. *et al.* (1996) ‘The α3 isoform protein of the Na+,K+-ATPase is associated with the sites of cardiac and neuromuscular impulse transmission’, *Circulation Research*, 78(5), pp. 870–879. Available at: https://doi.org/10.1161/01.RES.78.5.870.

Zahler, R. *et al.* (1997) ‘Sodium kinetics of Na,K-ATPase α isoforms in intact transfected HeLa cells’, *Journal of General Physiology*, 110(2), pp. 201–213. Available at: https://doi.org/10.1085/jgp.110.2.201.

Zhang, H.-Y. *et al.* (2009a) ‘Electrical coupling synchronises spinal motoneuron activity during swimming in hatchling *Xenopus* tadpoles’, *J Physiol*, 587, pp. 4455–4466. Available at: https://doi.org/10.1113/jphysiol.2009.173468.

Zhang, H.-Y. *et al.* (2009b) ‘Electrical coupling synchronises spinal motoneuron activity during swimming in hatchling *Xenopus* tadpoles’, *J Physiol*, 587, pp. 4455–4466. Available at: https://doi.org/10.1113/jphysiol.2009.173468.

Zhang, H.Y. *et al.* (2015) ‘Mechanisms underlying the activity-dependent regulation of locomotor network performance by the Na+ pump’, *Scientific Reports*, 5. Available at: https://doi.org/10.1038/srep16188.

Zhang, H.Y., Issberner, J. and Sillar, K.T. (2011) ‘Development of a spinal locomotor rheostat’, *Proceedings of the National Academy of Sciences of the United States of America*, 108(28), pp. 11674–11679. Available at: https://doi.org/10.1073/pnas.1018512108.

Zhang, H.Y. and Sillar, K.T. (2012) ‘Short-term memory of motor network performance via activity-dependent potentiation of Na +/K + pump function’, *Current Biology*, 22(6), pp. 526–531. Available at: https://doi.org/10.1016/j.cub.2012.01.058.

Zhao, Y. *et al.* (2021) ‘TPM, FPKM, or Normalized Counts? A Comparative Study of Quantification Measures for the Analysis of RNA-seq Data from the NCI Patient-Derived Models Repository’, *Journal of translational medicine*, 19(1). Available at: https://doi.org/10.1186/S12967-021-02936-W.

Zheng, S. *et al.* (2022) ‘Inhibition of the Sodium Potassium ATPase Alpha 3 (ATP1A3) Pump Function Alters Repolarization Time and is Proarrhythmic in Cardiac Myocytes’, *Circulation*, 146(Suppl_1). Available at: https://doi.org/10.1161/circ.146.suppl_1.12449.

Zou, S. *et al.* (2023) ‘The role of ATP1A3 gene in epilepsy: We need to know more’, *Frontiers in Cellular Neuroscience*, 17. Available at: https://doi.org/10.3389/fncel.2023.1143956.

Zouzoulas, A. *et al.* (2003) ‘Modulation of Na,K-ATPase by the γ subunit: Studies with transfected cells and transmembrane mimetic peptides’, *Journal of Biological Chemistry*, 278(42), pp. 40437–40441. Available at: https://doi.org/10.1074/jbc.M308610200.

Zúñiga-Ramírez, C. *et al.* (2019) ‘Generalized Dystonia and Paroxysmal Dystonic Attacks due to a Novel ATP1A3 Variant’, *Tremor and other hyperkinetic movements (New York, N.Y.)*, 9. Available at: https://doi.org/10.7916/tohm.v0.723.